THE EVOLUTION OF HYDROTHERMAL FLUIDS AT THE PIPELINE GOLD MINE, LANDER COUNTY, NEVADA

By Nigel John Frederick Blamey

Submitted in partial fulfillment of the requirements of the degree of Ph.D.

September 2000

Department of Earth and Environmental Science

New Mexico Institute of Mining and Technology

Socorro, New Mexico

ABSTRACT

Pipeline is a sediment-hosted, disseminated gold deposit located 120 km southwest of Elko, Nevada. Gold mineralization is argillization-hematite-silicification-gold in decalcified Roberts Mountains Formation. Pipeline and its extensions comprise a global resource of 13.13 million oz. gold and total mineralization reserves of 8.2 million oz.. Such large reserves and high tonnage make Pipeline an important deposit to study. In addition, samples could be collected at the commencement of mining activities before valuable information was lost by mining activities.

Until now, the genesis of Carlin-type deposits was considered enigmatic. Proposed sources of gold include magmatic, amagmatic, metamorphic and meteoric sources. Features of Carlin-type deposits remaining unanswered include the timing of gold mineralization, fluid sources, high-salinity fluid inclusions, the significance of carbonic fluid inclusions, a depositional mechanism, water-rock ratios for mineralizing fluids, and P-T conditions during gold mineralization. By applying a combination of analytical methods and field studies that are not widely used in Nevada, for the first time a coherent picture of mineralization processes and fluid sources of gold-bearing fluids was obtained that explain much of the contradictory evidence accumulated by previous studies. The objectives were to explore the genesis and timing of the Pipeline mineralization and to test the hypothesis that gold mineralization is coeval with decalcification in a Carlin-type deposit.

The study comprised field observations in addition to logging and sampling drillcore during 3 field seasons. Analytical methods applied include fluid inclusion

microthermometry, fluid inclusion gas analysis, fluid inclusion bulk crush leach, $^{40}Ar/^{39}Ar$ dating, clay analysis, petrographic microscopy, reflected-light microscopy and electron microprobe analysis.

Pipeline mineralization occurs in sheared, brecciated and decalcified Roberts Mountain Formation below the Roberts Mountains thrust. Mineralization is quartz, minor sericite, hematite, goethite, minor calcite, and finely disseminated gold.

A paragenetic sequence for the Pipeline deposit is established. Stage 1 comprises dark petroliferous calcite. Stage 2 is represented by white calcite and is thought to be coeval with the Antler orogeny. Stage 3 is quartz-sericite-calcite-pyrite-gold with veins occurring beneath the deposit and that are considered the hydrothermal feeders to the deposit. The stage 3 veins are linked to gold mineralization within the deposit by age dating and only stage 3 veins have gold selvages associated with them. Oxidation characterizes stage 4 with pseudomorph replacement of sulfides by Fe-oxides. Vuggy calcite, which occurs in veins and open space fillings in the ore deposit, represents stage 5 that locally predates the Basin- and-Range faulting.

Pipeline fluid inclusion studies identify 3 inclusion types. Type 1a are aqueous dominated with a minor vapor bubble. Type 1b are aqueous dominated with a minor carbonic phase and bubble. Type 2 inclusions have CO_2 and other gaseous species equal to or greater than the aqueous phase. Stage 1 calcite contains Type 1a inclusions, one population has methane-bearing clathrates with melting temperatures (Tm) up to 23.3°C whereas the second population are low salinity fluids. Stage 2 white calcite inclusions are Type 2 and the salinity ranges up to 0.8 eq. wt. % NaCl. Stage 3 vein and ore quartz contain aqueous Type 1 inclusions and Type 2 inclusions. Stage 3 quartz Type 1 inclusion

salinities range from 5 to 25 eq. wt. % NaCl and homogenization temperatures (T_h) range from 179° to 265°C. Hypersaline Type 1 inclusions have anomalous calcium-rich fluid with Ca/Na ratios of 0.8 to 1.4. Quartz-hosted stage 3, Type 2 inclusions are about 1:8 H_2O-CO_2, have salinities about 0.5 eq. wt. % NaCl and T_h ranges from 285° to 323°C. Calcite-hosted stage 3 inclusions are Type 1a, as are stage 5 calcite inclusions. Stage 3 calcite Th values range from 219° to 235°C and calculated salinities are 3.0 to 3.3 eq. wt. % NaCl. Stage 5 calcite Th values are ~125°C with low salinity values.

Gas analysis indicates stage 1 calcite inclusion fluids have 93.6 to 97.7 mol. % water and variable CO_2/CH_4 ratios between 0.5 and 40. The N_2/Ar ratios indicate meteoric and magmatic fluid components. Stage 2 calcite has high amounts of CO_2 that exceeds 50 mol. % for individual analyses, N_2/Ar ratios are around 100 and CO_2/CH_4 are about 100 indicating a meteoric source. Stage 3 quartz fluid inclusion gas analyses show that CO_2 varies from 0.5 to 8 mol. %. Carbon dioxide strongly correlates with H_2S, which varies from 0.03 to 0.00001 mol. %, and CO_2 inversely correlates with salinity. Fluid inclusion N_2/Ar ratios are >500 indicating a strong magmatic volatile component. Stage 5 calcite is dominated by fluids that have N_2/Ar ratios less than 100 and CO_2/CH_4 ratios ~1, indicating evolved fluids; total volatile contents are less than 1 mol. %.

Quartz bulk fluid inclusion crush leach followed by flame AA for cations and ion chromotography for anions show variable Ca/(Na+K) ratios. High ratios are paired with a high "missing" anion component, interpreted to be bicarbonate.

The only clay mineral present in ore zones is illite of $2M_1$ polytype. FWHM values of the first order illite peak are positively correlated with decalcification intensity ($R^2 = 0.41$).

Three thermal epochs are identified in the area. Mill Canyon stock biotite gives an $^{40}Ar/^{39}Ar$ plateau age of 152.2±0.3 Ma. Stage 3 hydrothermal sericite from quartz-sericite-calcite veins at Pipeline are dated at 92.0±0.3 Ma that coincides with age dates of alteration minerals by others ranging from 92 to 105 Ma. Age spectra of illite from ore zones have a strong Early Cretaceous component. Inherited argon results in discordant age spectra for some illite samples whereas in other samples, 8% recoil loss accounts for ages slightly older than 92 Ma. Tertiary dikes in the Cortez area give biotite and K-feldspar ages of 35 ~ 36 Ma.

Trapping pressures of inclusions (Pt) are estimated by isochores, MACFLINCOR and from estimates of the geothermal gradient. Estimates of the geothermal gradient, pressure and inclusion Th's, for stage 1 give a depth of ~5 km. Stage 2 calcite pressure estimates calculated by MACFLINCOR are ~1.5 kbar, corresponding to a minimum lithostatic load of ~5km. Stage 3 quartz was deposited at a pressure ~2000 bars. Stage 3 calcite isochores confirm lower pressures for calcite than quartz at any given temperature, suggesting calcite was deposited under lower pressure conditions.

The range in CO_2 contents of fluid inclusions, the range in fluid salinities that inversely correlate with CO_2, and correlation of CO_2 with H_2S is consistent with decalcification driven by carbonic acid:

$$H_2CO_3 + CaCO_3 = Ca^{++} + 2HCO_3^-$$

As CO_2 is consumed, spent fluids should increase in ionic strength and Ca^{++}; which is seen in both fluid inclusion and crush-leach analyses. The <1 % Fe in calcite released by calcite solution is available to form FeS_2, which explains the paired decrease in fluid inclusion CO_2 and H_2S. Calculations of ore fluid pH is 4.66 whereas in spent fluid the calculated

average pH is 5.9. Theoretical gold solubility based on fluid inclusion salinity and gas analysis, is calculated to be ~200 ppb in ore fluid and <2 ppb in spent fluid. Gold deposition is attributed to wall rock attack and sulfidization reactions that lowered fluid H_2S and thus destabilizing Au bisulfide complexes.

Calculated mass-balances of ore fluid to rock give relatively low ratios that are consistent with mineralization by magmatic fluids. Consumption of CO_2 during decalcification, Ca-production and change of gold solubility, are consistent with a water-rock ratio of about 6:1 by weight and explains the very localized alteration commonly observed in Carlin-type deposits.

Conclusions are that prior to gold mineralization were two periods of calcite veining in response to regional magmatic and tectonic events that did not produce gold mineralization. Gold mineralization was coeval with alteration and deposition of quartz during stage 3, around 92 Ma. Fluids derived from an intrusive body and charged with CO_2 penetrated the country rock through fractures and these fluids entered the permeable shear zones within the Roberts Mountains Formation. Decalcification occurred, liberating Fe^{++} which reacted with H_2S causing sulfidation. Spent ore fluids were Ca-rich brine that had salinities up to 25 eq. wt. % NaCl. The depletion of H_2S in ore solutions destabilized the gold bisulfide complexes and initiated gold deposition. Oxidization of the ore body was most likely by subsurface oxygenated waters and not a result of weathering. Following ore-body oxidation was calcite mineralization by evolved waters, and then Basin-and-Range faulting.

This work presents a internally self consistent body of data that yields an understanding of how Pipeline formed, and a genetic model that satisfies mass balance

calculations. Many Pipeline geochemical and physical characteristics are reported in other Carlin-type deposits. The implication is that most Carlin-type deposits have a similar genesis. That is, the driving force and major fluid source is magmatic. The CO_2 and H_2S charged fluids associated with an intrusive body provide a fluid that serves both to introduce gold and cause decalcification in one event. Gold mineralization is in response to sulfidization reactions. Fluid quantities are limited, hence there are low water-rock ratios and a localized alteration halo. Gold is associated with quartz and sericite mineralization. Depths can be as deep as 8 km, with mineralization under lithostatic pressure, hence, fluid inclusion Th measurements can yield far lower temperatures than mineralizing fluids. Carbonic fluid inclusions are the product of mild varying CO_2 composition that boiled when occasionally highly charged with CO_2. The oxidation event that replaced pyrite by Fe-oxides may not necessarily be supergene. Multiple intrusive and hydrothermal events occurred at or near the gold deposit, but principally one event introduced to gold.

ACKNOWLEDGMENTS:

I would like to express my deepest gratitude to my committee namely Drs. David Norman, Andrew Campbell, George Austin and Matt Heizler. I learned a great deal from the exceptional knowledge of Dave Norman, particularly on fluid inclusions and the handling of analytical data from the quadrupole mass spectrometer; he also helped by providing me with a research assistantship. Andrew Campbell always made me think very astutely about what I was doing and I invariably left his office with a more balanced objective. George and Matt always made time to discuss aspects of my research with me and I appreciated their constructive criticism. They all kept me focused and allowed me to reach my goal. I would also like to acknowledge the department of Geochemistry at New Mexico Institute of Mining and Technology and the New Mexico Bureau of Mines and Mineral Resources for the use of facilities for analyzing my samples; in the Bureau thanks go to Nelia Dunbar, Christopher McKee, Terry Thomas and Ibrahim Gundiler. Argon dating was conducted at the New Mexico Geochronological Research Laboratory; thanks also go to Lisa Peters and Richard Esser for their help. The department of Earth and Environmental Sciences nominated me for the Charles Park Fellowship and I acknowledge the assistance from the trust. Thanks to members of staff and fellow students who helped and encouraged me, particularly William Xavier Chavez, Beverley Chomiak, Patci Mills, and Felix Barreras. Financial support was received from the Graduate Students Association on campus for presenting at the 1999 GSA conference in Denver. On international affairs, Karen Schlue needs a big thanks for all her help. Thanks go to Kate Weatherall for helping me edit this document.

Placer Dome Inc. and Cortez Gold Mines are thanked for providing me with my research project, for funding the analyses and providing me with summer employment. Richard Duncan was instrumental in initiating the project. A special thanks goes to Robert Hays (Jnr.), the Chief Geologist at the Pipeline Mine as well as the geological staff with whom I worked. Dr John Muntean provided fruitful comments during the latter stages of my writing. Thanks also goes to the friends I made in Nevada including Michael Steenhoek, Bruce Cox, Robert Wilcox, George and Barbara Montgomery, James Sefton, and Paul Meyer.

Thanks to the good friends that I have made in Socorro and with whom I shared many a meal and chat; these include Samuel and Viola Lewis, Harry Epstein, Connie Sayre, as well as Kalman and Barbara Oravecz. During the last year when I needed a musical interlude, some great blues were provided by Gary, Kathy, Tami and Steve of the KGB Blues Band as well as the Kat Crosby Band; thanks for jamming guys.

This dissertation is written in the memory of family passed on.

The biggest risk that one could take in life is not taking one at all

TABLE OF CONTENTS

LIST OF FIGURES

LIST OF TABLES

CHAPTER 1

Introduction

The United States of America is currently the world's second biggest gold producer. The greatest domestic gold production occurs in Nevada from Carlin-type gold deposits. Exploration for these deposits commenced in the 1960's following the discovery of gold in the Carlin area (Teal and Jackson, 1997). Subsequent discoveries were made along a linear trend passing through the Carlin mine and elsewhere in north central Nevada. Discovered during the past ten years, Pipeline is one of the largest gold deposits in Nevada. The Pipeline Gold Mine is located in Lander County, approximately 120 km southwest of Elko, Nevada (Fig. 1.1) along a mineralized belt named the Battle Mountain/Eureka trend. Pipeline and its extensions comprise a global resource of 13.13 million oz. gold and total mineralization reserves of 8.2 million oz. (R.C. Hays, pers. comm.).

Carlin-type deposits are hydrothermal gold mineralization hosted in carbonate rocks. These deposits feature finely disseminated gold with low silver to gold ratios, exhibit a similar alteration style, and have a strong structural control. Occurring along regional mineralization trends, these deposits have northwest and northeast-trending faults, and are associated with elevated concentrations of As, Sb, Hg and Te. Pipeline exhibits features typical of Carlin-type deposits including decalcification (calcite removal), argillization, sub-micron gold, carbonate host rocks and mineralization control by shear zones.

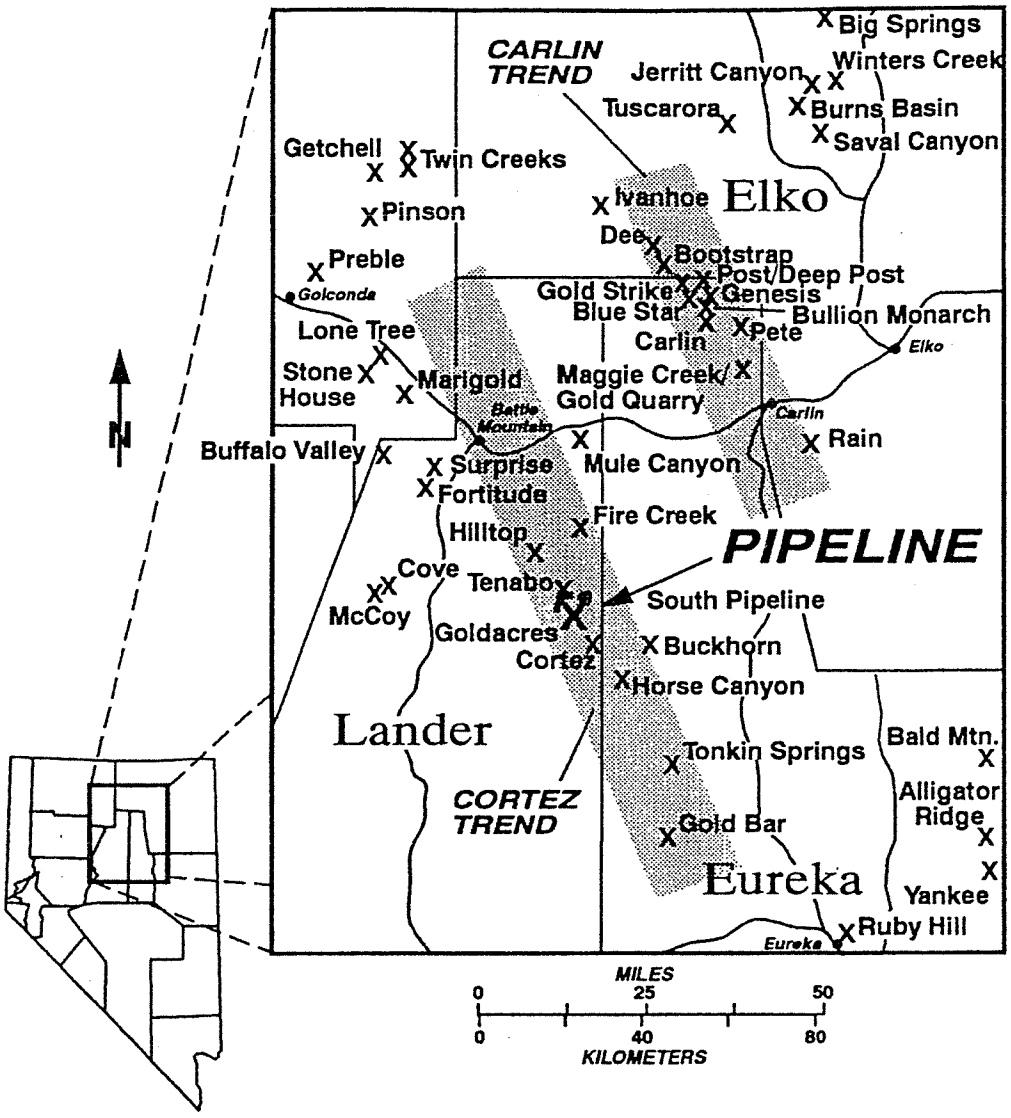

Figure 1.1 Location of the Pipeline deposit and several other gold deposits in Nevada (with permission from Foo et al., 1996). Shaded are the Battle Mountain-Eureka and Carlin trends.

Exploration of Carlin deposits has been driven by economic factors that dictate large, high-tonnage deposits that can be mined in an open pit. An understanding of Carlin-type deposit genesis is necessary for the successful exploration of new deposits, and the formation of predictive strategies to locate hidden reserves nearby known mineralization.

Important milestones influencing our understanding of Carlin-type deposits were made in the past 15 years. The concept of decalcification (also referred to as decarbonation) is recognized as the most prominent alteration style in Carlin-type deposits (Teal and Jackson, 1997). Decalcification refers to the dissolution of calcite to create a suitably porous and permeable host rock by decalcifying fluids. It was first documented at Carlin (Kuehn, 1989; Bakken 1990). These two studies describe hydrothermal fluid being focused along structural conduits and favorable stratigraphic units resulting in pre-ore decalcification, loss of density, coupled with increase of porosity and permeability. Decalcification of the silty limestone protolith at Carlin is more widespread and intense, this being attributed to the original porosity and permeability of the host rock (Teal and Jackson, 1997). In contrast, at Meikle, hydrothermal fluids did not react readily with the biosparitic protolith and therefore decalcification tends to be restricted to near high-angle conduits (Teal and Jackson, 1997). Decalcification is generally regarded as a ground-preparation event that is economically unimportant and separate in time from gold mineralization. However, calcite destruction and mineralization are commonly considered coeval in skarn and base metal replacements deposits. This leads to the question whether separate alteration and mineralization events are required in Carlin-type deposits.

Sulfidation is common in all Carlin-type deposits and is well documented at Twin Creeks by Stenger et al., 1998. Sulfur is introduced by hydrothermal fluid but Fe is locally sourced from ferroan-dolomites. Sulfide minerals are regarded as an important factor in Carlin-type deposits due to their strong association with gold, particularly arsenopyrite (Arehart et al., 1993a).

A variety of characteristics specific to individual deposits has prevented the development of one genetic model that would explain all Carlin-type deposits. In some deposits the mineralization controls are stratigraphic (Carlin and Pete) and in others faults control the mineralization (Gold Quarry and Griffin). Shear as opposed to breccia-style mineralization is also used by Teal and Jackson (1997) to contrast the differences within the greater group of Carlin-type deposits.

Dating of gold mineralization in Carlin-type deposits is restricted by the lack of datable minerals that are paragenetically linked with gold mineralization. In addition, Carlin-type deposits may be complicated by the potential for repeated hydrothermal activity driven by igneous events that span the Jurassic, Cretaceous, and Tertiary. Five gold-bearing events are reported (Groff et al., 1997) at Getchell and Twin Creeks, with the major gold mineralizing events occurring at 83 Ma and 42 Ma. Sub-micron gold is commonly associated with altered, decalcified sedimentary rocks as well as silicification and fine-grained pyrite (Kuehn, 1989; Bakken et al., 1989; and J. Cline, pers. comm.). In these alteration and mineralization conditions, the growth of potassium-rich minerals is not favored. As a result, age dating of Carlin-type deposits is restricted to alteration products, such as illite and sericite (Arehart et al., 1993), and potassium-bearing minerals from igneous rocks that pre or postdate gold mineralization (Groff, 1996.).

The timing of gold mineralization in Carlin-type deposits is strongly debated. Argon isotope dating of adularia has provided conclusive ages for Eocene hydrothermal events, particularly at Jerritt Canyon (Hofstra et al., 1999). Conclusive evidence for five gold mineralizing events is found at Getchell (Groff et al., 1997). Dating of clays from Carlin-type deposits (Arehart et al., 1993b) are generally problematic and inconclusive. It is unclear if gold mineralization and alteration require multiple events to form a Carlin-type deposit or if mineralization and alteration occur in a single event. Another issue that remains unresolved is whether the Eocene events documented in northeastern Nevada apply to their western counterparts along the Battle Mountain/Eureka trend. If the Eocene is such an important event, then why is the 83 Ma event at Getchell an important gold contributor?

The sources of gold-bearing fluids in Carlin-type deposits remain enigmatic (Arehart et al., 1993b; Kuehn and Rose, 1995; Cline et al., 1996; and Stenger et al., 1998). Meteoric fluids are regarded as important at Jerritt Canyon (Hofstra et al., 1999). Fluid inclusion microthermometry and O-H stable isotope analyses for the Carlin (Kuehn, 1989) and Cortez (Rye et al., 1974) mines led to the hypothesis that Tertiary volcanism causes circulating meteoric water which then leaches gold from crustal rocks. However, the spatial relationship of Carlin-type gold deposits with porphyry systems near the Bingham Canyon mine, Utah and the Bau district, Malaysia, led Sillitoe and Bonham (1990) to propose a magmatic component in the mineralizing fluids. In a similar theme to the magmatic hypothesis, Seedorf (1991) proposes a metamorphic model where the heat is provided by magmatic bodies. Ilchik and Barton (1996) propose an amagmatic model whereby gold is leached by basinal fluids which then are focused along faults. Since

multiple events are recognized at Getchell (Groff, 1996), it is reasonable to hypothesize multiple fluid sources and that their composition changed in time.

The Pipeline deposit provides an opportunity to examine an economically significant, large tonnage Carlin-type deposit prior to commencement of mining activities. Study of Pipeline is important because the genesis and timing of gold mineralization has not been documented, the deposit is economically significant, is a major gold producer in Nevada, mining was just starting and so the deposit could be observed in a pristine state before mining destroyed key evidence, and considerable drillcore was generated by an aggressive exploration program.

Objective

My objective is to determine the genesis of the Pipeline mineralization. Specifically, my objectives are to understand the gold depositional process , the chemistry of gold-ore solutions, the chemical signatures of dissolved gases that enable fluid source recognition, and to determine the age of mineralization. In so doing, I test the hypothesis that gold mineralization is coeval with decalcification in a Carlin-type deposit.

CHAPTER 2

BACKGROUND

History and Discovery

Mining activities in the Pipeline district (Fig. 2.1) began in 1862 with the discovery of silver in the Cortez and Mill Canyon areas (Foo et al., 1996). The production from these mining activities is uncertain, however, a flourishing community at the time suggests a lucrative operation. The Hilltop deposit was discovered in 1907 with gold hosted in quartz veins and breccia. Mining occurred between 1910 and 1934 (Lisle and Desrochers, 1988). The first mining activities at the Gold Acres deposit (Fig. 2.1) in 1935 produced >500,000 troy oz. of gold (Foo et al., 1996).

Placer Dome U.S., formerly known as American Exploration and Mining Co. (AMEX), began exploration within the district in 1959 and joined forces with Kennecott to form the Cortez Joint Venture (hereafter referred to as the CJV). Placer Dome U.S. controls 60% of the CJV stock and are the operators of the Pipeline mine whereas Kennecott hold the remaining 40%. During the 1960's, the United States Geological Survey (USGS) conducted mapping and sampling programs throughout the area. They reported anomalous gold hosted by oxidized and weathered silty carbonate outcroppings adjacent to the range front (Wells et al., 1969). Drilling by AMEX at the site led to the discovery of the Cortez Gold deposit which has produced 872,870 troy oz. of gold from 1969 to 1973 (Foo et al., 1996). The present unmined gold reserves at Cortez are estimated at 250,000 troy oz..

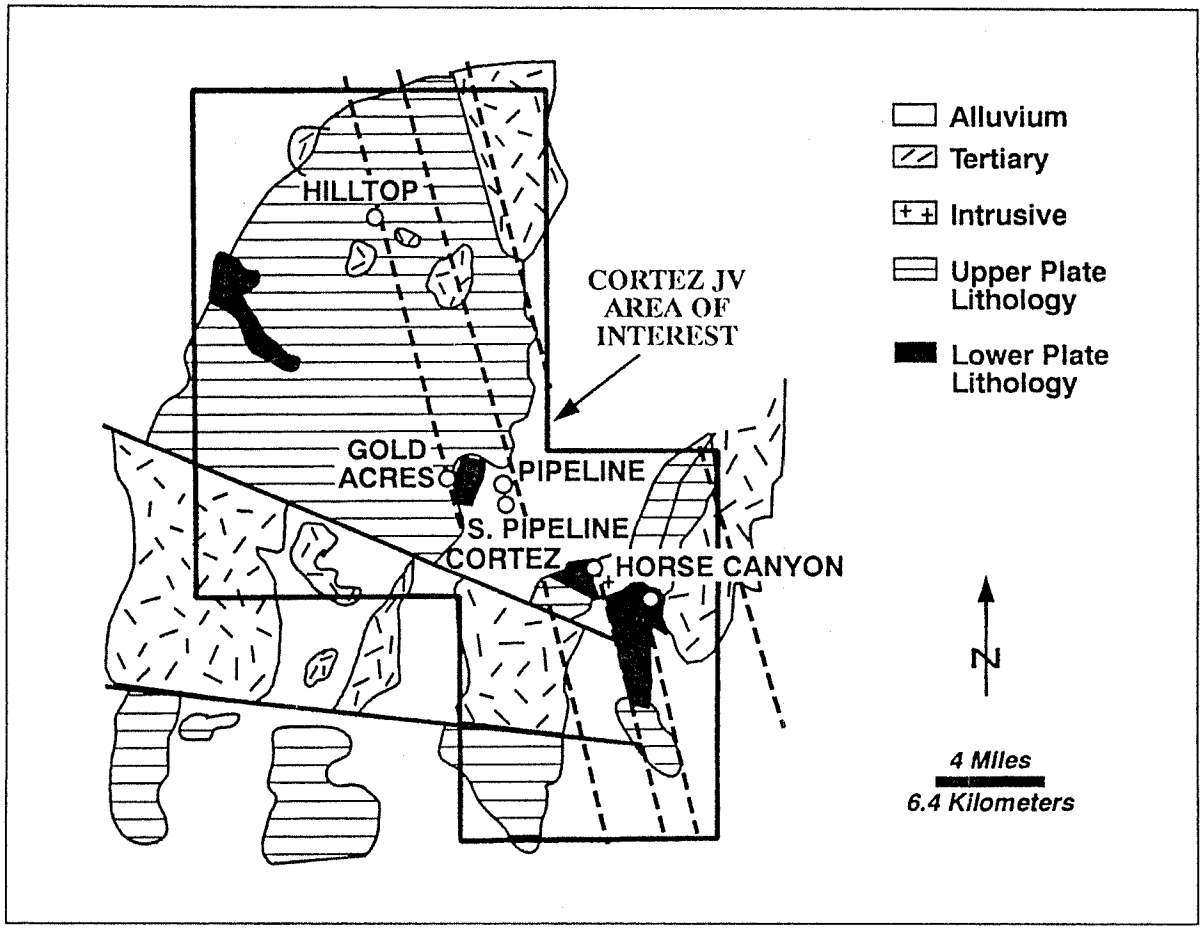

Figure 2.1. Simplified geology of the CJV area of interest. The Pipeline deposit is located along the eastern flank of the Shoshone range within a buried erosional window (Foo et al., 1996).

The Horse Canyon deposit, 6 km southeast of the Cortez Gold Mines mill site, was discovered in 1976. Approximately 385,000 troy oz. of gold were produced from 1983 to 1987 (Foo and Hebert, 1995).

The 1991 discovery of the Pipeline deposit resulted from condemnation drilling for Gold Acres heap leach pads (Foo et al., 1996). Two reverse-circulation drillholes were planned. Both intersected alteration and drillhole 91907 had a 35 m intersection averaging 10.5 g/ton gold (Foo et al., 1996). Pipeline's name refers to a water pipeline that traversed the area supplying water to the Gold Acres operations (R.C. Hays, pers. comm.).

Geological Setting

North Central Nevada Geologic History

During the Mississippian, northeastern Nevada was situated along a stable paleocontinental margin as indicated by regional stratigraphy and isotopic data (Stewart, 1980). A prism shaped, westward-thickening package of sediment was deposited from the outer margins of the paleocontinental shelf into an oceanic basin and facies changes led to a gradation from eastern shelf sediments into western deep basin equivalents (Teal and Jackson, 1997). Subsequent eastward-directed compressional tectonism associated with the Antler orogeny during the Late Devonian through Middle Mississippian resulted in region-scale north-south folding and imbricate thrusting of the western assemblage over the eastern assemblage (Roberts et al., 1958). The region continued to experience three less important, yet similar, compressional tectonic events during the Late Pennsylvanian

through Permian with the Humbolt orogeny, the Early Triassic Sonoma orogeny, and finally the Early Cretaceous Sevier orogeny (Teal and Jackson, 1997). It is unclear whether NNW-trending antiforms are a result of one specific compressional event or formed during more than one of the above mentioned events. Mid-Tertiary extension between 40 and 30 Ma is regarded by Hofstra et al. (1999) as the most important event in terms of gold mineralization in Nevada. "Dilation of faults and fractures during mid-Tertiary northwest-southeast extension may have controlled emplacement of igneous dikes and underlying intrusions, provided connections between deep fluid reservoirs and the meteoric-dominated regime in the upper crust, and served to focus flow of convecting meteoric water" (Hofstra et al., 1999).

Episodic intrusive activity that spans Late Triassic to Late Tertiary time indicates the gold belts of the Great Basin were subjected to high heat flow. There is a close spatial association between many of the Great Basin gold deposits and intrusive rocks of multiple ages. However, the role of igneous rocks in the possible formation of Great Basin gold deposits has remained enigmatic (Cline et al., 1996). In the Ely district evidence suggests that intrusive bodies are the source for gold in Carlin-type deposits (Seedorf, 1991). In other areas of Nevada the relationship is unclear and the timing of gold mineralization relative to intrusive bodies is poorly constrained.

Geology

The stratigraphy of central Nevada is comprised of shelf and deeper marine sediments. Terminology most commonly used in Nevada refers to miogeosynclinal and eugiosynclinal sediments. Thrusting has brought these time equivalent sediments, that

were once spatially separated on the continental shelf, into close proximity. Stratigraphy is therefore described in order of the Lower Plate rocks, also referred to as Eastern Assemblage, followed by the Upper Plate rocks or Western assemblage rocks. The stratigraphy of the region is complicated by facies changes within some units. The lower and upper plate assemblages are discussed separately.

Lower plate rocks: The oldest lower plate unit in Central Nevada is Middle Cambrian Hamburg Dolomite (Gilluly and Masursky, 1965). Gilluly and Gates (1965) describe this unit as being "composed almost wholly of highly broken and irregularly bedded dolomite." Hamburg dolomite is coarsely granular and largely recrystallized. Approximately 150 m thickness is exposed along the Northern Shoshone Range (Gilluly and Gates, 1965). Exposures of the Hamburg at Cortez are metamorphosed to a marble where it is in contact with the Mill Canyon stock (Gilluly and Masursky, 1965).

The Ordovician Eureka Quartzite overlies the Hamburg Dolomite and is a well sorted medium grained quartzite of high purity with accessory silt-sized grains, heavy minerals and pyrite. Corals and cross bedding within the Eureka quartzite suggest a shallow sea depositional environment.

The Hanson Creek Formation conformably overlies the Eureka Quartzite and comprises alternating beds of dark gray and very light gray dolomite with occasional thin limestone beds. The top of the formation contains interbedded chert with a prominent chert capping (for Type section, see Nolan et al., 1956).

Silurian Roberts Mountains Formation (SRM) conformably overlies the Hanson Creek Formation. It comprises thinly bedded to laminated carbonaceous silty limestones

and calcareous siltstones. Microscopically, the formation is about 80% calcite and 20% silt, comprised of 15% quartz, about 5% K-feldspar and minor muscovite flakes. Organic carbon and authigenic pyrite crystals are present. Graded bedding is observed in the thickest beds and fossil hash may be present. Formation thickness is estimated at 200 to 300 m. The Roberts Mountains Formation depositional environment is interpreted to be the transition between the siliceous rocks of the basin facies and the carbonate shelf facies (Gilluly and Masursky, 1965).

Devonian Wenban limestone postdates, and has a gradational boundary with the Roberts Mountains Limestone (Gilluly and Masursky, 1965) and the base of the Wenban is the first bioclastic bed above the thinly bedded SRM. The formation comprises thickly bedded bioclastic limestone with thinly bedded argillaceous limestone. Devonian Wenban differs from the Roberts Mountains Formation in age; bed thickness, which is generally 10 cm to 1 m; and siliceous content (Gilluly and Gates, 1965). Deposition is interpreted to have been within the moderately deep outer shelf environment (Stewart, 1980).

Upper plate rocks: Cambrian age rocks of upper plate are not exposed in the district. The first upper plate rocks are the Ordovician Valmy Formation which comprises a wide variety of rock types including quartzite, chert, greenstone, sandstone, siltstone, shale and very minor limestone.

Overlying the Valmy formation is the Silurian Elder Sandstone, comprised of predominantly fine-grained sandstone and interbedded siltstones. Most of the beds are laminated although some are crossbedded or ripple marked and do not part along the bedding as readily as the Roberts Mountains Formation (Gilluly and Gates, 1965).

The Devonian System overlying the Elder Sandstone comprises the Slaven Chert. Slaven Chert consists predominantly of black chert that has partings of dark carbonaceous shale and thinly bedded sandstone (Gilluly and Masursky, 1965).

Structural setting

Gold mining districts in north-central Nevada are aligned along the Carlin, Battle Mountain, and Getchell trends (Fig. 1.1). The Battle Mountain/Eureka, and Carlin trends were originally recognized by Roberts (1960) to be related to alignment of tectonic windows although the origin of these gold belts is not clear. Roberts proposed that the belts were related to "third order structures of Precambrian age" but that additional work is required to clarify the origin of the belts (Roberts, 1960). The trend also corresponds to a basement gravity gradient, consistent with either a terrane boundary, a strike-slip fault, or a major structure that is Jurassic or older in age (Grauch et al., 1995).

The Pipeline deposit is located along the Battle Mountain/Eureka trend in north-central Nevada, near the eastern flank of the Shoshone Range (Fig. 2.1). The deposit occurs within an erosional window of the Roberts Mountains thrust on the west side of Crescent Valley. Upper plate rocks above the Roberts Mountains thrust comprise allochthonous deep water siliceous sediments and volcanic rocks that have been thrust approximately 80 km during the Late Devonian Antler Orogeny over its time-equivalent, the Silurian Roberts Mountains Formation (Foo et al., 1996). The timing of structural and igneous events within the CJV area of interest is summarized in Table 2.1.

The major structural events that impacted the CJV from Jurassic times to the present are the NNW-trending Cortez fault and the Basin-and-Range extension. A model

Structure or intrusive	Date	Reference
Roberts Mountains Thrust	Late Devonian to Early Mississippian	Roberts et al., 1958
Mill Canyon Stock	151 K-Ar biotite	Guilluly and Masursky, 1965
Gold Acres Stock	149.6±6.9Ma U/Pb zircon	J.K.Mortensen, 2000, unpublished
Gold Acres Stock	104.8±0.02Ma U/Pb zircon	J.K.Mortensen, 2000, unpublished
Gold Acres Stock	98.8±2.0 Ma biotite	Silberman and McKee, 1971
Gold Acres Stock	92.8±1.0 K-Ar altered stock	Silberman and McKee, 1971
Quartz porphyry dike	94.3±1.9 K-Ar sericite	Silberman and McKee, 1971
Cortez dikes	34.5 Ma sericite + biotite	Wells et al., 1971
Caetano volcanics	34.4±1.1 Ma K-Ar biotite	J.D.Obradovich, unpublished
Caetano volcanics	32.6±1.1 Ma K-Ar sanidine	J.D.Obradovich, unpublished
Basin and range extension	11 Ma	McCormack and Hays, 1996

Table 2.1 Tectonic and intrusive dates for the CJV area.

to reconstruct the area is described by McCormack and Hays (1996) and is based on gravity, geologic, magnetic and topographic data. This model incorporates reversal of movement along low-angle detachment faults related to Basin and Range extension around 11 Ma, as well as strike-slip movement along the Cortez and Pipeline faults, connecting the Mill Canyon and Gold Acres stocks (Fig. 2.2).

Pipeline Deposit

Igneous rocks

The Mill Canyon stock has a 1000 m vertical exposure at Mount Tenabo. The stock is dominantly biotite-quartz monzonite but is variable in composition from a quartz diorite to an alaskite (Gilluly and Masursky, 1965). It may evolve through time from the former to the latter. In general the rock is porphyritic with feldspar phenocrysts containing An ranging from 25 to 55%. Biotite commonly has a reddish-brown hue and quartz commonly forms polycrystalline aggregates. Accessory minerals include magnetite, zircon and minor apatite. All are set in a mosaic of perthitic microcline. Sometimes hornblende is present but does not appear to be altered. Biotite is commonly poikilitic, enclosing plagioclase and quartz (Gilluly and Masursky, 1965).

Three dike types are reported within the area and have compositions of quartz porphyry, alaskite (like the stock), and augite syenite (Gilluly and Masursky, 1965). Quartz porphyry dikes are considered to be magmatically allied to the Caetano Tuff (Gilluly and Masursky, 1965). Dikes are mostly N to NNW trending and are controlled by

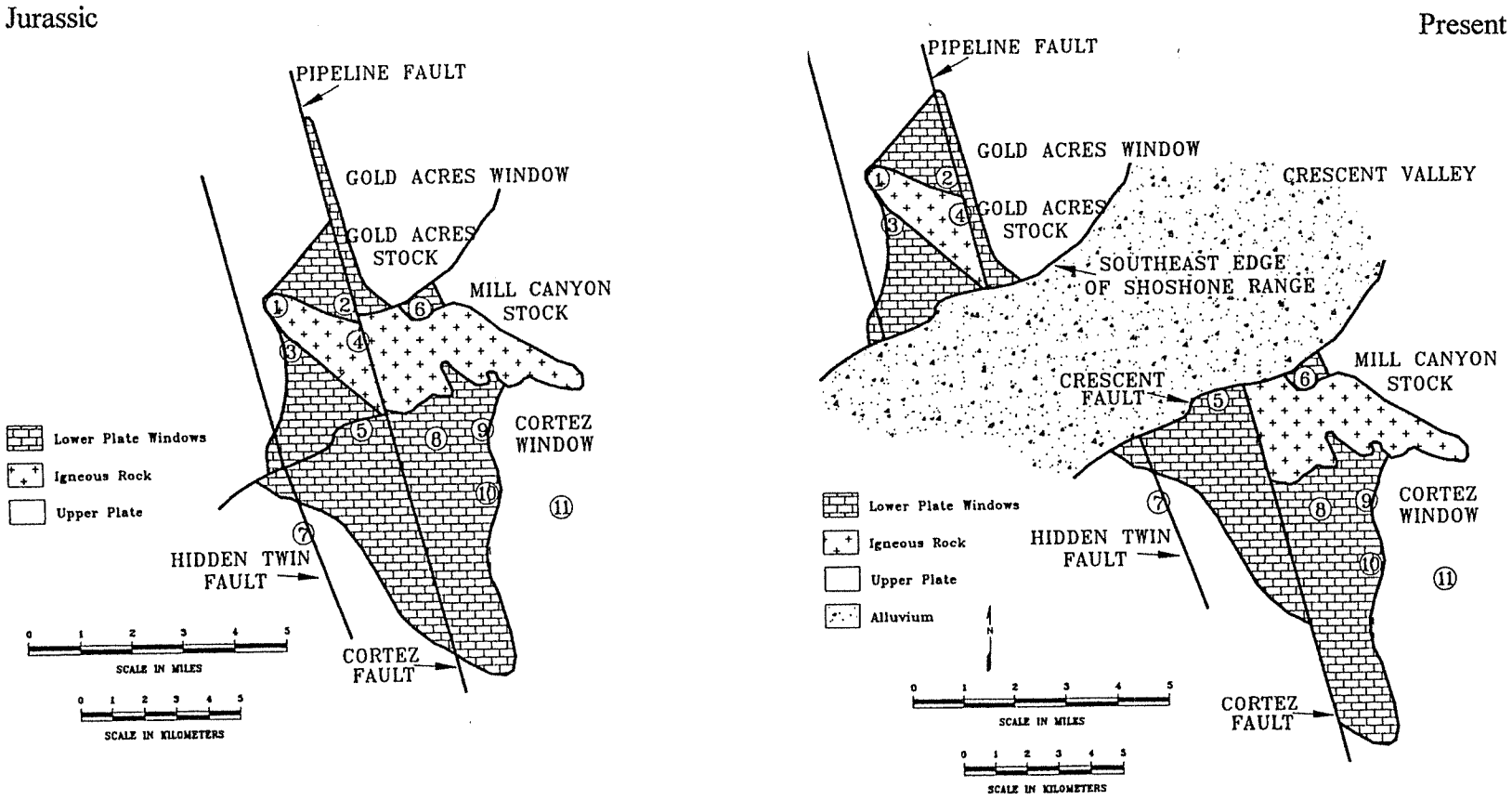

Figure 2.2 Foo et al. (1996) model for reconstruction of the Crescent Valley. The figures show the present (right) and reconstructed (left) positions of faults and intrusive bodies.

parallel faults. In the Cortez pits these dikes also turn parallel to bedding to form sills that were subsequently altered to smectite.

The Caetano Tuff is a body of welded and water-laid tuff with associated conglomerate and sandstone with outcrops starting a few km's south of the Pipeline Mine and continuing south into the Toiyabe Range. The thickness of the Caetano is estimated at 2500 m (Gilluly and Masursky, 1965).

Geology

Pipeline is located near the eastern flank of the Shoshone Range within Lander County, Nevada. The main ore zone, is 150 to 180 m below the surface, varying in thickness from 15 to 105 m, is tabular in shape, and dips at a low angle to the east. This zone extends about 760 m in the northerly direction and about 460 m in the easterly direction (Foo et al., 1996).

Pipeline was a "blind" deposit covered by alluvium and hosted within the Silurian Roberts Mountains Formation (SRM). Unaltered SRM is gray to black silty carbonate, thin to medium-bedded, thinly laminated with normal graded beds of 5 to 12 mm thickness. Carbonaceous content is estimated at 0.03% and the pyrite content is estimated at 0.003 to 0.01%; both are variable. Unaltered rock comprises silt-size particles of calcite (±80%), quartz (±15%), K-feldspar (±5%) and muscovite flakes (<1%) (Gilluly and Masursky, 1965). Roberts Mountains formation within the deposit is invariably altered to some degree. Altered SRM typically comprises 50 to 80% fine-grained to clay-sized quartz, 0 to 40% calcite, 5 to 50% illite, as well as accessory iron-oxides (Foo et al., 1996; and personal observations). Carbon has been removed by oxidation that

extends below the water table and to as much as 300 m below the surface, giving a gray-buff color to the SRM.

The Devonian Wenban limestone (DW) is exposed across the NNW-trending fault on the west side of the pit. It is not economically important because DW has not reacted to hydrothermal fluids like the SRM.

Bedding in the SRM generally dips 15-20° to the east, a product of Basin-and-Range tectonism (Foo et al., 1996). Within the deposit bedding is variable due to shearing, thrusting, and duplex formation. The primary ore controlling structure is a low-angle shear zone that varies from 3 m in thickness on the edge of the deposit to 105 m within the deposit (R.C. Hays, pers. comm.). Within the shear zone the rocks are sheared, deformed and brecciated; individual shear planes commonly exhibit fault drag of the immediately overlying strata. Shear zones are regarded as zones of imbricate thrusting subparallel to and beneath the Roberts Mountains Thrust (Foo et al., 1996).

High-angle faults are well documented by pit mapping and include a NNW-fault that strikes N15W to N20W. The Pipeline fault is the most prominent of these faults and dips 75-85° to the east, is sympathetic to the Cortez trend, and is interpreted to be an offset extension of the Cortez fault (McCormack and Hays, 1996). A N35W subvertical fault is recognized to truncate deep mineralization, but this in turn is truncated by a younger NE-striking, high-angle fault set of which the Fence fault is the most important (Fig. 2.3). Normally conjugate shear planes of the same age develop at about 30° or 60° to each other, however, although the faults are about 60° to each other, the lineations measured for these faults suggest that they are co-active rather than conjugate pairs (C. Tarnocai, pers. comm.). Movement along the NNW faults are reported as normal oblique

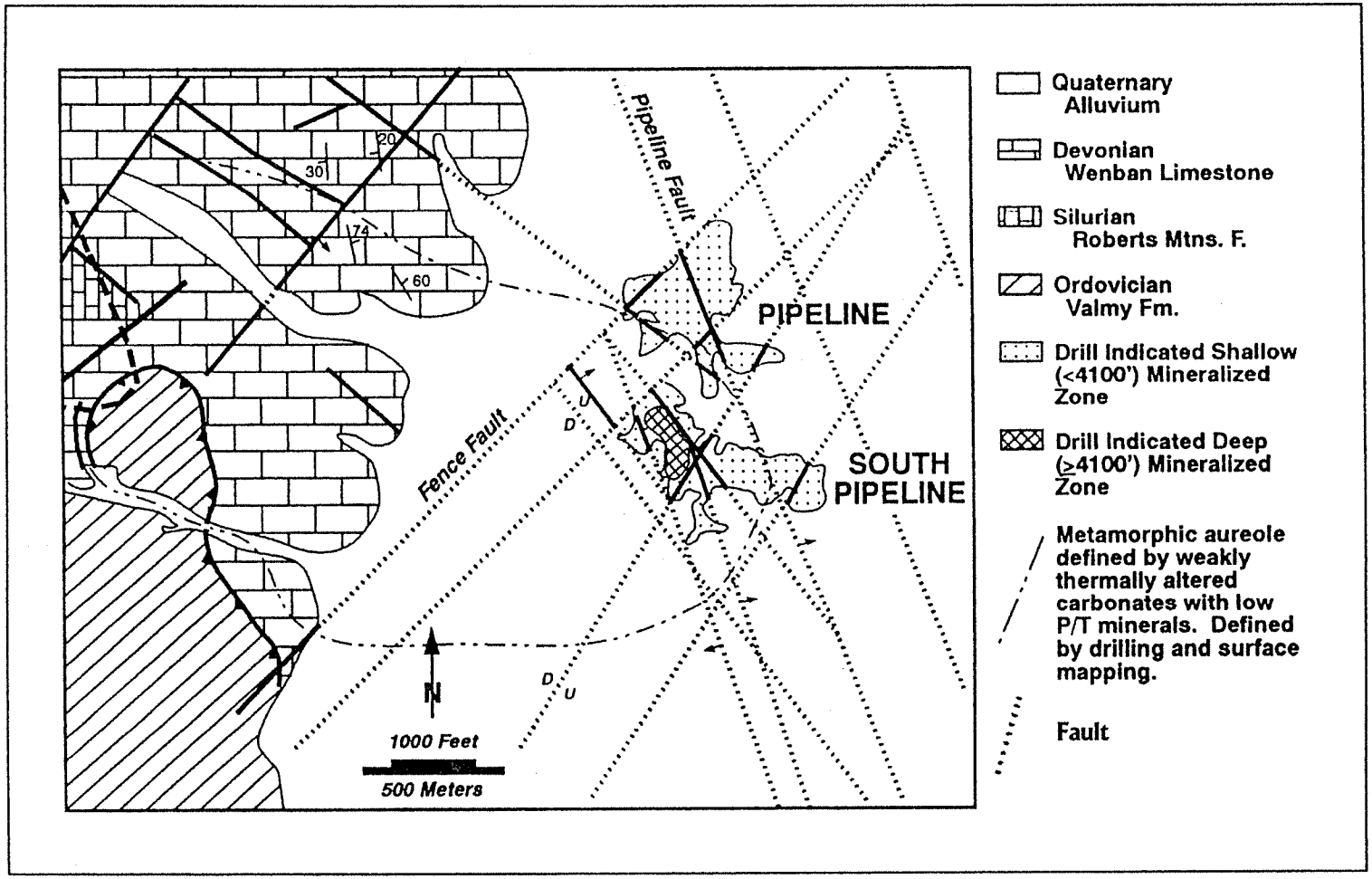

Figure 2.3. Simplified geologic map of the Pipeline and South Pipeline deposit areas showing faulting and outline of gold mineralization (Foo et al., 1996).

right slip whereas the NE faults have some normal movement with significant left slip (Foo et al., 1996). Both the NNW- and NE-trending faults are important ore controls.

Alteration

Alteration types include decalcification, silicification and argillization. Decalcification intensity is measured at the Pipeline mine by the reaction of the rock to 6:1 HCl acid. The amount of decalcification is visually estimated by the intensity of effervescence and by comparing this intensity to descriptions made on SRM of known decalcification intensity. Silicification is also documented within the Pipeline deposit. The silicification intensity is measured by comparing analytically determined intensities of silicification to a rock's response to a steel dental tool. Steel left behind on a drillcore after a steel dental tool has been scraped across the surface has a starting limit of 20% silicification. Argillization refers to the increase in argillic content. Most commonly this is a result of decalcification whereby the removal of calcite increases the bulk concentration of the insoluble components, including clay. The term sericitization refers to the growth of sericite such that new material is added without other components being removed.

Gold Mineralization

According to Foo et al. (1996) gold is not confined to a single alteration type, nor confined to shear zones. However, the most favorable host to gold mineralization occurs within shear zones that are decalcified, sericitized, and oxidized. Microscopically visible gold was reported by Foo et al. (1996) who concluded that "much of the gold occurs as submicroscopic, disseminated grains." Also, gold "was observed in and on silica, in and

on hematite, on pyrite, and in illitic or sericitic matrix material as well as discrete grains in open spaces and on fracture surfaces" (Foo et al., 1996). A link between gold and pyrite is inferred "from limonite and hematite pseudomorphs."

Previous Geochemical Studies

Fluid inclusion studies

Microthermometry: Studies of Carlin-type gold deposits incorporating fluid inclusion microthermometry include Radtke et al. (1980), Rye (1985), Kuehn and Rose (1995), Lamb (1995), Groff (1996), Kamali (1996), Cline et al. (1996), Simon (1999) and Cline et al. (2000). A common observation from many of the studies are homogenization temperatures ranging from 180° to 220°C. Most studies also report salinities of 1 to 7 eq. wt. % NaCl, however, some higher salinities near 20 eq. wt. % NaCl are reported at Purple Vein and Post/Betze (Lamb, 1995), at Lone Tree (Kamali, 1996), Getchell and Twin Creeks for main ore stage (Groff, 1996), and Turquoise Ridge (Cline et al., 2000). Hypersaline inclusions with daughter halite crystals are reported from Lone Tree (Kamali, 1996), Getchell and Twin Creeks (Groff, 1996).

Fluid inclusion microthermometry and interpretations at the Carlin mine by Radtke et al. (1980) suggest that gold mineralization and boiling during late-stage mineralization occurred at depths of <1 km. Recognition of CO_2-bearing inclusions at Jerritt Canyon (Hofstra et al., 1988) and Carlin (Kuehn, 1989) has led to the conclusion that gold mineralization occurred at depths of 1-5 km. Depth estimates at Getchell are a minimum of 1.2 km (Cline at al., 2000).

Gases: Known studies of Carlin-type deposits that involve fluid inclusion gas analysis are restricted to Bendrick (1989), Graney et al. (1991), Groff (1996), Kamali (1996) and Cline et al. (2000). Work by Bendrick (1989) added to the microthermometry of Kuehn (1989) and shows that volatile contents decrease in time whereas H_2S increases. The focus of both Groff (1996) and Kamali (1996) was to recognize fluid sources. In addition, Groff (1996) is able to show that gold mineralization is associated with fluids that have a high methane content and labeled the fluid as "organic-rich". Fluid source categorization based on He-N_2-Ar ternary discrimination diagrams identified magmatic, crustal, and meteoric components to fluids trapped within different minerals as fluid inclusions. In contrast, J. Cline (pers. comm.) uses gas analysis to test for differences between fluid inclusion populations rather than applying source recognition.

Radiometric dating within the CJV

Within the CJV, multiple dates are reported that span the Jurassic, Cretaceous and Tertiary (Table 2.1). A K/Ar age of 151 Ma is reported for fresh biotite for the Mill Canyon stock (Guilluly and Masursky, 1965). Despite the Crescent Valley reconstruction model of McCormack and Hays (1996) placing the Mill Canyon stock and Gold Acres stock in juxtaposition, only one date for the Gold Acres stock is within error of the 151 Ma date. Dating of zircon by U/Pb gives two ages, i.e., 149.6±6.9 Ma and 104.8±0.02 Ma (J.K. Mortensen, unpublished data). The sample submitted for dating was a composite from drillcuttings (R.C. Hays, pers. comm.) and therefore the existence of two discrete intrusive bodies should be considered. Biotite from the Gold Acres stock yields an age of 98.8±2.0 Ma and altered stock gives a K-Ar age of 92.8±1.0 Ma (Silberman and

McKee, 1971). Sericite from a quartz porphyry dike in the area gives a K-Ar date of 94.3±1.9 Ma (Silberman and McKee, 1971). The variance of ages for the Gold Acres stock presumably reflects thermal events and/or alteration that impacted the stock.

A hiatus separates Cretaceous igneous activity from Tertiary volcanism. Dikes at Cortez are dated as 34.5 Ma (sericite + biotite; Wells et al., 1971) and biotite from the Caetano volcanics to the south gives a K-Ar age of 34.4±1.1 Ma and sanidine gives 32.6±1.1 Ma (J.D. Obradovich, unpublished).

CHAPTER 3

ANALYTICAL METHODS

Field studies

More than 110 samples were collected and described during 3 field seasons (Appendix A). During this time, I logged several thousand feet of drillcore and had access to the open pit. Most vein material sampled originated from drillcore and was intact, whereas the material from the open pit was broken and displaced by blasting. Access to previously drilled core was granted, however, key drillcore intersecting ore zones in the original drilling program had been removed for metallurgical testing. Additional core was removed during skeletonization and only limited core remains.

Fluid Inclusions

I studied fluid inclusions by geothermometry, gas geochemistry, and bulk analysis of major ions. The basic assumptions are (1) the chemistry of fluid inclusions have not been modified since trapping occurred, and (2) the P-T-V conditions measured reflect the conditions at the time of trapping.

A Linkham TH600 heating-freezing stage and temperature controller is used to accomplish microthermometry. Doubly polished, 100-300 μm thick, rock sections for analysis were prepared by Spectrum Petrographics. Sections are removed from the microscope-slide backing by soaking in acetone prior to analysis. The instrument calibration is checked daily by use of a H_2O standard, and each week the calibration is checked using at least three standards. Data obtained between shifts in the calibration are

discarded. The analytical error in melting point determinations near 0°C is 0.1°C, whereas error in Th measurements in the temperature range of 200°C is 0.5°C.

The analysis of volatile species is done in vacuum using by the CFS (crush-fast scan) method (Norman et al., 1996). Samples are cleaned with potassium hydroxide, then distilled water, and then oven dried at about 60°C (at 100°C He is rapidly lost). Samples are then placed in crushers and evacuated while heating to about 60°C until a pressure $<10^{-7}$ Torr (10^{-8} mPascals) is attained. The analysis is performed by means of a Balzers QME125 quadrupole mass spectrometer operating in a fast-scan, peak-hopping mode. The CFS method involves opening inclusions by a swift crush in the vacuum chamber housing the mass spectrometer. Volatiles released are quickly removed by the vacuum pumping system within two seconds. Meanwhile, the pulse of inclusion volatiles is recorded by operating the quadruple in a fast scan mode with measurements every 150 to 200 msec. The mass peak areas are used to determine the concentration of each species using predetermined sensitivity factors and a peak-stripping algorithm designed by D.I. Norman. Opening a 10 to 20 μm inclusion, or group of smaller inclusions of equivalent volume, provides the ideal amount of volatiles for CFS analysis. Opening a 40 μm inclusion swamps the vacuum system and the system crashes. Five to twenty sequential crushes are made on about a 200 mg sample with the expectation that some crushes will be failures by opening too many or too few inclusions. Species routinely recorded are H_2, He, CH_4, H_2O, N_2, O_2, H_2S, Ar, C_3H_8, CO_2 and SO_2. In addition several crushes are done on a sample while monitoring CH_4, CO_2, C2-4 alkenes and alkanes, benzene and toluene. Ammonia is rarely detected because of the interference of secondary water peaks at m/e = 17 and 16; He at concentrations below 10 ppm is interfered with by the tail on the

H_2 peak; and CO peaks fall on those of CO_2, N_2, CH_4 and C2-7 organic species. Small amounts of admixed air is commonly detected during CFS measurements, which is estimated from the amount of O_2 measured. The source of air contamination is most likely air trapped on grain boundaries and micro-cracks. The concentrations of inclusion N_2, Ar and CO_2 can be corrected for air contamination assuming all O_2 measured represents admixed air. In general, analyses indicating admixed air are discarded because of the uncertainties in making an air correction. Air contamination is eliminated by prolonged baking. However, in the interest of expediency, and to minimize H_2 and He diffusion from inclusions, prolonged baking of samples is not done.

The instrument is calibrated with commercial gas mixtures, artificial inclusions filled with gas mixtures, and an in-house fluid inclusion standard. The gas water ratio of the standard inclusions (HF1) is known to about 0.1% by Penfield-tube analysis, thus allowing water calibration with an error less than 0.2%. Measurement precision is <5% for major gaseous species, and ~10% for the minor species.

Crush-leach analysis is done in order to measure ratios of fluid inclusion anions and cations. Methods used are described in detail in Norman et al. (1987) and Shepherd and Rankin (1998). In excess of 10 gm of quartz is placed in nitric acid to destroy any calcite. Samples are boiled in nitric acid to clean the surfaces. The nitric acid is decanted and the samples washed several times in deionized water. Samples then are boiled several times in ultra-pure, reverse osmosis, deionized water prior to placing them in electrolytic cells. The water in the electrolytic cells is changed daily until the current does not increase in a days operation from freed ions. Dried samples are placed in clean stainless steel tubes and crushed in a hydraulic press to open fluid inclusions. The powder produced is placed on a

sieve and a reverse osmosis leach bath removes the fluid inclusion salts. The leachate is reduced by evaporation in Teflon containers, then analyzed at the New Mexico Bureau of Mines and Mineral Resources by atomic absorption and ion chromatographic methods.

Argon Geochronology

The $^{40}Ar/^{39}Ar$ technique is an extension of the K-Ar technique. The sample must be irradiated with fast neutrons in a reactor thus converting some ^{39}K into ^{39}Ar. Unlike the K-Ar technique which requires the K concentration to be known precisely, ratios between Ar isotopes are analyzed. Also, the sample is incrementally heated *in vacuo* and the argon released during each heating step is analyzed separately to produce an apparent age spectrum. Another common form of display is the isochron plot. The $^{40}Ar/^{39}Ar$ technique is a relative method and requires the use of monitors of known age to determine a sample age. These monitors are used to determine the neutron flux parameter referred to as J. The $^{40}Ar/^{39}Ar$ technique also requires the measurement of ^{37}Ar and ^{36}Ar to determine interfering argon isotopes produced from K and Ca.

The K-bearing minerals found in the Pipeline deposit are very fine-grained illite and hydrothermal sericite. Some geologists regard illite and sericite to be the same mineral, however, sericite has slightly more potassium. Dating such fine-grained clay minerals may be problematic in that the recoil distance for ^{39}Ar radiation is comparable to the grain-size of illite. A brief explanation of recoil is given below to enable a better understanding of this potential problem in dating fine-grained materials.

Samples analyzed by the $^{40}Ar/^{39}Ar$ technique require irradiation in nuclear reactors. By absorbing a neutron, ^{39}K emits a proton and transmutes to $^{39}Ar_K$ and this reaction is expressed as ^{39}K (n,p) ^{39}Ar. The produced $^{39}Ar_K$, recoils with an energy of 177 keV (Onstott et al., 1995) displacing the $^{39}Ar_K$ from its original site by about 800 Å (McDougall and Harrison, 1988). Recoil may invalidate the assumption "that the $^{39}Ar_K$ produced during irradiation is distributed in a manner similar to the ^{40}K in a sample" (McDougall and Harrison, 1988). It is possible for $^{39}Ar_K$ to recoil out of the clay grain from where it was produced and embed itself in an adjacent grain. The effect of recoil can produce discordant age spectra in clay minerals, exsolved minerals, and altered minerals.

Clay Mineralogy

I selected seventeen samples for XRD analysis; i.e. two fault gouges and other samples which were primarily collected along section line 59200 where drillcore exists and different alteration types occur. This allows a comparison between alteration type relative to clay data.

Clay samples for XRD analysis are individually ground with deionized water in a mortar and pestle, and the resulting fluid is poured into a beaker. Deionized water is added to dilute the clay-water mixture and the sample is allowed to settle under gravity. After about 4 hours, a pipette is used to extract about 4 ml of solution from near the surface in order to capture a <4 μm fraction. The solution is allowed to coat one side of a glass slide and then left to evaporate. The clays in suspension are concentrated on the surface of the slide producing a basal section of the clay for XRD analysis. Clay-coated slides are placed in a Rigaku XRD spectrometer using monochromatic X-rays (using

curved crystals) from a Cu tube set to 40 kV and 25 mA. The goniometer is set to 0.03 °2θ per second. After the spectra are collected, X-ray patterns are produced using the WINJADE computer program.

Randomly orientated slides for polytype identification are produced by collecting about 1-2 gm of <4 μm clay material. Clay is allowed to dry and is then broken up and sprinkled onto a glass slide that is coated with petroleum jelly to act as an adhesive. The slide is immediately analyzed using the XRD spectrometer by the same method as previously described except that the dwell is increased about 5 to 10 times. Random mounts are used to examine the polytypes of illite where distinctive spectral lines enable the identification of each polytype (Table 3.1).

1M			$2M_1$		
	d (Å)	Intensity		*d* (Å)	Intensity
1	4.35	1½	1	4.29	1
2	4.12	1	2	4.09	1
3	3.66	5	3	3.88	3
4	3.07	5	4	3.72	3
5	2.93	1	5	3.49	3
6	2.69	2	6	3.20	3
			7	2.98	3½
			8	2.86	3
			9	2.79	2½

$2M_2$			3T		
	d (Å)	Intensity		*d* (Å)	Intensity
1	4.34	2	1	3.87	3½
2	3.90	3	2	3.60	3
3	3.68	4	3	3.11	3
4	3.52	4	4	2.88	4
5	3.21	4	5	2.68	1
6	3.07	4			
7	2.87	2			
8	2.81	2			

Table 3.1. Diagnostic XRD lines for 1M, $2M_1$, $2M_2$ and 3T polytypes of illite (Bailey, 1980).

CHAPTER 4

OBSERVATIONS AND RESULTS

Mine Geology

Alteration

Observations of the alteration styles confirmed those reported by Foo et al. (1996) and described by mine geologists. Several additional observations were made, particularly a paragenetic sequence of vein types.

Decalcification: Removal of calcite is commonly documented in drillcore at Pipeline. Total decalcification occurs in shear zones, however, a progressive decrease in the intensity of decalcification is documented perpendicular to the shear zones. Fresh, undecalcified SRM (Fig. 4.1) has a well-developed lamination that is emphasized by dusty pyrite. In the shear zones where decalcification is total, the lamination spacing decreases and laminations are enhanced by hematite (Fig. 4.2).

Decalcification has affected most of the deposit with shear zones exhibiting the strongest intensity. Locally, there is no reaction of the SRM to acid. Totally decalcified SRM is confined to the shear zones. Totally decalcified rock exhibits high porosity such that water dripped onto the rock surface is immediately absorbed and hand samples are discernibly less dense.

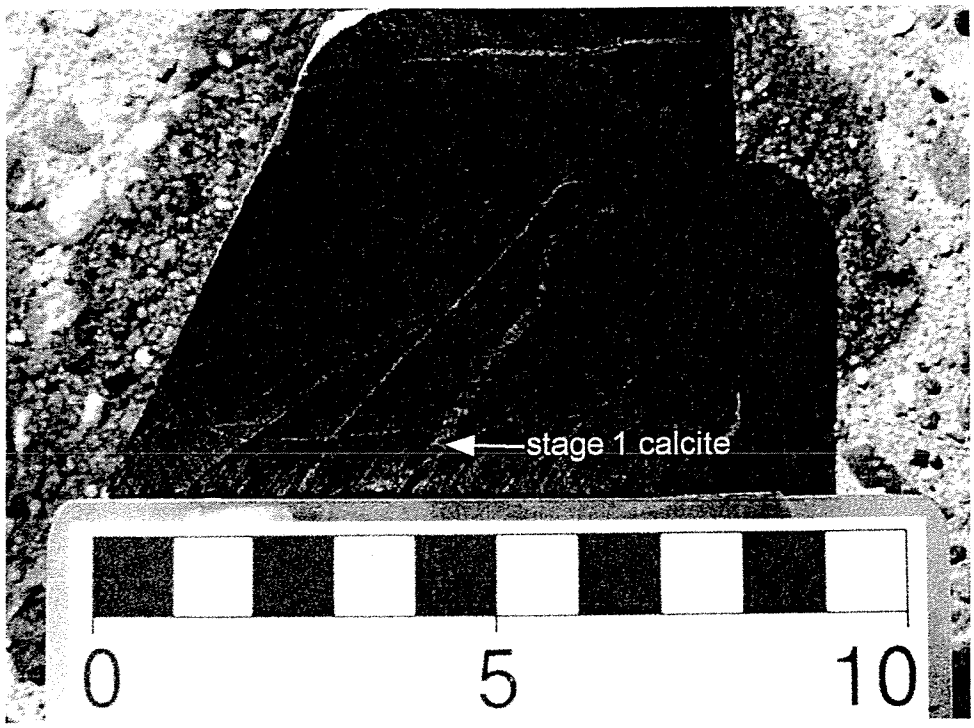

Figure 4.1 Photograph of fresh, carbonaceous SRM crosscut by a stage 1 dark calcite vein. The scale is in cm.

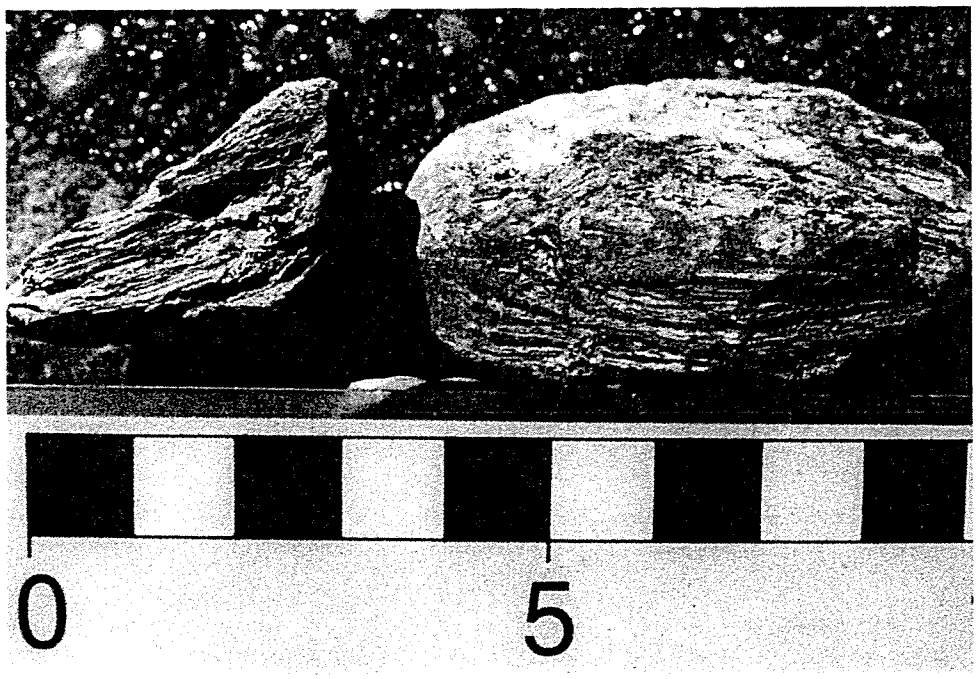

Figure 4.2 Photograph of totally decalcified, argillized and oxidized SRM. The mm-scale lamination is emphasized by hematite. The scale is in cm.

Silicification: Silicification occurs pervasively and as halos to quartz veins. Observations of thin sections and polished surfaces show that the filling of open space by quartz is the most common occurrence, whereas replacement by silica is less common. An example of silicification controlled by a fracture is shown in Figure 4.3 and emphasizes how silica penetrates the host rock to a depth of a few mm. Although the term "silicification" is commonly used by Nevada. At Pipeline, petrographic analysis indicated that silica was deposited as quartz rather than chalcedony; therefore, the term "ore quartz" is used to represent silicification.

Sulfidation: Pyrite-bearing haloes of up to 10 mm wide occur next to quartz carbonate veins below the deposit (Fig. 4.4). Sulfidation is not as extensive as decalcification and in Figure 4.3 the light brown decalcified halo extends beyond the dark specks that represent pseudomorph replacement of pyrite by Fe-oxides. Evidence for sulfidation within the ore zones is obscured by subsequent pseudomorph replacement to Fe-oxides.

Oxidation: Oxidation is divided into two types, iron-oxide development and carbon removal from dark carbonaceous SRM to produce a light yellow-brown colored rock. The entire ore zone is oxidized and the oxidation halo can extend to >300 m. Observations of drillcore confirm that Fe-oxide replacement of sulfides occurs slightly ahead of carbon removal.

Two iron-oxides are present, hematite and goethite. Red-colored hematite is spatially associated with shear zones and immediately above the shear zones where

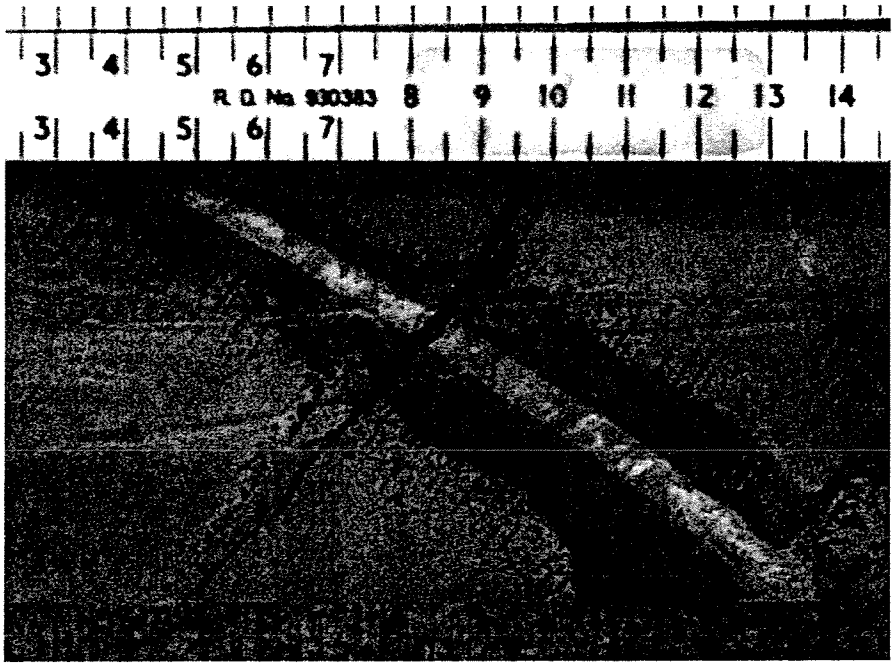

Figure 4.3 Photograph showing silicification of wallrock adjacent to a quartz vein. Note the decalcified halo (light brown) extends beyond the silicified halo as well as the halo of Fe-oxide that forms as pseudomorph replacement after pyrite. The scale is in cm.

Figure 4.4 Photograph of a stage 3 quartz-calcite vein in fresh SRM. Note the sulfidized halo that extends beyond the vein for several mm's. The scale is in cm.

decalcification is prominent. Hematite concentration is based on color intensity comparisons to known standards. Red laminations bearing fine-grained hematite are most common (Fig. 4.2), however, it also occurs in argillized zones where moderate to total decalcification has occurred. Goethite, is orange-brown and occurs as laminations and replacements. An interesting observation is that laminated goethite forms a zone above hematite. Interlaminated goethite and hematite is common. Goethite also occurs as pseudomorph replacements after pyrite.

Argillization: In most of the deposit the intensity of argillization is low but locally in shear zones argillization is so intense that rock has the consistency of putty. Argillization commonly is a residual accumulation of clay released by decarbonization of SRM and the rock has a light brown color. A second argillization type is the growth of illite to produce a distinctive off-white clay that occurs locally within the pit (Fig. 4.5). This off-white clay is commonly associated with good gold values and is thought to be the same material as the hydrothermal sericite that occupies quartz-calcite veins.

Several differences are recognizable between unaltered SRM several meters above the shear zones and the strongly altered ore horizon. Unaltered SRM is gray, calcareous, and has bedding planes of 3 to 15 mm separation containing syngenetic pyrite (Fig. 4.1). In contrast, altered SRM is off-white, totally decalcified, and has a ~1 mm bedding lamination separation emphasized by brick-red colored fine-grained hematite laminae (Fig. 4.2).

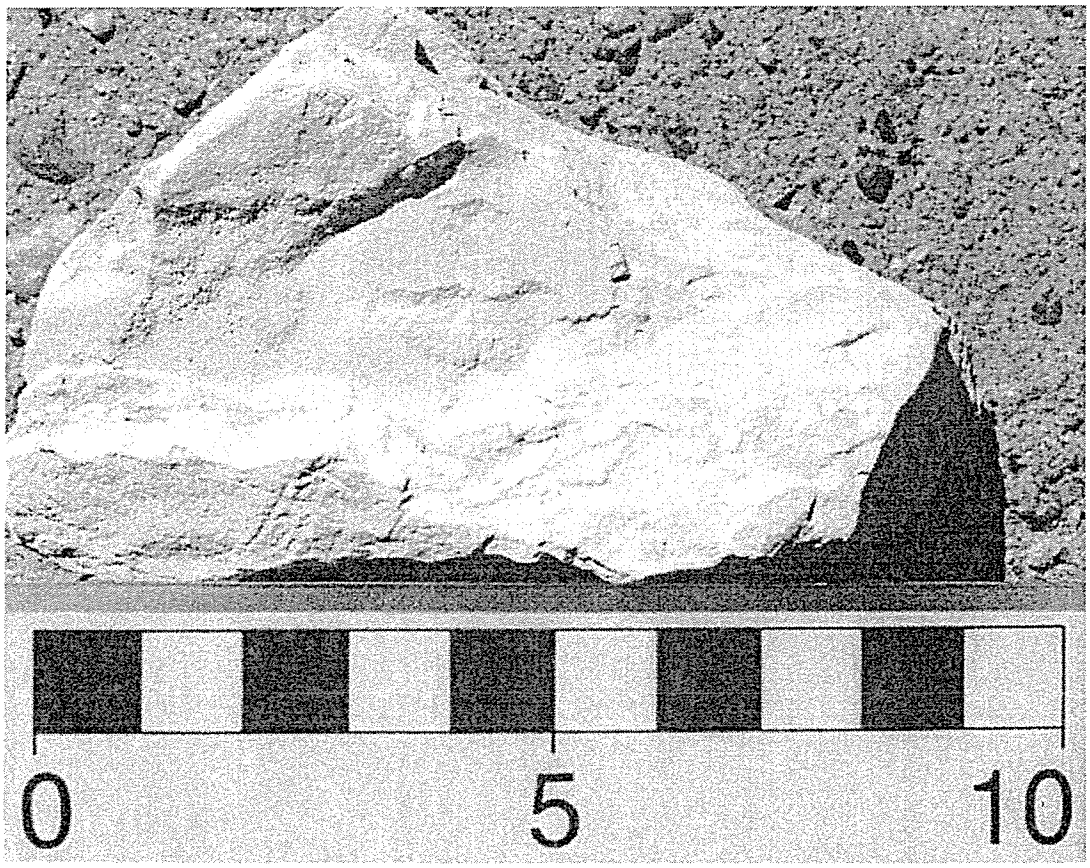

Figure 4.5 Strongly argillized, totally decalcified ore. This sample assayed 21 ppm gold. The scale is in cm.

Veins

Four vein types are recognized. Dark petroliferous calcite veins (VC-1) can be found above and below ore and shear zones. The distribution of these veins is unaffected by shear zones. Fluid inclusion sections show the dark coloration to be micron-sized carbonaceous matter.

A second vein set forms a stockwork of white undeformed-calcite veins (VC-2) and comprises up to 30% of the SRM that spatially underlies the shear zones but do not occur within the shear zones. The veins are anastamosing with a subvertical preferred orientation and crosscut styolites.

Quartz-sericite-calcite veins (VQ-3) occur beneath the deposit, whereas none are observed above the ore. A similarity is drawn between these veins and the vein systems that develop beneath massive sulfide deposits because they appear to be feeders to the tabular ore body. These quartz-sericite-calcite veins have a paragenetic sequence of sericite and quartz followed by the growth of euhedral quartz into open space, followed by calcite. The wallrock immediately adjacent to the vein has a silicified and sulfidized halo that is commonly 5 mm wide but does not exceed 10 mm. In two fresh SRM samples, scattered pyrite grains up to 1 mm occur (Fig. 4.4). Silicification is more difficult to observe in hand specimens than in thin section. In oxidized samples, the pyrite is replaced by Fe-oxides whereas the silicification is emphasized by a color contrast (Fig. 4.3). In oxidized samples, a decalcified halo that manifests itself as a paler shade between the grey-colored silicification and the slightly darker undecalcified rock (Fig. 4.3) is observed. The decalcified halo is larger than the silicified halo.

Vuggy calcite veins (VC-5) crosscut gold mineralization and are more abundant preipheral to the deposit than within it. Calcite crystals are commonly light brown in color and the habits observed include dogtooth spar, cockscomb and stubby drusey crystals. Most crystals are clear to translucent.

Gold Mineralization

Access to gold values obtained from logged core was limited. Section lines compiled by the author and mine geologists show a correlation between shear zones and gold values. All samples collected were examined with a binocular microscope for gold. Visible gold is rare, and polished ore thin sections fail to reveal gold, despite assays confirming good gold values. Two polished resin-impregnated samples of ore zones did not exhibit visible gold using a reflected-light microscope despite neutron activation confirming ppm levels of gold. The highest gold values of 21 ppm assayed by neutron activation came from a sample (NB-87) that is off white in color, totally decalcified, strongly sericitized, unsilicified, porous and hosted within a shear zone (Fig. 4.5).

One blasthole drilled in the Pipeline pit during 1998, yielded >2 oz per ton gold. Visible gold grains as large as 1 mm were recovered from the panned concentrate. These grains are the only case of visible gold observed by the author. In this concentrate, gold is intimately associated with Fe-oxide. Using the electron microprobe in SEM mode, crystalline gold with hopper-like surface textures is revealed (Fig. 4.6); this is inconsistent with the sub-micron sized gold generally associated with Carlin mineralization. The gold purity of these grains is high with microprobe analyses giving only up to 0.5% Ag, the remainder being gold. Some visible gold grains are associated with Fe-oxide (Fig. 4.7)

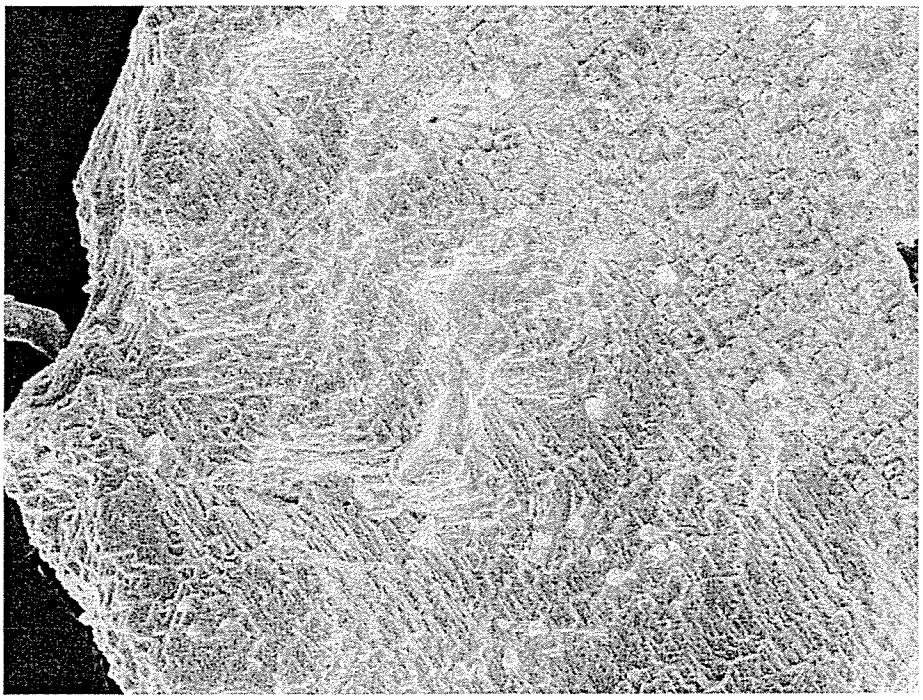

Figure 4.6 Electron microprobe image in SEM mode of a gold grain showing a hopper-like crystal growth pattern. The field of view is about 200 μm.

Figure 4.7 Electron microprobe image in SEM mode of a gold grain showing a close association with Fe-oxides (granular material). The field of view is about 100 μm.

although there is no information suggesting the relative timing of either phase. The images do, however, confirm the intimate association of gold and a Fe-oxide.

Fire assays from drillcore that hosted stage 1, 2 or 5 veins showed no gold values. In contrast, the sulfidized selvages of four stage 3 veins assayed by fire assay all confirmed gold values that varied from 0.3 to 1.0 ppm. The gold content of the wall rocks beyond the pyrite selvages is below detection.

Paragenetic Relationships

The paragenetic relationships at the Pipeline mine were determined from observations made in core, observations within the pit, regional crosscutting relationships and dating of K-bearing minerals. The mineral paragenesis is summarized in Table 4.1.

Crosscutting veins

The earliest mineralization (stage 1) are dark petroliferous calcite veins (Fig. 4.1). Stage 1 veins are, crosscut by all other veins, and are commonly deformed and crosscut by shear planes.

The dark-colored stage 1 veins are cut by VC-2 stage 2 veins (Fig. 4.8). These veins are not observed as fragments within the ore zones and their absence is attributed either to decalcification in the ore zones or the locations of drillholes.

Stage 3 quartz-sericite-calcite veins crosscut stage 1 and 2 veins. In one locality a stage 3 vein is truncated by a shear plane but this plane could be related to Basin-and-Range extension.

Time	Pre-Antler Orogeny	Antler Orogeny	Cretaceous		Pre Basin and Range	Basin and Range
Event	Stage 1	Stage 2	Stage 3	Stage 4	Stage 5	
Dark calcite						
White calcite						
Sericite						
Quartz						
Pyrite						
Gold						
Orpiment			?			
Vuggy calcite						
Alteration						
Silicification						
Decalcification						
Argillization						
Oxidation						
Shearing						
Brecciation						?

Table 4.1 Paragenetic sequence as recognized by veining, alteration and shearing at the Pipeline mine.

Figure 4.8 Photograph of stage 2 white calcite stockwork, crosscut by stage 6 calcite vein. The width of the drillcore is approximately 6 cm.

Oxidation postdates stage 3. Fresh pyrite is associated with stage 3 veins at depths >300 m whereas in the oxidized zone, pyrite is replaced by Fe-oxides.

Crosscutting both stage 3 veins and the oxidized ore body are vuggy, calcite veins (stage 5). Dipping layers of calcareous sediment (Fig. 4.9) have the same inclination as surrounding sediments. Since the local 10 to 20° dip is indicated to be the result of Basin-and-Range faulting, the sediment must predate this event. These veins must also postdate stage 4 oxidation. It is expected that acid fluids produced by the oxidation of pyrite would destroy calcite in stage 5 veins.

Ore deposit

Paragenetic relationships within the Pipeline deposit are poorly constrained. Unlike several other Carlin-type deposits (Cortez, Meikle), no intrusive bodies occur within Pipeline and so dating crosscutting igneous rocks is precluded. The Crescent Valley reconstruction model (McCormack and Hays, 1996) indicates that NNW-trending faulting postdates the Mill Canyon stock. The location of Pipeline on these NNW-trending lineaments suggests that the deposit must have formed after 152 Ma, the age of the Mill Canyon stock. NE-trending faults are observed and economic gold mineralization is abruptly terminated on the Fence fault. Poor gold values occur on the NW side of the Fence fault. This may indicate that major gold mineralization predated the NE-trending fabric but that minor remobilization could postdate the Fence fault.

No examples of early calcite veins are seen crosscutting the deposit. The only vein identified that crosscuts the deposit is stage 5 calcite. Ore zones within the deposit are

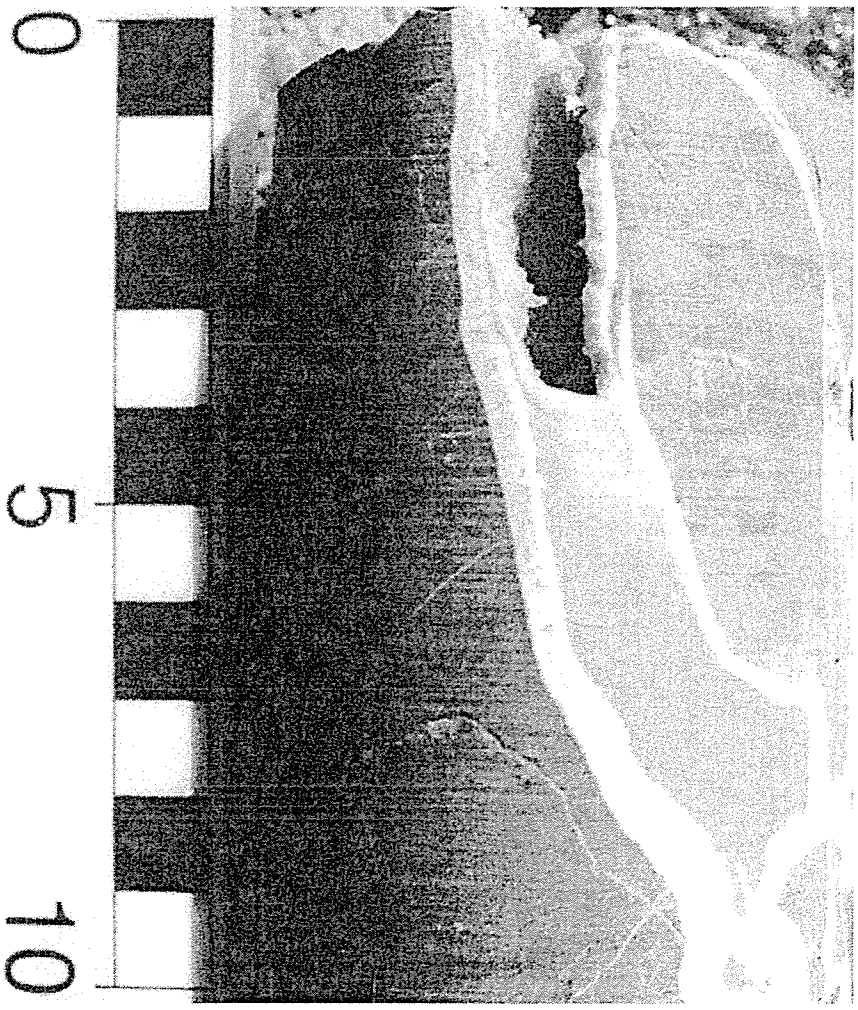

Figure 4.9 Photograph of a stage 4 vein showing the laminated calcareous sediment. The scale is in cm.

generally located along shear zones sympathetic to and underlying the Roberts Mountains thrust and must therefore postdate the Roberts Mountains thrust.

Ore zones are decalcified, gold-bearing, and exhibit local sericitization and silicification (ore quartz). A halo of oxidation extends beyond the ore zones and within this halo, Fe-oxides replace all sulfide minerals.

The link between gold mineralization in the deposit and the stage 3 veins below the deposit is made as follows. Only stage 3 veins have gold-bearing selvages. Sericite associated with stage 3 and in the ore zone illite give similar dates; this will be discussed later in the argon geochronology section.

Ore zones are currently represented by residual material after decalcification, that have up to 1 % hematite and gold is closely associated with the Fe-oxide. Oxidation of pyrite to form hematite is a potential decalcification mechanism in that acid is produced by the oxidation of pyrite. However, the ≤1 % hematite content of decalcified rock implies that insufficient acid could be produced during oxidation to account for removing >80 % of the rock volume by pyrite oxidation alone. Two decalcification events must have occurred at Pipeline. Oxidation of pyrite provides a sulfur source and therefore the oxidation event is coeval with the sporadic occurrence of barite peripheral to the deposit.

Fluid Inclusions

Microthermometry

Twenty-five fluid inclusion sections were studied. Microthermometry results are reported in Appendix B. The convention used to classify Pipeline fluid inclusions is based on the number of phases and the composition of these phases (Table 4.2).

Primary inclusions hosted in quartz are abundant, 5 to 20 μm in size, invariably elongated, and irregular in shape. Clusters of inclusions form zones that mimic the crystal habit of quartz (Fig. 4.10). Secondary inclusions occur either individually or as trails of

Inclusion Type	Description:
Type 1a (Fig. 4.11)	Two phase liquid and vapor inclusion that is liquid-dominated (aqueous) with a vapor bubble that is smaller than the aqueous phase. The inclusion may or may not exhibit clathrate melting behavior.
Type 1b (Fig. 4.12)	Three phase, liquid-dominated inclusion that has a vapor bubble that is smaller than the aqueous phase and minor liquid CO_2 at 10°C. The inclusion exhibits clathrate melting.
Type 2 (Fig. 4.13)	Three phase aqueous, CO_2-dominated inclusions that at 10°C have a small rim of aqueous fluid and >50% by wt. of liquid and gaseous mixture of CO_2 and other gaseous species.

Table 4.2 Fluid inclusion classification as recognized at Pipeline.

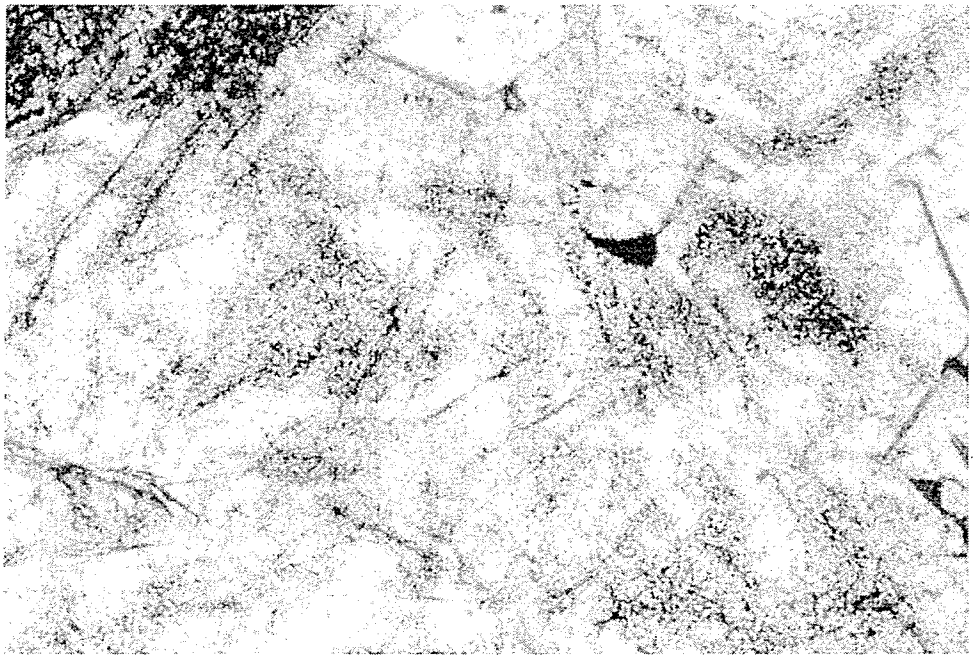

Figure 4.10 Stage 3 quartz grain (sample NB-99) showing primary, zoned fluid inclusions which mimic the crystal shape. The field of view is about 1200 μm.

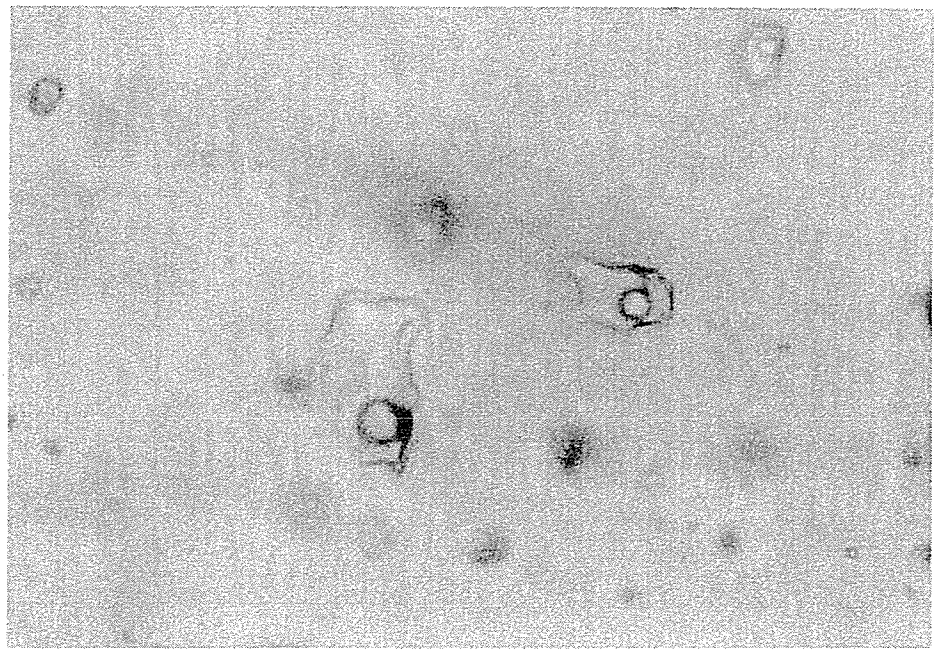

Figure 4.11 Type 1a fluid inclusions (stage 3 quartz; sample NB-33) comprising a dominant aqueous phase and a minor vapor phase. No carbonic phase is visible. The field of view is about 120 μm.

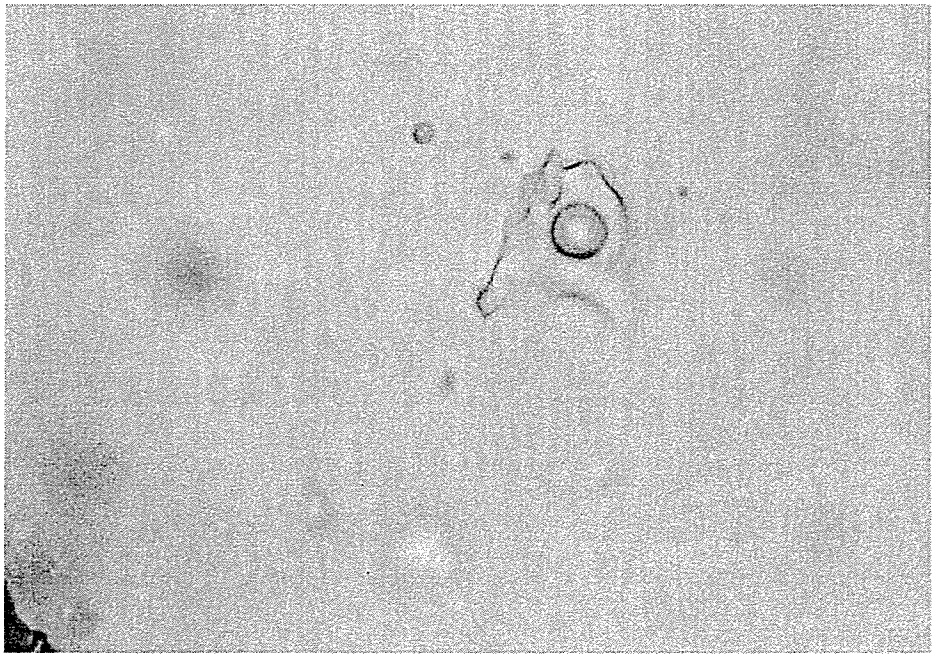

Figure 4.12 Type 1b fluid inclusion hosted in stage 3 quartz (sample NB-107). The inclusion comprises a major aqueous phase and a minor bubble. The bubble shows a vapor phase in the center, rimmed by liquid CO_2. The field of view is about 120 μm.

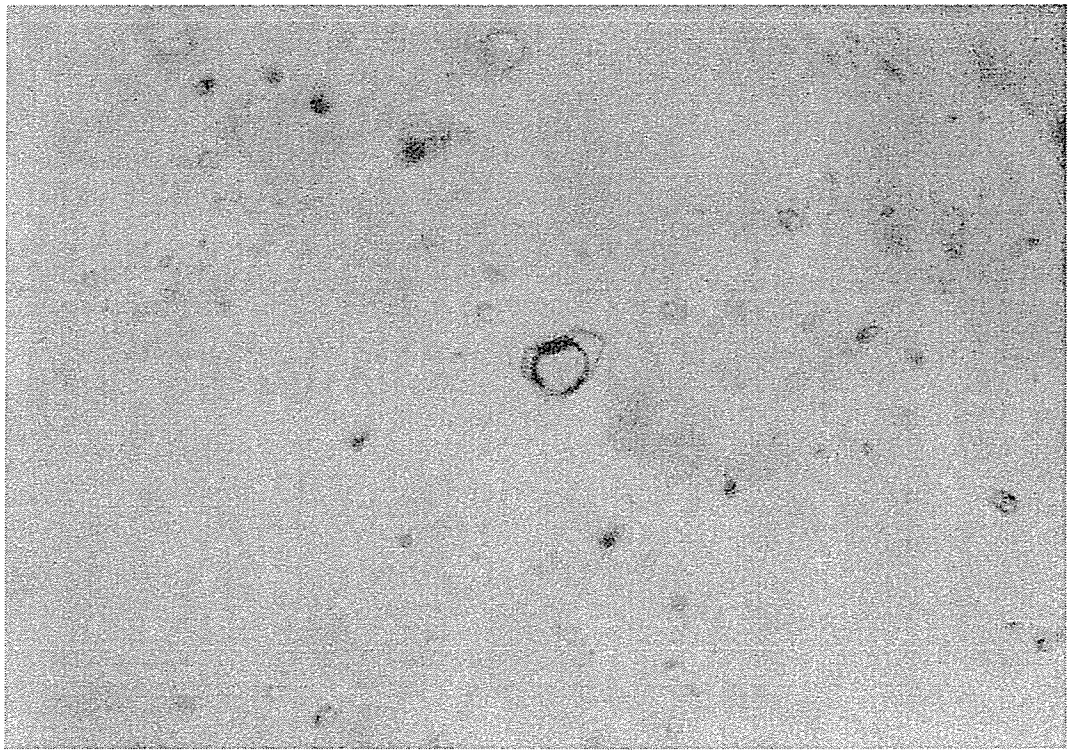

Figure 4.13 Type 2 fluid inclusion hosted in stage 3 quartz (sample NB-104). The inclusion comprises a dominant carbonic phase and a minor aqueous phase. The carbonic phase homogenizes to a liquid. The field of view is about 100 μm.

weakly orientated inclusions of 8 to 15 μm.

Inclusions hosted in calcite are commonly submicron in size, however, sparse visible inclusions of up to 8 μm occur. These visible inclusions are invariably rectangular.

Type 1a inclusions are aqueous-dominated with a vapor bubble generally exceeding 10% by volume (Fig. 4.11). On heating, the aqueous phase expands at the expense of the vapor phase until the inclusion homogenizes to a liquid at which point the bubble disappears. Upon freezing, ice forms at the expense of liquid and during subsequent thawing, the salinity of the inclusion in eq. wt. % NaCl is determined from the melting depression of ice below 0°C. Unlike the gentle melting of ice in contact with brine, clathrate melting occurs very rapidly and the disintegration of the solid phase occurs almost instantaneously. Final melting occurs above 0°C for inclusions that exhibit clathrate melting behavior. Inclusions are heated at a ramp rate of 2°C/min between -20° and 0°C to help stabilize the clathrate.

Type 1b inclusions are aqueous dominated, but at 10 °C annular rings of liquid CO_2 are visible (Fig. 4.12). The liquid CO_2 and vapor bubble may homogenize to a liquid or a vapor. All Type 1b inclusions exhibit clathrate melting behavior. Total homogenization is always to an aqueous phase.

Type 1 inclusions appear to have a broad range of CO_2. Those inclusions with very little CO_2 exhibit ice melting behavior. As the CO_2 content increases the melting behavior changes to clathrate melting and with more CO_2, visible rings of liquid CO_2 occur. The characteristics defining Type 1 inclusions reflect end member compositions of which an entire spectrum of compositions are present.

Type 2 inclusions are sparse and have a small aqueous phase (generally 10% by volume, perhaps none visible) and the remainder comprises a CO_2-rich phase that homogenizes to a liquid between 10° and 31°C (Fig. 4.13). Type 2 inclusions homogenize around 300°C from a major supercritical CO_2 phase and a minor aqueous phase, to a carbonic phase. On freezing, the CO_2 phase forms solid CO_2 between -90° and -100°C. This solid phase melts between -57° and -60°C. All Type 2 inclusions show clathrate melting behavior of the aqueous phase. Often it is impossible to discern if Type 2 inclusions are primary or secondary, however, in one case four Type 2 inclusions occurred in a line suggesting that they are secondary.

Stage 1 inclusions: Only one inclusion section out of four has visible aqueous inclusions. Black calcite has primary and secondary, 5 to 10 μm, Type 1a inclusions with about 98% fill. Submicron carbonaceous material is observed under the microscope and possibly represent polymerized hydrocarbons that were once hosted within fluid inclusions. Homogenization temperature (Th) measurements vary from 142° to 152°C. Melting temperature measurements (Tm) are bimodal. Ice melting temperatures (Tm_{ice}) are -0.8 ±0.4°C; inclusions exhibiting clathrate melting have Tm_{cl} from +1° to +23.2°C. The salinities of inclusions with Tm between -0.4° and -1.2°C calculated range from 0.7 to 2.2 eq. wt. % NaCl. Owing to clathrate melting behavoir in hydrocarbon-rich inclusions, the salinity cannot be accurately determined. Fluid-inclusion salinity can be estimated from clathrate melting, provided the gaseous species are known. Black calcite gas analyses presented below shows considerable analysis to analysis variation of the clathrate

forming species CO_2, CH_4, and C_3H_8, therefore estimating inclusion salinity from the clathrate melting temperatures is not possible. However, clathrate melting temperatures above 10.7°C indicate the presence of methane, and clathrate melting temperatures above 16°C suggest inclusions contain mixtures of CH_4 with heavier hydrocarbon species (Katz et al., 1959).

Stage 2 inclusions: The one fluid inclusion section examined was host to abundant fluid inclusions. All VC-2 fluid inclusions are primary, Type 2, 8 to 15 μm in size, and comprise about equal proportions by volume of water and a CO_2-rich phase. Homogenization of CO_2-liquid and vapor (Th_{CO2}) to liquid occurs between +23.2° and +25.5°C. These measurements correspond to a CO_2 density range of 0.72 to 0.75. Decrepitation of inclusions start at 200°C; all the inclusions decrepitated by 276°C before Th_{TOTAL} was reached. Measurement of Tm_{cl} varies from +9.6° to +11.5°C. The Tm_{cl} measured could result from additions of methane, which is confirmed by gas analysis, or attributed to either clathrate metastability or high pressure (Katz et al., 1959). The stability of CO_2 clathrate is extended to higher temperatures as the partial pressure of CO_2 increases (R. Bakker, pers. comm.). Fluid inclusion salinity of about 0.8 eq. wt. % NaCl is estimated assuming CO_2-clathrate melting.

Stage 3 inclusions: From ten stage 3 inclusion sections, a subset of six sections which were not contaminated by secondary inclusion trails were selected. Thermometric analyses of vein quartz and ore quartz analyses show similar results, therefore are discussed together. Quartz is host to primary Type 1a, 1b, and sparse Type 2 inclusions

of 2 to 20 mm in size (Fig. 4.10). Type 1 inclusion Th measurements range from 179° to 265°C (Fig. 4.14) and Tm measurements range from -26.0° to +10.1°C (Fig. 4.15). A general observation is that Th values of Type 1b are higher than Type 1a inclusions. Calculated inclusion salinities cluster in a large group with 5 to 10 eq. wt. % NaCl with some extraneous values as high as 25 eq. wt. % NaCl (Fig. 4.16). Samples that have salinities near 25 eq. wt. % NaCl exhibit eutectic melting of salt-hydrate to brine at temperatures of -21.1° to - 26.0°C. Assuming that the potassium contribution can be added to the Na budget, then the Ca/Na ratio of the inclusion is determined by the transition temperature of hydrohalite to ice (see Shepherd et al., 1985, p. 103). The range of calculated Ca/Na ratios for these very saline inclusions is 0.8:1 to 1.4:1.

Some Type 1a inclusions exhibit clathrate melting behavior. Liquid CO_2 is not observed in these inclusions (Fig. 4.11), however, this does not preclude that small annular rings of liquid CO_2 are present which could not be seen in the small-size inclusions. Measurements of sample NB99 zoned quartz crystals show a change in fluid chemistry with time. Fluid inclusions in the core have Tm_{ice} (ice melting temperature) values in the region of -5°C. Toward the outside of the same crystal, fluid inclusions exhibit clathrate melting behavior and Tm_{cl} (clathrate melting temperature) about +7°C (Fig. 4.17). The calculated salinities from Tm_{ice} and Tm_{cl} measurements are about 7 eq. wt. % NaCl.

In Type 1b inclusions liquid-CO_2 and vapor homogenize to liquid (Fig. 4.12), and Tm_{CO2} ranges from +13° to +23°C. A general increase in Th values are observed for Type 1b inclusions in comparison to Type 1a. The highest Type1 inclusion Th of 265°C was measured on a Type 1b inclusion.

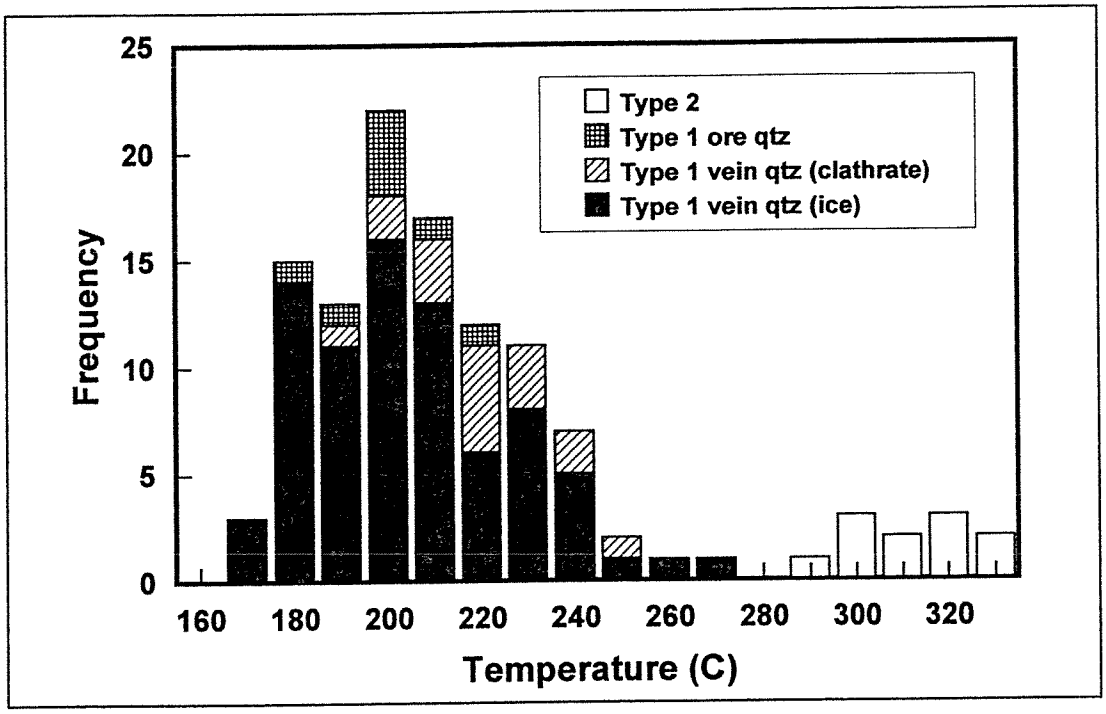

Figure 4.14 Histogram of Th's measured for all inclusions hosted in stage 3 quartz. Note that Type 2 inclusions have higher Th measurements than Type 1.

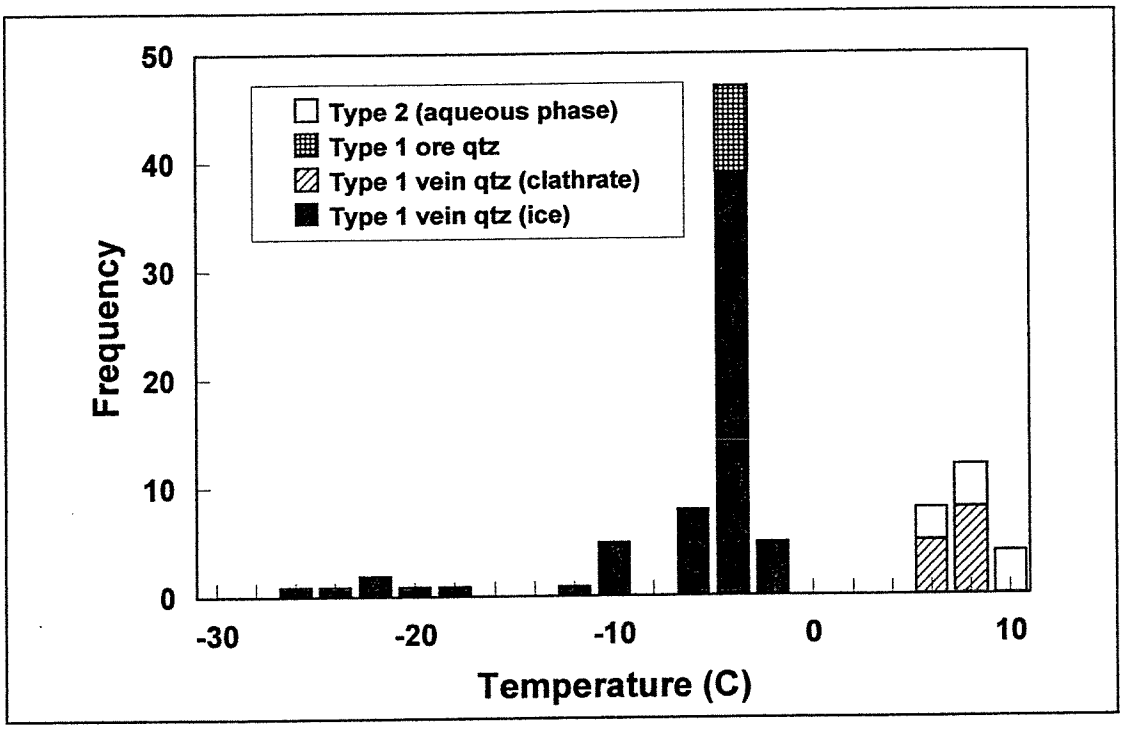

Figure 4.15 Histogram of Tm values measured for all inclusions hosted in stage 3 quartz.

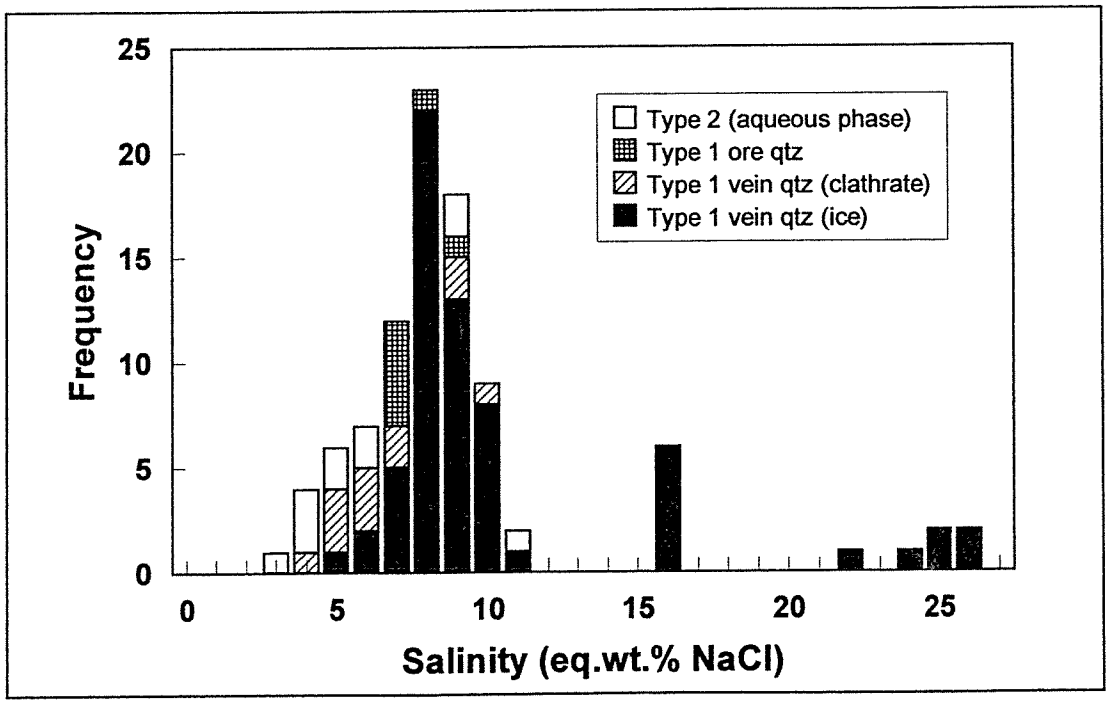

Figure 4.16 Histogram of salinity determined for all inclusions hosted in stage 3 quartz.

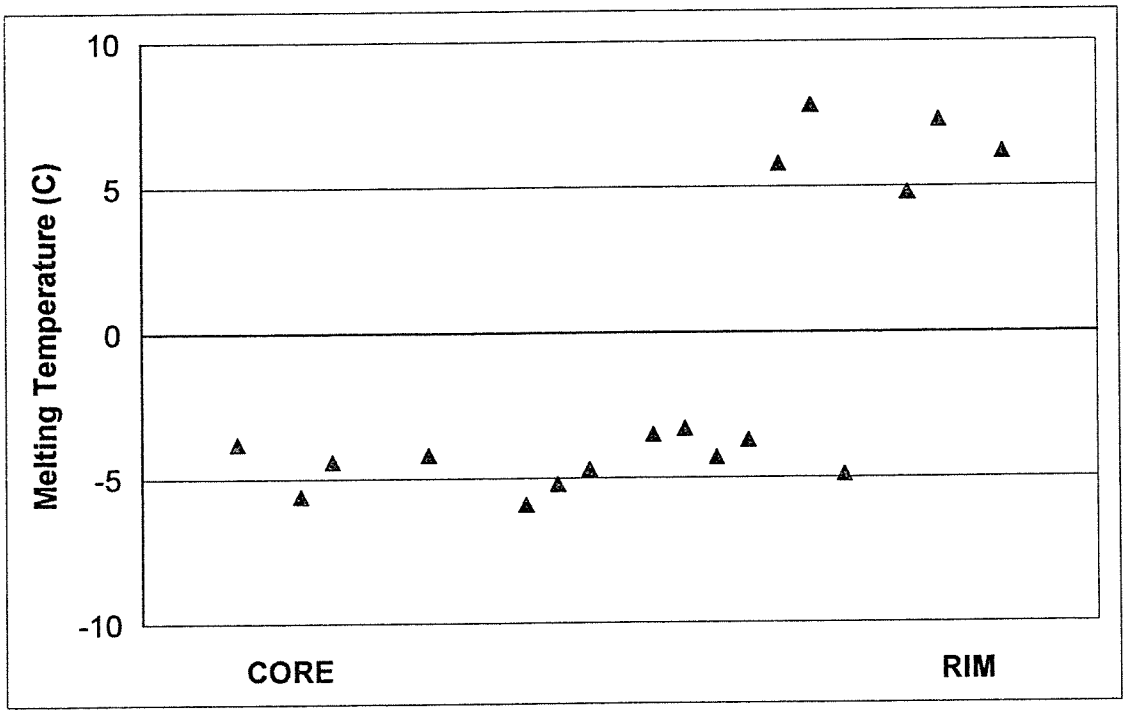

Figure 4.17 Distribution of Tm values for sample NB-99 (stage 3 quartz) showing ice melting behavior within the crystal core and clathrate melting at the rims.

Type 2 inclusions are sparsely distributed, are secondary and vary from 3 to 20 μm in size (Fig. 4.13). The aqueous phase of Type 2 inclusions exhibits clathrate melting (Fig. 4.15). Type 2 inclusion Th values vary from 295° to 323°C (Fig. 4.14). However, measurements are few because Type 2 inclusions readily decrepitate at temperatures >250°C. The inner non-aqueous liquid in Type 2 inclusions melts at about -59° to -58°C and corresponds to 9-12 mol. % CH_4 in the carbonic phase (Shepherd and Rankin, 1985). The inner liquid and vapor homogenize to liquid at +13° to +23°C. These measurements correspond to a CO_2 density range of 0.76 to 0.85. Calculated brine salinity ranges from 5 to 6 eq. wt. % NaCl, and the calculated salinity of the inclusion fluid as a whole is about 0.5 eq.wt. % NaCl.

Calcite exhibits primary fluid inclusions that commonly occur in zones (Fig. 4.18). Calcite-hosted fluid inclusions are generally submicron (Fig. 4.19) but some as large as 8 μm provide practical geothermometry measurements. Secondary inclusions are not observed. Calcite Tm_{ice} measurements range from -1.8° to -2.0°C and Th values range from 219° to 235°C. Calculated salinities are 3.0 to 3.3 eq. wt. % NaCl.

A single quartz-orpiment vein was recovered from a NNW-trending fracture within the Pipeline pit that shows some differences from the stage 3 quartz below the ore zones. This is possibly a stage 3 vein and it is therefore mentioned together with stage 3. The quartz is host to primary and pseudosecondary Type 1a and 1b fluid inclusions. These inclusions exhibit clathrate melting behavior; Tm_{cl} measurements range from +6.8° to +7.9°C. The Tm_{CO2} values for Type 1b inclusions range from -60.2° to -60.7°C and Th_{CO2} was measured from 21° to 27°C as homogenization proceeds to a liquid. Type 1a inclusion Th varies from 192.9° to 233.1°C. Type 1b Th values range from 303.3° to

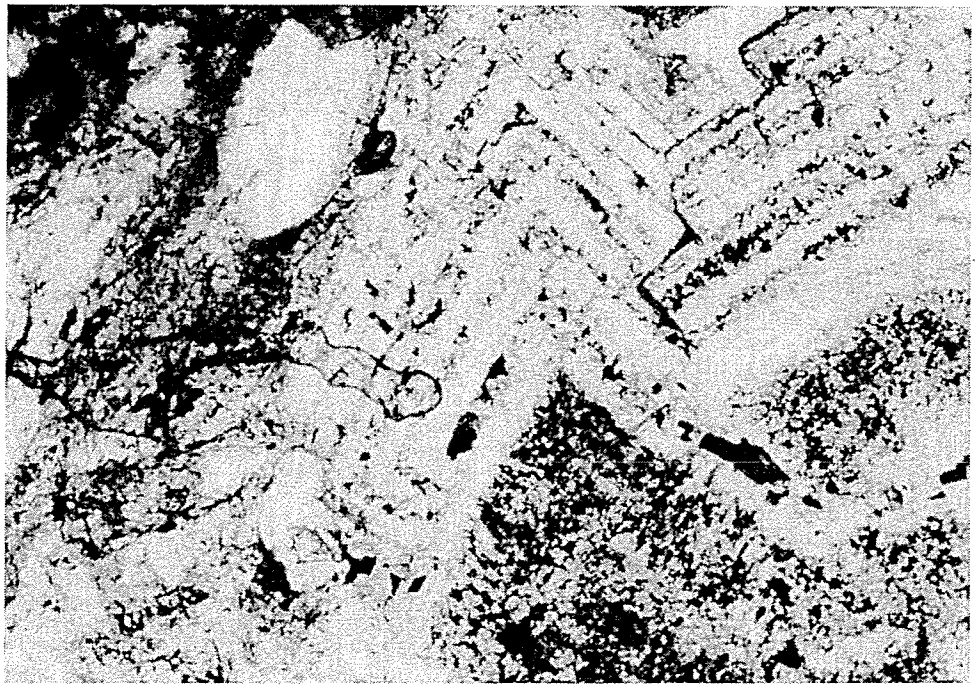

Figure 4.18 Primary, zoned fluid inclusions hosted in stage 3 calcite. The field of view is about 1200 μm.

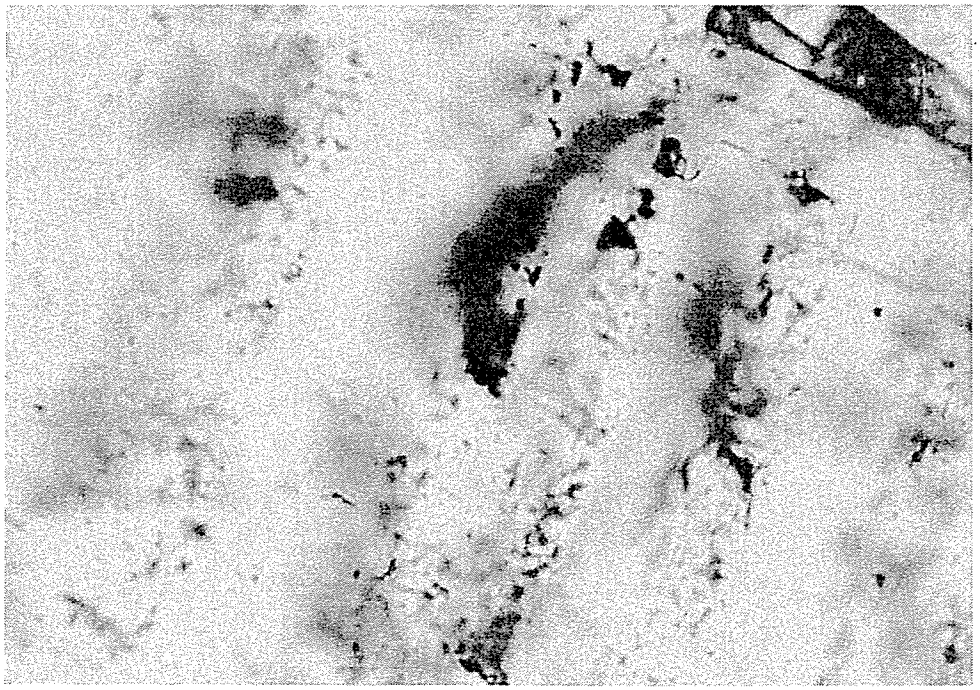

Figure 4.19 Primary, submicron, Type 1 fluid inclusions hosted in stage 3 calcite. The field of view is about 100 μm.

312.8°C. Estimated inclusion salinities, assuming CO_2 clathrate is observed, range from 5.15 to 6.88 eq. wt. % NaCl. Estimated inclusion CH_4/CO_2 ratios from the CO_2 melting point (Shephard et al., 1985) range from 0.31 to 0.34.

Gas Chemistry

The individual gas analyses from the quadrupole mass spectrometer are given in Appendix C. Forty-four samples (calcite = 21, quartz = 21, pyrite = 1, barite = 1) were analyzed yielding 531 analyses of the major volatile species and 118 analyses of the organic species. Table 4.3 gives representative analyses of each mineral analyzed.

Stage 1 and stage 2 calcite: Gaseous species comprise 2.27 to 6.43 mol.% of volatiles in VC-1 calcite and 50.88 to 70.05 % in VC-2 calcite. These ratios are in line with observations made on inclusion liquid to vapor relationships. On a CO_2/CH_4-N_2/Ar diagram (Fig 4.20; template from Norman et al., 1998), VC-1 inclusions show a range in composition from those with N_2/Ar <100 and CO_2 >CH_4 to inclusions that have N_2/Ar >100 and CH_4 >CO_2. In contrast all VC-2 analyses indicate similar CO_2/CH_4 ratios and a small range in N_2/Ar ratios (Fig. 4.20).

Stage 3 sericite-quartz-calcite: Quartz inclusion analyses show gaseous species ranging from 0.54 to 13.21 mol. %. The H_2S content is highly variable ranging from 0.00001 to 0.03 mol. % and CO_2 ranges from 0.22 to 11.3 mol. %.

Vein	VC-1	VC-2	VQ3	VC3	VC-4
Mineral	calcite	calcite	quartz	calcite	calcite
H2	0.718	0.095	0.085	0	0
He	0.0019	0.0065	0.00059	0.00019	0.0016
CH4	2.05	0.48	1.04	0.11	0.063
H2O	95.24	35.6	93.1	99.3	99.7
N2	0.197	0.36	0.19	0.031	0.14
O2	0.0106	0	0	0	0.025
H2S	0.00012	0.0027	0.013	0.0003	0.00022
Ar	0.00047	0.0028	0.00036	0.00033	0.0021
C3H8	0.01707	0.19	0.012	0.00104	0.00041
CO2	1.76	63.3	5.55	0.58	0.041
SO2	0.00014	0.0002	0.00004	0.00001	0.00004
CO2	95.8		84.4	91.2	
CH4	3.78		15.0	8.3	
C2H4	0.076		0.024	0.020	
C2H6	0.096		0.26	0.126	
C3H6	0.089		0.084	0.093	
C3H8	0.13		0.18	0.187	
C4H8	0.00007		0.011	0.0024	
C4H10	0.0015		0.004	0.0070	
C5H10	0		0	0	
C6H6	0.00001		0.00054	0.0021	
C7H8	0		0.00021	0.00046	

Table 4.3 Typical gas analysis for the sampled vein sets. The upper group are the traditional geothermal species that are analyzed. The lower group represent the carbon-bearing species, normalized to 100%.

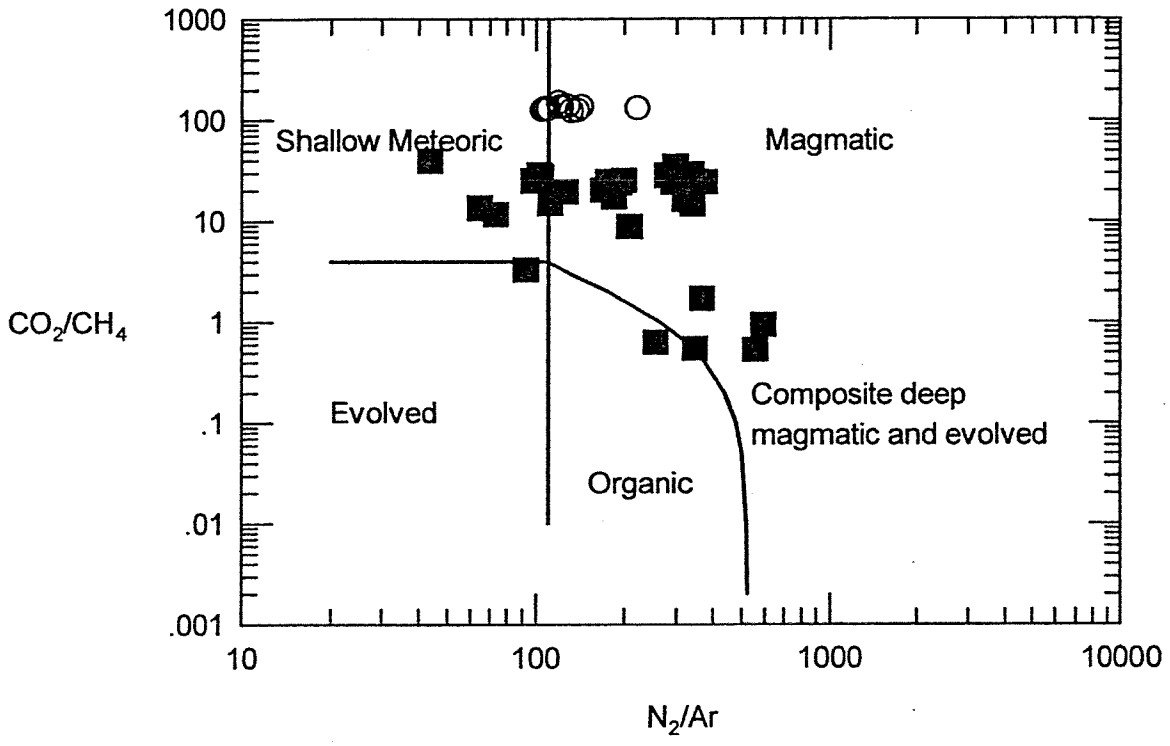

Figure 4.20 Discrimination CO_2/CH_4 vs N_2/Ar diagram for the stage 1 (solid squares) and stage 2 (open circles) calcite veins.

Plotting the quartz data on a CO_2/CH_4-N_2/Ar diagram shows a broad spread of CO_2/CH_4 ratios (Fig. 4.21). Most N_2/Ar ratios are well above 500 indicating a significant magmatic component.

A linear relationship exists between CO_2/CH_4 and H_2S (Fig. 4.22a and b). Analyses made on quartz samples bearing inclusions with 5 to 10 eq. wt. % NaCl salinities have higher H_2S levels than analyses of quartz that contain inclusions with 15 to 25 eq. wt. % NaCl (Fig. 4.22). A CO_2 versus total gas content shows a highly linear relationship between CO_2 and gas content of fluid inclusions, and that CO_2 and CH_4 concentrations are not coupled (Fig. 4.23). There is also no discernible relationship between N_2/Ar and total gas content.

Calcite inclusions generally have lower concentration of gaseous species and a different gas chemistry than inclusions hosted in quartz. Calcite gaseous species mostly range from 0.24 to 1.5 mol. %, although a few analyses indicate up to 5 mol. %. Calcite CO_2/CH_4 ratios are similar to those measured in quartz, but the N_2/Ar ratios are much lower (Fig. 4.21). There is appreciably less H_2S in calcite-hosted inclusions; analyses range from 0.001 to 0.00001 mol. % H_2S. Calcite analyses show a mixing relationship between a shallow meteoric and a composite magmatic-sedimentary sources (Fig. 4.21). A linear trend between between two end member compositions is shown in Figure 4.24 for calcite analyses.

Stage 5 vuggy calcite: The five samples of vuggy calcite analyzed had similar results for thirty-nine analyses. On a CO_2/CH_4-N_2/Ar diagram the data plots in the evolved field (Fig. 4.25).

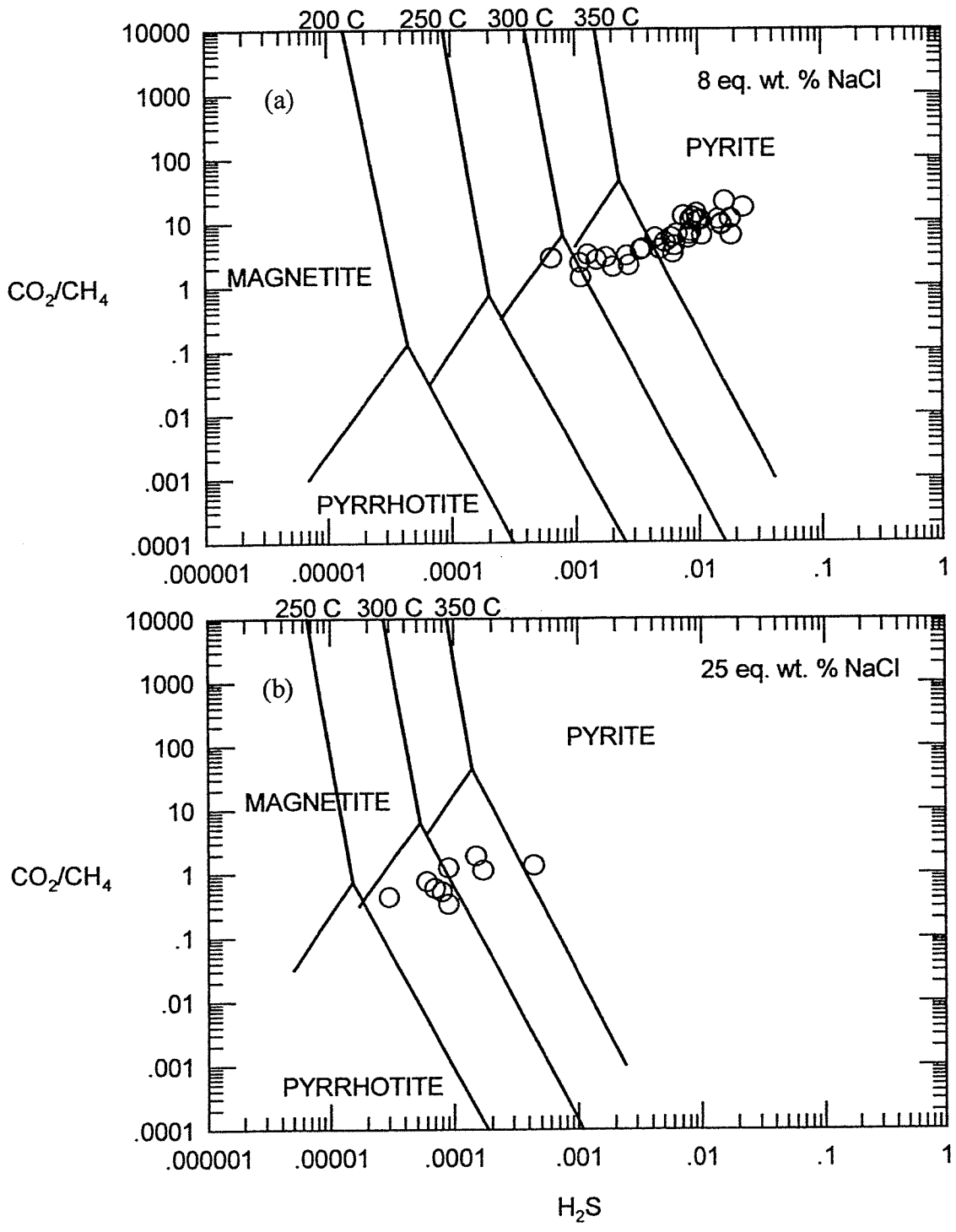

Figure 4.22 Plot of CO_2/CH_4 vs H_2S for non-hypersaline (a) and hypersaline stage 3 quartz. Corresponding stability fields for the magnetite-pyrite-pyrrhotite system are shown at varying temperature, calculated for 8 eq. wt. % NaCl (a) and 25 eq. wt. % NaCl (b). Note that the data points have a H_2S content that ranges from 0.001 to 0.03 mol.% for non-hypersaline samples whereas the H_2S content of hypersaline samples varies from 0.00003 to 0.0004 mol. %. This H_2S content corresponds to pyrite stability >300°C.

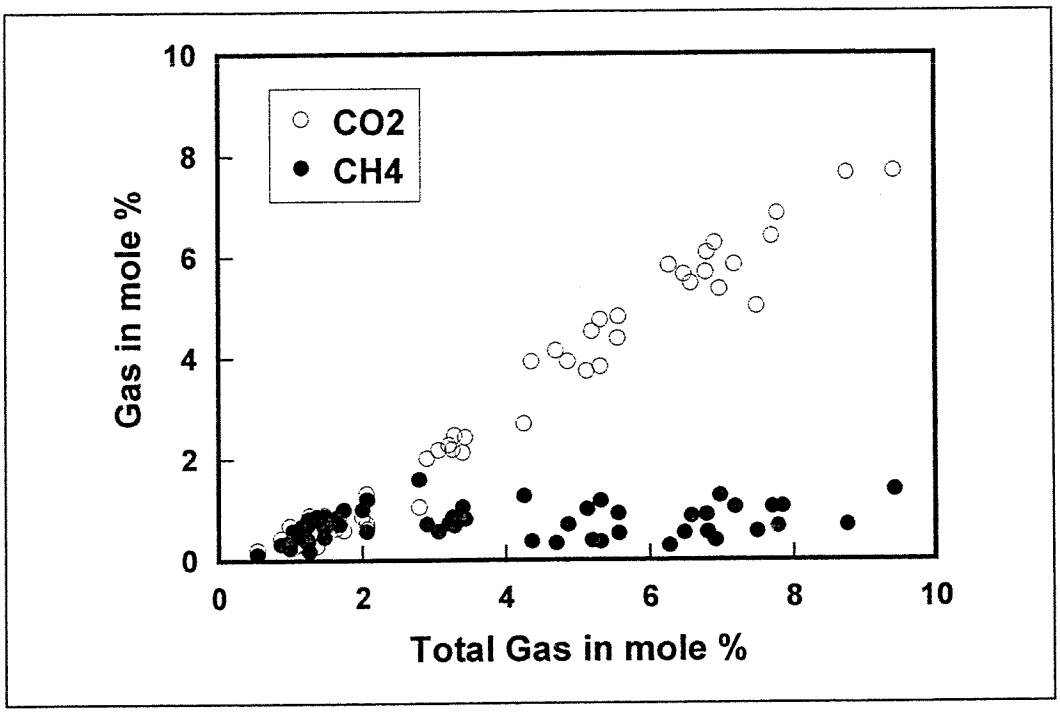

Figure 4.23 Comparison between CO_2 and CH_4 concentration as a function of total gas (excluding water) for the stage 3 quartz. Note that as the CO_2 content decreases, so does the total gas whereas CH_4 is constant.

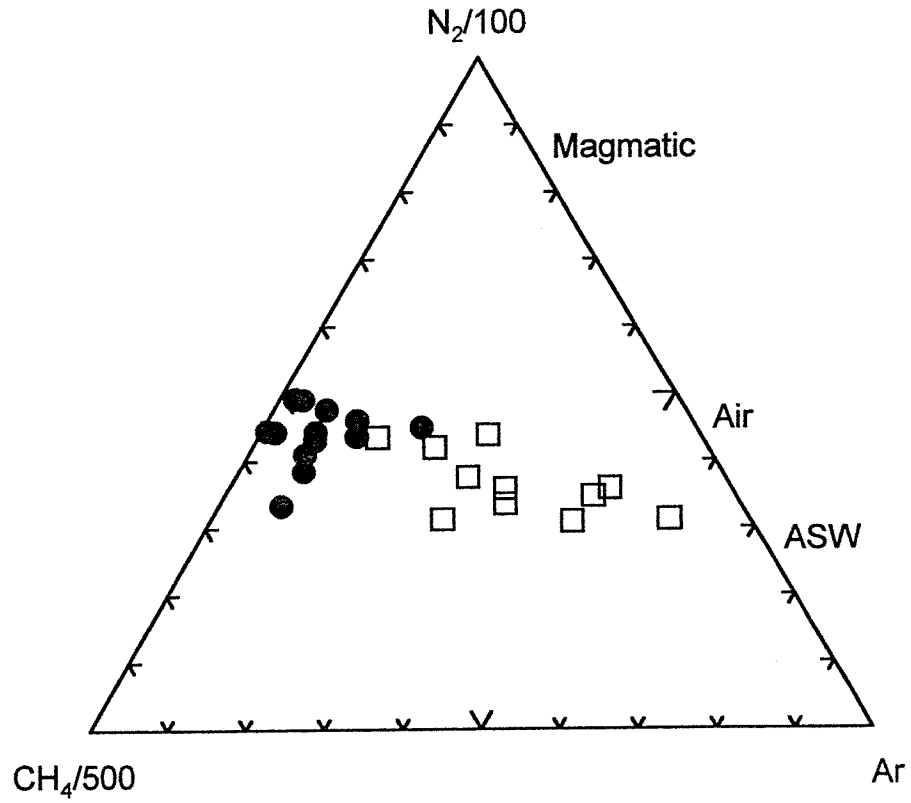

Figure 4.24 Comparison between the calcite (open squares) and quartz (solid circles) from the stage 3 vein set (sample NB-33 only) using the CH_4-N_2-Ar discrimination diagram. The calcite data plots in a line that has end member compositions corresponding to the quartz gas signature and air saturated water. Mixing is inferred.

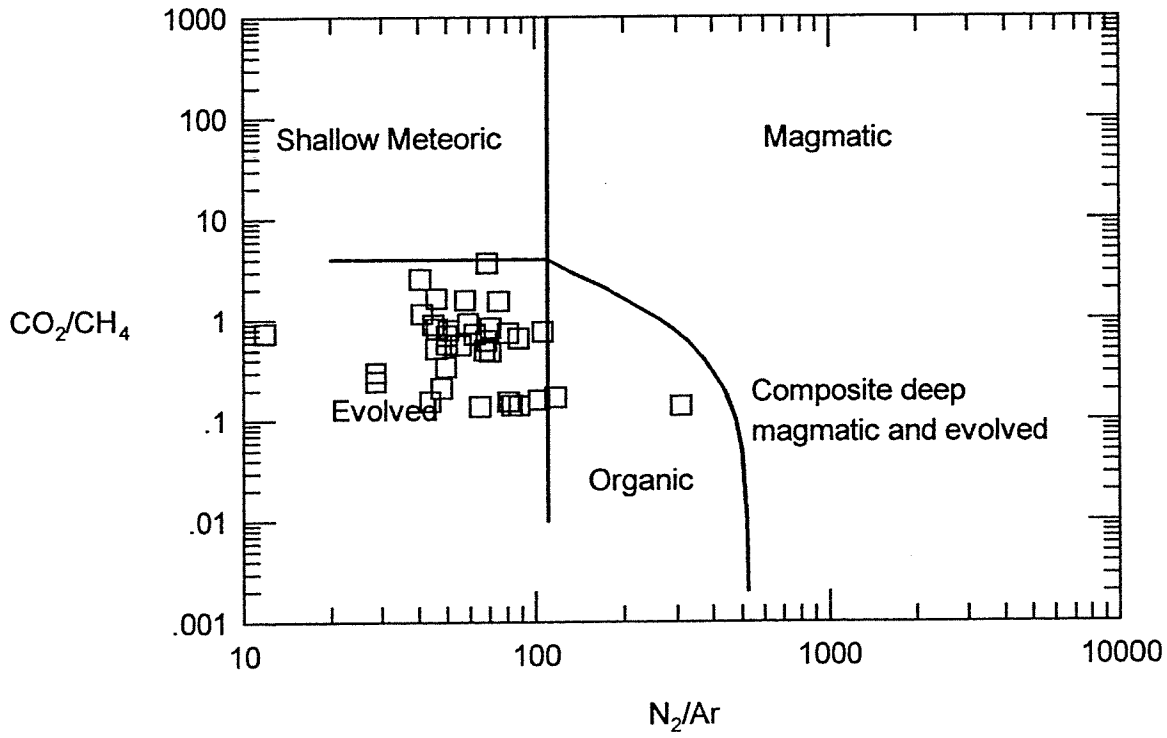

Figure 4.25 Discrimination CO_2/CH_4 vs N_2/Ar diagram for the stage 5 vuggy calcite.

Bulk cation and anion analysis

Five samples were analyzed for their anion and cation components. Results are shown in Table 4.4 and are graphically presented in Figure 4.26. The diagram shows a broader range in Ca than for Na and K, and two analyses show Ca > Na. One of these high Ca samples, NB-100, is host to the hypersaline fluid inclusions from which individual microthermometry measurements gave Ca/Na ratios as high as 1.4. The bulk cation analysis confirms microthermometry observations. The Na/K ratio varies from about 4 to 1. Applying the Fournier geothermometer (Fournier, 1981) yields values from 307° to 515°C. The geothermometer was calibrated to give acceptable values over the temperature range of 150° to 300°C and fluids with lower salinity.

Sample	NB-99	NB-100	NB-102	NB-103	NB-107
Na	5	12	13	21	22
K	4	3	13	5	11
Ca	41	35	24	24	17
Cl	7	30	11	37	40
F	1	1	3	2	2
Br	0	0	0	0	0
SO_4^{2-}	19	10	18	0	0
HCO_3^-	23	9	18	11	8

Table 4.4 Results of bulk ion leach converted into percentage of total ion budget (Appendix D). Cations comprise 50% of the total budget and the "missing" anion component is attributed to bicarbonate.

Major anions were analyzed and the results are shown in Table 4.4. Comparing the total cation charge against the total anion charge, the cations always exceed the anions (Appendix D). This "missing" anion component is attributed to bicarbonate. The bicarbonate component in % vs. the Ca/Na ratio is plotted in Figure 4.27. Samples with

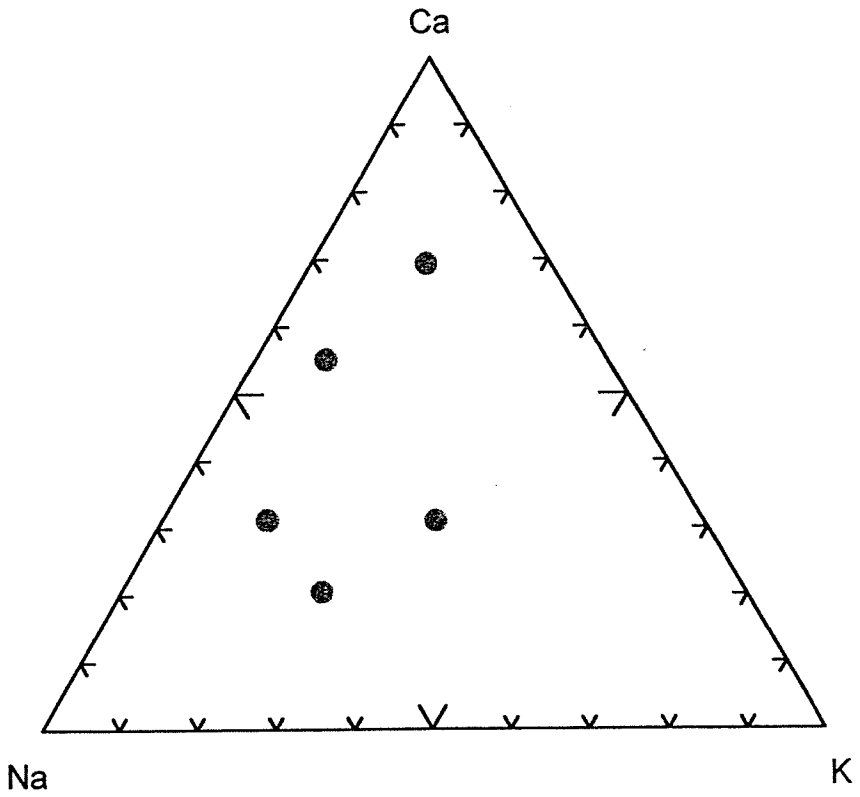

Figure 4.26 Ternary diagram for Ca-Na-K from the bulk cation leach. The high-Ca data corresponds to the hypersaline sample.

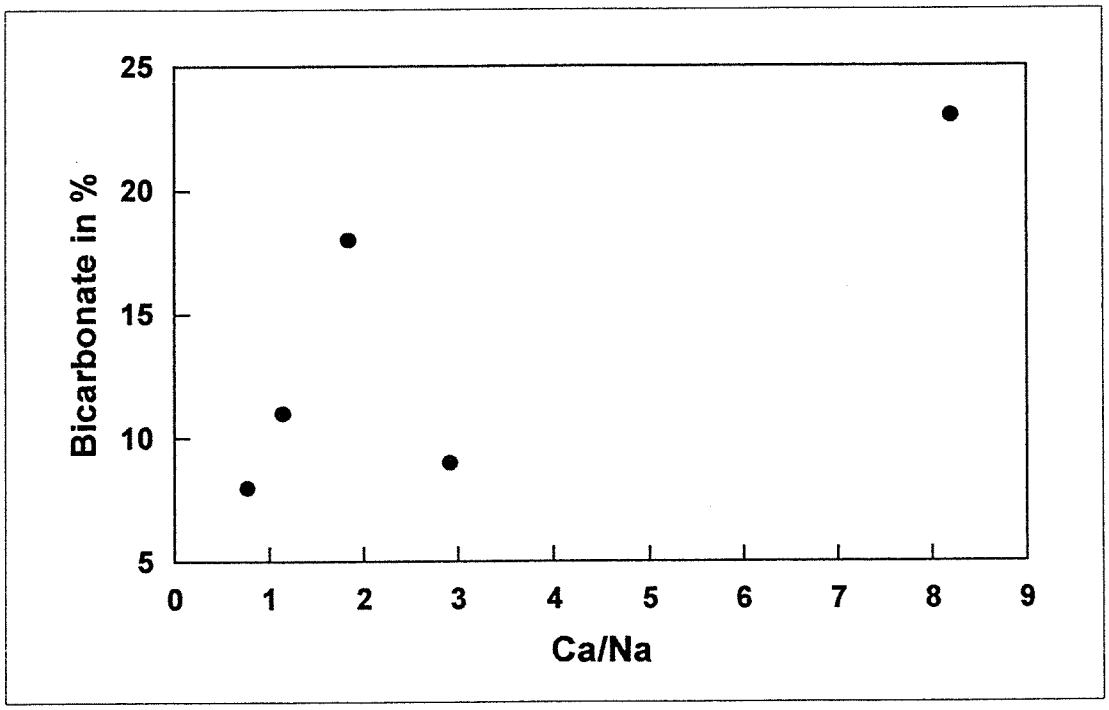

Figure 4.27 Plot of bicarbonate component in % vs. Ca/Na ratio. Highest bicarbonate correlates with highest Ca/Na whereas lowest bicarbonate correlates with lowest Ca/Na.

highest bicarbonate are those with high Ca/Na ratios, whereas samples with a low bicarbonate have low Ca/Na ratios.

Argon Geochronology

The furnace incremental heating age spectrum method was used to analyze all samples. Abbreviated analytical methods for the dated samples are given in Appendix E. The argon isotopic results are listed in Appendix F; all errors are 2σ unless otherwise stated.

Both the K-feldspar and biotite from sample 93271 collected at South Trench exhibit simple age spectra with a plateau for greater than 90% of the gas release (Fig. 4.28b). The biotite has a weighted mean age for steps C through I of 35.88±0.14 Ma with an MSWD for these steps of 4.93. Slightly elevated MSWD indicate scatter which can not be accounted for by analytical uncertainties. The radiogenic yield for the plateau steps is about 95%, and the K/Ca ratio decreases towards the final heating steps. The K-feldspar has a weighted mean age for all the steps of 35.72±0.06 Ma and an MSWD of 1.04.

The biotite and K-feldspar pair from Cortez have slightly younger apparent ages than the South Trench sample. Biotite has a plateau for ~89% of the ^{39}Ar released giving a weighted mean age of 35.80±0.24 Ma and is analytically indistinguishable from the biotite in sample 93271 (Fig. 4.28a). In contrast, the Cortez K-feldspar heating spectrum

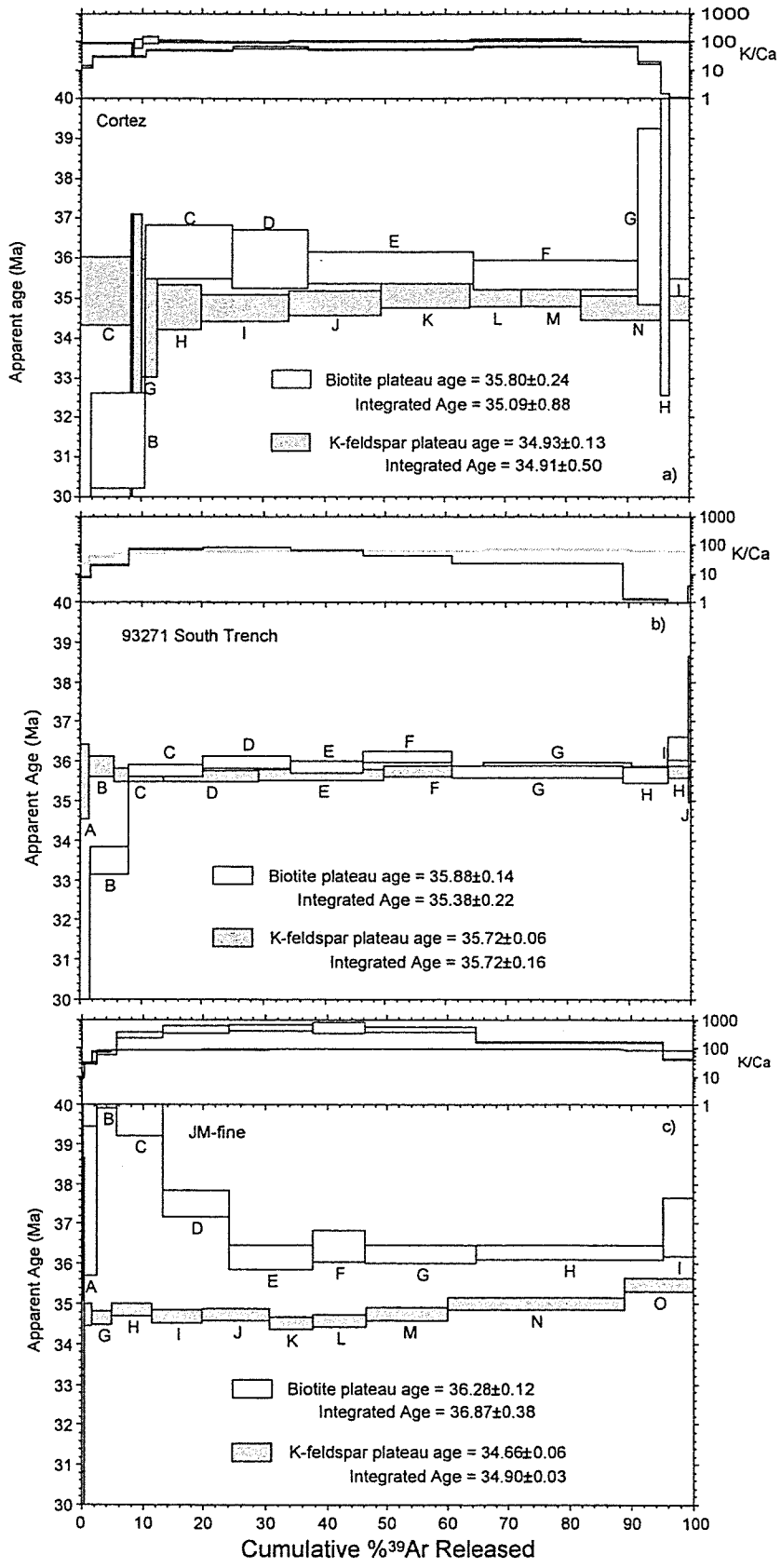

Figure 4.28 Age spectra for all K-feldspar - biotite pairs collected from Eocene dikes.

is flat for 100% of the gas released with a weighted mean age of 34.93±0.13 Ma (MSWD is 0.93).

The biotite and K-feldspar pair from the dike that crosscuts the Mill Canyon stock in a drillhole is referred to as JM-fine. The age spectra for the biotite and K-feldspar are more complex than the Cortez and 93271 biotites (Fig. 4.28c). The biotite age spectrum is disturbed and exhibits ages that are older than the biotite in the Cortez and 93271 samples. Initial heating steps yield old ages and are followed by a plateau segment with an age of 36.28±0.12 Ma (Fig. 4.28c). In contrast, the K-feldspar has an age spectrum that is flat for the first ~50% of the gas released with a plateau age of 34.66±.06 Ma. The final three steps rise to ~35.5 Ma.

Isochron analyses are reported for several samples. The isochron plots are shown in Figure 4.29 for the samples yielding Eocene apparent ages and the results are reported in Appendix F. The isochron ages are analytically indistinguishable from the plateau ages, however, there are greater uncertainties associated with the isochron ages in comparison to the plateau ages. The final three heating steps from the JM-fine K-feldspar lie on a relatively poor isochron with a MSWD of 11.1. The isochron has a trapped initial $^{40}Ar/^{36}Ar$ value of 603±100 and an apparent age of 34.78±0.47 Ma. This age is within error of the plateau age determined for the initial heating steps and may indicate that the apparent age gradient is related to excess argon in large diffusion domains (Foster et al., 1990).

The Mill Canyon stock is intersected by a reverse-circulation drillhole on the east side of the valley. The sample of Mill Canyon stock is referred to as JM-coarse and is host

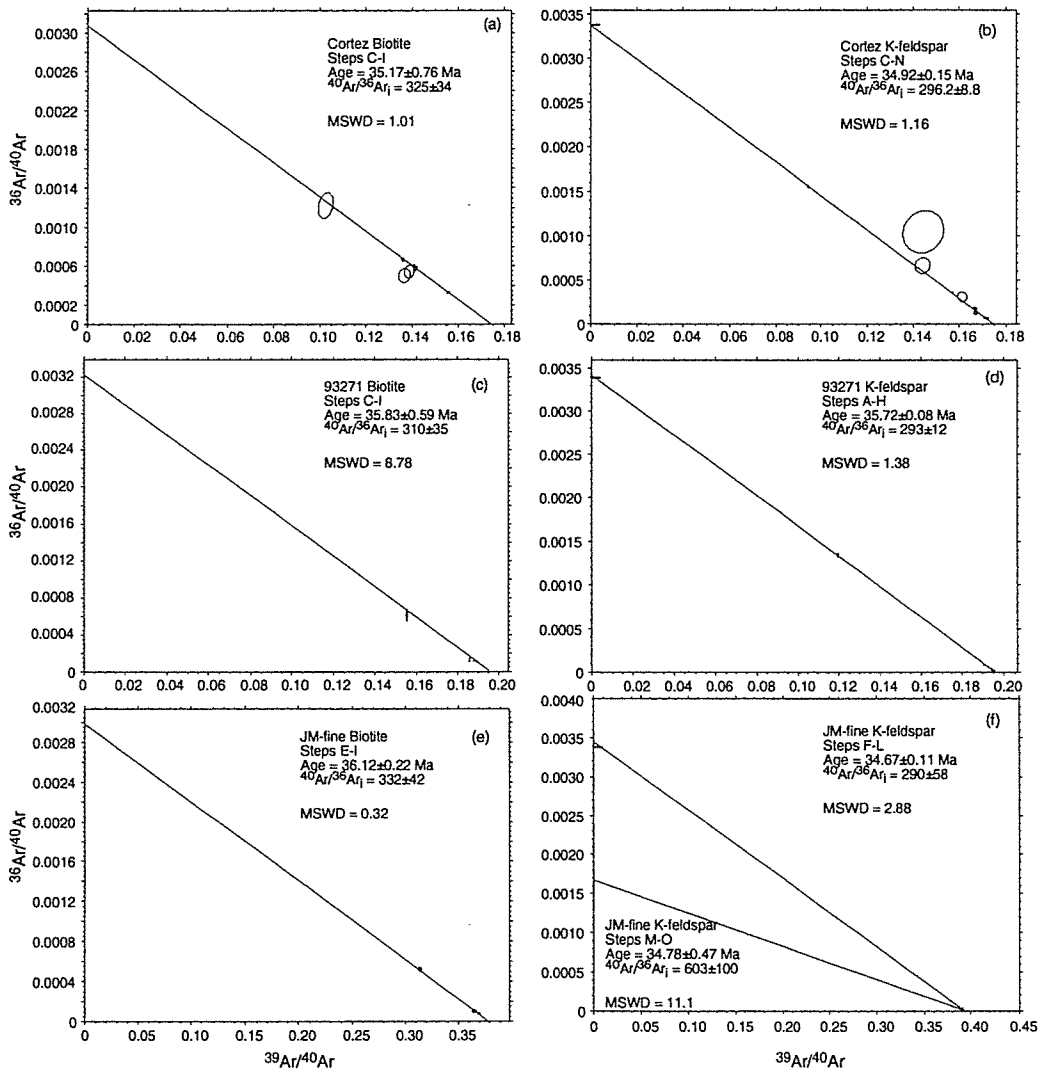

Figure 4.29 Isochron diagrams for biotite and K-feldspars from samples that yield Eocene apparent ages.

to coarse, fresh biotite and K-feldspar. The biotite has a flat age spectrum with a plateau age of 152.24±0.33 Ma, whereas the K-feldspar yields an age gradient ranging from about 50 to 150 Ma (Fig. 4.30).

Sample NB-102 is the only stage 3 vein that is host to hydrothermal sericite. Thin section shows the sericite has variable grain size with a maximum grain size of ~20 μm (Fig. 4.31). In contrast, electron microprobe backscatter images show that the material used for dating comprises a mosaic of fine-grained white mica (Fig.4.32), closely associated with quartz. Using the electron microprobe in point quantitative analysis mode, the sericite was analyzed and the K_2O, Al_2O_3 and SiO_2 are reported in Table 4.5.

#	Al_2O_3	P_2O_5	TiO_2	MgO	CaO	MnO	Na_2O	K_2O	Al_2O_3	SiO_2	Total	K_2O/ Al_2O_3	SiO_2/(Al_2O_3+ K_2O)
1	4.00	0.02	0.00	0.09	0.05	0.01	0.01	1.12	4.00	70.69	76.00	0.28	13.8
2	3.08	0.02	0.03	0.08	0.04	0.02	0.02	0.76	3.08	83.81	87.85	0.25	21.8
3	1.62	0.01	0.00	0.05	0.03	0.03	0.04	0.41	1.62	94.27	96.45	0.24	46.4
4	1.81	0.01	0.01	0.04	0.04	0.01	0.00	0.44	1.81	75.39	77.78	0.25	33.5
5	2.57	0.06	0.00	0.11	0.05	0.00	0.03	0.65	2.57	94.11	97.58	0.27	29.2
6	2.82	0.00	0.01	0.07	0.05	0.00	0.02	0.75	2.82	92.35	96.07	0.29	25.9
7	3.45	0.03	0.00	0.08	0.02	0.00	0.02	1.00	3.45	82.39	87.01	0.29	18.5
9	2.18	0.00	0.03	0.08	0.05	0.00	0.03	0.49	2.18	81.06	83.94	0.27	30.3
10	2.75	0.00	0.00	0.10	0.05	0.00	0.03	0.74	2.75	82.27	85.94	0.27	23.6

Table 4.5 Electron microprobe analysis of NB-102 sericite. Note the consistent K_2O/Al_2O_3 ratios whereas the $SiO_2/(Al_2O_3+K_2O)$ ratios are variable.

The sericite displays a complex age spectrum (Fig. 4.33a). Overall there is a decrease in the apparent ages from heating steps A to J, followed by a dramatic drop in apparent age for the ensuing steps. The drop in apparent age observed for steps K through P coincides with a decrease in radiogenic yield and the lowest K/Ca ratios.

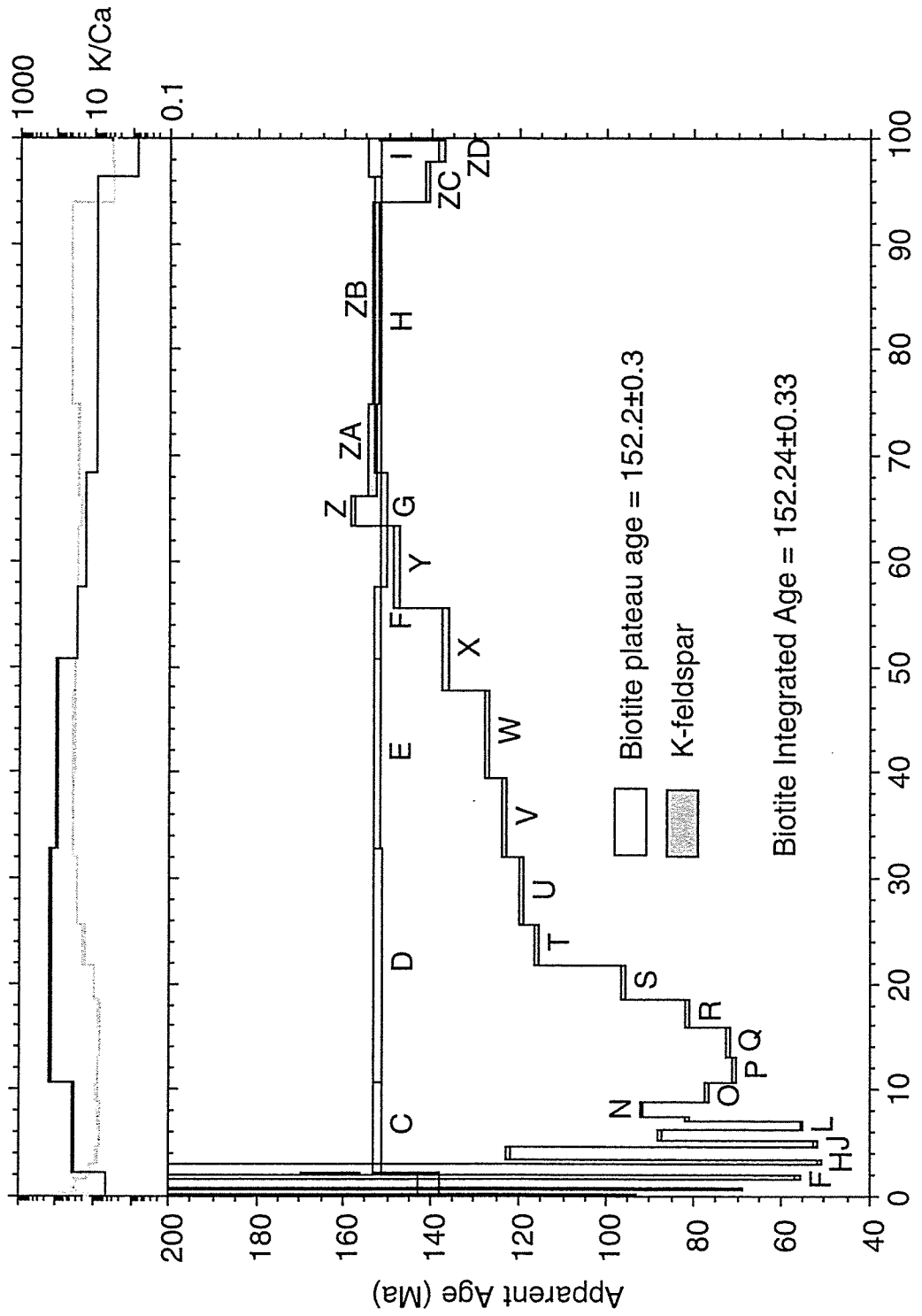

Figure 4.30 Mill Canyon stock (JM-coarse), biotite and K-feldspar age spectra. This sample was collected from the Mill Canyon stock near Cortez Gold Mines.

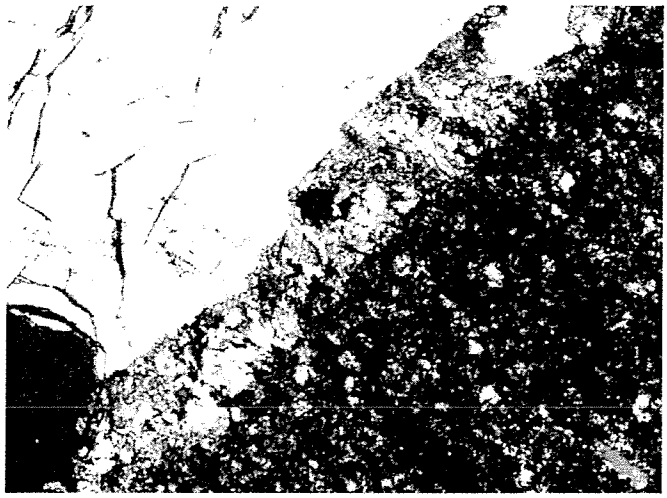

Figure 4.31 Photograph of stage 3 coarse-grained, hydrothermal sericite. The field of view is 1200 μm.

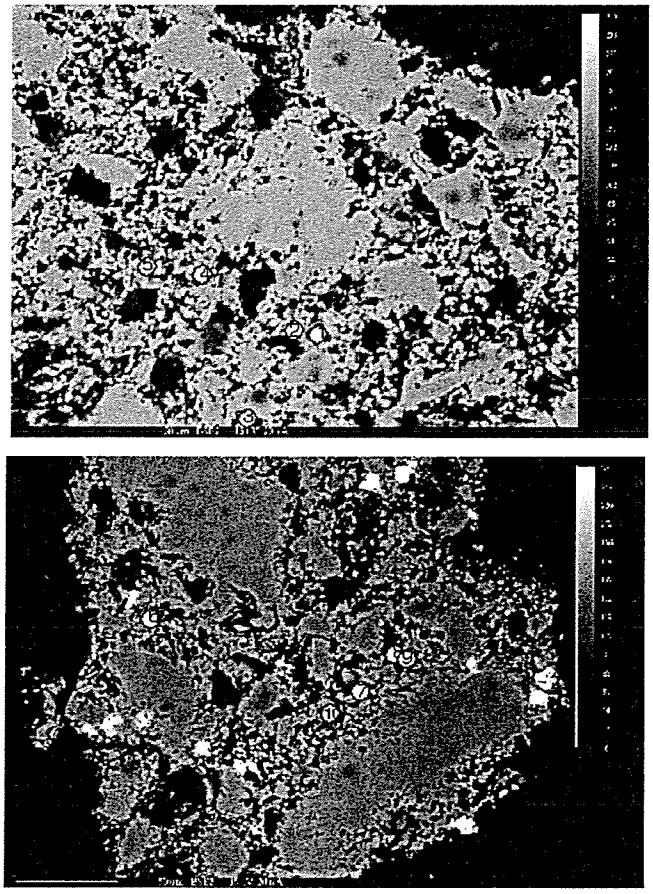

Figure 4.32 Electron microprobe image in backscatter mode of stage 3 sericite and quartz. The image shows a mosaic of fine-grained sericite and closely associated quartz. The uniform grey areas are quartz. Point analyses are indicated.

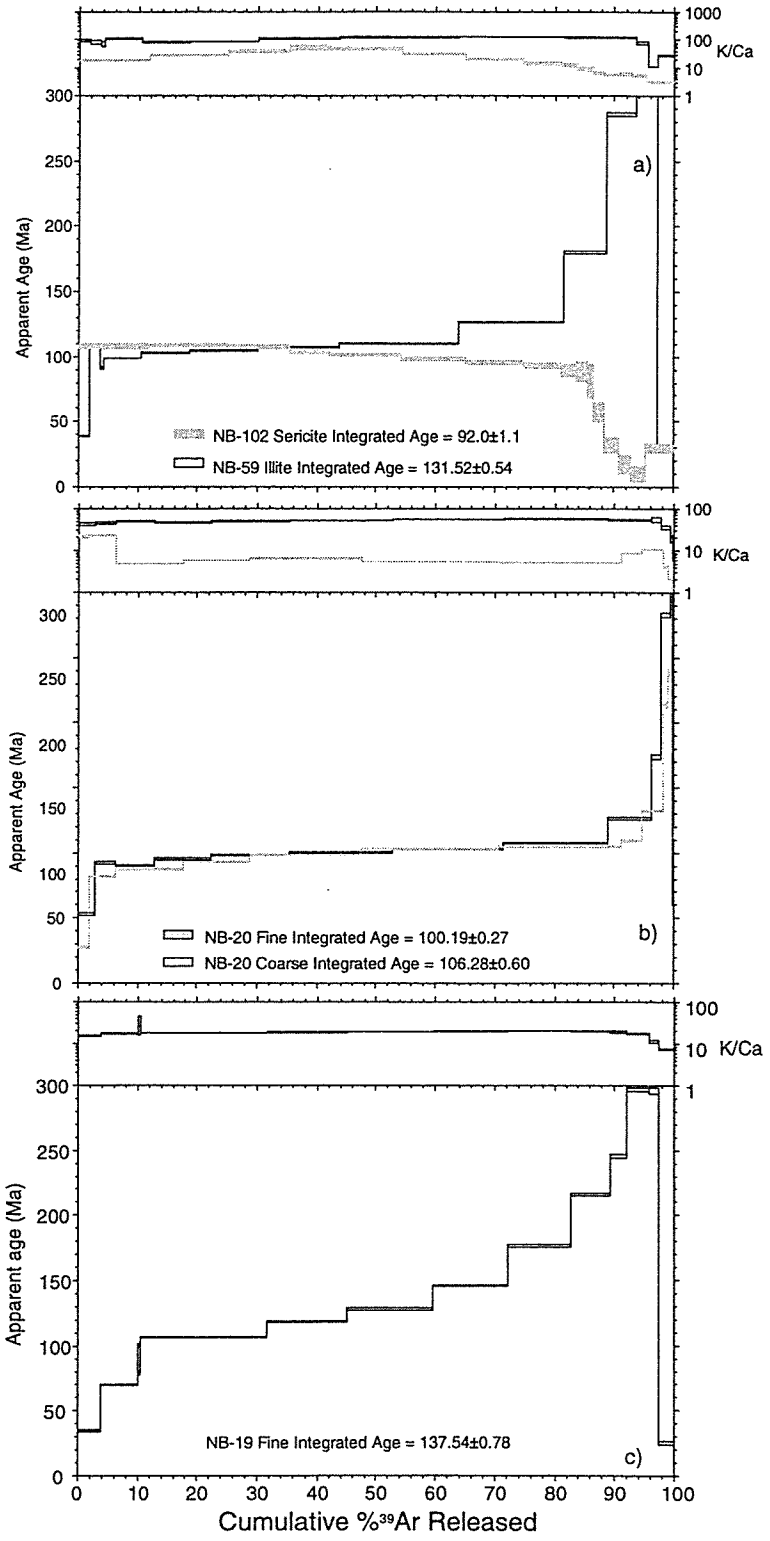

Figure 4.33 Illite age spectra from mineralized zones, argillized zones and faults.

A sample of illite from a mineralized zone (sample NB-20) was separated into a coarse and fine clay fraction. Both coarse and fine-grained fractions show discordant age spectra that steadily climb from about 90 to greater than 250 Ma (Fig. 4.33b). Both size fractions yield nearly identical results, however, the K/Ca values for the fine fraction is almost an order of magnitude lower than the coarse fraction. The radiogenic yield is 100% for nearly all the heating steps.

Illite from a very strongly argillized zone (sample NB-59), also shows a discordant age spectrum (Fig. 4.33a). The spectrum is dominated by steps with apparent ages between 100 and 110 Ma followed by a sharp rise to ages as old as 400 Ma, accompanied by a large drop at the fusion step. The radiogenic yield is almost 100% for heating steps E through N.

An argillized sample from which the clay minerals have been separated is represented by sample NB-19. The age spectrum is discordant with the first heating step being about 35 Ma followed by an age increase for ensuing steps (Fig. 4.33c). There is no plateau evident although there are several heating steps giving ages older than Cretaceous. As with the other illite spectra, the ages climb to very old values near the end of the heating steps followed by a drop for the fusion steps.

Clay Mineralogy

Clay minerals in the Fence Fault gouge and a NNW-trending fault in the Crescent Pit are illite and kaolinite in a 6:4 ratio (see Fig. 4.34). The first order illite peaks are

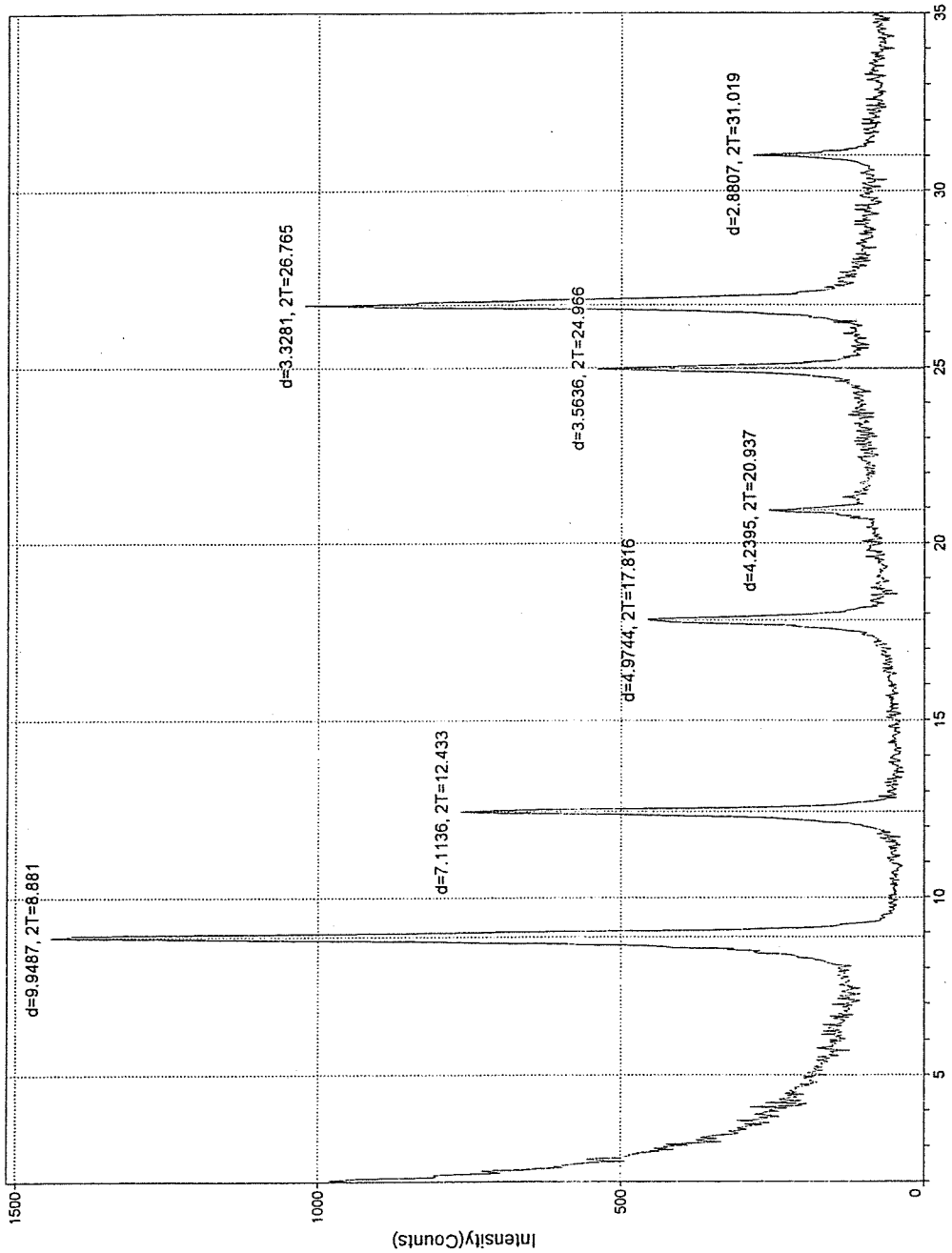

Figure 4.34 Basal section x-ray diffraction pattern for the clay fraction separated from the fault gouge of the Fence Fault. The d-spacing and intensity of the peaks correspond to illite and kaolinite in 6:4 ratio.

sharp. The clay mineralogy of the other fault gouges comprise illite with less than 5% kaolinite or smectite.

Illite is the only clay present in samples collected from mineralized zones (Fig. 4.35). Kaolinite is absent in all samples tested from mineralized zones but was detected in some unaltered samples outside the ore zones. Random mount spectral analysis shows that illite $2M_1$ polytype dominates, but the presence of 1M polytype is not ruled out (see Fig. 4.36; the diagnostic spectral lines for each polytype are reported in Table 3.1). Spectral lines corresponding to 1M polytype are barely discernible, but identification of the $2M_1$ polytype is conclusive.

Sixteen analyses show that the clay minerals analyzed from mineralized and/or altered SRM collected along section line 59200, and in drillhole DP104, are exclusively illite. However, in drillhole DP104, accessory kaolinite is present.

The FWHM refers to the full width of the XRD peak at half maximum intensity (Drits, et al., 1997) and is also known as the Kubler Index (Kubler, 1964). Smaller FWHM values correspond to a high degree of sample crystallinity. Samples with broader peaks and higher FWHM values are indicative of more poorly crystalline materials. The crystallinity index of illite is calculated using the FWHM of the 001 illite XRD reflection and the data is reported in Table 4.6. The FWHM of all illite analyzed ranges from 0.198 to 0.418. Comparing FWHM to alteration type (Table 4.6), the FWHM correlates with decalcification intensity ($R^2 = 0.2$) and to argillization intensity ($R^2 = 0.41$).

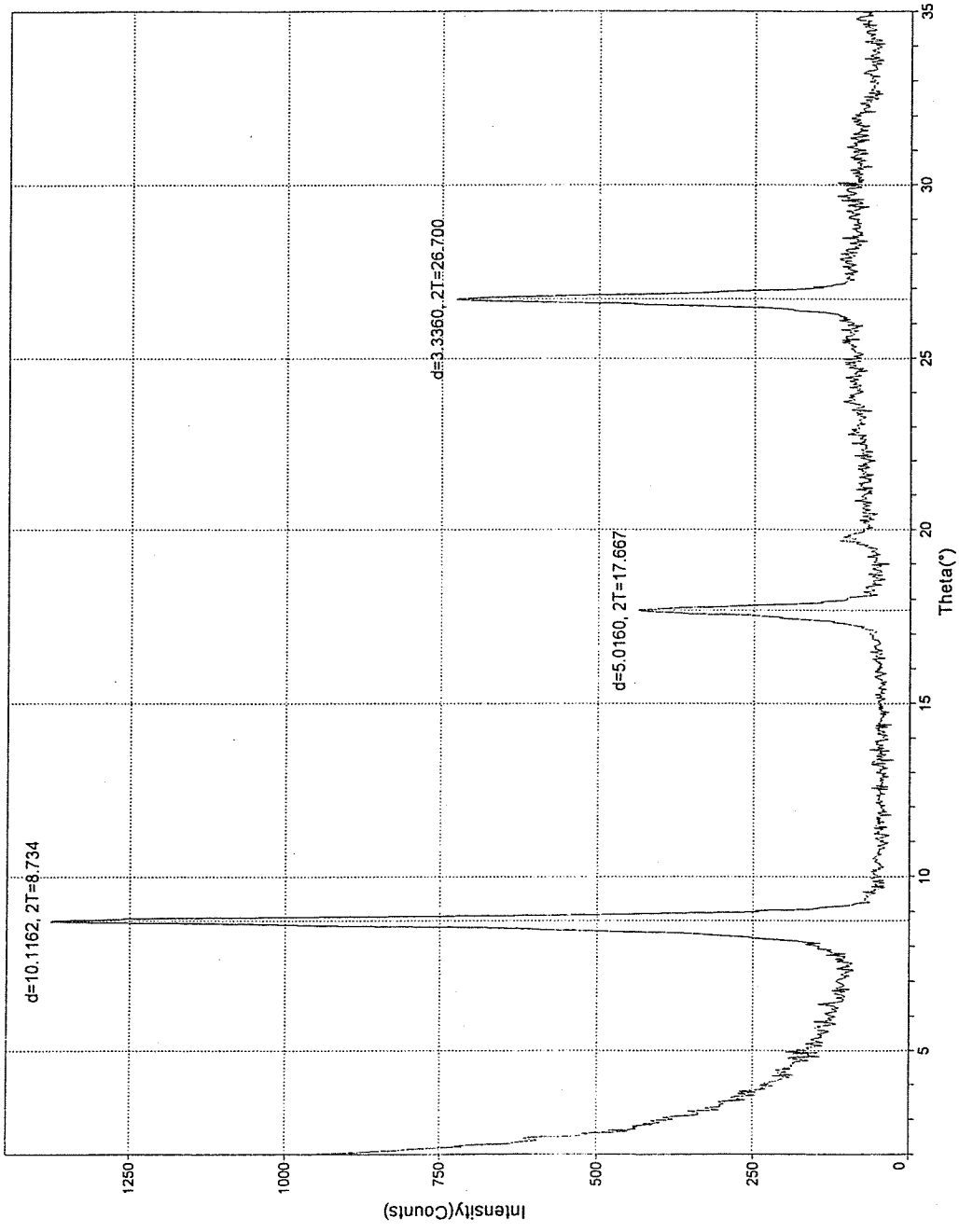

Figure 4.35 Basal section x-ray diffraction pattern for the clay fraction separated from a gold-rich ore zone (Sample NB-20). The d-spacing of these peaks correspond to illite.

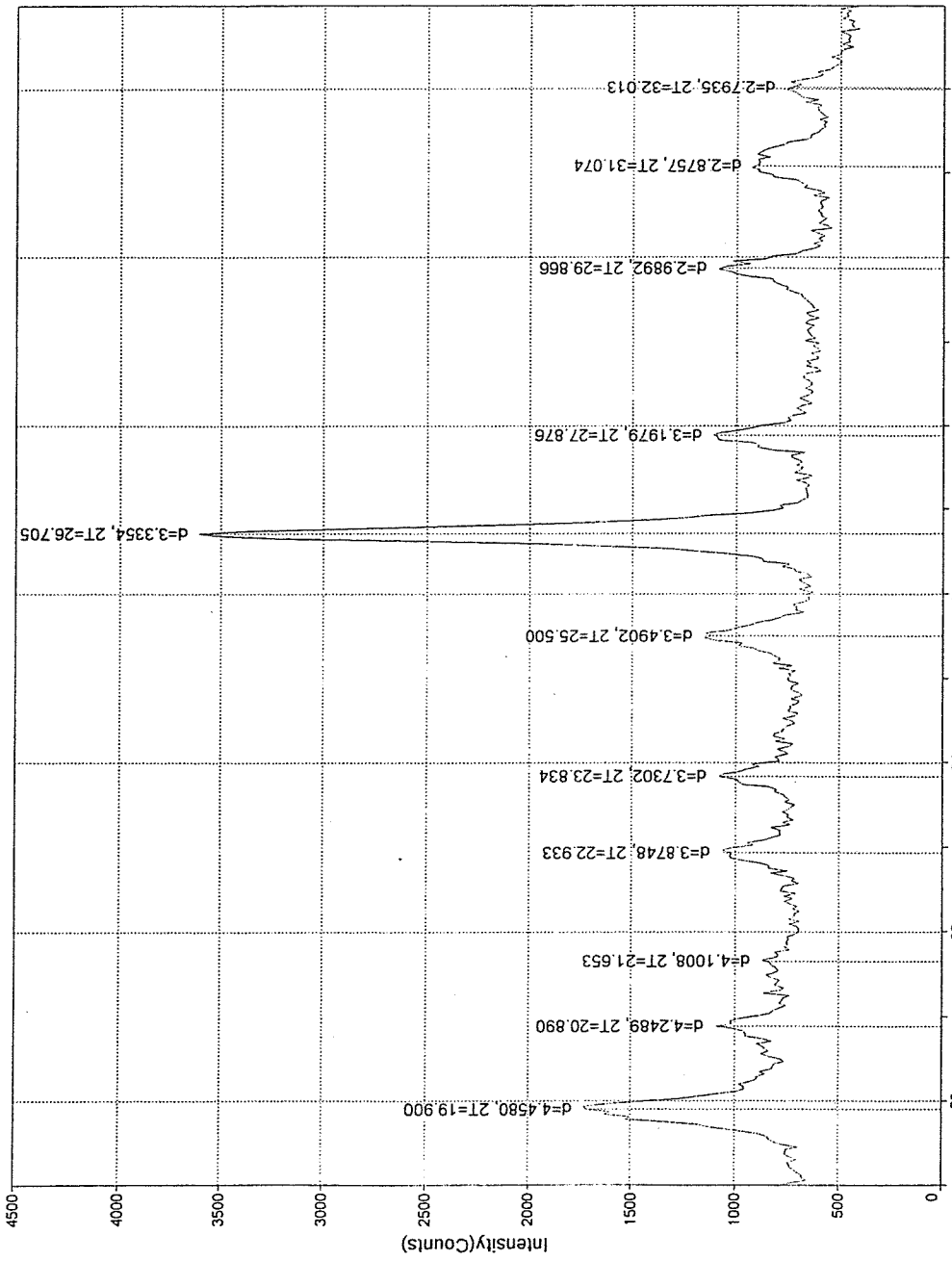

Figure 4.36 Random mount x-ray diffraction pattern for the clay fraction separated from a gold-rich ore zone (Sample NB-20). The d-spacing of these peaks correspond to the illite $2M_1$ polytype.

Sample	FWHM	Decalcification intensity in %	Argillization intensity in %	Silicification intensity in %	Fe-oxide content in %
NB-19	0.326	100	30	20	
NB-20	0.341	100	30	0	0.3
NB-57	0.355	40	30	0	0
NB-58	0.334	20	30	0	0
NB-59	0.357	100	30	0	0.05
NB-60	0.345	100	30	0	0.3
NB-62	0.289	100	20	10	0
NB-63	0.370	50	20	0	0.1
NB-65	0.305	100	30	0	1
NB-66	0.262	80	30	0	1
NB-67	0.380	100	20	0	0.3
NB-68	0.241	100	20	0	0.1
NB-69	0.298	60	25	0	0.3
NB-70	0.198	0	5	0	0
NB-73	0.248	50	20	0	0.05
NB-74	0.418	80	30	0	0
NB-75	0.210	0	15	0	0

Table 4.6 Kubler index of first order illite peaks from x-ray diffraction patterns of all samples. The various alteration intensities are given. Note that the lowest FWHM value occurs in the decalcified samples where alteration is absent.

CHAPTER 5

DISCUSSION

Pressure Estimation

The trapping pressures of inclusions (Pt) are estimated several ways. Pressure can be estimated from geologic information about the burial depths assuming hydrostatic or lithostatic pressure. Pressure is estimated from isochores when Tt is known. Isochores are calculated using MACFLINCOR, inputting Tm and Th data, and gas analyses (Brown et al., 1995). However, MACFLINCOR does not allow input of all gaseous species measured by the quadrupole mass spectrometer, hence pressure estimates made with MACFLINCOR are low. The minimum Pt is most correctly estimated from the gas analyses, Th, and salinity data. The assumption is that Pt is the sum of all the volatile inclusion species partial pressures calculated at Tt (calculated pressures are in Appendix G; the formulae for Henry's Law constants is in Appendix H):

$$Pt = P_{H2O} + P_{CO2} + P_{CH4} + P_{N2} + \ .....$$

Stage 1

This calcite is unusual in that it hosts clathrate that melts as high as 23.3°C. This is used to estimate a minimum Pt. Clathrate is stable above 0°C provided a confining pressure exists because methane enters the ice "cage" and holds the ice structure together above normal melting temperatures of ice. Graphs from Katz et al. (1959) show that a

pure methane clathrate can exist at 23.3°C provided the pressure exceeds 5000 psi or 360 bar (equivalent to a lithostatic load of 1.3 km).

Using the sum of the partial pressures at Th gives a total pressure of 1550 bars, equivalent to ~6 km depth if lithostatic conditions are assumed. Since boiling did not occur, 1550 bars is taken as a minimum pressure.

An alternative approach to estimating pressure is by geothermal gradient difference. Stage 1 Th's are approximately 125°C above ambient conditions. If a geothermal gradient of 25°C/km is assumed, then rock temperatures of 150°C is reached at 5 km depth.

Stage 2 white calcite

Constraints on the pressure-temperature conditions for stage 2 calcite veins are complicated by fluid inclusion decrepitation. However, a measured maximum decrepitation temperature of 276°C places a lower bound on Th. Isochores calculated using MACFLINCOR suggests a minimum Pt between 1200 and 1450 bars assuming Pt ≥276°C (see Fig. 5.1). This pressure corresponds to a lithostatic load of about 5 km.

Stage 3 sericite-quartz-calcite

The presence of Type 2 inclusions indicates fluid boiling, however there are no Type 1 inclusions with similar Th values. Rather, a 100°C difference in the homogenization temperatures is measured between Type 1 and Type 2 fluid inclusions. Fluid inclusion observations and gas analysis indicate there is a range in CO_2/H_2O ratios in stage 3 Type 1 inclusions hosted in quartz. Fluid boiling occurs when $P_{H2O} + P_{CO2} + P_{CH4} + ...$ exceed the

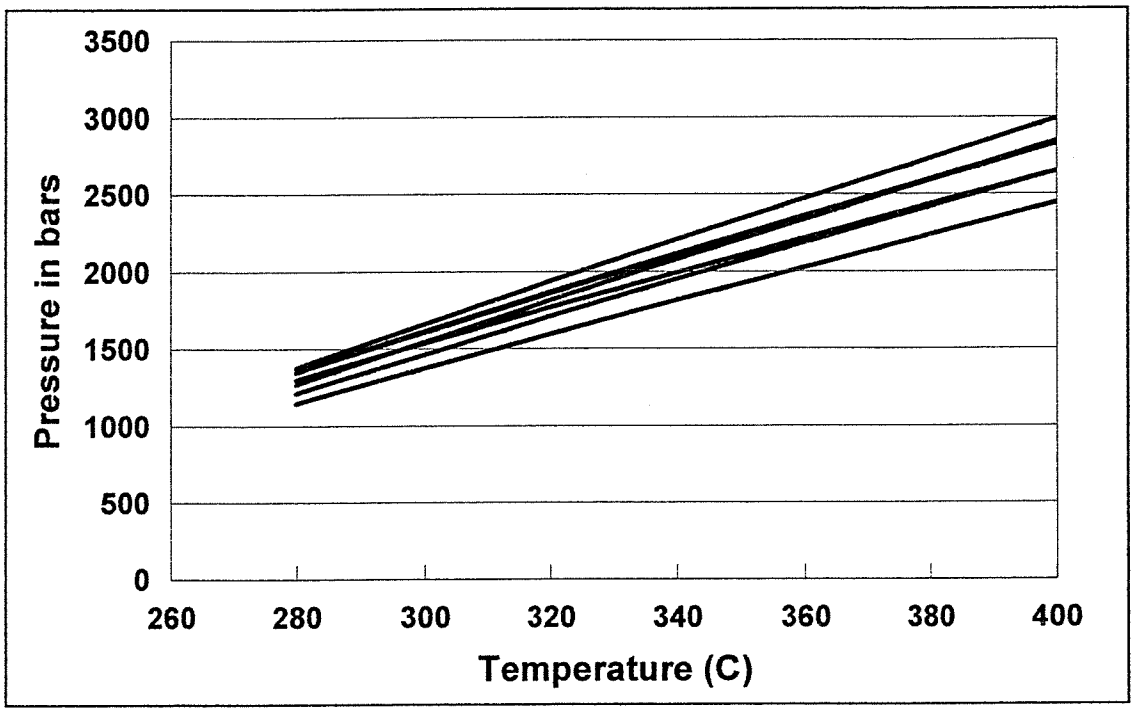

Figure 5.1 Isochore plot for stage 2 white calcite.

confining pressure (Pc). Assuming a near constant Pt and Tt, boiling would occur when fluids were most charged with gaseous species. During times of low gas contents, fluid pressures would be <Pc, and Th measurements will yield a temperature <Tt. Another possibility is that Type 2 inclusions reflect injection of a CO_2-dominated vapor into ore fluid. Some but not all of the CO_2 dissolved in the ore fluids as the low density vapor phase moved quickly upward through the ore solution. To test the idea that Type 1 and Type 2 inclusions were trapped under similar P-T conditions, assume that Type 2 inclusions were trapped under boiling conditions when 2 phases, liquid and vapor were present, hence Th = Tt. Hence, Pt and Tt can be estimated by the crossing isochore method when fluids of differing composition were trapped under similar P-T conditions. The similarity of Type 2 inclusion Th values, and their occurrence together along fractures indicates Type 2 fluids existed during Pipeline mineralization, and are not a product of post-mineralization changes in fluid inclusions. Type 2 inclusions are not the product of pinching off. They show similar Th values and all homogenize to vapor that does not agree with pinching off. Type 2 inclusions occur in all sections examined, and occur in clusters. Type 2 inclusion presence therefore suggests that for a short time during Pipeline mineralization, CO_2 increased sufficiently to induce phase separation of a carbonic phase.

Gas-corrected isochores are calculated for stage 3 vein and ore quartz geothermometry data and the results are presented in Appendix G. Type 2 fluid inclusions have calculated homogenization pressures of 1910 to 2423 bar; most data points occur around 305°C and about 2000 bar pressure (Fig. 5.2). Assuming Type 2 inclusions were trapped during phase-separation conditions, Th = Tt, and Pt can be calculated from either isochore calculation, or by the partial pressure method. MACFLINCOR calculations show Type 2

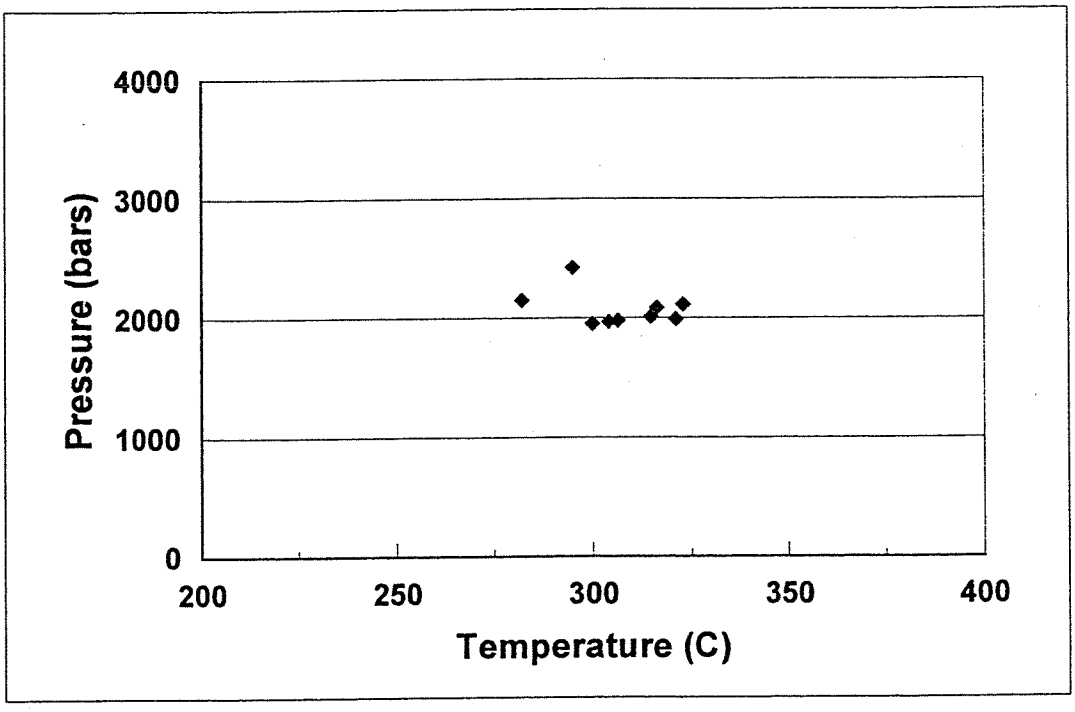

Figure 5.2 Homogenization conditions for all Type 2 inclusions hosted in quartz. Note that there is a general clustering of points in the temperature range 290° to 323°C and pressure range 1900 to 2200 bars.

inclusions comprise of about 0.71 to 0.75 mole fraction CO_2. Gas-corrected isochores of Type 1 inclusions intersect the zone defined by the Type 2 inclusions (Fig. 5.3). Hence, it shows that the assumption that Type 1 and Type 2 inclusions were trapped under similar P-T conditions is permissible. It follows then that Th measured for most Type 1 inclusions are considerably less that Tt.

Stage 3 calcite gas-corrected isochores were calculated in order to show if calcite was formed under similar P-T conditions as quartz. Stage 3 calcite isochores do not intersect stage 3 vein and ore quartz gas-corrected isochores. For any given temperature, $Pt_{calcite}$ is less than Pt_{qtz} (Fig. 5.4). The diagram shows a calcite Pt = ~1200 bars if stage 3 calcite Tt was 300°C, the stage 3 quartz Type 2 Th values.

Stage 5 calcite

Stage 5 calcite pressure estimates are poorly constrained. The open-space filling and presence of calcareous sediment suggest that calcite was deposited under hydrostatic conditions. A depth of a few 100 m is possible for stage 5 calcite.

Fluid Inclusions

Stage 1 dark calcite

Two fluid inclusion populations are hosted within the dark calcite veins. Microthermometry shows one population whose Tm is slightly below 0°C whereas a second population exhibits clathrate melting behavior above 0°C, indicating hydrocarbon species. The highest reported fluid inclusion clathrate melting temperature for a methane-

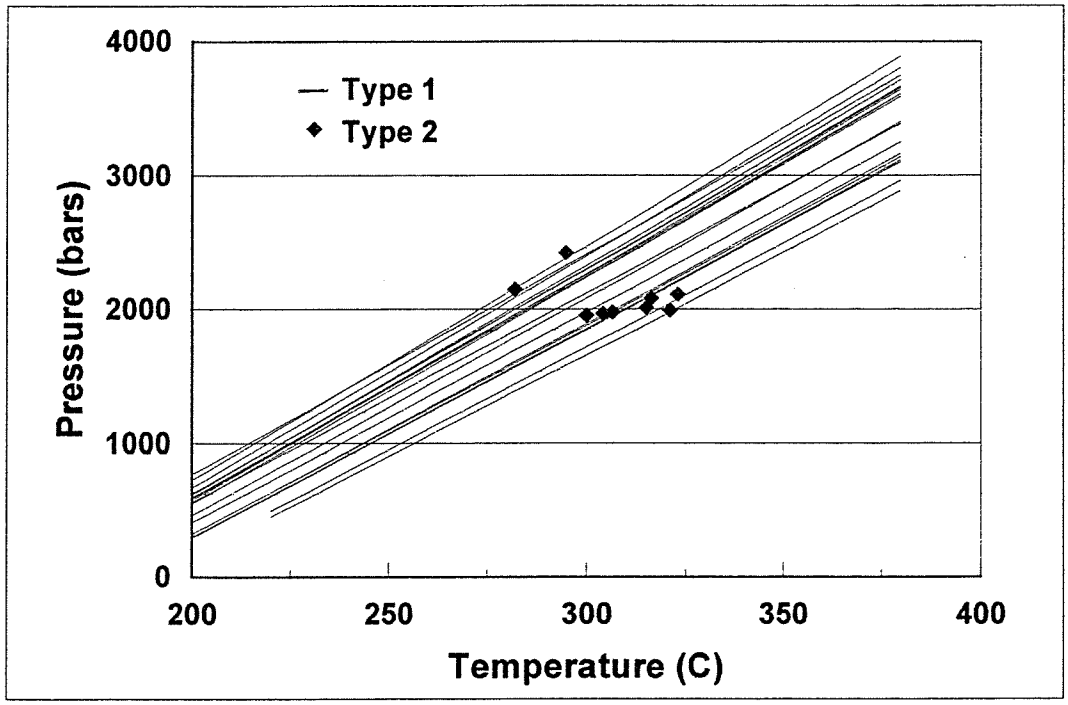

Figure 5.3 Comparison between stage 3 Type 1 isochores from sample NB-47 and all Type 2 inclusions showing that the Type 1 isochores intersect the zone in which Type 2 inclusions trapped.

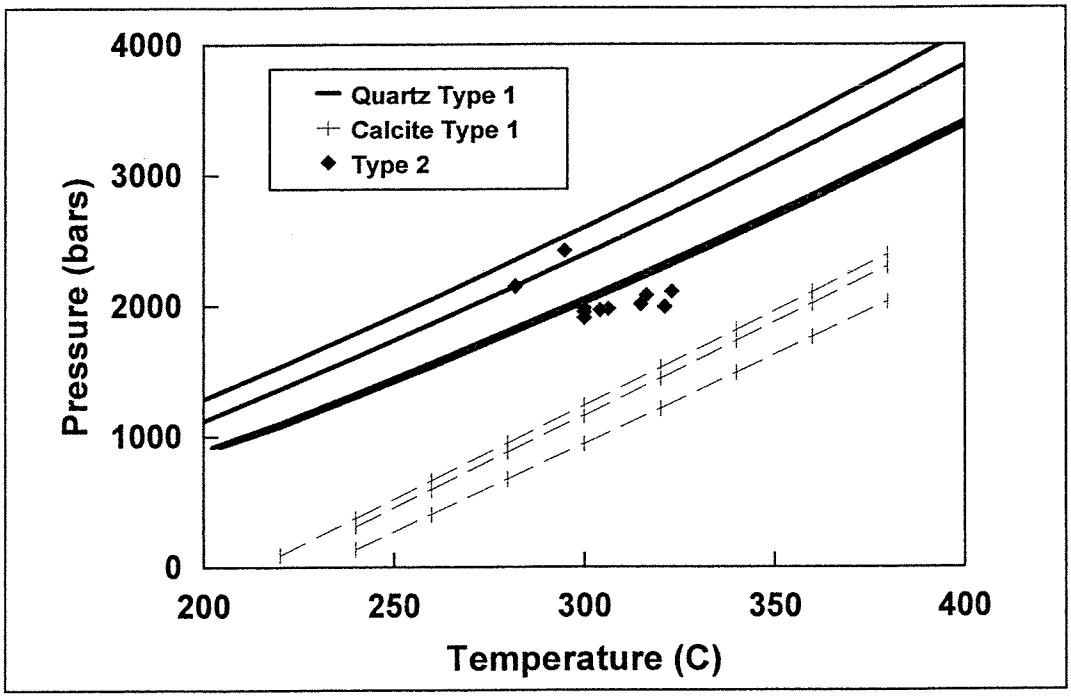

Figure 5.4 Isochore plot comparison between stage 3 quartz and calcite for the same sample, both have been corrected for the partial pressure of dissolved gases. For any given temperature, the pressure within the calcite inclusions is considerably lower.

bearing gas hydrate is 17°C (Yonaka, 1996) whereas my measurements are as high as 23.3°C. Gas analysis shows two populations of inclusions, one is methane-poor with CO_2/CH_4 >2 whereas the other population is methane-rich with CO_2/CH_4 <2 (Appendix C). It makes sense to correlate the methane-bearing clathrate inclusions identified by microthermometry with the methane-rich population recognized in the gas analysis data. Non-clathrate inclusions are correlated with the low CH_4 gas population. The N_2/Ar vs. CO_2/CH_4 plot (Fig. 4.20) shows a meteoric component. Inclusion volatiles with high N_2/Ar ratios and low CO_2/CH_4 ratios explained by the breakdown of proteins to produce both CH_4 and N_2 (Norman et al., 1999) but these generally plot in the organic field. It is possible that N_2/Ar were higher in Early Mesozoic times when these inclusions were trapped. The N_2/Ar ratio of most inclusions based on present day N_2/Ar suggest a magmatic component to the fluids. But, the data could equally well represent a hyperbolic mixing curve between a CH_4-N_2 rich pore fluid and a shallow meteoric water.

Calcite has reverse solubility, but is also deposited from hydrothermal solutions by boiling and loss of dissolved CO_2 (Heinrich et al., 1989; Simmons, 1999). There is no evidence of boiling, therefore the best explanation is that calcite deposition is a consequence of heating. The most plausible explanation is that deposition of calcite resulted from downward penetrating cool groundwaters, however, saturation of vein fluids with calcite by addition of magmatic CO_2 cannot be ruled out.

The lower N_2/Ar ratios in some inclusions agree with this interpretation. The hydrocarbon-rich aqueous and dark hydrocarbon-bearing inclusions are best explained as admixed pore hydrocarbon-rich fluids from the SRM. The Th of 145°C is above the maturation temperature of petroleum and well into the natural gas temperature window.

The suggestion of protein breakdown from gas data agrees with rising temperature.

A fracturing event allows downward flow of shallow ground water through the limestones and siltstones of the SRM. Cross cutting relationships and deformation of dark calcite veins indicate fracturing occurred before the Antler orogeny. From the estimated Tt, a minimum depth of this event is estimated at ~5 km assuming a geothermal gradient of 25°C/km and 25°C surface temperature.

Stage 2 white calcite

Similar Th_{CO2}, salinity and phase volume ratios for stage 2 inclusions indicate calcite deposition by a fluid with a chemistry remaining constant over time. Homogenization temperatures were not obtained for stage 2 calcite, but the highest measured decrepitation temperature of 276°C is a possible lower constraint on Th. However, calcite deforms easily, hence there is a possibility that stretching occurred in these high-pressured inclusions during measurement thus increasing Th values. Above 300°C, equal volumes of CO_2 and H_2O are completely miscible in low salinity fluids (Bowers and Helgeson, 1983). The homogeneous nature of inclusions suggests that the chemistry is a miscible mixture of CO_2 and H_2O controlled by equilibrium between fluids and wall rock, which suggests a temperature >300°C. The high density of the CO_2 phase in these inclusions confirms that the stage 3 calcite developed under relatively high pressures. If calcite decrepitated before significant stretching occurs, isochores for the white calcite give a pressure of about 1.3 kbar at 276°C. Since Th is higher than the decrepitation temperature and most likely above 300°C, 1.5 kbar is taken to be a realistic minimum pressure. Therefore, a minimum lithostatic pressure corresponding to about

6 km depth existed during precipitation of the calcite. Data from the stage 3 mineralization gives a pressure of about 1.9 to 2.2 kbar, therefore, if this pressure is the load of upper plate rocks, then the isochore can be used to constrain temperature. By applying 1.9 to 2.2 kbar pressure to the isochore of white calcite, a corresponding trapping temperature of 320° to 340°C is determined.

The CO_2/CH_4 vs. N_2/Ar discrimination diagram (Fig. 4.20) shows the white calcite has a meteoric gas signature of a separated gas phase (Norman and Moore, 1997). It could well be that ground water N_2/Ar ratios differed from the 32-54 ratio recorded today. This is consistent with the average fluid salinity of <1 eq. wt. % NaCl, of which a portion is dissolved CO_2. There is no evidence to support fluid boiling, hence deposition of calcite is considered in response to an increase in fluid temperatures.

Stage 3 quartz-sericite-calcite

The data and isochore calculations indicate that Type 1 and Type 2 inclusions were derived from a fluid of variable CO_2 content and salinity at approximately 300°C and 2 kb. The range in observed Th values can be explained with the aid of Figure 5.6 that shows phase relationships in the CO_2-NaCl-H_2O system calculated for a salinity of 8 eq. wt. % NaCl. Figure 5.5 shows that phase separation (boiling) occurs at 300°C in fluids that have CO_2 >12 mol. %. Further it shows that inclusions trapped with less than 12 mol. % CO_2 will show a range in Th that will be proportional to amount of CO_2. The gas analyses show aqueous inclusion CO_2 ranging up to 11.5 mol. % and Type 2 inclusions with about 89 mol. % CO_2. Clathrate melting observations agree with a variable CO_2 content of inclusions. Hence, the data are consistent with a mineralizing fluid with

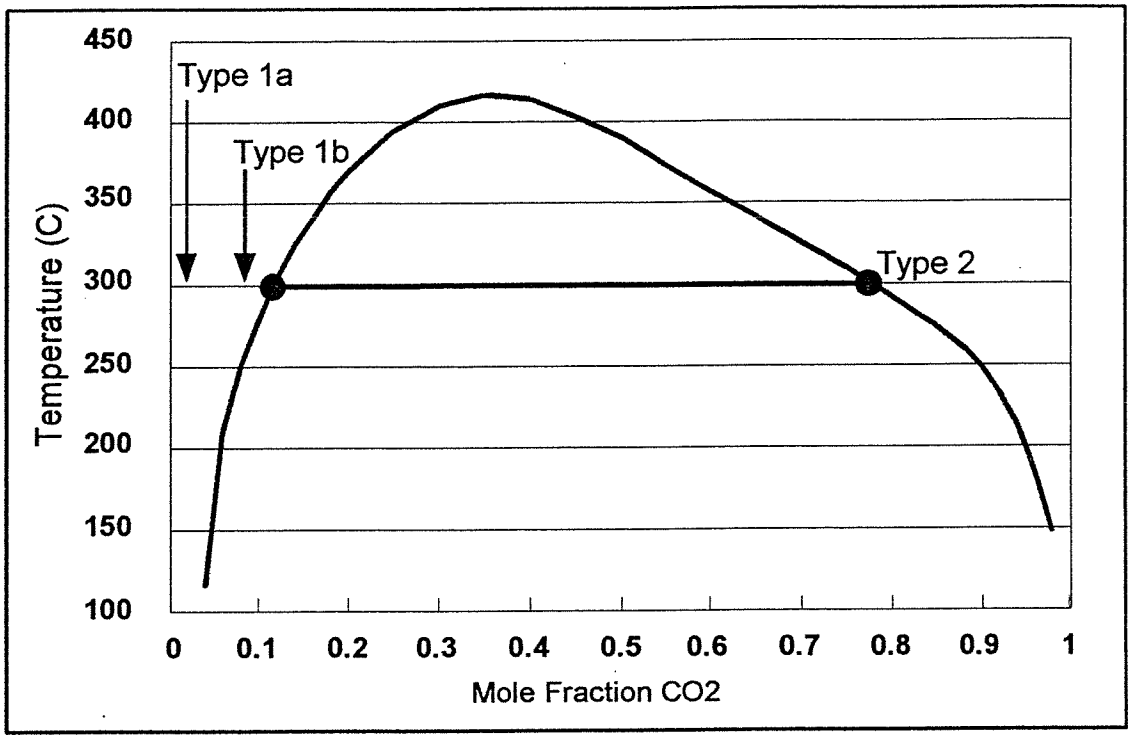

Figure 5.5 Immiscibility curve for brine (8 eq. wt. % NaCl) and CO_2 at 2000 bar. Type 1a inclusion CO_2 content is low and this group plots on the left of the diagram. Type 1b has more CO_2 and plots close to the solvus curve. Type 2 inclusion CO_2 content is high and this group plot on the right.

variable CO_2 content that boiled on rare occasions that resulted in trapping Type 2 inclusion fluids. As mentioned before, this may be the result of fluids with >12 mol. % CO_2 or admixing a CO_2-rich vapor. The reason no Type 1 inclusions with Th ~300°C were measured could be due to chance, preferential trapping of Type 2 inclusion fluids, or that Type 1 inclusions trapped during boiling events were smaller in size, and hence overlooked.

Kuehn and Rose (1995) report CO_2-vapor-filled inclusions in Carlin mineralization, similar to the Type 2, and they postulate that these CO_2-rich inclusions are the result of a throttle-controlled change from lithostatic to hydrostatic pressures. I observed Type 2 inclusions in quartz veins several tens of meters below the ore zone and observed no increase in abundance of Type 2 inclusions in mineralized gold-bearing ore quartz, which follows from Kuehn and Rose's model. The data suggests that Pt does not change during quartz deposition. A pressure of about 2 kb can only be lithostatic for a hydrostatic pressure of 2 kb would require an unreasonable depth of mineralization. Hence, lithostatic or near lithostatic conditions prevailed during quartz deposition and silicification, which implies lithostatic conditions exist during gold mineralization.

The distribution of Th values can be explained by examination of a CO_2-NaCl-H_2O phase diagram (Fig. 5.6). The behavior of a Type 1 inclusions below Tt depends on the CO_2 content and is predictable. At Tt the inclusion pressure is Pt but as the inclusion cools, an inclusion with little CO_2 will follow P-T conditions corresponding to an isochore until the aqueous phase contracts sufficiently to develop a vapor bubble. Inclusions with more than about 3 mol. % CO_2, which gas analysis indicates is most Type 1 inclusions and trapped at 300°C, will initially cool along a line defined by the isochore until the solvus is

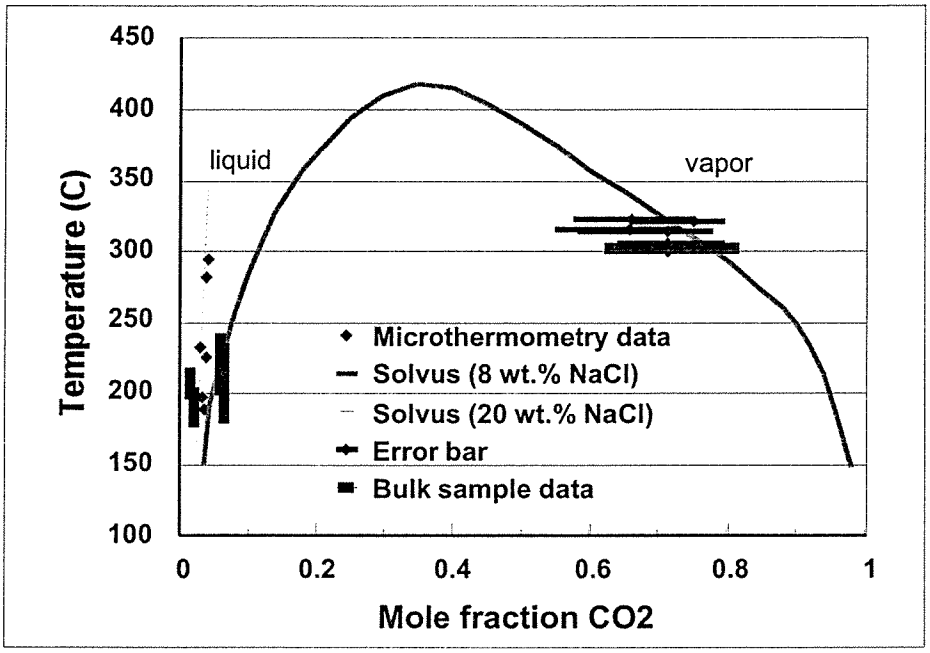

Figure 5.6 Plot of Th and CO_2 mole fraction determined from microthermometry for Type 1 (solid diamonds) and Type 2 (showing error bars). For bulk samples the Th range and gas analysis data is used to constrain a solid box to show the range for individual samples. Superimposed is the CO_2-H_2O-NaCl solvus curve calculated for 8 eq. wt. % NaCl (Bowers and Helgeson, 1985) and part of the solvus curve for 20 eq. wt. % NaCl (Takenouchi and Kennedy, 1965).

intersected. Thus, a spread of Th will reflect the CO_2 content and not necessarily Tt.

Plotting stage 3 data on a CO_2-NaCl-H_2O P-T solvus diagram shows that the distribution of Th measurements obtained is consistent with trapping temperatures of ~300°C and trapping pressures of ~2 kbar. Curves are plotted for the CO_2-H_2O-NaCl system at 8 eq. wt. % NaCl (Bowers and Helgeson, 1985) and 20 eq. wt. % NaCl (Takenouchi and Kennedy, 1965). Other gaseous species are ignored due to the lack of equations of state. Type 2 fluid inclusions cluster on the vapor side of the solvus curve indicating they represent a trapped vapor phase, as might be expected by boiling a fluid. Corresponding Type 1 inclusions with ~10 mol. % CO_2 were not observed on the left side of the solvus curve but are predicted. A plausible explanation is the "wetting" effect of non-aqueous phases causing more Type 2 inclusions to be trapped than Type 1. It follows that more observations might increase the chances of observing Type 1 inclusion whose composition plots to the solvus curve at 300°C. Alternatively, the solvus curve is affected by change of salinity, presence of other gases and change of pressure.

Quartz gas analysis data give N_2/Ar ratios >500, indicating magmatic fluids (Fig. 4.21). The data supports a magmatic fluid source for Carlin-type deposits, orginally proposed by Sillitoe and Bonham (1990).

Calcite isochores and calcite inclusion gas analyses are compatible with calcite mineralization occurring under different pressures than quartz. The calcite isochores do not intersect the P-T conditions measured for the stage 3 Type 2 inclusions, nor do they intersect stage 3 quartz Type 1 inclusion isochores. Therefore, deposition under lower pressures than prevalent during quartz mineralization is indicated, assuming Tt was the same or less. Gas analysis shows stage 3 calcite depositing fluids contain a shallow

meteoric component mixed with a magmatic fluid (Fig. 4.21). Entering stage 3 veins during lithostatic conditions is impossible for meteoric fluids because lithostatic pressures imply there are no fluid conduits to the water table. However, it is possible for meteoric fluids to migrate downwards into the deposit under less than lithostatic pressure. Meteoric fluids are expected to be saturated with calcite from contact with carbonate sediments. Deposition of calcite is explained by heating, as meteoric fluids descended, due to its reverse solubility. Veins with similar mineralogy are known to occur in other Carlin-type deposits (J. Cline, pers. comm.; Kuehn and Rose, 1995).

Stage 5 calcite

Stage 5 calcite has N_2/Ar ratios that are consistent with air saturated water ratios. Approximately equal CO_2/CH_4 ratios are lower than meteoric waters and plots on a N_2/Ar -CO_2/CH_4 discrimination diagram in the evolved field. The increase in abundance of stage 5 calcite peripheral to the deposit suggests that a thermal source is responsible for circulating ground water during stage 5.

Clay Minerals

The dominance of illite in rocks that display ore mineralization is attributed to hydrothermal alteration. This is supported by the correlation between illite peak FWHM and degree of alteration in comparison to unmineralized SRM. The dominance of the $2M_1$ illite polytype also confirm mineralizing temperatures of 200° to 370°C (Lonker and Fitz Gerald, 1990; Weaver and Boekstra, 1984; and Yoder and Eugster, 1955).

Disappearance of kaolinite suggests that some illite formed at the expense of kaolinite. The indicated intergrown sericite and quartz suggests that illite in the most intensely mineralized area is of hydrothermal origin. Presence of illite inherited from SRM cannot be ruled out, however, the relationship between FWHM and alteration suggests that illite crystals grew during ore mineralization.

The presence of both illite and kaolinite in the fault gouges is attributable to incorporation of clay minerals from lithologies flanking the faults. Reaction of clay minerals to a hydrothermal fluid is ruled out because this would require an acid pH that is hard to explain in carbonate-rich terrain. Downward percolating waters along the fault that could alter illite to kaolinite is possible.

Based on electron microprobe images of stage 3 sericite, the material analyzed shows varying SiO_2 content whereas the K/Al ratio remains relatively constant. The electron microprobe has the ability to resolve crystals greater than 3 μm. However, the variability of SiO_2 in the microprobe data (Table 4.5) is consistent with sericite and quartz intergrown on a micron or sub-micron scale. If the sericite comprised a mixed-layer clay or if a second discrete clay occurred, differences in the K/Al ratio would be expected. This is not true as only SiO_2 varies. A plausible explanation is that fine- grained quartz occurs intergrown with the sericite.

Argon Geochronology

Igneous rocks

Argon ages obtained from minerals derived from intrusive rocks generally record

the time that the mineral closes to radiogenic argon loss. For biotites from relatively rapidly cooled rocks, the closure temperature is ~350°C (Harrison et al., 1985). K-feldspars commonly contain variable diffusion length scales (domains) due to their complex microstructures and thus have variable argon closure temperatures. The diffusion domains generally have closure temperatures that range from ~175° to 300°C (Lovera et al., 1989). Sample 93271 biotite and K-feldspar yield analytically indistinguishable plateau ages, whereas there is a measurable discordance of ~0.8 to 1.5 Ma for mineral pairs from Cortez dikes and JM-fine (Appendix F). Also, the JM-fine biotite plateau of 36.28±0.12 Ma is older than the essentially identical biotite ages from the other two Eocene dike samples. All three Eocene dike K-feldspars yield statistically different plateau ages, and the youngest K-feldspar comes from the Mill Canyon Eocene dike (JM-fine) and gives the oldest biotite age (Appendix F). The age discordance between mineral pairs and between similar minerals from different Eocene dike samples are linked to variations in closure temperatures and/or actual age differences of the samples. However, there is no simple cooling or intrusive history that explains all the age results from these samples. For instance, if the 1.5 Ma age discordance between biotite and K-feldspar from JM-fine is related to overall cooling from ~350° to 200°C between 36.2 and 34.7 Ma, why does 93271 (South trench dike) yield concordant mineral ages? Additionally, if these rocks are emplaced at depths between ~1 to 2 km, how can protracted cooling be explained? Answers could lie in the accuracy of the mineral ages or within the geological/thermal history. It is often observed that biotites yield ages older than coexisting sanidines from ash-flow tuffs and that the sanidines provide the most accurate age estimate. Perhaps the apparent discordance between the biotite and K-feldspar pairs for these samples is

attributed to inaccuracies in the biotite ages, thus making the K-feldspars the most reliable mineral for estimating the dike ages. Using the K-feldspar plateau ages indicates that the dikes were emplaced between 35.7 to 34.7 Ma. Alternatively, if the biotite ages are correct, the dike emplacement ages may be ~36.3 Ma and the K-feldspar ages represent cooling and/or partial resetting associated with post emplacement reheating associated with multiple heating events. The age of these Eocene rocks cannot be more precise, however, all results indicate that these rocks were intruded between 34.5 to 36.2 Ma.

The Mill Canyon stock (JM-coarse) sample has a biotite apparent age of 152.24±0.33 Ma. This age is interpreted to be the time of cooling through ~350°C and suggests that it is derived from a Jurassic pluton. The K-feldspar has a much more complex age spectrum, but can be understood in terms of post-emplacement argon loss. The initial excess argon observed in the first few percent of argon released obscures the age of final argon loss, however, ages get as young as ~50 Ma. Because this sample is spatially associated with JM-fine, an Eocene dike, it is suggested that the last time for argon loss from JM-coarse K-feldspar was ~35 Ma.

During step-heating of K-feldspars for the generation of the age spectrum, diffusion coefficients are calculated based on the duration of the heating steps and the amount of released ^{39}Ar (e.g., McDougall and Harrison, 1988). The diffusion coefficients are plotted on an Arrhenius diagram from which the argon kinetic parameters (activation energy, frequency factor) are obtained. These kinetic parameters are then used to model the argon retentivity of each diffusion domain and combined with the age spectrum to obtain a quantitative thermal history for the sample (Lovera et al., 1989). The thermal history is obtained by forward modeling the age spectrum, that is, by trial and error,

thermal histories are imposed upon the kinetic parameters until a calculated age spectrum matches that of the measured age spectrum. Results of multiple diffusion domain modeling conducted on JM-coarse K-feldspar are shown in Figure 5.7. The first models assume the pluton cooled quickly in the Jurassic and the K-feldspar only lost argon at ca. 35 Ma (Fig. 5.7). The calculated age spectra show that reconciling the measured age gradient between ca. 100 to 150 Ma is not possible without too much argon loss during the initial part of the spectrum. This suggests that the thermal history that produced the measured age gradient is more complex than this model.

Considering that many gold deposits in Nevada are associated with Cretaceous magmatic systems (e.g., Groff et al., 1997) thermal models incorporating reheating at ca. 100 Ma were tried. After numerous iterations, a good fit between the measured and modeled age spectra was obtained by using two short duration thermal events, one at ca. 110 and ca. 35 Ma (Fig. 5.8). The 110-Ma event serves to produce the age gradient from about 110 to 150 Ma, while the younger event causes the argon loss measured over the initial 10% of the spectrum. It is emphasized that other thermal models can also produce the measured spectrum. For instance, slow cooling throughout the Early Cretaceous could cause argon loss similar to a discrete event at 110 Ma. Also, the late Cretaceous ages may be related to argon loss associated with cooling during this time rather than an Eocene thermal event. Thus, the calculated models require some geological insight toward presenting a geologically relevant thermal history.

An Eocene event causing argon loss from the Mill Canyon stock K-feldspar is entirely plausible due to the spatial association with the Eocene JM-fine sample. The

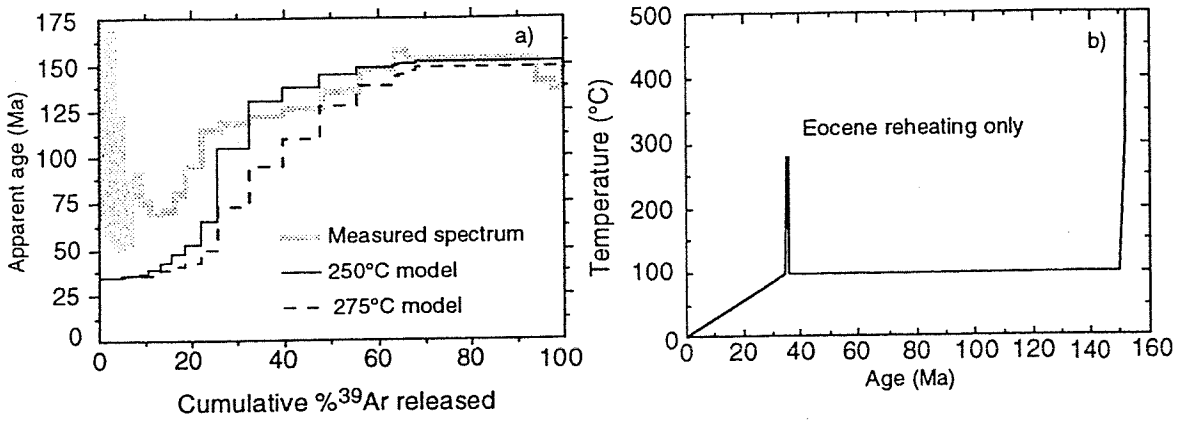

Figure 5.7 (a) Model and measured age spectra for JM-coarse K-feldspar, (b) thermal history. The poor fit between the measured and modeled spectra suggests a more complex thermal history is required to explain the age data.

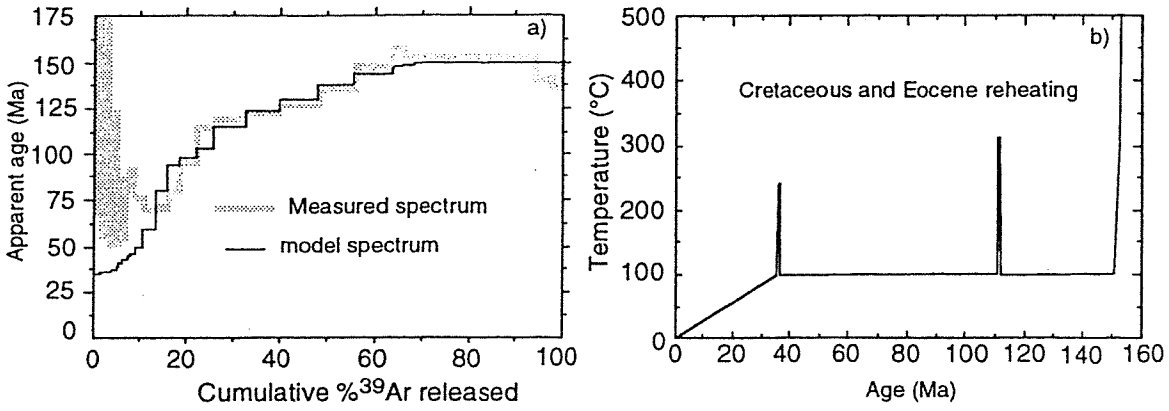

Figure 5.8 (a) Model and measured age spectra for JM-coarse K-feldspar, (b) thermal history. Using both Cretaceous and Eocene reheating events produces a calculated age spectrum which closely matches the measured spectrum.

Cretaceous event is more speculative which leads onto the discussion of the illite/sericite data.

Clay and sericite

Despite the overall complexity of the illite and sericite spectra, recorded ages for large segments of the spectra are typically 90 to 110 Ma (Fig. 4.33). The old apparent ages observed in the high-temperature heating steps are interpreted to be related to incomplete degassing of inherited clay grains. Based on the age spectra alone, it is not possible to ascertain if the ca. 100 Ma ages are associated with new clay growth or if the detrital clays are heated sufficiently to cause nearly complete argon loss. However, mineral stability fields of illite and kaolinite, based on the K^+/H^+ ratio, show that the fluids associated with the stage 3 veins and ore mineralization are more than capable of reacting with kaolinite to create fresh illite.

Dating of clay minerals from Carlin-type deposits have been largely unsuccessful (Arehart et al., 1993a; Folger et al., 1996). The Eocene hydrothermal event is regarded as an important gold epoch in Nevada (Teal and Jackson, 1997), and dating of adularia has provided convincing evidence for Eocene mineralization. However, in some deposits clay minerals are the only K-bearing minerals that can be used for dating by the $^{40}Ar/^{39}Ar$ method. Two factors can lead to anomalously old $^{40}Ar/^{39}Ar$ when analyzing clay. Inherited argon from nondegassed clay is observed in some age spectra. Second, clay minerals are very fine-grained, and variably crystalline, making recoil during irradiation a serious consideration. Retention of ^{39}Ar in clay minerals is dependent upon the degree of crystallinity (Dong et al., 1995) with progressive ^{39}Ar loss occurring in poorly crystalline

materials.

At Jerritt Canyon, $^{40}Ar/^{39}Ar$ dating of diagenetic mica from altered and unaltered samples was unsuccessful in recording younger hydrothermal resetting events (Folger et al., 1996). The authors argue that the failure to measure younger apparent ages is because the hydrothermal temperatures were too low (120°-260°C) or the duration of the heating interval too short to reset the isotopic system.

For stage 3 sericite (NB-102), inherited argon is not a problem due to its known hydrothermal origin at ~300°C. Similarly, the hydrothermal origin of the sericite suggests that the material dated is well-crystallized and coarse-grained enough for recoil loss not to be a concern. Electron microprobe spot analyses show that the sericite has consistent K/Al ratios but that silicon varies (Table 4.5), implying that quartz is intergrown with the sericite. Microprobe data show a fine-grained sericite closely associated with quartz (Fig. 4.32). This being the case, ^{39}Ar recoil from sericite into quartz explains the age spectrum (Fig. 4.33a). The last 20% ^{39}Ar released coincides with a decrease in radiogenic yield and the lowest K/Ca ratio. The apparent drop in K/Ca is interpreted to result in differential recoil implantation of ^{37}Ar and ^{39}Ar into the intergrown quartz. Since the recoil distance for $^{39}Ar_K$ is about 65% less than for $^{37}Ar_{Ca}$, it follows that the K/Ca ratio decreases if recoil occurred into quartz from sericite. Assuming the recoil of ^{39}Ar out of the sample is negligible, the integrated age for sample NB-102 is the accepted age. In addition, the 92.0±0.3 Ma integrated age is within error of a 92.8±1.0 Ma K-Ar date reported for an alteration event in Gold Acres (Silberman and McKee, 1971). Therefore, the 92.0 Ma age is regarded as geologically meaningful.

The Pipeline illite samples dated give ages suggestive of Cretaceous mineralization.

The age spectra from the coarse- and fine- grained illite from sample NB-20 at Pipeline, are both discordant but have similar ages with many heating steps at ~100 Ma (Fig. 4.33). Sample NB-20 gives a Kubler Index of 0.341 and is regarded as well-crystalline, but according to the results of Dong et al. (1995), loss of ^{39}Ar by recoil is still a consideration. Dong et al. (1995) provide a formula to calculate the amount of ^{39}Ar loss due to recoil based on the illite crystallinity (Kubler Index), that being:

$$43.8 * (\Delta 2\theta) - 6.74$$

Applying a Kubler Index (measured as FWHM) of 0.341, the ^{39}Ar loss is calculated at 8%. This would indicate that the age spectrum could not correspond to an Eocene clay which recoiled ^{39}Ar to give an Early Cretaceous age. The integrated age of 100.19±0.27 Ma for fine-grained illite from NB-20 when corrected for 8% ^{39}Ar recoil loss, yields an integrated age of ~92 Ma. This recalculated age is very similar to the integrated age from stage 3 hydrothermal vein sericite. Sample NB-19 has a FWHM of 0.362 which corresponds to 9% ^{39}Ar recoil loss. The integrated age of this sample is 137.54 Ma which suggests that inherited argon could be a factor. Older ages (~300 Ma) at Jerritt Canyon are attributed to temperatures of 120°-260°C (Arehart et al., 1995) under which resetting failed to occur. However, hydrothermal temperatures at Pipeline were 300°-320°C. I attribute the ~50°C higher temperatures at Pipeline to be the reason for partial resetting of argon systematics in illite.

Summary

The thermal history of the area is summarized as follows. Intrusion of the Mill Canyon stock occurred during the Jurassic and cooled to 350°C by 152.2±0.3 Ma. The

Gold Acres stock is probably part of the same intrusive body, but has been spatially separated by faulting that predates the Early Cretaceous vein set. Hydrothermal activity during the Early Cretaceous caused alteration in the Gold Acres deposit and the same fluids developed sericite-quartz-calcite veins in the Pipeline feeder zones along with alteration and mineralization in the Pipeline deposit. During the Eocene, extension allowed dikes to intrude the crust, provide heat and partially reset the K-feldspars within the Mill Canyon stock. Fluids penetrating existing faults caused partial resetting or growth of illite hosted in fault gouges. The Eocene event is significant elsewhere in Nevada (Groff et al., 1997; C. Henry, pers. comm.; J. Cline, pers. comm.; J. Muntean, pers. comm.; Hofstra et al., 1999), however, there is no evidence linking gold mineralization to a thermal event during the Eocene at Pipeline.

Timing of Gold Mineralization

Despite the lack of adularia for $^{40}Ar/^{39}Ar$ dating purposes, constraints can be put on the timing of gold mineralization. First, hydrothermal sericite dated at 92.0 Ma is paragenetically part of the quartz calcite veins that have pyrite-bearing and gold-bearing sidewalls. Fluid inclusion data from this vein set strongly supports more than two orders of magnitude reduction in H_2S, the key compound for gold transportation as a bisulfide complex. Second, $^{40}Ar/^{39}Ar$ dating of illite collected from gold-bearing ore zones indicate either a resetting or new growth event during the Early Cretaceous (Fig. 4.33a and 4.33b). The intergrowth of Early Cretaceous illite and gold is recognized at Getchell (Cline et al., 2000) and although illite and gold intergrowth is reported at Pipeline (Foo et al., 1996), no

date is reported. Unlike northeastern Nevada where Eocene ages dominate reported gold mineralization (Hofstra et al., 1999), no evidence can be found at Pipeline to support mineral or gold deposition during the Eocene. Third, samples containing ore quartz (silicification) from the ore zones are gold-bearing.

Geochemical Constraints

Calculations of pH were performed for the two stage 3 fluid inclusion end member salinities. The pH for the moderate salinity (±8 eq. wt. % NaCl) fluid is calculated from the dissociation of carbonic acid in brine of 8 wt. % NaCl. Carbon-dioxide amount is an average value taken from gas analysis. Activity coefficients are calculated from ionic strength (I) using the Debye-Hückel equation (Helgeson and Kirkham, 1974). The pH for the moderate salinity fluid is 4.66 and is calculated as follows:

Given: CO_2 = 5.5 mole % or 2.91 Molar
NaCl = 8 eq. wt. % or 1.37 Molar
T = 300°C
P = 2000 bar
log K = -9.98338
gamma $_{HCO3-}$ = 0.3045

Reaction:

$$H_2CO_3 = H^+ + HCO_3^-$$

$$m_{CO2} = m_{H2CO3} + m_{HCO3-}$$

$$m_{CO2} \cong m_{H2CO3} \qquad \text{since } m_{H2CO3} >> m_{HCO3-}$$

$$\log K = -pH + \log \gamma_{HCO3-} + \log HCO_3^- - \log m_{CO2}$$

$$pH = -\log K + \log \gamma_{HCO3-} + \log HCO_3^- - \log m_{CO2}$$

$$= 9.98338 - 0.516 + \log HCO_3^- - \log 2.91$$

Since $H^+ = HCO_3^-$

Then $\log HCO_3^- = -pH - \log \gamma_{H+}$

$2\,pH = 9.98338 - 0.516 - (-0.325) - 0.464$

$pH = 4.66$

A different approach is taken for the hypersaline fluid and is based on the equilibrium between carbonic acid, calcium ions, calcite and pH. The CO_2 value was obtained by averaging gas analyses, Ca^{++} is from fluid inclusion Tm data. Ionic strength is assumed to be = 4 based on salinity measurements and γ activity coefficients were determined using the Debye-Hückel equation.

Given: CO_2 = 0.767 mol. % or 0.422 Molar

Ca = 1.01 Molar

T = 300°C

P = 2000 bar

log K = -9.538

gamma $_{Ca++}$ = 0.0132

I = 4

Reaction:

$$H_2CO_3 + Ca^{2+} = CaCO_3 + 2H^+$$

$\log K = -2\,pH - \log a_{Ca2+} - \log m_{CO2}$

$2\,pH = -\log K - \log \gamma_{Ca2+} - \log m_{Ca2+} - \log m_{CO2}$

$= 9.538 - \log 0.0132 - \log 1.01 - \log 0.422$

$= 11.788$

$pH = 5.89$

The hypothesis that acidic hydrothermal fluids react with the limestones in Carlin deposits to cause decalcification is proposed by Kuehn (1989) and Bakken (1990). I, therefore, propose that the moderate salinity, high-CO_2 fluid is the source fluid that entered the deposit and caused decarbonation. Calculations show that this fluid would dissolve about

1.35 moles of $CaCO_3$ per kg of solution. This would increase fluid "salinity" to about 20 eq. wt. % NaCl, increasing Ca^{++} to about that of Na^+, increasing HCO_3^- in solution. This remarkably agrees with my data indicating the 15 to 25% salinity fluid that has Ca>Na and elevated HCO_3^-.

Gold solubility calculations were performed using thermodynamic data drawn from SUPCRT92 (Johnson et al., 1992) and Benning and Seward (1996). The logK value used to determine the ionization of metal gold to the Au^+ state ($Au^0 + H^+ = Au^+ + ½H_2$) is taken from SUPCRT92. The solubility of the bisulfide species ($AuHS^0$ and $Au(HS)_2^-$) is calculated using the formulae of Benning and Seward (1996). Gaseous species that participate in the reactions include H_2 and H_2S. The fugacities of these gases are calculated knowing their concentration from the quadrupole analyses and calculating gas fugacities using Henry's Law gas constants (Appendix H). The activity coefficients are calculated as indicated above. I developed a spreadsheet to calculate gold solubility that considers all the above mentioned factors and gives the Au solubility for both $AuHS^0$ and $Au(HS)_2^-$ species. The spreadsheet allows parameters such as pH, salinity, gas concentration, and temperature to be varied.

Taking the pH and salinity conditions established for stage 3 quartz samples, gold solubility was calculated for individual gas analyses because H_2 and H_2S are the principle variables in calculating gold. Gold solubility for stage 3 quartz has two populations (Fig. 5.9). Samples with hypersaline inclusions (eg. NB-100) give <2 ppb solubility whereas the samples with about 8 eq. wt. % NaCl, give a range of 20 to >500 ppb gold solubility. The gold solubility in ~8 eq. wt. % fluid is consistent with an ore fluid whereas the gold solubility in the more saline fluids is consistent with a spent fluid.

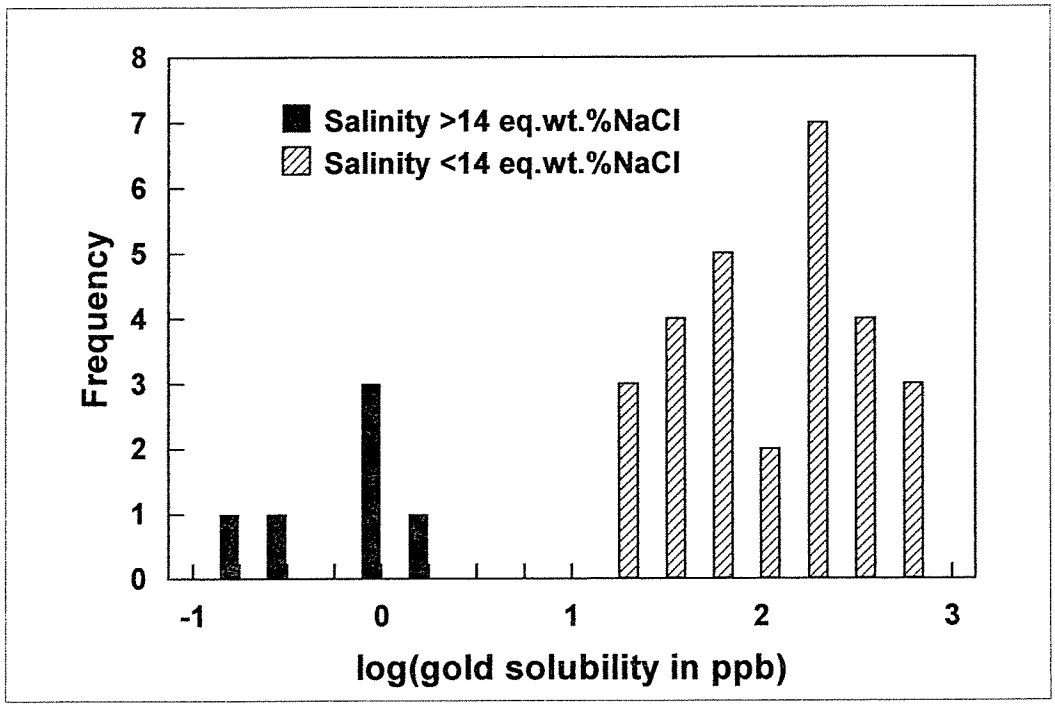

Figure 5.9 Histogram of calculated gold solubility for hypersaline (>14 eq. wt. % NaCl) and non-hypersaline (<14 eq. wt. % NaCl) stage 3 quartz inclusions. Solubility is calculated using the gas analysis of individual crushes and correcting for salinity.

Laboratory experiments (Seward, 1973) show that if all other factors, including a_{H2S} is maintained constant and only temperature is varied, then a maximum gold solubility around 250°C occurs (Fig. 5.10). Trapping temperature is indicated to be about 300°C, therefore a decrease in fluid temperature cannot account for Pipeline gold mineralization. Loss of H_2S by sulfidation reactions will result in gold deposition. Accepting that carbonic acid is responsible for decarbonation reactions, the strong linear relationship between fluid inclusion H_2S and CO_2 indicates that gold at Pipeline was deposited during decarbonization, presumably by sulfidation occurring concurrently with wall-rock alteration. Analysis of SRM show a ready supply of available Fe.

I question the concept that a_{H2S} is constant and that gold saturation occurs at 250°C. It is shown by Norman et al. (1997) that in hydrothermal systems the H_2S content of a fluid is buffered by the assemblage pyrite-magnetite-pyrrhotite. The fugacity of H_2S increases at higher temperatures. Unlike laboratory generated conditions, the a_{H2S} of hydrothermal systems extends the gold solubility to higher temperatures. I calculated the a_{H2S} at various temperatures along with the gold solubility buffered by pyrite-magnetite-pyrrhotite and take into account fugacities of gases and activities of ionic species. Figure 5.11 gives the gold solubility maxima around 350°C, maintaining constant pH = 4.66, H_2 = 0.0468 mol. %, ionic strength = 1.37. Assuming equilibrium of magnetite-pyrite-pyrrhotite or at least magnetite-pyrite, implies gold saturation can occur at temperatures below 350°C (in contrast to Fig. 5.10). However, since gold saturation occurs at 350°C then it follows that saturation at 300°C is more likely.

The H_2S content of stage 3 quartz indicates a source at T >300°C, and at mineralization temperature fluids had excess H_2S. Data plot as expected from a

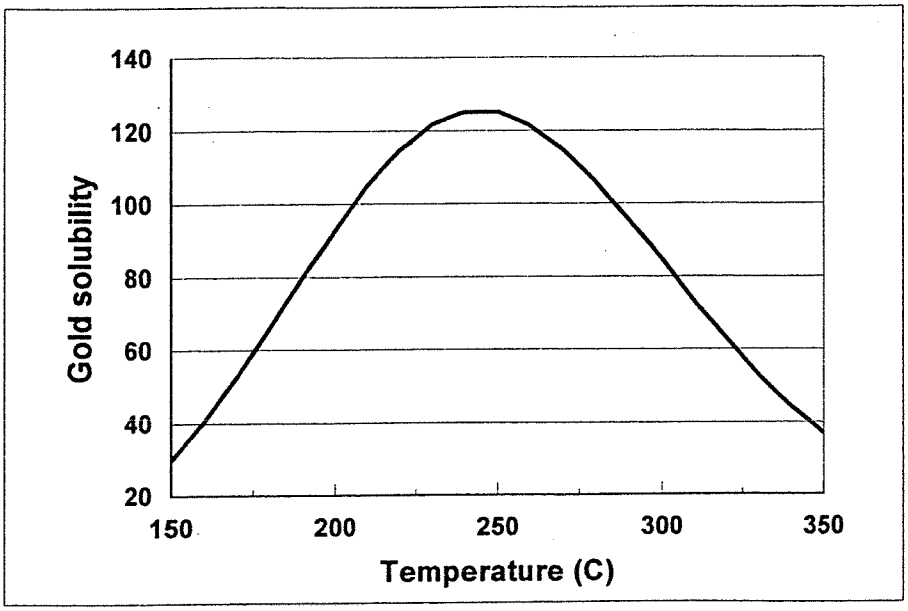

Figure 5.10 Theoretical gold solubility for the $Au(HS)^0$ complex at varying temperature based on constant salinity, H_2, H_2S and pH. The chemistry is taken from sample NB-33 ; I = 1.37, H_2 = 0.0468 mol. %, H_2S = 0.0133 mol. %. Note that the solubility maxima occurs around 250°C.

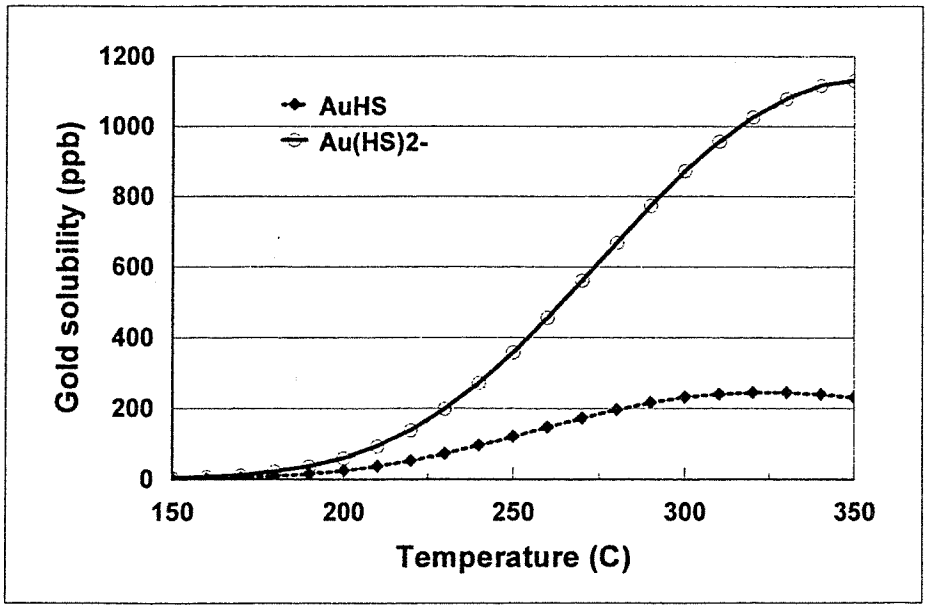

Figure 5.11 Theoretical gold solubility for the $Au(HS)^0$ and $Au(HS)_2^-$ complexes at varying temperature but constant salinity, H_2 and pH (chemistry is based on sample NB-33; I = 1.37, H_2 = 0.0468 mol. %). The H_2S content is calculated as temperature varies by assuming that fluid H_2S is buffered by magnetite-pyrite-pyrrhotite and keeping H_2 constant at 0.0468 mol. %. Note that maximum gold solubility is around 350°C.

sulfidation reaction between a hotter source that was in equilibrium with pyrite-magnetite coming into contact with cooler rocks.

Water-rock Ratios

The term water-rock ratio is used to give the ratio between the mass of hydrothermal fluid that reacted with a unit mass of rock is calculated by two methods for Pipeline ore fluids.

Consumption of CO_2: The calculations for the consumption of CO_2 is based on following reactions:

$$H_2O + CO_2 = H_2CO_3$$

$$CaCO_3 + H_2CO_3 = Ca^{2+} + 2HCO_3^-$$

Applying these reactions, one mole of CO_2 is required to react with one mole of calcite. Gas data shows that the average CO_2 content before reaction is about 5.5 mole % and the CO_2 in >14 eq. wt. % NaCl inclusions is about 0.7 mole %. Assuming the higher salinity fluids represent spent solutions then this translates into consumption of 4.8 mole % CO_2 (ie., 2.67 moles CO_2 per kg of fluid). The SRM contains 80 % $CaCO_3$ (Gilluly and Masursky, 1965) or about 8 moles of calcite per kg of rock. The required minimum water-rock ratio for the decarbonization reaction is therefore 8 / 2.67 ≅ 3.

Production of Ca^{++} from acid attack on limestone: Water-rock ratio is calculated a second way by assuming the spent fluids have about 25 eq. wt. % NaCl and a Ca/Na ratio of 1. Since fluid prior to decalcification had 8 eq. wt. % NaCl or 1.4M NaCl, and

assuming minimal Ca^{++}, then the spent fluid acquires about 1.4M Ca^{++}. The water to rock ratio is calculated by dividing the 8 moles of calcite in average SRM by the 1.4M Ca^{++} in solution giving a water to rock ratio of ~6. Both methods of calculation suggest water-rock ratios of Pipeline were low.

Gold deposition: Given a water-rock ratio of about 5, and assuming ore fluids were saturated in gold, the amounts of gold deposited by Pipeline fluids is calculated. Assuming an average gold concentration of 100 ppb based on calculations illustrated in Figure 5.9, each 1 kg of ore solution would deposit about 200 μg gold. The amount of gold in 1 kg of rock would be 200 μg * 5 (W/R ratio) * 10 (factor from decarbonization) = 10 mg/kg. The published grade for Pipeline is about 7 mg/kg. This calculation further enforces the general accuracy of the W/R calculation and the calculation of gold solubility.

Source of Fluids

The fluid sources at Pipeline are meteoric fluids, evolved fluids and magmatic fluids. The N_2/Ar ratio of fluid inclusions indicate meteoric, evolved and minor magmatic fluids in all stages of calcite mineralization. Calcite depositing fluids typically have low amounts of dissolved solids and low H_2S contents. During both stage 1 and stage 2, higher N_2/Ar suggest the mineralizing event was intrusive driven. Gold mineralization at Pipeline is associated with a fluid that has N_2/Ar >500 indicating a strong magmatic component. These fluids have elevated salinity and H_2S and variable amounts of CO_2, high enough at times to boil. Only magmatic fluids reacted with wall rocks which parallels

our understanding of magmatic fluids that are expected to be out of equilibrium with cooler country rocks.

Stage 1 calcite shows crustal sources (Fig. 4.20), one with a meteoric component, an evolved fluid and possibly a magmatic component. Stage 2 calcite has a strong meteoric signature, but the N_2/Ar ratio is slightly elevated. Quartz from the stage 3 veins has a gas signature consistent with a magmatic fluid that has evolved by interaction with crustal rocks (Fig. 4.21). The reason for the scatter in Figure 4.21 is attributed to consumption of CO_2 during decalcification that decreases the CO_2/CH_4 ratio. Gas analyses from stage 3 quartz are consistent with the magmatic source model of Sillitoe and Bonham (1990) and Berger and Bagby (1991). Stage 3 calcite analyses indicate mixing between the fluid from which the quartz was deposited and air saturated water (Fig. 4.24). The stage 5 vuggy calcite has a strong evolved gas signature with no indication of a magmatic component.

Implications for this study on genetic models for Carlin-type deposits

This study provides a consistent data set whereby field observations agree with fluid inclusion data and the chemical mass balance works. Several enigmatic aspects about Carlin-type deposits could be answered at Pipeline and include (1) the significance of carbonic fluid inclusions, (2) the hypersaline fluid inclusion chemistry and why they develop, (3) the source of gold mineralizing fluids, (4) P-T conditions during gold mineralization, (5) coeval gold mineralization and alteration, (6) an ore genesis mechanism that satisfies mass balance constraints, (7) low water-rock ratios, (8) localized alteration

haloes, and (9) the spatial relationship of Carlin-type deposits to Cretaceous or Jurassic plutons.

Magmatic activity is seen as the driving force at Pipeline and supplier of ore fluids. This is indicated by (1) N_2/Ar ratios of source fluids, (2) dating that links gold mineralization to intrusive activity and alteration, (3) a special fluid that was out of equilibrium with country rock and had a special chemistry (elevated H_2S and CO_2) not represented during other hydrothermal events, and (4) coincident with a zone of contact metamorphism around an intrusive body.

Fluid inclusion Th values ~200°C for Type 1 inclusions are similar to other Carlin-type deposits. However, these inclusions require a large pressure correction as Tt is ~300°C.

Carbonic fluid inclusions were reported at Carlin (Kuehn and Rose, 1995) but the presence of carbonic inclusions at Pipeline, both below and within ore zones, suggest that a pressure throttle did not exist. Changing CO_2 content adequately explains the development of carbonic inclusions even though sporadic phase separation occurred. High CO_2 is important for decalcification, the principle alteration style in Carlin-type deposits.

Low water-rock ratios are confirmed, implying limited alteration; this is compatible with limited fluids from a magmatic body. Limited fluid shows why significant amounts of gold are deposited despite no large scale meteoric water involvement. Mass balance calculations for gold deposition and decalcification are accounted for in a coeval event.

The oxidation event that replaced pyrite by Fe-oxides may not necessarily be supergene. Oxidation in Pipeline and other deposits could be magmatically driven during

the Eocene with oxidizing fluids migrating laterally rather than vertically.

Evidence to support Eocene gold mineralization is lacking at Pipeline, unlike deposits in Northeastern Nevada. Early Cretaceous gold mineralization at Pipeline is possibly an end-member example of Carlin-type deposits in the broader perspective. Cretaceous gold mineralization serves both to introduce gold and cause decalcification in one event. Eocene igneous activity was the driving mechanism behind circulating groundwater that caused oxidation of sulfide minerals, releasing gold. Gold was mobilized over short distances within Pipeline whereas in other deposits, circulating ground water leached gold from suitable host rocks and deposited gold in suitably prepared ground.

Genetic Model

The stage 1 dark petroliferous calcite veins are precursors to gold mineralization. Stage 1 calcite was deposited in fractures within the Roberts Mountains Formation prior to the Antler Orogeny. Depth of formation is estimated at 5 km and about 150°C. Hydrocarbons present within the fluid inclusions were locally derived. Fluid movement could be related to a magmatic event.

West- over east-directed movement along the Roberts Mountains thrust during the Antler orogeny resulted in emplacement of Upper Plate rocks on top of Lower Plate rocks. Sympathetic shears developed in the SRM, close to and subparallel to the Roberts Mountains thrust. One of the shears broadened at what is now the Pipeline deposit. Immediately underlying the shear planes, stage 2 calcite stockwork deposited from

meteoric fluid that descended downward in newly-formed fractures, under P-T conditions exceeding 300°C at ~6 km depth.

Emplacement of the Mill Canyon and Gold Acres stocks as one intrusive body occurred during the Jurassic, ca. 152 Ma. Subsequent NNW-trending faulting, which is either Jurassic or Cretaceous in age, displaced the pluton along the Cortez - Pipeline fault to form two separate bodies.

At 92.0±0.3 Ma a second intrusive body was emplaced in the Gold Acres stock area. Hydrothermal fluids caused sericitic alteration in parts of the Gold Acres stock and fluids also reacted with calcareous country rock to form a skarn. The emplacement of the intrusive body caused tension in the country rock and opening of fractures up which hydrothermal fluids flowed. Stage 3 sericite and quartz were deposited on the sidewalls of the veins and limited sulfidation and gold mineralization occurred. The hydrothermal fluids entered the shear zones where permeability was highest following ground preparation during the Antler orogeny. Pressure-temperature conditions that existed were 300°C and 2000 bar lithostatic. Fluctuations of CO_2 content in the ore fluids caused minor fluid immiscibility. Decalcification reactions liberated Ca^{++}, HCO_3^- and minor Fe^{++} ions increasing the ionic strength of the fluid and is reflected as an increase of salinity reported in eq. wt. % NaCl. The Fe^{++} scavenged H_2S in solution to form pyrite and in so doing dropped the solubility of gold as a bisulfide complex by two orders of magnitude. The mineralization model is summarized in Figure 5.12. Silicification occurred locally as a response to drop in temperature. Calculations give the mass of ore fluid to rock in the deposit at a maximum of 6:1. Toward the end of the event, fracturing extended outwards from the deposit. As the hydrothermal system collapsed, meteoric fluids under hydrostatic

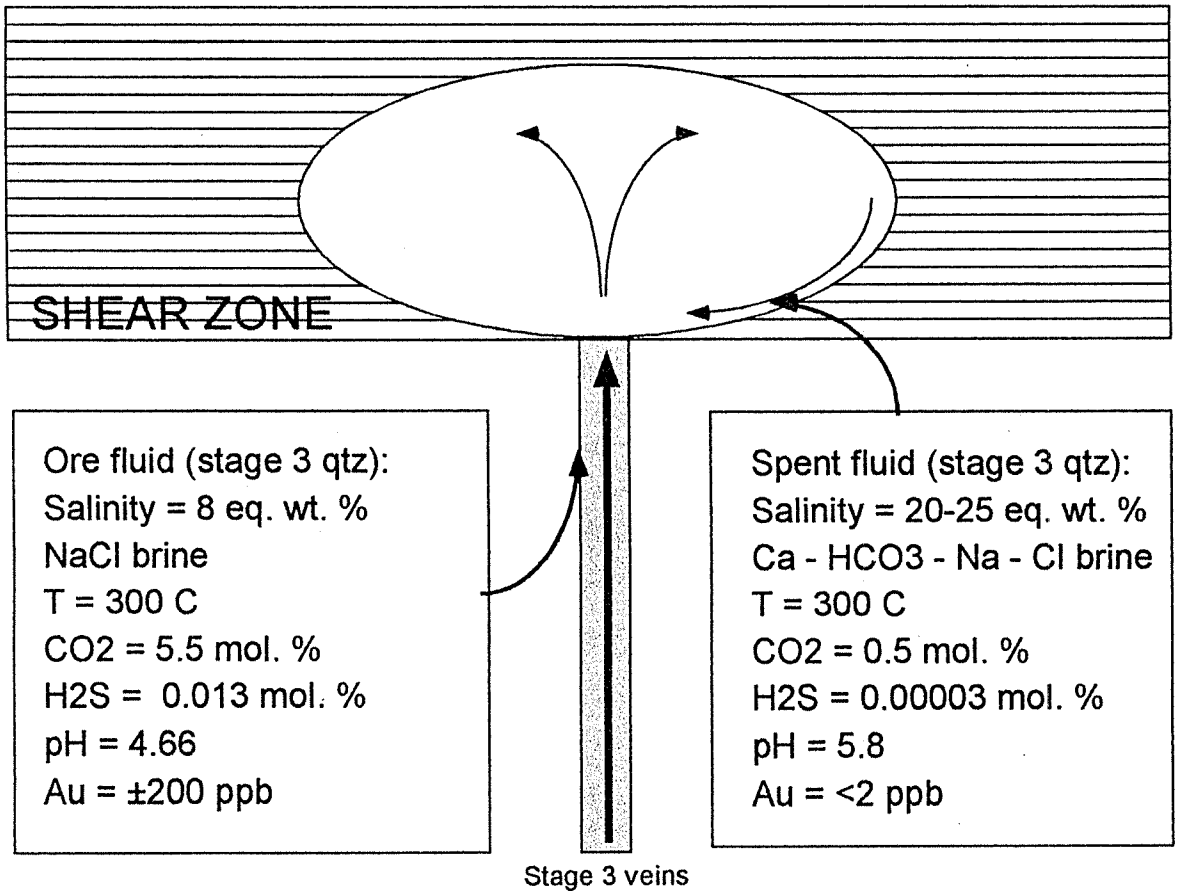

Figure 5.12 Schematic model for Pipeline gold mineralization during stage 3 showing the chemical differences between the ore fluid and the spent fluid.

conditions penetrated the country rock. Minor calcite was deposited from the fluids as they warmed up.

Stage 4 oxidation of the deposit occurred between 92 and 11 Ma, prior to development of stage 5 veins. Circulating meteoric water caused replacement of pyrite by Fe-oxides; acidic fluids were produced by the oxidation process and possibly induced further decalcification. Stage 3 calcite that may have been deposited in the deposit was destroyed. Oxidizing fluids did not penetrate above the shear zones to any extent and migration of oxidizing fluids appears to have been lateral rather than vertical. It is not known if this event was coeval with ~34-35 Ma dike emplacement in the region; the magmatic activity was potentially a heat source to drive circulating meteoric water.

Post-oxidiation, stage 5 vuggy calcite was precipitated in open fractures that occur above, within, and below the deposit. During one precipitation cycle, a calcareous sediment was deposited. Drusey calcite subsequently covered this sediment.

Basin-and-Range extension at around 11 Ma tilted the deposit by about 15°. Pipeline was nearly exposed by erosion prior to 11 Ma but was buried by basin fill sediments as Crescent Valley formed.

CHAPTER 6

CONCLUSION

My conclusions are summarized as follows:

(1) The Pipeline deposit is the result of a single, Early Cretaceous, hydrothermal event, in which ore solutions dissolved calcite and deposited gold and pyrite. Field evidence does not exist which supports any other significant gold-bearing event. Calcite veining occurred during 2 events before stage 3 mineralization but were not gold-mineralizing events.

(2) Gold mineralization occurs at ~300°C at 2 kbar pressure under lithostatic conditions (an equivalent of ~8 km depth).

(3) Ore solutions with magmatic components, salinity about 8 eq. wt. % NaCl, and up to 8 mol. % CO_2 migrated up subvertical fractures into the Pipeline structural zone. The slightly acidic ore fluids (pH ~4.66) reacted with calcite in the Roberts Mountain Formation resulting in decalcification as the fluid mineralized and altered the Formation.

(4) Gold deposition is the result of sulfidation. Iron released by decalcification reacted with H_2S to form pyrite, resulting in a breakdown of bisulfide-gold complexes, and gold deposition.

(5) Mineralization occurs with no measurable change in fluid P or T, and mineralization resulted in spent ore solutions with up to 25 eq. wt. % NaCl salinity and >1.0 Ca/Na ratios. Calcite removal resulted in volume loss, increasing insoluble components such as silt, pyrite and clay particles. Later, under non-lithostatic

pressures, near surface fluids enter fractures and deposit calcite.

(6) The source fluids associated with gold mineralization have a distinctive gas signature i.e., a magmatic component and most likely originating from a skarn where the magmatic fluids reacted with carbonaceous calcareous rocks at ~400°C. The ore fluids have greater than 3 mol.% CO_2, H_2S in the order of 0.01 mol.%, 0.5 to ~1 mol.% CH_4, and N_2/Ar >500.

(7) The N_2/Ar ratio of the ore fluid gas exceeds 500 that is consistent with a magmatic fluid component. Meteoric and evolved fluids are recognized by gas analysis and are associated with both calcite mineralization.

(8) Timing, gas ratios, and fluid chemistry indicate gold mineralization was the product of magmatic activity which agrees with the Sillitoe and Bonham (1990) model that magmatic fluids are responsible for Carlin-type gold mineralization.

(9) The process in which Type 2 (CO_2-dominated) inclusions form differs from the model proposed by Kuehn and Rose (1996). I see the process as a result of intermittent boiling in response to varying fluid CO_2 contents. Type 2 inclusions form once the CO_2-brine solvus is reached. P-T conditions are unchanged.

(10) Three thermal epochs occur. The first occurs at 152 Ma and is related to the intrusion of the Mill Canyon and Gold Acres stock. The second thermal epoch occurred about 92 Ma; stage 3 gold mineralization, and alteration of Gold Acres stock are within this time frame. The third thermal epoch is represented by dikes ~34 to 35 Ma.

(11) Dating of stage 3 vein sericite gives an integrated age of 92.0±0.3 Ma. Illite from ore zones give integrated ages that can be interpreted to be consistent with stage 3.

(12) Oxidation of the deposit occurs prior to Basin-and-Range extension and possibly during the Eocene.

REFERENCES

Arehart, G.B., Chryssoulis, S.L., and Kesler, S.E., 1993a, Gold and arsenic in iron sulfides from sediment-hosted disseminated gold deposits: Implications for depositional processes: ECONOMIC GEOLOGY, v. 88, p. 171-185.

Arehart, G.B., Foland, K.A., Naeser, C.W., and Kesler, S.E., 1993b, $^{40}Ar/^{39}Ar$, K/Ar, and fission track geochronology of sediment-hosted disseminated gold deposits at the Post-Betze, Carlin Trend, northeastern Nevada: ECONOMIC GEOLOGY, v. 88, p. 622-646.

Bailey, S.W., 1980, Structures of layer silicates: *in* Brindley, G.W., and Brown, G., eds., Crystal structures of clay minerals and their X-ray identification: Mineralogical Society, United Kingdom, 123 p.

Bakken, B.M., 1990, Gold mineralization, wall rock alteration, and the geochemical evolution of the hydrothermal system in the main orebody, Carlin Mine, Nevada: Ph.D. dissertation, Stanford University, 200 p.

Bakken, B.M., and Einaudi, M.T., 1989, Volume-loss and mass transportation during hydrothermal alteration and weathering, Carlin Gold Mine, Nevada: Geological Society of America Abstracts with Programs, v. 21, no. 6, p. 295.

Benning, L.G., and Seward, T.M., 1996, Hydrosulphide complexing of Au(I) in hydrothermal solutions from 150-400°C and 500-1500 bar: Geochimica Cosmochimica Acta, v. 60, p. 1849-1971.

Bendrick, M.B., 1989, Mass spectrometric analysis of gases in fluid inclusions from the Carlin gold deposit, Eureka County, Nevada: Masters thesis, University of Tulsa, 134 p.

Berger, B.R., and Bagby, W.C., 1991, The geology and origin of carlin-type gold deposits, *in* Foster, R.P., Gold metallogeny and exploration: Blackie and son, Glasgow, p. 210-248.

Bowers, T.S., and Helgeson, H.C., 1983, Calculation of the thermodynamic and geochemical consequences of non-ideal mixing in the system H_2O-CO_2-NaCl on phase relations in geologic systems: Equation of state for H_2O-CO_2-NaCl fluids at high pressures and temperatures: Geochimica Cosmochimica Acta, v. 47, p. 1247-1275.

Brown, P.E., Hageman, S.G., and Vanko, D.A., 1995, Macflincor and its application to fluids in Archean lodegold deposits: Geochimica et Cosmochimica Acta, v. 59, p. 3943-3952.

Cline, J.S., Hofstra, A.H., Rye, R.O., and Landis, G.P., 1996, Stable isotope and fluid inclusion evidence for a deep sourced ore fluid at the Getchell, Carlin-type, gold deposit, Nevada: PACROFI VI, Abstract Volume, p. 33-35.

Cline, J.S., Cail, T., Weaver, K., and Shigehiro, M., 2000, The Geochemistry of the Getchell Carlin-type gold deposit; Geology and ore deposits 2000: The Great Basin and Beyond, Geological Society of Nevada, Program with Abstracts, p. 42.

Dong, H., Hall, C.M., Peacor, D.R., and Halliday, A.N., 1995, Mechanisms of Argon Retention in Clays revealed by laser ^{40}Ar-^{39}Ar dating, Science, v. 267, p. 355-359.

Drits, V., Srodon, J., and Eberl, D.D., 1997, XRD measurement of mean crystalline thickness of illite and illite/smecite: Reappraisal of the Kubler Index and the Scherrer Equation, Clay and Clay Minerals, v. 45, p. 461-475.

Drummond, S.E., 1981, Boiling and mixing of hydrothermal fluids: Chemical effects on mineral precipitation: Ph.D. Dissertation, Pennsylvania State University, 380 p.

Folger, H.W., Snee, L.W., Mehnert, H.H., and Hofstra, A.H., 1996, Significance of K-Ar and $^{40}Ar/^{39}Ar$ dates from mica in Carlin-type gold deposits: Evidence from the Jerritt Canyon District, Nevada, *in* Coyner, A.R., and Fahey, P.L., eds., Geology and Ore Deposits of the American Cordillera: Geological Society of Nevada Symposium Proceedings, Reno/Sparks, Nevada, April 1995, p. 41-60.

Foo, S.T., Hays, Jr., R.C., and McCormack, J.K., 1996, Geology and mineralization of the Pipeline Gold Deposit, Lander County, Nevada, *in* Coyner, A.R., and Fahey, P.L., eds., Geology and Ore Deposits of the American Cordillera: Geological Society of Nevada Symposium Proceedings, Reno/Sparks, Nevada, April 1995, p. 95-109.

Foo, S.T., and Hebert, J.P., 1987, Geology of the Horse Canyon deposit, Eureka County, Nevada, *in* Bulk Mineable Precious Metals Deposits of the Western U.S., Reno, Nevada: 1987, Geological Society of Nevada Guidebook for Field Trips, p. 326-332.

Foster, D.A., Harrison, T.M., Copeland, P., and Heizler, M.T., 1990. Effects of excess argon within large diffusion domains on K-feldspar age: Geochim. et Cosmochim. Acta., v. 54, p. 1699-1708.

Fournier, R.M., 1986, Carbonate transport and deposition in the epithermal environment: Reviews in Economic Geology, v. 2, p. 63-72.

Fournier, R.O., 1981, Application of water chemistry to geothermal exploration and reservoir engineering; *in* Ryback, L., and Muffler, L.J.P., Eds., Geothermal Systems: Principles and case histories, Wiley New York, p.109-143.

Giggenbach, W.F., 1981, Geothermal mineral equilibria: Geochim. et Cosmochim. Acta., v. 45, 393-410.

Gilluly, J., and Masursky, H., 1965, Geology of the Cortez Quadrangle Nevada: Geological Survey Bulletin 1175, 117 p.

Graney, J.R., Kesler, S.E., and Jones, H.D., 1991, Application of gas analysis of jasperoid inclusion fluid to exploration for micron gold deposits, Journal of Geochemical Exploration, v. 42, p. 91-106.

Grauch, V.J.S., Jachens, R.C., and Blakely, R.J., 1995, Evidence for a basement feature related to the Cortez disseminated gold trend and implications for regional exploration in Nevada: ECONOMIC GEOLOGY, v. 90, p. 203-207.

Groff, J.A., 1996, Geochronology and origin of auriferous fluids for the Getchell and Twin Creeks mines, Humbolt County, Nevada, Unpublished Ph.D. dissertation: Socorro, New Mexico Institute of Mining and Technology, 291 p.

Groff, J.A., Heizler, M.T., McIntosh, W.C., and Norman, D.I., 1997, $^{40}Ar/^{39}Ar$ dating and mineral paragenesis for Carlin-type gold deposits along the Getchell trend, Nevada: Evidence for Cretaceous and Tertiary gold mineralization: ECONOMIC GEOLOGY, v. 92, p. 601-622.

Harrison, T.M., Duncan, I., and McDougall, I., 1985, Diffusion of ^{40}Ar in biotite: temperature, pressure and compositional effects: Geochim. et Cosmochim. Acta., v. 49, p. 2461-2468.

Heinrich, C.A., Henley, R.W., and Seward, T.M., 1989, Hydrothermal Systems: Adelaide, South Australia, Australian Mineral Foundation, 74 p.

Helgeson, H.C., and Kirkham, D.H., 1974, Theoretical prediction of the thermodynamic behavior of aqueous electrolytes at high pressures and temperatures; II, Debye-Hückel parameters for activity coefficients and relative partial molal properties: American Journal of Science, v. 274, p. 1199-1261.

Henley, R.W., Truesdell, A.H., and Barton, P.B., 1984, Metals in hydrothermal fluids, *in* Fluid-mineral equilibria in hydrothermal systems: Society of Economic Geology Reviews in Economic Geology, v. 1, p. 115-127.

Hofstra, A.H., Northrop, H.R., Rye, R.O., Landis, G.P., and Birak, D.J., 1988, Origin of sediment-hosted gold deposits by fluid mixing; evidence from jasperoids in the Jerritt Canyon gold district, Nevada, U.S.A.: Bicentennial gold, Geological Society of Australia Abstracts, v. 22, p. 284-289.

Hofstra, A.H., Snee, L.W., Rye, R.O., Folger, H.W., Phinisey, J.D., Loranger, R.J., Dahl, A.R., Naeser, C.W., Stein, H.J., and Lewchuk, M., 1999, Age constraints on Jerrit Canyon and other Carlin-Type deposits in the Western United States - Relationship to Mid-Tertiary extension and magmatism: Economic Geology, v. 94, p. 769-802.

Ilchik, R.P., and Barton, M.D., 1996, Physical and chemical contraints for an amagmatic origin of Carlin-type gold deposits, a source-sink approach, *in* Coyner, A.R., and Fahey, P.L., eds., Geology and ore deposits of the American Cordillera: Geological Society of Nevada Symposium Proceedings, Reno/Sparks, Nevada, April 1995, p. 687-708.

Johnson, J.W., Oelkers, E.H., and Helgeson, H.C., 1992, SUPCRT92: A software package for calculating the standard molal thermodynamic properties of minerals, gases, aqueous species, and reactions from 1 to 5000 bar and 0°C to 1000°C: Computers and Geosciences, v. 18, p. 899-947.

Kamali, C., (1996), Mineralogy and geochemistry of the Lone Tree mine, Humboldt County, Nevada: Unpub. M.S. thesis, New Mexico Institute of Mining and Technology.

Katz, D.L., Cornell, D., Kobayashi, R., Poetmann, F.H., Vary, J.A., Elenbaas, J.R., and Weinaug, C.F., 1959, Handbook of natural gas engineering: McGraw-Hill Book Company, New York, 802 p.

Kubler, B., 1964, Clays as indicators of metamorphism: Revue de I'Institut Francais du Petrole, v. 19, p. 1093-1112.

Kuehn, C.A., 1989, Studies of disseminated gold deposits near Carlin, Nevada: evidence for a deep geologic setting of ore formation: Ph.D. dissertation, Pennsylvania State University, University Park, 418 p.

Kuehn, C.A., and Rose, A.W., 1995, Carlin gold deposits, Nevada: Origin in a deep zone of mixing between normally pressured and overpressured fluids: ECONOMIC GEOLOGY, v. 90, p. 17-36.

Lamb, J.B., 1995, A petrographic fluid inclusion study of the Purple Vein and Post/Betze orebodies, Carlin, Nevada: Masters thesis, University of Nevada, Las Vegas, 111 p.

Lisle, R.E., and Desrochers, G.J., 1988, Geology of the Hilltop Gold Deposit, Lander County, Nevada: *in* Schafer, R.W., Cooper, J.J., and Vikre, P.G., eds., Bulk mineable precious metal deposits of the Western United States, p. 101-116.

Lonker, S.W., and Fitz Gerald, J.D., 1990, Formation of coexisting 1M and 2M polytypes of illite from an active hydrothermal system: American Mineralogist, v. 75, p. 1282-1289.

Lovera, O.M., Richter, F.M., and Harrison, T.M., 1989, $^{40}Ar/^{39}Ar$ thermochronometry for slowly cooled samples having a distribution of domain sizes: J. Geophy. Res., v. 94, n. 17, p. 971-935.

McCormack, J.K., and Hays, Jr., R.C., 1996, Crescent Valley: A model for reconstruction of district mineralization in the Basin and Range, *in* Coyner, A.R., and Fahey, P.L., eds., Geology and ore deposits of the American cordillera: Geological Society of Nevada Symposium Proceedings, Reno/Sparks, Nevada, April 1995, p. 635-646.

McDougall, I., and Harrison, T.M., 1988, Geochronology and Thermochronology by the $^{40}Ar/^{39}Ar$ method. Oxford University Press, New York, 212 p.

Nolan, T.B., Merriam, C.W., Williams, J.S., 1956, The stratigraphic section in the vicinity of Eureka, Nevada: U.S.Geol. Professional Paper 276, 77 p.

Norman, D.I., and Sawkins, F.J., 1987, Analysis of gases in fluid inclusions by mass spectrometer: Chemical Geology, v. 61, p. 110-121.

Norman, D.I., and Moore, J.N., 1997, Gaseous species in fluid inclusions: a fluid tracer and indicator of fluid processes [abs.]:European current research on fluid inclusions, No. XIV, Nancy, France, Abstracts, p. 243-244.

Norman, D.I., Chomiak, B.A., and Moore, J.N., 1998, Approaching equilibrium from the hot and cold sides in the FeS_2-FeS-Fe_3O_4-H_2S-CO_2-CH_4 system in the light of fluid inclusion gas analysis, *in* Arehart, G.B., and Hulston, J.R., eds., Proceedings of the 9th International Symposium on Water-Rock Interaction: Rotterdam, A.A. Balkema, p. 565-568.

Norman, D.I., and Moore, J.N., 1999, Methane and excess N_2 and Ar in geothermal fluid inclusions: 24th Workshop on Geothermal Reservoir Engineering, California, Stanford University, Proceedings, p. 196-202.

Onstott, T.C., Miller, M.L., Ewing, R.C., Arnold, G.W., and Walsh, D.S., 1995, Recoil refinements: Implications for the $^{40}Ar/^{39}Ar$ dating technique: Geochim. et Cosmochim. Acta., v. 59, p. 1821-1834.

Prini, R.F., and Crovetto, R., 1989, Evaluation of data on solubility of simple apolar gases in light and heavy water at high temperature, J. Phys. Chem. Ref. Data, v. 18, p. 1231-1243.

Radtke, A.S., Rye, R.O., and Dickson, F.W., 1980, Geology and stable isotope studies of the Carlin gold deposit, Nevada: ECONOMIC GEOLOGY, v. 75, p. 641-672.

Roberts, R.J., 1960, Alinement of mining district in north-central Nevada, *in* Geological Survey research 1960: U.S.Geological Survey Professional Paper 400-B, p. B17-B19.

Roberts, R.J., Hotz, P.E., Gilluly, J., and Ferguson, H.G., 1958, Paleozoic rocks of north-central Nevada: American Association of Petroleum Geologists Bulletin, v. 42, p. 2813-2857.

Rye, R.O., Doe, B.R., and Wells, J.D., 1974, Stable isotope and lead isotope study of the Cortez, Nevada, gold deposit and surrounding area: Journal of Research of the U.S. Geological Survey, v. 2, n. 1, p. 13-23.

Rye, R.O., 1985, A model for the formation of carbonate-hosted disseminated gold deposits based on the geologic, fluid-inclusion, geochemical, and stable-isotope studies of the Carlin and Cortez deposits, Nevada: U.S. Geological Survey Bulletin 1646, p. 35-42.

Seedorf, E., 1991, Magmatic, extension, and ore deposits of Eocene to Holocene age in the Great Basin; mutual effects and preliminary proposed genetic relationships, *in* Raines, G.L., Lisle, R.E., Schafer, R.W., and Wilkinson, W.H., eds., Geology and Ore Deposits of the Great Basin: Geological Society of Nevada Symposium Proceedings, Reno/Sparks, Nevada, 1990, p. 133-178.

Seward, T.E., 1973, Thio complexes of gold and the transport of gold in hydrothermal ore solutions: Geochimica et Cosmochimica Acta, v. 37, p. 379-399.

Shepherd, T.J., and Rankin, A.H., 1998, Fluid inclusion techniques of analysis: Reviews in Economic Geology, v. 10, p. 125-149.

Shepherd, T.J., Rankin, A.H., and Alderron, D.H.M., 1985, A practical guide to fluid inclusion studies: Glasgow and London, Blackie & Son Ltd., 239 p.

Silberman, M.L., and McKee, E.H., 1971, K-Ar ages of granitic plutons in north-central Nevada: Isochron/West, no. 71-1, p. 15-32.

Sillitoe, R.H., and Bonham, H.F., 1990, Sediment-hosted gold deposits: distal products of magmatic- hydrothermal systems: Geology, v. 18, p. 157-161.

Simmons, S.F., Arehart, G., Simpson, M.P., Mauk, J.L., 1999, Origin of massive calcite veins in the Golden Cross low-sulphidation, epithermal Au-Ag deposit, New Zealand: ECONOMIC GEOLOGY, v. 95, p. 99-112.

Steiger, R.H., and Jager, E., 1977, Subcommission on geochronology: Convention on the use of decay constants in geo- and cosmochronology. Earth Planet. Sci. Letters, v. 36, p. 359-362.

Stenger, D.P., Kesler, S.E., Peltonen, D.R., and Tapper, C.J., 1998, Deposition of gold in Carlin-type deposits: The role of sulfidation and decarbonation at Twin Creeks, Nevada: ECONOMIC GEOLOGY, v. 93, p. 201-215.

Stewart, J.H., 1980, Geology of Nevada: Nevada Bureau of Mines and Geology Special Publication 4, 132 p.

Takenouchi, S., and Kennedy, G.C., 1965, The solubility of carbon dioxide in NaCl solutions at high temperatures and pressures: American Journal of Science, v. 263, p. 445-454.

Teal, L., and Jackson, M., 1997, Geologic overview of the Carlin Trend Gold Deposits and descriptions of recent deep discoveries, SEG Newsletter, October 1997, no. 31, p. 12-25.

Truesdell, A.H., 1976, GEOTHERM, a geothermometric computer program for hot spring systems: Proc. 2nd U.N. Symp. on the development of Geothermal Resources, San Francisco, 1975, v. 1, p. 831-836.

Weaver, C.E., and Boekstra, B.R., 1984, Illite-mica, *in*, Weaver, C.E., ed., Shale slate metamorphism in Southerna Appalachians: Elsevier, Amsterdam, p. 67-199.

Wells, J.D., Stoiser, L.P., and Elliot, J.E., 1969, Geology and geochemistry of the Cortez gold deposit, Nevada: ECONOMIC GEOLOGY, v. 64, p. 526-537.

Wells, J.D., Elliot, J.E., and Obradovich, J.D., 1971, Age of the igneous rocks associated with ore deposits, Cortez-Buckhorn area, Nevada: United States Geological Survey Prof. Paper 750-C, p. C127-C135.

Yoder, H.S., and Eugster, H.P., 1955, Synthetic and natural muscovites: Geochimica et Cosmochimica Acta, v. 8, p. 225-280.

Yonaka, B.E., 1994, Gold-bearing granitoids of southern Ghana, West Africa: Unpublished masters thesis: Socorro, New Mexico Institute of Mining and Technology, 181 p.

APPENDIX A

SAMPLE LIST

Sample #	Drillhole	Depth(ft)	Remarks
NB-1	DP-412	604.9	Dark calcite vein with banding.
NB-2	DP-413	867.5	Last crystallizing phase of stubby coxcomb clear calcite on top of rhombohedral calcite.
NB-3	DP-412	305	Botriodal calcite with earlier crystallized phase removed.
NB-4	DP-412	393.5	Clear and white calcite with small core of light brown colored calcite.
NB-5	DP-413	895.5	Quartz from qtz-carbonate vein.
NB-6	DP-412	929	Calcite (pale brown) ontop of botrioidal Mn oxide which itself coats orange fine-grained calcite.
NB-7	DP-432	633.5	Buff carbonate sediment infilling vugs.
NB-8	DP-471	515.7	Euhedral barite occurring as thin tabular laths as late-stage vuggy infillings (thought to be supergene).
NB-9	DP-452	296.7	Quartz vein.
NB-10	DP-471	515.7	Barite. Vuggy infillings.
NB-11	DP-422	644.6	Calcite dogtooth spar (light brown color) from vug.
NB-12	Crescent pit		Calcite vein striking 155 degrees.
NB-13	DP-424	448	Calcite which postdates the tannish calcareous sediment.
NB-14	DP-472	450	Barite from vug.
NB-15			Southwest fault gouge zone collected 27' south of G14 on 4900 level. It trends N40E.
NB-16			N40E fault gouge zone (Fence Fault) collected at G20, 4900 level Stage 1.
NB-17			N40E fault gouge collected at G21, 4900 level Stage 1.
NB-18			N5W (fault gouge of Pipeline orientation collected at G8, 4860 level, CP.
NB-19	DP-476	880	Argillization which is superimposed upon silicification producing light fish-belley gray color.
NB-20	DP-98	486	30 percent argillization with laminae of hematite (0.3%).
NB-21	DP-76	584.3	
NB-22	DP-471	520	Tannish strongly argillized material.
NB-23	DP-468	343.5	
NB-30	DP-504	819	Porphyroblastic scapolite in fresh to slightly bleached host rock.
NB-31	DP-507	630.5	Breccia-filling which resembles concrete.

NB-32	DP-511	1200	Dark calcite vein (first calcite event).
NB-33	DP-511	1200	Younger qtz carbonate vein with initial euhedral qtz followed by pyrite, followed by infill of white calcite. Vein dips 75 degrees below horizontal.
NB-34	DP-98	655-660	White calcite vein with galena.
NB-35	DP-504	1105	Quartz carbonate vein in slightly sheared, moderately carbonaceous to fresh host rock. Quartz rim with calcite core.
NB-36	DP-504	1140	Quartz vein in slightly sheared moderately carbonaceous host rock.
NB-37	DP-504	1403.4	Quartz carbonate filled shear in fresh host rock.
NB-38	DP-507	746.1	Quartz carbonate vein whereby quartz appears to postdate the calcite; hosted within light tan moderately argillized SRM.
NB-39	DP-507	724	Calcite veins with tannish sediment filling coated by clear drusey calcite.
NB-40	DP-520	785.8	Gray mottled calcite vein hosted in tan weakly argillized SRM.
NB-41	DP-520	994.2	2" thick white quartz vein. Qtz appears to replace calcite.
NB-42	DP-520	784	Two white calcite veins.
NB-43	DP-521	912	Abundant dark calcite veins.
NB-44	DP-521	1002.8	Quartz carbonate vein with euhedral qtz grown from the sidewall and infilled by calcite.
NB-45	DP-521	1152	Quartz filled shear hosted by carbonaceous SRM.
NB-46	DP-525	1116.5	Dark calcite vein.
NB-47	DP-536	923.2	Quartz carbonate vein with euhedral qtz and core of white calcite.
NB-48	DP-532	903.8	Quartz carbonate vein with euhedral qtz and infill of calcite.
NB-49	DP-536	1097	Moderate silicification in strongly carbonaceous, microbrecciated, welded zone.
NB-50	DP-511	1286.2	Quartz filled shear hosted in strongly carbonaceous SRM.
NB-51	DP-532	1081	Framboidal pyrite in weakly carbonaceous SRM.
NB-52	DP-536	1124.5	Brecciation and microbrecciation in strongly carbonaceous SRM with breccia fill of sulphides almost totally replaced by goethite.
NB-53	DP-523	900	Goethitic fracture filling within microbrecciated host rock.
NB-54	DP-511	1354	Microbrecciation in strongly carbonaceous SRM within sheared interval.
NB-55	DP-532	1222.5	Microbrecciated shear zone with calcite microveining within carbonaceous SRM.

NB-56	DP-511	1313.7	Folded tiger stripe with replacement pyrite, hosted by moderately carbonaceous SRM.
NB-57	DP-104	599	Grayish tan, moderately to strongly argillized SRM.
NB-58	DP-113	476	Whiteish tan strongly argillized SRM with goethite fracture surfaces.
NB-59	DP-113	486	Off-white strongly sericitised, totally decalcified SRM.
NB-60	DP-435	585	Moderately hematitic, strongly argillized, sheared SRM.
NB-61	DP-507	736.3	Tannish vuggy sediment.
NB-62	DP-104	494.5	Grayish brownish tan moderately argillized SRM.
NB-63	DP-104	510-520	Moderately argillized SRM with goethite fracture coatings and Mn oxides.
NB-64	DP-104	520-530	Moderately argillized SRM with high Mn oxides.
NB-65	DP-104	577	Tan moderately argillized SRM.
NB-66	DP-104	681	Red moderately hematitic, moderately to strongly argillized SRM.
NB-67	DP-105	440	Weakly oxidised, moderately argillised SRM.
NB-68	DP-105	577	Weakly oxidised, moderately argillized SRM with high Mn oxide content.
NB-69	DP-111	680	Weakly hematitic, moderately to strongly argillized SRM.
NB-70	DP-111	825	Weakly argillized, limey calcareous siltstone below a shear zone.
NB-71	DP-111	849	Weakly hematitic, moderately argillized interbed within limey calcareous siltstone.
NB-72	DP-111	882	Weakly oxidized, moderately argillized SRM.
NB-73	DP-113	260	Moderately argillized SRM.
NB-74	DP-113	540	Brownish tan, moderately argillized SRM.
NB-75	DP-113	680	Brownish tan, moderately argillized SRM.
NB-76	DP-105	562	Quartz vein hosted in oxidised SRM (Qtz appears to postdate the oxidation).
NB-77	DP-495	710,4	7mm dark calcite vein hosted in grayish tan SRM.
NB-78	N25W		White calcite vein in Crescent pit.
NB-79	DP-428	424,5	White calcite from vug with Mn-oxide predating calcite and calcareous sediment postdating.
NB-80	DP-460	382	Quartz filling in vug.
NB-81	DP-412	1253	Quartz filled shear zone with styolites.
NB-82	DP-511	1171,3	Fresh 1mm-sized pentagonal-dodecahedral pyrite in gray moderate to strongly argillised SRM.
NB-84	DP-532	1508,5	Light gray flame-like calcite veining which postdate styolites hosted in SRM.
NB-85	DP-532	1508,5	Creamish white calcite vein which dips 60 from horizontal and crosscuts NB-84. Core of vein becomes more clearer.

NB-86	DP-532	1508,5	Slightly creamish white calcite vein which postdates NB-84 and NB-85 and is weakly vuggy. Mn-oxide coating formed on sidewall prior to calcite deposition.
NB-87	Pit		Off-white, totally decalcified, very strongly argillized SRM.
NB-88	DP-633	753,5'	Tannish, totally decalcified, porous, bleached SRM.
NB-89	DP-633	981,5'	Fresh, weakly carbonaceous, unaltered SRM.
NB-90	DP-633	955'	Recrystallized pyrite aggregate hosted in fresh SRM.
NB-91	DP-618	558,5'	Very strong limonite in very strongly argillized sheared zone.
NB-92	DP-618	551'	Very strong hematite with goethite and minor Mn in very strongly argillized shear zone.
NB-93	DP-618	555'	Very strong Mn oxides in very strongly argillized shear zone.
NB-94	DP-633	1054'	Microbreccia of silicified, weakly carbonaceous SRM filled in with darkish gray quartz. Quartz matrix is estimated at 70 percent.
NB-95	DP-602	360,5'	Quartz vein with oxidised pyrite. One crystal of stibnite occurs in a vug and paragenetically postdates the quartz.
NB-96	DP-603	437'	50 percent silicification of SRM.
NB-97	DP-616	688'	Very strong silicification in sheared zone. Silicification appears to postdate shearing.
NB-98	DP-602	365,5'	1" quartz vein parallel to bedding which has secondary calcite microveins. The sample infills a shear.
NB-99	DP-630	1385'	1" quartz vein dipping about 10 degrees to core axis and is probably related to the weak to moderate silicification in the hosting moderately carbonaceous SRM. Vein has 1mm quartz followed by 0,2mm chalcedony and then infilling by quartz.
NB-100	DP-632	855'	1" quartz carbonate vein dipping 45 degrees to core axis. Quartz is euhedral and primary.
NB-101	DP-633	1054'	Microbreccia with quartz matrix within weakly carbonaceous, silicified SRM.
NB-102	DP-641	915,5'	12 mm quartz chalcedony vein dipping 160 degrees and striking subparallel to bedding (dips opposite to bedding).
NB-103	DP-641	718,5'	4cm quartz vein dipping 150 degrees which has secondary calcite (look out for secondary FI).
NB-104	DP-641	778,5'	1" quartz carbonate vein dipping 150 degrees and comprises euhedral quartz and infilling of white calcite.

NB-105	DP-617	699,5'	15mm quartz carbonate vein dipping 130 degrees. The calcite has a slight orange stain.
NB-106	DP-640	865'	1" quartz carbonate vein (maybe same as NB-104)
NB-107	Pit 4440 level		Quartz vein with bladed quartz collected by TGT. Orientation of vein is N10W dip 81NE. Later infilling of openspace by orpiment and rare stibnite.
NB-108	DP-451	381'	Quartz vein with boxworks after sulphide minerals. Euhedral quartz occurs.
NB-109	Gold Acres		Mineralized quartz vein collected by Charles Tarnocai.
NB-110	Gold Acres		Mineralized quartz vein collected by Charles Tarnocai.
NB-111	DP-640	821,2'	A 4cm wide quartz-pyrite-carbonate vein dipping 30 degrees to core axis. Pyrite is zoned, occuring predominantly on one sidewall. Quartz paragenetically postdates pyrite whereas calcite postdates quartz.
NB-112	DP-640	803'	Almost black, moderately carbonaceous, laminated SRM with very sparse dust pyrite and about 5 percent fine crackle white calcite veins.

Collar positions of the drillholes from which samples were collected

Drillhole	Easting	Northing	Elevation
DP-76	102436.65	59169.39	5058.08
DP-98	102450.19	59401.40	5059.38
DP-104	102641.23	59200.41	5050.53
DP-105	102839.40	59200.41	5044.43
DP-111	103041.18	59201.73	5048.57
DP-113	102241.59	59200.17	5064.03
DP-412	102910.33	57748.36	5024.11
DP-413	103151.26	57638.23	5019.45
DP-422	104631.59	56963.63	4991.09
DP-424	104427.01	56759.90	4989.37
DP-428	104422.42	56379.58	4982.26
DP-432	103656.88	56396.23	4990.21
DP-435	104046.73	59192.16	5043.23
DP-451	103004.44	54512.01	4970.81
DP-452	103105.20	54412.42	4967.25
DP-460	103488.94	54822.62	4964.92
DP-468	103558.91	55849.50	4985.87
DP-471	103347.12	55989.31	4992.23
DP-472	103157.33	55844.15	4995.50
DP-476	104300.29	59076.04	5039.64
DP-495	104735.33	56275.19	4976.61
DP-504	101838.83	58513.54	5077.18
DP-507	103735.74	58099.83	5026.23
DP-511	102529.98	58380.88	5047.24
DP-520	103020.63	57798.63	5020.61
DP-521	103125.16	57894.38	5018.18
DP-523	103313.88	57922.78	5012.57
DP-525	103517.53	57899.45	5014.06
DP-532	103920.39	57478.13	5008.06
DP-536	103415.82	57609.83	5011.13
DP-602	103996.40	55333.13	4965.02
DP-603	104078.70	55444.07	4966.58
DP-616	104036.50	56220.16	4982.40
DP-617	103777.90	56311.69	4993.43
DP-618	103563.40	56310.61	4989.62
DP-630	103315.60	57018.26	5006.60
DP-632	102445.30	56908.01	4798.04
DP-633	102316.60	57117.33	4797.95
DP-640	102285.42	58424.38	4740.00
DP-641	101971.06	58580.52	4780.00

APPENDIX B

Sample	Mineral	Type	L+V=L Th	Tm(ice)	Salinity	L+V=L ThCO2	TmCO2	CO2 Vol. Fraction
NB-33	Quartz	primary	188.4	-5.4	8.41			
NB-33	Quartz	primary	179.4	-5.2	8.14			
NB-33	Quartz	primary	218.7					
NB-33	Quartz	primary	187.5					
NB-33	Quartz	primary	192.8					
NB-33	Quartz	primary	210.8					
NB-33	Quartz	primary	199.3					
NB-33	Quartz	primary	198.4					
NB-33	Quartz	secondary	>250			+17.8	-57.6	0.07
NB-33	Quartz	secondary	282.1	+4.7	9.44	+20.8		0.07
NB-33	Quartz	secondary	>295	+4.0	10.49	+27.5		0.07
NB-33	Quartz	primary	202.5	-4.9	7.73			
NB-33	Quartz	primary	204.5	-5.1	8			
NB-33	Calcite	primary	222.8	-1.8	3.06			
NB-33	Calcite	primary	218.7	-2	3.39			
NB-33	Calcite	primary	240	-2	3.39			
NB-33	Calcite	primary	235.3					

Sample	Mineral	Type	Th	Tm	Salinity
NB-47	Quartz	primary	172.8	-6.4	9.71
NB-47	Quartz	primary	181.7	-6.3	9.58
NB-47	Quartz	primary	175.6	-6.4	9.71
NB-47	Quartz	primary	174.9	-6.4	9.71
NB-47	Quartz	primary	178.2	-6.3	9.58
NB-47	Quartz	primary	180.6	-6.3	9.58
NB-47	Quartz	primary	202.1	-5.1	7.96
NB-47	Quartz	primary	203.9	-4.6	7.25
NB-47	Quartz	primary	179.2	-5	7.82
NB-47	Quartz	primary	177.2	-5.2	8.1
NB-47	Quartz	primary	178.8	-5.1	7.96
NB-47	Quartz	primary	179.6	-5.1	7.96
NB-47	Quartz	primary	186.2	-5.2	8.1
NB-47	Quartz	primary	173.5	-5.1	7.96
NB-47	Quartz	primary	175.5	-5.1	7.96
NB-47	Quartz	?	194.1	-4.9	7.68
NB-47	Quartz	?	195.6	-4.5	7.105
NB-47	Quartz	secondary	168.6	-3	4.86
NB-47	Quartz	?	188.9	-4	6.37
NB-47	Quartz	?	194	-4.4	6.96
NB-47	Quartz	?	195.3	-4.6	7.25
NB-47	Calcite	primary	176.8	-3.8	6.08
NB-47	Calcite	primary	168.4	-3	4.86
NB-47	Calcite	primary	168.7	-3.3	5.32
NB-47	Calcite	primary	169.2	-3	4.86
NB-47	Calcite	primary	167.4	-3.4	5.47
NB-47	Calcite	primary	155.2	-3	4.86
NB-47	Quartz	?	194	-4.4	6.96
NB-47	Quartz	?	195.3	-4.6	7.25
NB-47	Calcite	primary	176.8	-3.8	6.08
NB-47	Calcite	primary	168.4	-3	4.86
NB-47	Calcite	primary	168.7	-3.3	5.32

Sample	Mineral	Type	Th	Tm	Salinity			
NB-47	Calcite	primary	169.2	-3	4.86			
NB-47	Calcite	primary	167.4	-3.4	5.47			
NB-47	Calcite	primary	155.2	-3	4.86			
			Th(Celcius)	Tm(Celcius)	Salinity			
NB-99	Quartz	primary	235.4					
NB-99	Quartz	primary	220.3					
NB-99	Quartz	primary	242.3	-3.8	6.16			
NB-99	Quartz	primary	238.7					
NB-99	Quartz	primary	237.2	-5.6	8.68			
NB-99	Quartz	primary	217.1	-4.4	7.02			
NB-99	Quartz	primary	231.6					
NB-99	Quartz	primary	239.5					
NB-99	Quartz	primary	224.1	-4.2	6.74			
NB-99	Quartz	primary	228.2					
NB-99	Quartz	primary	220.6					
NB-99	Quartz	primary	199.3	-5.9	9.08			
NB-99	Quartz	primary	198	-5.2	8.14			
NB-99	Quartz	primary	206.3	-4.7	7.45			
NB-99	Quartz	primary	228.3					
NB-99	Quartz	primary	222.8	-3.5	5.71	Near edge		
NB-99	Quartz	primary	203.5	-3.3	5.41	Near edge		
NB-99	Quartz	primary	205.2	-4.3	6.88	Near edge		
NB-99	Quartz	primary	216.9	-3.7	6.01	Near edge		
NB-99	Quartz	primary	240.6	+5.8	6.88	Near edge		
NB-99	Quartz	primary	218.5	+7.8	3.87	Near edge		
NB-99	Quartz	primary	226	-4.9	7.73	Near edge		
NB-99	Quartz	primary	204.1			At edge		
NB-99	Quartz	primary	229.8	+4.8	8.28	At edge		
NB-99	Quartz	primary	208.8	+7.3	4.65	At edge		
NB-99	Quartz	primary	199.2			At edge		
NB-99	Quartz	primary	193.5	+6.2	6.3	At edge		
NB-99	Calcite	primary	142.2	+1.2				
NB-99	Calcite	primary	141.5	+0.8				
		Type	Th(Celcius)	Tm(Celcius)	Eq.wt.%NaC	Lco2	Tm co2	Ca/Na
NB-100	Quartz	Secondary	162	-11.4	15.37			
NB-100	Quartz	Secondary	165.1	-11.3	15.27			
NB-100	Quartz	Secondary	194.4	-11.9	15.86			
NB-100	Quartz	Secondary	171.9	-11.4	15.37			
NB-100	Quartz	Secondary	189.3	-12	15.96			
NB-100	Quartz	Secondary	181.4	-11.9	15.86	+16 to +18		
NB-100	Quartz	Primary	211.5	-21.1	23.11			
NB-100	Quartz	Primary	196.6	-19.4	21.96			
NB-100	Quartz	Primary	192.7	-26	25.66			1.4
NB-100	Quartz	Primary	218.5	-23.4				0.55
NB-100	Quartz	Primary	197.8	-23.7	24.5			0.65
NB-100	Quartz	Primary	207.4	-25.1	25.26			1.2

			Th	Tm(ice)	Salinity
NB-102	Quartz	Primary	265.5	-4.9	7.73
NB-102	Quartz	Primary	224.4	-4.9	7.73
NB-102	Quartz	Primary	253.2	-4.6	7.31
NB-102	Quartz	Primary	234.5	+5.4	
NB-102	Quartz	Primary	237.8	+7.5	ice metastability?
NB-102	Quartz	Primary	215.4	>10	ice metastability?
NB-102	Quartz	Primary	217.1	>10	ice metastability?
NB-102	Quartz	Primary	213.8	+7.1	ice metastability?

		L+V=L Th	Tm(ice)	Salinity	L+V=L ThCO2	TmCO2	CO2 Vol. Fraction
NB-104	Quartz	229.3					
NB-104	Quartz	>180	+7.9				
NB-104	Quartz	211.6	+7.1				
NB-104	Quartz	>200	+4.6				
NB-104	Quartz	196.5	-5.3	8.28			
NB-104	Quartz	204.6	-5.2	8.14			
NB-104	Quartz	198.1	-5.2	8.14			
NB-104	Quartz	223.6	+7.0	5.68			
NB-104	Quartz	>250			+23.4	-58.8	0.9
NB-104	Quartz	>300	+7.3	5.15	+19.6	-59.7	0.88
NB-104	Quartz	>300	+7.2	5.33	+20.4	-59.7	0.88
NB-104	Quartz	304.2	+7.6	4.62	+15.8	-57.7	0.88
NB-104	Quartz	306.4	+8.5	2.96	+17.8	-57.6	0.88
NB-104	Quartz	321.1	+8.2	3.52	+26.7	-58.2	0.9
NB-104	Quartz	323	+7.8	4.26	+23.2	-58.3	0.85
NB-104	Quartz	316.3	+8.2	3.52	+23.0	-58.2	0.85
NB-104	Quartz	314.9	+8.3	3.33	+23.4	-58.2	0.88

		Th	Tm(ice)	Salinity	ThCO2 to Liq
NB-106	Quartz	206.9	-6.2	9.47	
NB-106	Quartz	211.8			
NB-106	Quartz	211.3			
NB-106	Quartz	187.9	-6.2	9.47	
NB-106	Quartz	191.3	-6.1	9.34	
NB-106	Quartz	>300	+7.6		+12.9
NB-106	Quartz	197.8	-6	9.21	
NB-106	Quartz	190.7	-8.1	11.81	
NB-106	Quartz	179.5	-7.4	10.98	
NB-106	Quartz	181.3	-6.5	9.86	
NB-106	Quartz	195.9	-6.6	9.98	
NB-106	Quartz	204.2	-6.8	10.24	
NB-106	Calcite	204.7	0	ice metastability?	
NB-106	Calcite	172.8	-0.1	ice metastability?	
NB-106	Calcite	184.2	0	ice metastability?	

			L+V=L Th	Tm(ice)	Salinity	L+V=L ThCO2	TmCO2	CO2 Vol. Fraction
NB-107	Quartz		192.9	+7.3	5.154	23		0.05
NB-107	Quartz		233.1	+7.1	5.507	23		0.05
NB-107	Quartz		225.2	+7.2	5.331	23		0.05
NB-107	Quartz		224	+7.3	5.154	23		0.05
NB-107	Quartz		310	+7.2	5.331	24.1		0.4
NB-107	Quartz		310	+6.8	6.028	23.8		0.4
NB-107	Quartz		221.6	+7.1	5.507	23		0.05
NB-107	Quartz		310	+7.2	5.331	25.8		0.35
NB-107	Quartz		227.8	+7.4	4.976	26.8		0.07
NB-107	Quartz		220.1	+7.9	4.074	23		0.08
NB-107	Quartz		214.7	+7.8	4.256	23		0.07
NB-107	Quartz		210.5	+6.3	6.878	23		0.06
NB-107	Quartz		203.7	+7.9	4.074	23		0.06
NB-107	Quartz		227.9	+7.8	4.256	23		0.06
NB-107	Quartz		308.7	+7.3	5.154	24.9		0.45
NB-107	Quartz		312.8	+7.3	5.154	25.2		0.45
NB-107	Quartz		310.3	+7.3	5.154	23.8		0.5

			L+V=L Th	Tm(ice)	Salinity	L+V=L ThCO2	TmCO2	CO2 Vol. Fraction
NB-84	Calcite		>267	+9.6	0.825	+24		0.45
NB-84	Calcite		>267	+9.6	0.825	+23.2		0.5
NB-84	Calcite		>267			+23.4		0.5
NB-84	Calcite		>267			+23.2		0.55
NB-84	Calcite		>267			+25.5		0.55
NB-84	Calcite		>267			+25.4		0.45
NB-84	Calcite		>267			+25.3		0.5
NB-84	Calcite		>267	+10.1		+24.0	-61.6	0.45
NB-84	Calcite		>267	+11.5		+23.2		0.5
NB-84	Calcite		>267	+9.6	0.825	+23.4		0.5
NB-84	Calcite		>267			+23.2		0.55

			Th	Tm	Salinity
NB-44	Quartz	primary	177.2	-7.2	10.73
NB-44	Quartz	primary	185	-5.8	8.95
NB-44	Quartz	primary	198	-5.7	8.81
NB-44	Quartz	primary	178.5	-5.5	8.55
NB-44	Quartz	primary	187.1	-5.5	8.55
NB-44	Quartz	primary	188.7	-6.1	9.34

		Th	Tm	Salinity
NB-1	Calcite		-0.4	
NB-1	Calcite	146.5	-1.2	
NB-1	Calcite	142.3	-1.1	
NB-1	Calcite	150.3	-0.6	
NB-1	Calcite	150.7	-0.8	
NB-1	Calcite	149.1	+1.8	
NB-1	Calcite	152	-0.4	
NB-1	Calcite	124.2	+2.9	
NB-1	Calcite	145.1	+12.9	
NB-1	Calcite	145.5	+21.1	
NB-1	Calcite	149	+23.3	

Sample	Mineral	Crush	Counts	Ar Max.	H2	He	CH4	H2O	N2	O2	H2S	Ar	CnHm	CO2	SO2
NB-1	Calcite	5390A			0.32372	0	0.08936	97.4952	1.23136	0.02961	0.00068	0.00593	0.00442	0.80111	0.00018
NB-1	Calcite	5390B			0.19850	0	0.24266	97.6763	1.00020	0.03573	0.00078	0.0108	0.0074	0.80574	0.00066
NB-1	Calcite	5390C			0.23582	0.03744	0.20335	96.2122	0.46982	0.03568	0.00054	0.00728	0.00663	2.77804	0.00077
NB-1	Calcite	5390D			0.10213	0.03093	0.09922	95.0161	0.69156	0.04441	0.00602	0.01584	0.01461	3.94778	0.00843
NB-1	Calcite	5390E			0.36280	0	0.43028	93.7667	0.30190	0.02958	0.00496	0.00413	0.01092	5.07990	0.00083
NB-1	Calcite	5390G			0.12228	0.00665	0.09415	97.1353	0.22068	0.01686	0.00039	0.00224	0.00202	2.39477	0.000087
NB-1	Calcite	5390K			0.92900	0.00062	2.21812	95.4432	0.15589	0.00879	0.000078	0.00045	0.01888	1.21875	0.00027
NB-1	Calcite	5390L			0.58566	0.00034	1.73944	96.4221	0.11472	0.00795	0.0000094	0.00045	0.0189	1.10570	0.00015
NB-1	Calcite	5390M			0.59875	0	1.98626	95.3099	0.20251	0.01218	0.00011	0.00034	0.0164	1.86724	0.000015
NB-1	Calcite	5390N			0.64801	0.00369	2.32866	95.4298	0.30637	0.01156	0.00015	0.00055	0.01703	1.24579	0.00011
NB-1	Calcite	5390O			0.83096	0.00499	1.96818	93.5757	0.20537	0.01241	0.00024	0.00056	0.01414	3.38072	0.00017

		Crush	Counts	Ar Max.	H2	He	CH4	H2O	N2	O2	H2S	Ar	CnHm	CO2	SO2
NB-7	Calc Sed	5745A	3914970	0.00596	0.00000	0.00136	0.00000	99.28357	0.49755	0.08691	0.00044	0.00596	0.00072	0.12347	0.00002
NB-7	Calc Sed	5745B	2179129	0.00548	0.00000	0.00146	0.02210	99.44859	0.37563	0.06481	0.00024	0.00548	0.00022	0.08138	0.00009
NB-7	Calc Sed	5745C	2059691	0.00691	0.00000	0.00258	0.08037	99.18751	0.51746	0.08055	0.00021	0.00691	0.00039	0.12400	0.00002
NB-7	Calc Sed	5745D	4159612	0.00909	0.00000	0.00130	0.22775	99.04573	0.45362	0.12999	0.00048	0.00909	0.00129	0.13069	0.00006
NB-7	Calc Sed	5745E	7386391	0.00692	0.00000	0.00111	0.18327	99.23124	0.38641	0.08646	0.00041	0.00692	0.00116	0.10300	0.00002
NB-7	Calc Sed	5745F	8903441	0.00620	0.00000	0.00111	0.13182	99.29899	0.38659	0.07835	0.00033	0.00620	0.00091	0.09567	0.00003
NB-7	Calc Sed	5745J	6536523	0.00905	0.00000	0.00035	0.10093	99.03522	0.63696	0.13154	0.00048	0.00905	0.00108	0.08439	0.00000

NB-10	Barite	Crush	Counts	Ar Max.	H2	He	CH4	H2O	N2	O2	H2S	Ar	CnHm	CO2	SO2
NB-10	Barite	5748A			0	0	0.00898	99.693	0.00636	0.0142	0.000167	0.00017	0.000188	0.277	0.000015
NB-10	Barite	5748B			0	0.00148	0.0353	99.736	0.0104	0.0109	0.000199	0.000149	0.000294	0.205	0.000012
NB-10	Barite	5748C			0	0.000553	0.0342	99.546	0.00366	0.0104	0.000178	0.000011	0.000468	0.404	0.00002
NB-10	Barite	5748D			0	0.00247	0.0349	99.461	0	0.005573	0.000126	0.000011	0.000455	0.495	0.000029
NB-10	Barite	5748E			0	0.0041	0.102	99.368	0.0266	0.0199	0.000592	0.000251	0.00116	0.477	0.000097
NB-10	Barite	5748F			0	0.000787	0.0368	99.411	0.00601	0.0137	0.000169	0.000028	0.000535	0.531	0.000026
NB-10	Barite	5748G			0	0.00138	0.0469	99.473	0.008	0.016	0.000203	0.000028	0.000561	0.454	0.000039

		Crush	Counts	Ar max.	H2	He	CH4	H2O	N2	O2	H2S	Ar	CnHm	CO2	SO2
NB-32		5848A	3860696	0.002979	0.015753	0.000227	0.225401	93.484450	0.960733	0.001002	0.001702	0.002979	0.008014	5.299741	0.000000
NB-32		5848B	2966724	0.002013	0.024688	0.000887	0.195842	96.006340	0.682456	0.000686	0.001185	0.002013	0.004875	3.081042	0.000000
NB-32		5848C	4879834	0.002927	0.000000	0.002543	0.185764	93.306340	0.989446	0.000651	0.001540	0.002927	0.008470	5.502327	0.000000
NB-32		5848D	1566848	0.002829	0.083008	0.000907	0.112740	95.658920	0.933269	0.002591	0.001741	0.002829	0.004816	3.199183	0.000000
NB-32		5848	4204847	0.002802	0.000000	0.001081	0.153047	94.718470	0.935484	0.001820	0.001963	0.002802	0.006513	4.178830	0.000000
NB-32		5848F	4976033	0.004804	0.000000	0.002990	0.254422	89.385830	1.429271	0.002263	0.004001	0.004804	0.014108	8.902298	0.000017
NB-32		5848J	5248198	0.003236	0.000000	0.001454	0.192169	93.872180	1.216143	0.004813	0.001934	0.003236	0.007142	4.700921	0.000000
NB-32		5848K	9106990	0.003906	0.000000	0.001413	0.266619	92.055160	1.146448	0.000736	0.002541	0.003906	0.010518	6.512652	0.000014
NB-32		5848L	5466009	0.005161	0.000000	0.002037	0.255714	90.965880	1.434950	0.008786	0.002624	0.005161	0.011527	7.313306	0.000020
NB-32		5848M	6568289	0.003299	0.000000	0.000842	0.147167	95.135150	1.040955	0.004875	0.001255	0.003299	0.005856	3.660598	0.000001
NB-32		5848N	7915872	0.003546	0.000000	0.001295	0.175553	93.905750	1.192998	0.001798	0.001685	0.003546	0.007414	4.709964	0.000000
NB-32		5848O	9851422	0.003215	0.000000	0.001283	0.173974	94.351360	1.119840	0.002625	0.001337	0.003215	0.006816	4.339557	0.000000
NB-32		5848P	4866642	0.003486	0.000000	0.000830	0.297020	94.134900	1.187687	0.003095	0.001032	0.003486	0.007353	4.364590	0.000000
NB-32		5848Q	5659156	0.003955	0.000000	0.001422	0.317668	93.284680	1.269948	0.004845	0.001582	0.003955	0.008930	5.106990	0.000000

NB-36	Quartz	Crush	Counts	Ar Max.	H2	He	CH4	H2O	N2	O2	H2S	Ar	CnHm	CO2	SO2
NB-36	Quartz	5831A	13368400	0.000211	0.000000	0.000448	0.171363	98.019370	0.199747	0.000000	0.003361	0.000211	0.003206	1.602262	0.000026
NB-36	Quartz	5831B	4769098	0.000225	0.038605	0.001069	0.281784	94.485210	0.056265	0.000000	0.008294	0.000225	0.009394	5.119340	0.000037
NB-36	Quartz	5831C	3855259	0.000174	0.025215	0.000000	0.216828	95.443850	0.112557	0.000000	0.007858	0.000174	0.007256	4.186436	0.000000
NB-36	Quartz	5831D	6310762	0.000053	0.000000	0.000771	0.200303	95.346900	0.141715	0.000000	0.009302	0.000053	0.006945	4.293973	0.000043
NB-36	Quartz	5831E	9487064	0.000182	0.000000	0.000062	0.261061	95.004620	0.164915	0.000000	0.009158	0.000182	0.007582	4.552555	0.000041
NB-36	Quartz	5831F	10030760	0.000195	0.000000	0.000143	0.222561	95.078510	0.175260	0.000000	0.008045	0.000195	0.008131	4.507300	0.000049
NB-36	Quartz	5831J	3650279	0.000282	0.228558	0.000000	0.582108	94.545080	0.183968	0.000000	0.008257	0.000282	0.011735	4.440290	0.000000
NB-36	Quartz	5831K	6676615	0.000210	0.054117	0.000000	0.387792	96.174320	0.080600	0.000000	0.006534	0.000210	0.008731	3.287914	0.000000
NB-36	Quartz	5831L	15497420	0.000170	0.000000	0.000811	0.248982	96.525000	0.146570	0.000000	0.005605	0.000170	0.007083	3.065904	0.000043
NB-36	Quartz	5831M	15090220	0.000137	0.000000	0.001476	0.216917	96.828950	0.145759	0.000000	0.005108	0.000137	0.005719	2.796031	0.000041
NB-36	Quartz	5831N	9693801	0.000128	0.000452	0.000000	0.258923	97.010150	0.112259	0.000000	0.004980	0.000128	0.005325	2.607905	0.000000
NB-36	Quartz	5831O	12888560	0.000145	0.000000	0.001430	0.213268	96.781370	0.117387	0.000000	0.004475	0.000145	0.006040	2.875999	0.000025
NB-36	Quartz	5831P	9260945	0.000136	0.000000	0.000000	0.205482	96.689320	0.103302	0.000000	0.005177	0.000136	0.005648	2.991056	0.000022
NB-36	Quartz	5831Q	9795414	0.000133	0.000000	0.000000	0.230537	96.896220	0.106405	0.000000	0.004344	0.000133	0.005558	2.756904	0.000022

		Crush	Counts	Ar Max.	H2	He	CH4	H2O	N2	O2	H2S	Ar	CnHm	CO2	SO2
NB-34	Calcite	5746A			0	0.000729	0.105	98.124	0.0541	0	0.000134	0.001632	0.0015	1.7	0.000029
NB-34	Calcite	5746B			0	0.00141	0.0796	97.921	0.051	0	0.00011	0.000544	0.00221	1.94	0.000022
NB-34	Calcite	5746C			0	0.00108	0.0796	97.378	0.0612	0	0.000088	0.0012	0.00204	2.455	0
NB-34	Calcite	5746D			0	0.000493	0.125	96.781	0.0619	0.00332	0.000151	0.000656	0.00385	3.02	0.000025
NB-34	Calcite	5746E			0	0.00107	0.078	97.941	0.0342	0	0.000055	0.000241	0.00215	1.943	0.000016
NB-34	Calcite	5746F			0	0.00128	0.0976	97.594	0.0717	0	0.000162	0.000938	0.00308	2.226	0.000018
NB-34	Calcite	5746J			0	0.000423	0.0936	97.146	0.0569	0	0.000084	0.000765	0.00268	2.696	0.000001
NB-34	Calcite	5746K			0	0	0.107	96.559	0.0474	0	0.000058	0.00062	0.00322	3.28	0.000012
NB-34	Calcite	5746L			0	0.000367	0.0851	97.426	0.0715	0	0.000088	0.000986	0.00254	2.41	0.000018
NB-34	Calcite	5746M			0	0.000433	0.0774	97.58	0.1	0	0.0001	0.00172	0.00246	2.23	0.000006
NB-34	Calcite	5746N			0	0.0002	0.0883	97.186	0.111	0	0.000118	0.00174	0.00295	2.6	0.000005
NB-34	Calcite	5746P			0	0.000453	0.0778	97.645	0.0629	0	0.000091	0.00078	0.00254	2.207	0.000021
NB-34	Calcite	5746Q			0	0.000286	0.0685	97.495	0.108	0	0.000115	0.00235	0.00197	2.31	0.000009
NB-34	Calcite	5746R			0	0.000383	0.0933	97.564	0.0838	0	0.000185	0.00123	0.00287	2.246	0.000028
NB-34	Calcite	5746S			0	0.000021	0.0973	97.462	0.077	0	0.000155	0.00103	0.00298	2.35	0.000036
NB-34	Calcite	5746T			0	0.000642	0.0783	97.89	0.0648	0	0.000114	0.000909	0.00222	1.957	0.000018
NB-34	Calcite	5746U			0	0.0011	0.112	96.918	0.1335	0	0.000227	0.00199	0.00354	2.81	0.000022
NB-34	Calcite	5746V			0	0.000908	0.132	96.294	0.118	0	0.000264	0.00202	0.00443	3.43	0.000025

		Sample	Counts	Ar max	H2	He	CH4	H2O	N2	O2	H2S	Ar	CnHm	CO2	SO2
NB-43	Calcite	5861A	13353060	0.000960	1.682224	0.000043	0.228761	91.98646	0.190877	0.034814	0.010776	0.000960	0.010518	5.854364	0.000183
NB-43	Calcite	5861B	5961918	0.001596	0.026583	0.000000	0.171387	94.80742	0.166154	0.008587	0.006277	0.001596	0.006128	4.805873	0.000003
NB-43	Calcite	5861C	9718400	0.001527	0.000000	0.000000	0.156337	95.10228	0.157135	0.008977	0.007199	0.001527	0.005770	4.560764	0.000014
NB-43	Calcite	5861D	12199240	0.001096	0.000000	0.000000	0.131608	97.72803	0.122523	0.007539	0.003452	0.001096	0.002586	2.003143	0.000020
NB-43	Calcite	5861E	8292313	0.001023	0.017609	0.000000	0.198311	95.73127	0.128890	0.003678	0.006782	0.001023	0.004895	3.907521	0.000021
NB-43	Calcite	5861F	14221260	0.000873	0.000000	0.000370	0.236966	95.42583	0.160228	0.001607	0.007499	0.000873	0.006173	4.160423	0.000039
NB-43	Calcite	5861J	9866821	0.000898	0.000000	0.000000	0.287976	92.37776	0.157767	0.000000	0.012351	0.000898	0.009985	7.153229	0.000032
NB-43	Calcite	5861K	13690290	0.000855	0.000000	0.000093	0.251595	93.53643	0.163965	0.000000	0.008462	0.000855	0.009016	6.029544	0.000040
NB-43	Calcite	5861L	15707320	0.000917	0.000000	0.001865	0.392088	91.45277	0.154869	0.000000	0.012375	0.000917	0.014511	7.970525	0.000093
NB-43	Calcite	5861M	522755	0.001729	1.748810	0.000000	2.649343	68.79783	0.447177	0.002107	0.012718	0.001729	0.034082	26.306210	0.000000

		Crush	Counts	Ar Max.	H2	He	CH4	H2O	N2	O2	H2S	Ar	CnHm	CO2	SO2
NB-47	Quartz	6061A	2096815	0.0000719	0	0.0006045	0.1124231	97.63969	0.0442663	0	0.0024923	0.0000719	0.0029949	2.197497	0.0000332
NB-47	Quartz	6061B	1508904	0.0000637	0	0.0004052	0.1527035	97.76558	0.061164	0	0.0024467	0.0000637	0.0026549	2.015054	0
NB-47	Quartz	6061C	2543105	0.0000621	0	0.0009174	0.1508304	98.14724	0.0687116	0	0.0019482	0.0000621	0.0025863	1.627715	0.0000451
NB-47	Quartz	6061D	1021501	0.0001123	0	0.0028748	0.3119783	96.68582	0.0200555	0	0.0037005	0.0001123	0.0046796	2.970887	0
NB-47	Quartz	6061F	2170470	0.0000833	0	0.0015459	0.2299575	97.58023	0.0908486	0	0.0016636	0.0000833	0.0034689	2.092149	0.0001435
NB-47	Quartz	6061J	4165967	0.0000604	0	0.0012491	0.1122563	98.0655	0.085047	0	0.0020904	0.0000604	0.0025181	1.731254	0.0000838
NB-47	Quartz	6061K	1583162	0.0000822	0	0.0020006	0.1721286	97.20409	0.085643	0	0.0019777	0.0000822	0.0034269	2.530559	0.0001761
NB-47	Quartz	6061N	4480185	0.0000615	0	0.0016276	0.093094	98.15904	0.0947686	0	0.0020156	0.0000615	0.0025612	1.646809	0.0000701
NB-47	Quartz	6061O	5569970	0.000069	0	0.0017289	0.0890884	98.13785	0.0770375	0	0.002165	0.000069	0.0028753	1.689163	0.000103

		Crush	Counts	Ar Max.	H2	He	CH4	H2O	N2	O2	H2S	Ar	CnHm	CO2	SO2
NB-47	Calcite	6056B	10027390	0.000081	0	0.0045446	0.1008174	98.45542	0.0547837	0	0.0008853	0.000081	0.0033735	1.380039	0.0001432
NB-47	Calcite	6056C	8337252	0.0000524	0	0.0010801	0.0721521	98.60174	0.0366589	0	0.0004126	0.0000524	0.0021825	1.285745	0.0000307
NB-47	Calcite	6056D	7143973	0.0000728	0	0.0010631	0.0911884	98.04115	0.0183292	0	0.0007336	0.0000728	0.0030315	1.844469	0.0000285
NB-47	Calcite	6056E	7865752	0.0000437	0	0.0013314	0.0766649	98.74147	0.0092736	0	0.0003116	0.0000437	0.0018227	1.169096	0.0000285
NB-47	Calcite	6056F	11710710	0.0002412	0	0.0076716	0.1542457	97.05801	0.067039	0	0.0011686	0.0002412	0.0075656	2.703899	0.000151
NB-47	Calcite	6056J	10131690	0.0001526	0	0.0043493	0.1517741	96.99197	0.0904313	0	0.0008536	0.0001526	0.0063587	2.75413	0.0001477
NB-47	Calcite	6056K	9834060	0.0001312	0	0.0033394	0.1503735	97.26543	0.0547749	0	0.0007045	0.0001312	0.0054658	2.51983	0.0001
NB-47	Calcite	6056L	9187300	0.0001314	0	0.0014305	0.122768	96.87359	0.0593591	0	0.0005186	0.0001314	0.0054754	2.9368	0.0000503
NB-47	Calcite	6056M	9188462	0.0001193	0	0.001329	0.1063492	97.121	0.0546061	0	0.0004517	0.0001193	0.0049689	2.711232	0.0000633
NB-47	Calcite	6056N	8605552	0.0001196	0	0.0012988	0.1089512	97.04345	0.0506221	0	0.0004822	0.0001196	0.004985	2.790181	0.0000371

		Crush	Counts	Ar Min	H2	He	CH4	H2O	N2	O2	H2S	Ar	CnHm	CO2	SO2
NB-78	Calcite	6057A	7365414	0.00149	0.00000	0.00112	0.04539	99.81807	0.10805	0.01411	0.00015	0.00149	0.00000	0.01157	0.00004
NB-78	Calcite	6057B	4742081	0.00668	0.00000	0.00138	0.03504	99.44621	0.40264	0.10132	0.00055	0.00668	0.00000	0.00617	0.00002
NB-78	Calcite	6057C	6877001	0.00373	0.00000	0.00038	0.02994	99.66788	0.23604	0.05781	0.00031	0.00373	0.00001	0.00389	0.00001
NB-78	Calcite	6057D	7679501	0.00143	0.00000	0.00078	0.03203	99.86224	0.08728	0.01455	0.00010	0.00143	0.00000	0.00155	0.00002
NB-78	Calcite	6057E	8066802	0.00073	0.00000	0.00080	0.04208	99.87890	0.06884	0.00635	0.00010	0.00073	0.00005	0.00212	0.00004
NB-78	Calcite	6057I	9207132	0.00211	0.00000	0.00168	0.06137	99.75428	0.15135	0.02486	0.00026	0.00211	0.00021	0.00381	0.00006
NB-78	Calcite	6057J	9636624	0.00091	0.00000	0.00208	0.07004	99.81428	0.09513	0.01287	0.00022	0.00091	0.00029	0.00412	0.00006
NB-78	Calcite	6057K	8292410	0.00121	0.00000	0.00099	0.03672	99.85226	0.09277	0.01362	0.00013	0.00121	0.00001	0.00226	0.00002

		Sample	Counts	Ar max.	H2	He	CH4	H20	N2	O2	H2S	Ar	CnHm	CO2	SO2
NB-79		5838B	24007580	0.000797	0.051146	0.000733	0.147929	99.65356	0.135307	0.008137	0.000448	0.000797	0.000778	0.001070	0.000086
NB-79		5838C	27556970	0.002892	0.331062	0.015277	0.426138	98.71806	0.403896	0.032921	0.002504	0.002892	0.005085	0.061741	0.000415
NB-79		5838D	17151890	0.000429	0.000000	0.000000	0.040012	99.88842	0.064635	0.006435	0.000063	0.000429	0.000000	0.000000	0.000013
NB-79		5838E	22545540	0.001710	0.028444	0.000000	0.106354	99.62551	0.201776	0.030562	0.000369	0.001710	0.000265	0.004958	0.000052
NB-79		5838F	21486360	0.001285	0.017840	0.000067	0.102834	99.67937	0.150007	0.019984	0.000393	0.001285	0.000304	0.027877	0.000049
NB-79		5838J	23949310	0.001496	0.126572	0.000438	0.197899	99.41885	0.195949	0.020174	0.000661	0.001496	0.001167	0.036678	0.000112
NB-79		5838K	28327980	0.002602	0.304462	0.005571	0.404680	98.81334	0.381932	0.035786	0.002070	0.002602	0.003931	0.045277	0.000356
NB-79		5838L	27682080	0.001926	0.139242	0.000928	0.262123	99.28806	0.255940	0.026294	0.001215	0.001926	0.002178	0.021884	0.000207
NB-79		5838M	26994870	0.002489	0.214651	0.004850	0.306419	99.09988	0.302242	0.035283	0.001549	0.002489	0.002707	0.029671	0.000256
NB-79		5838O	22988530	0.001222	0.002113	0.000000	0.095569	99.71963	0.136953	0.020459	0.000306	0.001222	0.000267	0.023438	0.000045

		Crush	H2	He	CH4	H2O	N2	O2	H2S	Ar	CnHm	CO2	SO2
NB-80	Quartz	5830A	1.85	0	0.564	92.51	0.0357	0	0.0156	0.000613	0.00504	5.014	0.000299
NB-80	Quartz	5830B	0.031	0	0.66	92.213	0.241	0	0.00994	0.000497	0.00764	6.84	0.0002
NB-80	Quartz	5830C	0.276	0	0.694	91.232	0.128	0	0.0184	0.000329	0.0083	7.643	0.000251
NB-80	Quartz	5830D	0.037	0	0.534	93.526	0.24	0	0.0106	0.000271	0.00725	5.644	0.000166
NB-80	Quartz	5830E	0.011	0.000934	0.523	94.426	0.209	0	0.0155	0.000248	0.00635	4.807	0.000148
NB-80	Quartz	5830F	0.0597	0.00157	0.556	93.204	0.0813	0	0.0146	0.000049	0.0072	6.076	0.000162
NB-80	Quartz	5830J	0	0	0.388	94.792	0.288	0	0.00913	0.00022	0.0075	4.514	0.000127
NB-80	Quartz	5830K	0	0.000905	0.376	95.625	0.0532	0	0.00872	0.000121	0.00698	3.928	0.00007
NB-80	Quartz	5830L	0.0335	0.00116	0.283	93.727	0.104	0	0.0165	0.000061	0.0086	5.825	0.000116
NB-80	Quartz	5830M	0.0469	0.00276	0.38	93.093	0.177	0	0.0232	0.000051	0.01	6.266	0.000114
NB-80	Quartz	5830N	0	0.000164	0.339	95.291	0.219	0	0.00764	0.000045	0.00815	4.135	0.000063
NB-80	Quartz	5830O	0.0202	0.00195	0.354	94.677	0.177	0	0.00969	0.000003	0.00872	4.75	0.000096

		Crush	Counts	Ar Max.	H2	He	CH4	H2O	N2	O2	H2S	Ar	CnHm	CO2	SO2	Problem
NB-84	Calcite	6492C			0.110461	0.006173	0.529836	29.05445	0.242463	0	0.003397	0.001099	0.178623	69.8735	0	H2O
NB-84	Calcite	6492F			0.108977	0.008272	0.518926	33.25959	0.205817	0	0.002849	0.001957	0.165075	65.7284	0.000136	H2O
NB-84	Calcite	6492H			0.10088	0.006429	0.485662	32.73355	0.350715	0	0.002511	0.002464	0.175187	66.1425	0.000101	H2O
NB-84	Calcite	6492I			0.08007	0.003378	0.333934	49.12681	0.25939	0	0.002443	0.002175	0.149394	50.04222	0.000185	H2O
NB-84	Calcite	6492J			0.082774	0.006913	0.41442	44.65445	0.368368	0	0.002718	0.003349	0.190073	54.27676	0.000185	H2O
NB-84	Calcite	6492K			0.087398	0.005645	0.414445	42.68807	0.37018	0	0.002629	0.00307	0.18192	56.24643	0.000212	H2O
NB-84	Calcite	6492L			0.091461	0.006877	0.48223	35.73901	0.38912	0	0.00283	0.003624	0.210096	63.07455	0.000206	H2O
NB-84	Calcite	6492M			0.105916	0.008275	0.513276	27.17211	0.424925	0	0.003142	0.003311	0.216677	71.55214	0.000235	H2O
NB-84	Calcite	6492N			0.088424	0.005396	0.446935	37.97552	0.398844	0	0.002646	0.003279	0.198903	60.87968	0.000372	H2O
NB-84	Calcite	6492O			0.09816	0.006956	0.598017	23.33063	0.433216	0	0.001749	0.003143	0.205654	75.32231	0.00016	H2O
NB-84	Calcite	6492P			0.087692	0.006688	0.505493	35.69197	0.469197	0.005099	0.002482	0.003557	0.229241	62.99816	0.000418	H2O

		Crush	Counts	Ar Max	H2	He	CH4	H2O	N2	O2	H2S	Ar	CnHm	CO2	SO2	Problem
NB-85	Calcite	6059A	15365470	0.001144	0.000000	0.004035	0.079509	99.834540	0.054835	0.008172	0.000541	0.001144	0.000465	0.016616	0.000147	CO2
NB-85	Calcite	6059B	11439740	0.000086	0.000000	0.002217	0.049602	99.936460	0.003769	0.000000	0.000121	0.000086	0.000000	0.007683	0.000050	CO2
NB-85	Calcite	6059C	10918630	0.000160	0.000000	0.001835	0.056395	99.920160	0.013300	0.000000	0.000120	0.000160	0.000000	0.007961	0.000054	
NB-85	Calcite	6059D	13160050	0.000776	0.000000	0.004292	0.128243	99.764000	0.079896	0.000000	0.000738	0.000776	0.001418	0.020470	0.000178	
NB-85	Calcite	6059E	13332010	0.000460	0.000000	0.004006	0.090609	99.834420	0.053867	0.000000	0.000469	0.000460	0.000782	0.015365	0.000130	
NB-85	Calcite	6059J	11338890	0.000643	0.000000	0.002205	0.080630	99.847900	0.056582	0.000000	0.000301	0.000643	0.000546	0.011300	0.000106	
NB-85	Calcite	6059K	11019190	0.000120	0.000000	0.002061	0.072288	99.877600	0.037301	0.000000	0.000218	0.000120	0.000311	0.010007	0.000085	
NB-85	Calcite	6059L	10526690	0.000612	0.000000	0.001975	0.067477	99.880420	0.039779	0.000000	0.000166	0.000612	0.000233	0.009273	0.000071	
NB-85	Calcite	6059M	11908440	0.000863	0.000000	0.004032	0.110244	99.796240	0.069877	0.000000	0.000527	0.000863	0.001076	0.016999	0.000158	

		Crush	Counts	Ar Min	H2	He	CH4	H2O	N2	O2	H2S	Ar	CnHm	CO2	SO2	Problem
NB-86	Calcite	6058A	2426384	0.00106	0.00000	0.00003	0.01623	99.88970	0.04297	0.00842	0.00003	0.00106	0.00000	0.04155	0.00000	
NB-86	Calcite	6058B	2230480	0.00074	0.00000	0.00034	0.06705	99.83289	0.03325	0.00506	0.00000	0.00074	0.00026	0.06042	0.00000	
NB-86	Calcite	6058C	4125322	0.00027	0.00000	0.00145	0.04013	99.89896	0.02859	0.00000	0.00001	0.00027	0.00008	0.03048	0.00002	
NB-86	Calcite	6058D	6561870	0.00000	0.00000	0.00121	0.03849	99.91090	0.01335	0.00000	0.00006	0.00000	0.00005	0.03591	0.00002	Ar
NB-86	Calcite	6058E	6162266	0.00076	0.00000	0.00182	0.02392	99.88219	0.04388	0.00968	0.00006	0.00076	0.00000	0.03767	0.00000	
NB-86	Calcite	6058I	5980367	0.00001	0.00000	0.00019	0.04711	99.93385	0.00243	0.00000	0.00000	0.00000	0.00044	0.01598	0.00000	Ar

		Crush	Counts	Max.Ar	H2	He	CH4	H2O	N2	O2	H2S	Ar	CnHm	CO2	SO2	
NB-95	Quartz	6213A	1054143	0.00147	0.00000	0.00016	0.06433	97.10921	0.03321	0.01192	0.00034	0.00147	0.00366	2.77568	0.00002	
NB-95	Quartz	6213B	2609008	0.00012	0.00000	0.00110	0.07859	96.55620	0.00000	0.00000	0.00034	0.00012	0.00495	3.35882	0.00000	
NB-95	Quartz	6213F	1519068	0.00011	0.00000	0.00052	0.16914	96.95767	0.00000	0.00000	0.00018	0.00011	0.00454	2.86778	0.00016	
NB-95	Quartz	6213G	3560079	0.00044	0.00000	0.00092	0.18181	97.46474	0.00000	0.01282	0.00031	0.00044	0.00375	2.33510	0.00011	
NB-95	Quartz	6213K	2143727	0.00037	0.00000	0.00068	0.07426	96.77299	0.00000	0.00371	0.00031	0.00037	0.00403	3.14350	0.00013	
NB-95	Quartz	6213L	1058250	0.00009	0.00000	0.00022	0.09568	96.42011	0.00000	0.00000	0.00000	0.00009	0.00376	3.48010	0.00013	
NB-95	Quartz	6213M	1361330	0.00008	0.00000	0.00016	0.10631	97.02309	0.00000	0.00989	0.00019	0.00008	0.00324	2.85702	0.00010	
NB-95	Quartz	6213N	2194647	0.00007	0.00000	0.00063	0.06712	97.49698	0.00000	0.00000	0.00001	0.00007	0.00281	2.43236	0.00009	
NB-95	Quartz	6213O	1003762	0.00010	0.00000	0.00046	0.07895	96.43775	0.00000	0.00000	0.00019	0.00010	0.00403	3.47847	0.00015	

		Crush	Counts	Max.Ar	H2	He	CH4	H2O	N2	O2	H2S	Ar	CnHm	CO2	SO2	Problem
NB-96	Silica	6250C	1675087	0.00302	0.00000	0.00081	0.37486	97.06500	0.08843	0.03016	0.00071	0.00302	0.00476	2.43213	0.00011	
NB-96	Silica	6250D	1339959	0.00006	0.00000	0.00005	0.24926	98.89598	0.01172	0.00015	0.00003	0.00006	0.00157	0.84116	0.00002	
NB-96	Silica	6250F	482840.8	0.00016	0.00000	0.00000	0.58114	97.85554	0.05241	0.00044	0.00000	0.00016	0.00296	1.50728	0.00008	
NB-96	Silica	6250G	681837.5	0.00009	0.00000	0.00000	0.43796	97.43814	0.00000	0.00000	0.00021	0.00009	0.00370	2.11997	0.00002	
NB-96	Silica	6250K	6012581	0.00089	0.00000	0.00000	0.15626	99.32164	0.03496	0.00545	0.00013	0.00089	0.00127	0.47939	0.00003	
NB-96	Silica	6250L	3123.061	0.02175	9.90034	0.02472	49.20501	0.00000	2.37820	0.05295	0.00000	0.02175	0.90633	37.53245	0.00000	H2O

		Crush	Counts	Max.Ar	H2	He	CH4	H2O	N2	O2	H2S	Ar	CnHm	CO2	SO2	Problem
NB-97	Quartz	6214A	1540362	0.00045	0.00000	0.00026	0.23269	97.71711	0.00139	0.00809	0.00016	0.00045	0.00309	2.03667	0.00007	
NB-97	Quartz	6214B	907633.4	0.00126	0.00000	0.00003	0.26498	98.06175	0.07107	0.01952	0.00009	0.00126	0.00280	1.57846	0.00005	
NB-97	Quartz	6214C	3373780	0.00095	0.00000	0.00121	0.29310	97.56363	0.04411	0.01832	0.00014	0.00095	0.00328	2.07516	0.00008	
NB-97	Quartz	6214D	1580188	0.00039	0.00000	0.00012	0.12715	97.71397	0.00000	0.00732	0.00008	0.00039	0.00256	2.14833	0.00006	N2
NB-97	Quartz	6214	1361364	0.00006	0.00000	0.00018	0.19549	97.03239	0.00000	0.00000	0.00017	0.00006	0.00345	2.76819	0.00009	N2
NB-97	Quartz	6214F	958220.1	0.00008	0.00000	0.00023	0.27454	97.15855	0.00000	0.00000	0.00008	0.00008	0.00339	2.56313	0.00009	N2
NB-97	Quartz	6214G	515159	0.00033	0.00000	0.00009	0.25016	97.30639	0.00000	0.00779	0.00018	0.00033	0.00288	2.43214	0.00005	low,N2
NB-97	Quartz	6214K	917414.9	0.00008	0.00000	0.00024	0.32032	97.57936	0.00722	0.00498	0.00000	0.00008	0.00318	2.08465	0.00005	
NB-97	Quartz	6214L	1604874	0.00008	0.00000	0.00020	0.19352	97.28046	0.00000	0.03543	0.00022	0.00008	0.00315	2.48696	0.00007	N2
NB-97	Quartz	6214M	1535295	0.00006	0.00000	0.00031	0.16995	97.66319	0.01437	0.00595	0.00002	0.00006	0.00270	2.14344	0.00007	

		Crush	Counts	Ar Max.	H2	He	CH4	H2O	N2	O2	H2S	Ar	CnHm	CO2	SO2	Problem
NB-99	Quartz	6324A	651796	0.00045	0.00000	0.00115	0.32595	92.92352	0.03106	0.00000	0.00085	0.00045	0.01058	6.70622	0.00019	
NB-99	Quartz	6324B	545883	0.00001	0.00000	0.00172	0.31282	92.65728	0.00000	0.00000	0.00135	0.00001	0.01134	7.01521	0.00027	
NB-99	Quartz	6324D	518277	0.00025	0.00000	0.00167	0.64047	93.77675	0.09080	0.00000	0.00092	0.00025	0.01031	5.47880	0.00028	
NB-99	Quartz	6324E	668262	0.00124	0.00000	0.00109	0.37563	95.11384	0.07623	0.00000	0.00062	0.00124	0.00934	4.42188	0.00013	
NB-99	Quartz	6324F	2851073	0.00218	0.00000	0.00248	0.24192	95.17368	0.03232	0.00150	0.00055	0.00218	0.00739	4.53778	0.00020	N2
NB-99	Quartz	6324G	1382007	0.00042	0.00000	0.00138	0.16769	94.00031	0.01815	0.00000	0.00127	0.00042	0.00903	5.80154	0.00023	

		Crush	Counts	Max. Ar	H2	He	CH4	H2O	N2	O2	H2S	Ar	CnHm	CO2	SO2	
NB-100	Quartz	6216A	2065210	0.00001	0.00000	0.00111	0.71843	98.32487	0.06205	0.00000	0.00009	0.00001	0.00059	0.89280	0.00004	
NB-100	Quartz	6216B	665488.2	0.00004	0.02064	0.00084	1.20117	97.93796	0.11504	0.00000	0.00000	0.00004	0.00163	0.72264	0.00007	
NB-100	Quartz	6216C	1032062	0.00005	0.00000	0.00241	1.59640	97.20547	0.13474	0.00000	0.00000	0.00005	0.00199	1.05896	0.00004	
NB-100	Quartz	6216D	1286822	0.00003	0.00000	0.00141	1.00283	98.00095	0.13190	0.00000	0.00000	0.00003	0.00121	0.86167	0.00002	
NB-100	Quartz	6216E	3174728	0.00002	0.00000	0.00166	0.46714	98.52834	0.22188	0.00000	0.00000	0.00002	0.00136	0.77958	0.00002	
NB-100	Quartz	6216F	1120701	0.00002	0.00000	0.00061	1.00805	98.25744	0.13625	0.00000	0.00007	0.00002	0.00091	0.59664	0.00004	
NB-100	Quartz	6216G	1545827	0.00003	0.00000	0.00098	0.74929	98.37671	0.15531	0.00000	0.00000	0.00003	0.00139	0.71632	0.00001	
NB-100	Quartz	6216K	3317613	0.00026	0.00000	0.00076	0.83594	98.36558	0.16132	0.00000	0.00006	0.00026	0.00090	0.63517	0.00002	
NB-100	Quartz	6216L	1530231	0.00019	0.00000	0.00024	1.20135	97.92727	0.23794	0.00000	0.00008	0.00019	0.00102	0.63191	0.00000	
NB-100	Quartz	6216M	3738335	0.00016	0.00000	0.00095	0.88410	98.09772	0.11550	0.00000	0.00002	0.00016	0.00128	0.90023	0.00002	
NB-100	Quartz	6216N	3467158	0.00010	0.00000	0.00071	0.68674	98.53203	0.13344	0.00000	0.00001	0.00010	0.00134	0.64561	0.00002	

		Crush	Counts	Max. Ar	H2	He	CH4	H2O	N2	O2	H2S	Ar	CnHm	CO2	SO2	Problem
NB-100	Calcite	6217A	5686678	0.00041	0.00000	0.00125	0.14190	98.62723	0.05804	0.00000	0.00004	0.00041	0.00214	1.16894	0.00007	H2O, H2
NB-100	Calcite	6217B	6137726	0.00008	0.00000	0.00031	0.07543	98.91894	0.00000	0.00000	0.00001	0.00008	0.00139	1.00380	0.00005	
NB-100	Calcite	6217C	2451721	0.00031	0.00000	0.00000	0.05144	99.37001	0.01321	0.00000	0.00000	0.00031	0.00067	0.56434	0.00002	
NB-100	Calcite	6217D	7698231	0.00029	0.00000	0.00000	0.12696	99.30807	0.01348	0.00030	0.00000	0.00029	0.00069	0.55020	0.00001	
NB-100	Calcite	6217E	4810260	0.00035	0.00000	0.00000	0.28420	98.75375	0.01862	0.00000	0.00000	0.00035	0.00120	0.94185	0.00003	
NB-100	Calcite	6217F	8475448	0.00027	0.00000	0.00025	0.13216	99.12617	0.00970	0.00035	0.00000	0.00027	0.00090	0.73015	0.00003	
NB-100	Calcite	6217J	10898840	0.00011	0.00000	0.00034	0.07165	99.28859	0.01321	0.00000	0.00000	0.00011	0.00097	0.62510	0.00003	
NB-100	Calcite	6217K	10423720	0.00003	0.00000	0.00003	0.06933	99.14677	0.00571	0.00000	0.00002	0.00003	0.00119	0.77691	0.00004	

		Crush	Counts	Max. Ar	H2	He	CH4	H2O	N2	O2	H2S	Ar	CnHm	CO2	SO2	Problem
NB-101	Quartz	6211A	1104967	0.00509	0.00000	0.00000	0.20680	99.03116	0.29207	0.00000	0.00010	0.00509	0.00171	0.46301	0.00005	v.low
NB-101	Quartz	6211B	371256.7	0.01130	0.14487	0.00000	0.19525	98.59070	0.54073	0.00906	0.00011	0.01130	0.00225	0.50566	0.00006	v.low
NB-101	Quartz	6211C	1506552	0.00385	0.00000	0.00000	0.18470	99.02052	0.24958	0.00000	0.00006	0.00385	0.00190	0.53938	0.00003	v.low
NB-101	Quartz	6211D	688940.9	0.00734	0.01137	0.00000	0.31858	98.42022	0.43682	0.00497	0.00000	0.00734	0.00275	0.79789	0.00006	v.low
NB-101	Quartz	6211E	1170819	0.00253	0.00000	0.00012	0.18255	98.98097	0.13656	0.00000	0.00010	0.00253	0.00233	0.69474	0.00010	
NB-101	Quartz	6211F	1362152	0.00355	0.00000	0.00000	0.10280	99.32558	0.18846	0.00020	0.00008	0.00355	0.00139	0.37792	0.00002	
NB-101	Quartz	6211J	1123529	0.00155	0.00000	0.00000	0.15401	99.44701	0.11233	0.00000	0.00000	0.00155	0.00222	0.28286	0.00002	
NB-101	Quartz	6211K	904615.5	0.00535	0.00000	0.00000	0.26443	99.08123	0.29564	0.00000	0.00000	0.00535	0.00276	0.35060	0.00000	
NB-101	Quartz	6211L	699766.3	0.00230	0.00000	0.00000	0.26876	99.15573	0.13719	0.00000	0.00000	0.00230	0.00269	0.43332	0.00002	
NB-101	Quartz	6211M	729406.5	0.00341	0.01199	0.00000	0.24802	98.99156	0.21237	0.00000	0.00000	0.00341	0.00191	0.53073	0.00000	
NB-101	Quartz	6211N	813691.9	0.00219	0.00000	0.00000	0.23616	99.06855	0.14213	0.00000	0.00000	0.00219	0.00238	0.54858	0.00000	
NB-101	Quartz	6211O	840129.7	0.00282	0.00000	0.00000	0.22596	98.99679	0.15942	0.00000	0.00000	0.00282	0.00289	0.61210	0.00004	

		Crush	Counts	Max. Ar	H2	He	CH4	H2O	N2	O2	H2S	Ar	CnHm	CO2	SO2	Problem
NB-103	Quartz	6249A	200127.4	0.00005	0.00000	0.00000	0.57486	97.94026	0.15538	0.00000	0.00110	0.00005	0.00194	1.32646	0.00000	low
NB-103	Quartz	6249B	4941354	0.00002	0.00000	0.00152	0.41415	98.80122	0.21377	0.00000	0.00111	0.00002	0.00287	0.56521	0.00015	CH4, CO2
NB-103	Quartz	6249C	1173384	0.00010	0.00000	0.00070	0.68735	96.71080	0.11750	0.00000	0.00340	0.00010	0.00427	2.47593	0.00006	
NB-103	Quartz	6249D	4170253	0.00005	0.00000	0.00142	0.81569	96.55255	0.18889	0.00000	0.00264	0.00005	0.00532	2.43330	0.00013	
NB-103	Quartz	6249E	489206.4	0.00011	0.00000	0.00000	1.05883	96.58871	0.22052	0.00000	0.00203	0.00011	0.00440	2.12540	0.00011	v.low
NB-103	Quartz	6249F	1521147	0.00004	0.00000	0.00000	0.24724	99.01335	0.05447	0.00000	0.00064	0.00004	0.00152	0.68275	0.00005	
NB-103	Quartz	6249G	2112697	0.00018	0.00000	0.00156	1.27478	95.73946	0.27579	0.00000	0.00274	0.00018	0.00742	2.69789	0.00018	
NB-103	Quartz	6249J	879303.9	0.00011	0.00000	0.00000	0.73303	96.78619	0.19011	0.00000	0.00127	0.00011	0.00450	2.28478	0.00013	v.low
NB-103	Quartz	6249K	905473.7	0.00010	0.00000	0.00023	0.71103	97.08931	0.17855	0.00000	0.00178	0.00010	0.00418	2.01484	0.00008	v.low
NB-103	Quartz	6249L	940702.6	0.00011	0.00000	0.00035	0.85467	96.73643	0.20789	0.00000	0.00150	0.00011	0.00462	2.19441	0.00012	

		Crush	Counts	Ar max.	H2	He	CH4	H2O	N2	O2	H2S	Ar	CnHm	CO2	SO2	Problem
NB-104	Quartz	6428C	1754199	0.001538	0.000000	0.001874	1.001931	87.004550	0.000000	0.000000	0.005538	0.001538	0.013268	11.971250	0.000039	N2
NB-104	Quartz	6428D	925850.8	0.000640	0.000000	0.001829	1.105392	89.427210	0.000000	0.000000	0.005141	0.000640	0.009901	9.449888	0.000000	N2
NB-104	Quartz	6428E	1511005	0.001207	0.000000	0.001197	1.114775	89.883150	0.000000	0.000000	0.003223	0.001207	0.008760	8.987660	0.000017	N2
NB-104	Quartz	6428F	1540030	0.001251	0.000000	0.001712	1.136998	90.014150	0.000000	0.000000	0.001964	0.001251	0.007931	8.835995	0.000000	N2
NB-104	Quartz	6428G	2764011	0.000987	0.000000	0.001378	1.136540	92.747290	0.000000	0.000000	0.001736	0.000987	0.006182	6.105889	0.000004	N2
NB-104	Quartz	6428N	3863585	0.001176	0.000000	0.001007	0.898000	93.566710	0.000000	0.000954	0.000610	0.001176	0.005534	5.525978	0.000025	N2
NB-104	Quartz	6428O	1521158	0.001351	0.000000	0.001536	1.209754	90.256720	0.000000	0.003569	0.001382	0.001351	0.007769	8.517919	0.000000	N2
NB-104	Quartz	6428P	1044577	0.001571	0.000000	0.001945	1.108470	87.308460	0.000000	0.000000	0.001707	0.001571	0.010053	11.567800	0.000000	N2

		Crush	Counts	Ar max.	H2	He	CH4	H2O	N2	O2	H2S	Ar	CnHm	CO2	SO2	Problem
NB-104	Calcite	6430A	785410.4	0.000005	0.000000	0.000000	0.102539	98.909500	0.000000	0.000000	0.000000	0.000005	0.001135	0.986816	0.000012	
NB-104	Calcite	6430B	538771.7	0.000341	0.000000	0.000097	0.327185	98.682010	0.013781	0.000000	0.000000	0.000341	0.003499	0.973085	0.000000	
NB-104	Calcite	6430C	419819.2	0.000407	0.000000	0.000000	0.018351	99.368100	0.017705	0.000230	0.000000	0.000407	0.000370	0.594841	0.000000	CH4, CO2
NB-104	Calcite	6430D	2524585	0.000372	0.000000	0.000463	0.060753	99.406040	0.008358	0.000000	0.000000	0.000372	0.000867	0.523112	0.000029	.strong,CO2
NB-104	Calcite	6430E	4440892	0.000997	0.000000	0.000680	0.011735	99.574490	0.042580	0.010313	0.000062	0.000997	0.000328	0.358794	0.000011	low
NB-104	Calcite	6430F	968764.8	0.000461	0.000000	0.000002	0.004133	99.651460	0.016063	0.003328	0.000160	0.000461	0.000244	0.324145	0.000000	
NB-104	Calcite	6430G	6083811	0.001024	0.000000	0.001771	0.024563	99.447840	0.091506	0.005570	0.000119	0.001024	0.001074	0.426471	0.000061	CH4,CO2
NB-104	Calcite	6430H	9239875	0.000284	0.000000	0.000251	0.004111	99.759120	0.006522	0.001983	0.000000	0.000284	0.000173	0.227558	0.000003	
NB-104	Calcite	6430I	**********	0.000275	0.000000	0.000920	0.032587	99.708360	0.016414	0.001687	0.000176	0.000275	0.000377	0.239145	0.000057	
NB-104	Calcite	6430J	4516559	0.000288	0.000000	0.000000	0.017709	99.495360	0.006632	0.001070	0.000002	0.000288	0.000363	0.478565	0.000011	
NB-104	Calcite	6430K	7364627	0.000275	0.000000	0.000022	0.011594	99.526670	0.007345	0.001166	0.000000	0.000275	0.000352	0.452558	0.000013	
NB-104	Calcite	6430L	**********	0.000216	0.000000	0.000116	0.024316	99.486620	0.002982	0.000020	0.000046	0.000216	0.000449	0.485219	0.000025	
NB-104	Calcite	6430M	**********	0.000361	0.000000	0.000513	0.018937	99.561720	0.019213	0.001715	0.000061	0.000361	0.000359	0.397086	0.000030	

		Crush	Counts	Max. Ar	H2	He	CH4	H2O	N2	O2	H2S	Ar	CnHm	CO2	SO2
NB-107	Quartz	6209A	735832.6	0.00029	0.00000	0.00163	0.21868	95.52840	0.21131	0.00000	0.00138	0.00029	0.01195	4.02532	0.00134
NB-107	Quartz	6209C	5549299	0.00020	0.00000	0.00071	0.14868	95.41310	0.20247	0.00000	0.00079	0.00020	0.00822	4.22581	0.00022
NB-107	Quartz	6209D	7571808	0.00034	0.00000	0.00220	0.16175	96.33165	0.48191	0.00000	0.00152	0.00034	0.01436	3.00641	0.00021
NB-107	Quartz	6209E	4702521	0.00019	0.00000	0.00009	0.12389	94.21039	0.03460	0.00000	0.00083	0.00019	0.00783	5.62233	0.00004
NB-107	Quartz	6209F	8867061	0.00024	0.00000	0.00175	0.13284	94.33173	0.05452	0.00000	0.00064	0.00024	0.00985	5.46861	0.00006
NB-107	Quartz	6209G	9679538	0.00007	0.00000	0.00164	0.13459	94.59941	0.05568	0.00000	0.00137	0.00007	0.01062	5.19656	0.00006
NB-107	Quartz	6209K	3837124	0.00021	0.00000	0.00084	0.13518	93.64553	0.05601	0.00000	0.00062	0.00021	0.00860	6.15314	0.00009
NB-107	Quartz	6209L	2682901	0.00021	0.00000	0.00047	0.20268	93.39180	0.05861	0.00000	0.00071	0.00021	0.00860	6.33710	0.00003
NB-107	Quartz	6209M	3787845	0.00017	0.00000	0.00049	0.09653	94.38718	0.02784	0.00000	0.00047	0.00017	0.00719	5.48027	0.00003
NB-107	Quartz	6209N	3798337	0.00021	0.00000	0.00035	0.12948	93.57909	0.02175	0.00000	0.00094	0.00021	0.00855	6.25981	0.00004
NB-107	Quartz	6209O	2820668	0.00021	0.00000	0.00066	0.14680	92.40850	0.03046	0.00000	0.00065	0.00021	0.00880	7.40410	0.00004
NB-107	Quartz	6209P	7099338	0.00021	0.00000	0.00135	0.13405	94.25304	0.06170	0.00000	0.00059	0.00021	0.00873	5.54050	0.00003

		Crush	Counts	Max. Ar	H2	He	CH4	H2O	N2	O2	H2S	Ar	CnHm	CO2	SO2	Problem
NB-108	Quartz	6208A	1765782	0.00001	0.00000	0.00075	0.11389	99.45970	0.21236	0.00000	0.00000	0.00001	0.00022	0.21309	0.00000	
NB-108	Quartz	6208B	1042204	0.00005	0.00000	0.00072	0.18243	98.73631	0.19226	0.00000	0.00020	0.00005	0.00229	0.88573	0.00004	CH4
NB-108	Quartz	6208C	3607321	0.00005	0.00000	0.00188	0.32752	99.12994	0.09599	0.00000	0.00044	0.00005	0.00211	0.44208	0.00005	CO2
NB-108	Quartz	6208D	1378197	0.00011	0.00000	0.00059	0.40216	98.76000	0.07206	0.00000	0.00015	0.00011	0.00441	0.76052	0.00010	
NB-108	Quartz	6208E	1090154	0.00005	0.00000	0.00002	0.43840	98.78320	0.10075	0.00000	0.00000	0.00005	0.00224	0.67536	0.00003	
NB-108	Quartz	6208I	854680.8	0.00009	0.00000	0.00003	0.71008	98.75185	0.16884	0.00000	0.00001	0.00009	0.00357	0.36557	0.00005	
NB-108	Quartz	6208J	1025691	0.00009	0.00000	0.00005	0.68164	98.84555	0.15530	0.00000	0.00000	0.00009	0.00391	0.31354	0.00001	
NB-108	Quartz	6208K	516465.4	0.00028	0.03151	0.00000	0.81436	98.75181	0.16650	0.00000	0.00000	0.00028	0.01186	0.22390	0.00007	
NB-108	Quartz	6208L	731511.4	0.00034	0.02076	0.00007	0.86609	98.64111	0.17281	0.00000	0.00009	0.00034	0.01418	0.28487	0.00003	
NB-108	Quartz	6208M	2067356	0.00005	0.00000	0.00053	0.58967	98.97416	0.18035	0.00000	0.00003	0.00005	0.00228	0.25294	0.00005	
NB-108	Quartz	6208O	5015312	0.00004	0.00000	0.00060	0.39361	98.99125	0.16798	0.00000	0.00017	0.00004	0.00159	0.44477	0.00004	

		Crush	Counts	Max. Ar	H2	He	CH4	H2O	N2	O2	H2S	Ar	CnHm	CO2	SO2	Problem
NB-109	Quartz	6212A	105467.9	0.00017	1.58862	0.00114	0.92499	89.27659	0.08163	0.00000	0.00208	0.00017	0.00693	8.11786	0.00018	
NB-109	Quartz	6212C	1087376	0.00015	0.00000	0.00021	0.32666	98.19670	0.03440	0.00000	0.00013	0.00015	0.00278	1.43891	0.00006	
NB-109	Quartz	6212D	1078297	0.00037	0.00000	0.00241	0.67149	90.88541	0.00000	0.00000	0.00022	0.00037	0.01551	8.42464	0.00033	
NB-109	Quartz	6212E	73510.05	0.00023	0.76706	0.00134	0.88000	92.32441	0.18747	0.00000	0.00000	0.00023	0.00974	5.82998	0.00000	v.Low
NB-109	Quartz	6212F	105662.2	0.00325	0.45454	0.00000	1.49042	92.04359	0.19224	0.00000	0.00000	0.00325	0.01601	5.79982	0.00014	v.low
NB-109	Quartz	6212G	5540874	0.00004	0.00000	0.00278	0.38822	98.86997	0.17116	0.00000	0.00000	0.00004	0.00180	0.56602	0.00003	H2,CH4,H2C
NB-109	Quartz	6212H	1110376	0.00018	0.00000	0.00175	1.02873	94.49899	0.16997	0.00000	0.00000	0.00018	0.00760	4.29281	0.00015	
NB-109	Quartz	6212I	418749.2	0.00023	0.06225	0.00122	1.08189	95.79124	0.13892	0.00000	0.00000	0.00023	0.00962	2.91476	0.00009	
NB-109	Quartz	6212M	3027328	0.00009	0.00000	0.00236	0.56799	98.02115	0.19972	0.00000	0.00000	0.00009	0.00367	1.20504	0.00007	CH4
NB-109	Quartz	6212N	3206894	0.00018	0.00000	0.00201	0.15550	93.90902	0.08541	0.00000	0.00070	0.00018	0.01309	5.83384	0.00026	N2
NB-109	Quartz	6212O	1780039	0.00037	0.00000	0.00209	0.25222	90.22281	0.02765	0.00000	0.00048	0.00037	0.01531	9.47940	0.00002	
NB-109	Quartz	6212P	829630.9	0.00046	0.00000	0.00276	0.42974	86.84009	0.00793	0.00000	0.00062	0.00046	0.01927	12.69959	0.00000	
NB-109	Quartz	6212Q	94230.18	0.00110	0.24360	0.00413	1.39441	69.79996	0.00000	0.00000	0.00033	0.00110	0.04592	28.51164	0.00000	Low

		Crush	Counts	Max.Ar	H2	He	CH4	H2O	N2	O2	H2S	Ar	CnHm	CO2	SO2	Problem
NB-110	Quartz	6240A	194658.1	0.00020	0.38296	0.00000	0.90896	96.41021	0.01678	0.00000	0.00033	0.00020	0.00824	2.27251	0.00000	
NB-110	Quartz	6240B	345681.1	0.00016	0.13112	0.00000	0.36784	97.14555	0.00000	0.00000	0.00000	0.00016	0.00652	2.34896	0.00002	
NB-110	Quartz	6240C	1693117	0.00028	0.00000	0.00354	0.28732	97.57693	0.56592	0.00000	0.00089	0.00028	0.01178	1.55332	0.00029	N2,CO2
NB-110	Quartz	6240D	1322954	0.00019	0.00000	0.00101	0.27086	95.43567	0.00554	0.00000	0.00055	0.00019	0.00771	4.27851	0.00015	
NB-110	Quartz	6240E	70441.4	0.00180	0.75119	0.00000	1.51561	88.15727	0.10286	0.00000	0.00108	0.00180	0.02058	9.44924	0.00036	
NB-110	Quartz	6240F	392827.8	0.00022	0.04600	0.00000	0.78718	94.99339	0.16521	0.00000	0.00026	0.00022	0.00906	3.99879	0.00013	
NB-110	Quartz	6240G	350918	0.00028	0.02127	0.00128	0.91271	92.58345	0.08308	0.00000	0.00000	0.00028	0.01182	6.38611	0.00027	
NB-110	Quartz	6240H	422850.6	0.00061	0.00000	0.00331	1.24041	84.41102	0.00000	0.00000	0.00069	0.00061	0.02555	14.31844	0.00058	N2
NB-110	Quartz	6240I	615208.7	0.00044	0.00000	0.00236	0.63690	89.53461	0.00000	0.00000	0.00031	0.00044	0.01829	9.80711	0.00040	N2

		Crush	Counts	Max. Ar	H2	He	CH4	H2O	N2	O2	H2S	Ar	CnHm	CO2	SO2
NB-111	Pyrite	6248A	849680.3	0.00024	0.00000	0.00000	0.03260	98.83224	0.08934	0.00000	0.00009	0.00024	0.00117	1.04425	0.00009
NB-111	Pyrite	6248B	609390.8	0.00052	0.00000	0.00000	0.04056	99.26064	0.02824	0.00000	0.00008	0.00052	0.00006	0.66988	0.00000
NB-111	Pyrite	6248C	3506683	0.00049	0.00000	0.00000	0.05278	97.81666	0.14092	0.00000	0.00011	0.00049	0.00345	1.98555	0.00004
NB-111	Pyrite	6248D	3750622	0.00032	0.00000	0.00000	0.06025	98.06673	0.24168	0.00000	0.00009	0.00032	0.00302	1.62786	0.00004

DP-624 549'		Crush	Counts	Max. Ar	H2	He	CH4	H2O	N2	O2	H2S	Ar	CnHm	CO2	SO2
DP-624 5	Calcite	6218A	2637950	0.00061	0.00000	0.00000	0.00500	99.95068	0.02809	0.00733	0.00005	0.00061	0.00002	0.00821	0.00000
DP-624 5	Calcite	6218B	4265408	0.00051	0.00000	0.00000	0.00727	99.95833	0.02101	0.00449	0.00001	0.00051	0.00000	0.00838	0.00000
DP-624 5	Calcite	6218C	7598424	0.00038	0.00000	0.00124	0.00836	99.96114	0.01767	0.00222	0.00000	0.00038	0.00000	0.00900	0.00000
DP-624 5	Calcite	6218E	9382840	0.00034	0.00000	0.00071	0.01046	99.96053	0.01571	0.00361	0.00002	0.00034	0.00001	0.00861	0.00000
DP-624 5	Calcite	6218F	12715780	0.00025	0.00000	0.00133	0.00720	99.97270	0.01147	0.00326	0.00003	0.00025	0.00002	0.00374	0.00000
DP-624 5	Calcite	6218I	3909535	0.00011	0.00000	0.00000	0.01485	99.95980	0.00517	0.00073	0.00002	0.00011	0.00003	0.01927	0.00000

		Crush	Counts	Ar Max.	H2	He	CH4	H2O	N2	O2	H2S	Ar	CnHm	CO2	SO2
NB-4	Calcite	"5391A			0.02481	0.08885	0.26179	97.2355	1.36029	0.25232	0.00109	0.11459	0.19215	0.19328	0.14664
NB-4	Calcite	"5391B			0.52223	0	0.47595	98.5801	0.20244	0.01415	0.02045	0.00709	0.01754	0.14353	0.0065
NB-4	Calcite	"5391C			0.43474	0	0.32661	98.6625	0.27085	0.04656	0.00714	0.00543	0.00667	0.22927	0.00144
NB-4	Calcite	"5391D			0.15035	0	0.14122	99.2272	0.28005	0.04808	0.0051	0.00474	0.0034	0.1308	0.00122
NB-4	Calcite	"5391E			0.4324	0.04474	0.22082	98.9573	0.13132	0.05598	0.00243	0.0015	0.00414	0.14564	0.00047
NB-4	Calcite	"5391F			0.72365	0.14958	0.58104	98.0155	0.2714	0.03465	0.02551	0.00951	0.02319	0.14304	0.00949
NB-4	Calcite	"5391J			0.27618	0	0.15471	99.3008	0.10502	0.04065	0.00157	0.0013	0.0025	0.1143	0.00029
NB-4	Calcite	"5391K			0.17459	0.02134	0.13185	99.5424	0.04508	0.01313	0.00127	0.00067	0.00194	0.06607	0.00024
NB-4	Calcite	"5391L			0.43654	0	0.36641	98.8877	0.13817	0.01962	0.00861	0.00279	0.00771	0.12536	0.00215
NB-4	Calcite	"5391M			0.30485	0.04017	0.24297	99.1664	0.09421	0.0225	0.00296	0.00134	0.00383	0.11745	0.00059
NB-4	Calcite	"5391N			0.32102	0.04063	0.21264	99.1684	0.08937	0.0237	0.00267	0.00131	0.00365	0.13344	0.00052

		Crush	Counts	Ar Max.	H2	He	CH4	H2O	N2	O2	H2S	Ar	CnHm	CO2	SO2
NB-45	Quartz	5873B			0.879	0.000433	1.886	91.928	0.306	0	0.00756	0.000709	0.0296	4.963	0.000139
NB-45	Quartz	5873C			0.302	0.00457	1.018	91.819	0.0583	0	0.00347	0.00014	0.0287	6.765	0.000098
NB-45	Quartz	5873D			0.327	0.00377	1.17	93.385	0.208	0	0.00426	0.00534	0.0388	4.84	0.00004
NB-45	Quartz	5873E			0.93	0.00341	1.989	91.752	0.528	0	0.00529	0.00568	0.0267	4.76	0.000041
NB-45	Quartz	5873F			0.772	0.00403	1.805	93.281	0.1815	0	0.00377	0.0067	0.0377	3.904	0.000049
NB-45	Quartz	5873G			0.282	0.00333	0.828	93.628	0.308	0	0.0027	0.00358	0.0213	4.92	0.000062
NB-45	Quartz	5873K			0.097	0.00132	0.872	94.157	0.288	0	0.0022	0.00508	0.0328	4.543	0.000022

		Sample	H2	He	CH4	H2O	N2	O2	H2S	Ar	CnHm	CO2	SO2
NB-33	Quartz	5846B	0.04007	0	1.0585	92.1513	0.273	0	0.01078	0.001224	0.0126	6.4406	0.000064
NB-33	Quartz	5846C	0.11	0	0.69849	95.1225	0.127227	0	0.004524	0.000202	0.007926	3.9288	0
NB-33	Quartz	5846D	0.1963	0	0.5756	96.9341	0.1003	0	0.003572	0.000177	0.005756	2.1813	0.000021
NB-33	Quartz	5846E	0.03756	0.001353	0.8897	93.2174	0.1467	0	0.006761	0.000064	0.011978	5.687	0.000056
NB-33	Quartz	5846F	0.26294	0	0.9989	94.8633	0.11388	0	0.004963	0.000279	0.0116	3.7385	0.000023
NB-33	Quartz	5846G	0.03701	0.000334	1.038	92.2921	0.20973	0	0.01858	0.000085	0.012587	6.3879	0.000057
NB-33	Quartz	5846H	0.060166	0	0.918156	94.4357	0.18867	0	0.005465	0.000118	0.0107	4.3759	0.000041
NB-33	Quartz	5846I	0.08587	0.001095	1.0492	92.8296	0.1703	0	0.006119	0.00003	0.013167	5.84	0.000054
NB-33	Quartz	5846J	0.031713	0	0.8714	93.4297	0.17365	0	0.00857	0.000501	0.010287	5.466	0.000043
NB-33	Quartz	5846M	0.03757	0.003073	1.6103	86.7862	0.23298	0	0.008747	0.000513	0.021395	11.298	0.000072
NB-33	Quartz	5846N	0.042226	0.001011	1.385	90.5725	0.28916	0	0.008318	0.000414	0.016812	7.6767	0.000036
NB-33	Quartz	5846O	0.124645	0	1.16731	94.6775	0.1851	0	0.006306	0.000332	0.007854	3.82423	0.000011
NB-33	Quartz	5846P	0.040523	0.000746	1.26937	93.0304	0.2745	0	0.006485	0.000684	0.01002	5.3568	0.000032
NB-33	Calcite	5847A	0	0.000099	0.0689	99.443	0.0422	0	0.000183	0.000791	0.000814	0.44	0
NB-33	Calcite	5847C	0	0	0.112	99.442	0.0271	0	0.00041	0.00015	0.000942	0.417	0.000032
NB-33	Calcite	5847D	0	0	0.133	99.38	0.033	0	0.000499		0.000994	0.452	0.000039
NB-33	Calcite	5847E	0	0	0.11	99.243	0.0247	0	0.000351	0.000268	0.00113	0.62	0.000007
NB-33	Calcite	5847F	0	0.000304	0.133	98.998	0.0213	0	0.000508	0.000201	0.00148	0.844	0
NB-33	Calcite	5847G	0	0	0.118	99.24	0.0249	0	0.000298	0.000087	0.00112	0.615	0.000007
NB-33	Calcite	5847K	0	0	0.0898	99.212	0.0245	0	0.000226	0.000366	0.00102	0.669	0.000003
NB-33	Calcite	5847L	0	0.000109	0.099	99.217	0.0247	0	0.00023	0.000243	0.00108	0.657	0.000004
NB-33	Calcite	5847M	0	0.00131	0.111	99.29	0.0361	0	0.0003	0.00024	0.00117	0.559	0.000014
NB-33	Calcite	5847N	0	0.000024	0.114	99.148	0.0262	0	0.000229	0.000207	0.001317	0.71	0.000007
NB-33	Calcite	5847O	0	0.000019	0.0827	99.518	0.0386	0	0.000123	0.000523	0.000558	0.356	0.000003
NB-33	Calcite	5847P	0	0.000368	0.122	99.26	0.0468	0	0.000206	0.000635	0.000893	0.566	0.000004

APPENDIX D

Sample	NB-99	NB-100	NB-102	NB-103	NB-107
Na	0.96	3.38	0.87	1.24	1.05
K	0.9	0.85	0.9	0.3	0.5
Ca	4.2	5.2	0.8	0.7	0.4
Cl	1.44	8.76	0.77	2.16	1.87
F	0.16	0.14	0.18	0.14	0.12
Br	0.01	0.04	<0.01	0.02	0.01
SO_4^{2-}	1.92	1.53	0.62	0	0

Results of bulk ion leach with results reported in ppm. Cations are analyzed by AA whereas anions are analyzed by ion chromotography.

APPENDIX E

Sample preparation and irradiation:
Mineral separate obtained with standard heavy liquid and magnetic techniques. Clays obtained via floation methods.
Samples were irradiated in machined Al discs at the Univ. of Michigan Ford Reactor
along with neutron flux monitor Fish Canyon Tuff sanidine, (FC-1) with an assigned age of 27.84 Ma (Deino and Potts, 1990), relative to Mmhb-1 at 520.4 Ma (Samson and Alexander, 1987).

Instrumentation:
Mass Analyzer Products 215-50 mass spectrometer on line with automated all-metal extraction system.
Mo double-vacuum resistance furnace:
All samples step-heated.
Reactive gases removed by reaction with 3 SAES GP-50 getters, 2 operated at ~450°C and
1 at 20°C. Gas also exposed to a W filament operated at ~2000°C.

Analytical parameters:
NM-64 data: Irradiation duration 24 hours
Electron multiplier sensitivity averaged 1.0×10^{-16} moles/pA.
Total furnace system blanks plus backgrounds were about:
1500, 10, 3, 11, 11 x 10^{-18} moles at masses 40, 39, 38, 37, and 36, respectively for temperatures <1300°C.
$(^{40}Ar/^{39}Ar)_K = 0.025 \pm 0.005$; $(^{36}Ar/^{37}Ar)_{Ca} = 0.00026 \pm 0.00002$; and $(^{39}Ar/^{37}Ar)_{Ca} = 0.00065 \pm 0.00005$.
NM-80 data: Irradiation duration 24 hours
Electron multiplier sensitivity averaged 1.0×10^{-16} moles/pA.
Total furnace system blanks plus backgrounds were about:
1450, 20, 2, 1, 5 x 10^{-18} moles at masses 40, 39, 38, 37, and 36, respectively for temperatures <1300°C.
$(^{40}Ar/^{39}Ar)_K = 0.021 \pm 0.002$; $(^{36}Ar/^{37}Ar)_{Ca} = 0.00026 \pm 0.00002$; and $(^{39}Ar/^{37}Ar)_{Ca} = 0.00065 \pm 0.00005$.
NM-95 data: Irradiation duration 24 hours
Electron multiplier sensitivity averaged 1.0×10^{-16} moles/pA.
Total furnace system blanks plus backgrounds were about:
700, 8, 0.5, 4, 5 x 10^{-18} moles at masses 40, 39, 38, 37, and 36, respectively for temperatures <1300°C.
$(^{40}Ar/^{39}Ar)_K = 0.024 \pm 0.002$; $(^{36}Ar/^{37}Ar)_{Ca} = 0.00028 \pm 0.000005$; and $(^{39}Ar/^{37}Ar)_{Ca} = 0.00078 \pm 0.00003$.
NM-100 data: Irradiation duration 50 hours
Electron multiplier sensitivity averaged 1.0×10^{-16} moles/pA.
Total furnace system blanks plus backgrounds were about:
1000, 10, 1, 0.5, 3 x 10^{-18} moles at masses 40, 39, 38, 37, and 36, respectively for temperatures <1300°C.
$(^{40}Ar/^{39}Ar)_K = 0.0275 \pm 0.0001$; $(^{36}Ar/^{37}Ar)_{Ca} = 0.00028 \pm 0.000003$; and $(^{39}Ar/^{37}Ar)_{Ca} = 0.00076 \pm 0.00002$.

J-factors determined to a precision of ± 0.1% by CO_2 laser-fusion of 4 single crystals from each of 4 or 6 radial positions around the irradiation tray.
Correction factors for interfering nuclear reactions were determined using K-glass and CaF_2 and are as follows:

Age calculations:
Total gas ages and errors calculated by weighting individual steps by the fraction of ^{39}Ar released.
Plateau ages calculated for the indicated steps by weighting each step by the inverse of the variance.
Plateau age errors calculated using the method of (Taylor, 1982).
MSWD values are calculated for n-1 degrees of freedom for plateau ages.
If the MSWD is outside the 95% confidence window (cf. Mahon, 1996; Table 1), the error is multiplied by the square root of the MSWD.
Isochron data regressed using York (1969) method.
Decay constants and isotopic abundances after Steiger and Jäger (1977).
All final errors reported at $\pm 2\sigma$, unless otherwise noted.

APPENDIX F

ID	Temp (°C)	$^{40}Ar/^{39}Ar$	$^{37}Ar/^{39}Ar$	$^{36}Ar/^{39}Ar$ (x 10^{-3})	$^{39}Ar_K$ (x 10^{-16} mol)	K/Ca	$^{40}Ar^*$ (%)	^{39}Ar (%)	Age (Ma)	±1σ (Ma)
Cortez Biotite, wt. = 0.93 mg, J=0.0034332, NM-64, Lab#=7709-01										
A	*600*	*25.89*	*0.0387*	*82.27*	*15.8*	*13.2*	*6.0*	*1.9*	*9.6*	*3.0*
B	*750*	*9.400*	*0.0170*	*14.41*	*74.7*	*29.9*	*54.4*	*10.6*	*31.42*	*0.60*
C	850	7.385	0.0100	4.956	123	51.0	79.8	25.0	36.16	0.34
D	920	7.090	0.0083	4.065	104	61.6	82.7	37.1	35.96	0.37
E	1000	7.134	0.0093	4.324	235	54.9	81.7	64.6	35.76	0.20
F	1075	6.454	0.0075	2.126	230	68.1	89.9	91.5	35.58	0.19
G	1110	7.238	0.0287	3.968	33.0	17.8	83.5	95.4	37.0	1.1
H	1180	9.782	0.3364	11.99	12.5	1.5	63.8	96.8	38.3	2.8
I	1210	7.338	0.4471	3.830	27.2	1.1	84.7	100.0	38.1	1.3
total gas age			n=9		855	51.8			**35.09**	**0.88***
plateau		MSWD=1.31	n=7	steps C-I	764	54.7		89.4	**35.80**	**0.24***
NB-20 Fine Illite, wt. = 3.95 mg, J=0.0034782, NM-64, Lab#=7672-01										
B	500	5.426	0.0228	3.388	59.8	22.4	81.1	1.8	27.41	0.61
C	550	13.93	0.0220	1.964	139	23.2	95.7	6.1	81.73	0.30
E	625	14.49	0.1031	0.6720	377	4.9	98.5	17.8	87.41	0.21
F	650	15.32	0.0855	0.3578	356	6.0	99.2	28.8	92.90	0.22
G	675	16.15	0.0779	0.2538	606	6.6	99.4	47.4	98.03	0.23
H	700	16.95	0.0919	0.2286	749	5.6	99.5	70.5	102.87	0.22
I	730	17.33	0.0976	0.2807	669	5.2	99.4	91.2	105.00	0.23
J	760	18.12	0.0589	0.4635	111	8.7	99.1	94.6	109.36	0.39
K	800	22.15	0.0473	0.9291	117	10.8	98.7	98.2	132.16	0.40
L	850	37.14	0.1254	3.260	28.2	4.1	97.4	99.1	213.8	1.3
M	950	42.56	0.2413	7.092	16.3	2.1	95.1	99.6	237.6	2.1
N	1250	23.39	0.4009	14.46	14.1	1.3	81.8	100.0	116.2	2.4
total gas age			n=12		3243	7.0			**100.19**	**0.27**
NB-20 Coarse Illite, wt. 3.52 mg, J=0.0034500, NM-64, Lab#=7674-01										
B	500	9.379	0.0120	3.018	85.7	42.5	90.2	2.8	52.66	0.43
C	550	15.46	0.0109	1.554	108	46.7	96.9	6.3	92.15	0.36
D	600	14.75	0.0104	0.4704	203	49.1	98.9	12.9	89.84	0.27
E	625	15.62	0.0107	0.4446	288	47.5	99.0	22.3	95.10	0.25
F	650	16.04	0.0104	0.2153	406	49.1	99.5	35.4	98.01	0.22
G	675	16.36	0.0099	0.1624	532	51.3	99.6	52.7	100.05	0.24
H	700	16.84	0.0093	0.2020	576	54.9	99.5	71.4	102.83	0.23
I	730	17.59	0.0090	0.1848	542	56.8	99.6	89.0	107.31	0.24
J	760	20.85	0.0094	0.4129	220	54.5	99.3	96.1	126.21	0.32
K	800	29.05	0.0093	0.5130	49.4	54.7	99.4	97.8	173.66	0.75
L	850	49.10	0.0138	2.013	51.0	37.1	98.7	99.4	282.75	0.95
M	950	86.03	0.0271	8.198	12.0	18.9	97.2	99.8	463.0	3.1
N	1250	24.53	0.0735	43.72	6.25	6.9	47.3	100.0	71.8	5.7
total gas age			n=13		3079	51.6			**106.28**	**0.60***

ID	Temp (°C)	$^{40}Ar/^{39}Ar$	$^{37}Ar/^{39}Ar$	$^{36}Ar/^{39}Ar$ (x 10^{-3})	$^{39}Ar_K$ (x 10^{-16} mol)	K/Ca	$^{40}Ar^*$ (%)	^{39}Ar (%)	Age (Ma)	±1σ (Ma)
NB-19 Illite, wt.= 4.07 mg, J=0.0034297, NM-64, Lab#=7676-01										
B	500	8.202	0.0326	8.626	83.7	15.6	68.6	3.8	34.50	0.48
C	550	12.70	0.0291	3.831	140	17.5	90.9	10.1	70.04	0.31
D	600	13.59	0.0194	-4.4523	5.44	26.4	109.5	10.4	89.8	5.8
E	625	17.95	0.0276	0.8412	468	18.5	98.5	31.6	106.21	0.23
F	650	19.99	0.0272	0.4759	298	18.7	99.2	45.0	118.71	0.28
G	675	21.61	0.0267	0.4778	322	19.1	99.2	59.6	128.05	0.29
H	700	24.71	0.0258	0.5383	279	19.8	99.3	72.3	145.73	0.35
I	730	30.20	0.0250	0.6925	232	20.4	99.2	82.8	176.54	0.49
J	760	37.36	0.0251	0.9964	143	20.3	99.2	89.2	215.75	0.49
K	800	42.99	0.0261	1.366	60.2	19.5	99.0	92.0	245.84	0.77
L	850	52.59	0.0292	1.424	82.8	17.5	99.2	95.7	296.84	0.76
M	950	53.42	0.0448	5.091	37.2	11.4	97.1	97.4	295.5	1.2
N	1250	5.126	0.0700	3.327	57.5	7.3	80.4	100.0	25.34	0.61
total gas age			n=13		2209	18.5			**137.54**	**0.78***
Cortez K-feldspar, wt. = 0.88 mg, J=0.0034276, NM-64, Lab#=7705-01										
C	800	10.63	0.0058	16.45	164	88.4	54.0	8.2	35.19	0.43
E	900	6.960	0.0103	7.218	10.0	49.8	69.0	8.7	29.5	3.8
F	900	6.975	0.0059	4.619	26.3	85.8	80.1	10.0	34.2	1.4
G	1000	6.217	0.0045	1.896	52.3	113.1	90.6	12.6	34.50	0.74
H	1100	6.008	0.0050	1.031	145	101.4	94.5	19.9	34.78	0.28
I	1200	6.028	0.0050	1.113	288	101.8	94.1	34.2	34.75	0.17
J	1250	5.827	0.0047	0.3657	304	109.2	97.7	49.4	34.87	0.15
K	1300	5.869	0.0048	0.4003	292	107.2	97.6	63.9	35.06	0.16
L	1350	6.011	0.0046	0.7785	175	111.9	95.8	72.7	35.25	0.23
M	1400	6.000	0.0046	0.7441	195	111.2	95.9	82.4	35.24	0.22
N	1750	6.391	0.0050	2.338	352	101.4	88.8	100.0	34.76	0.16
total gas age			n=11		2003	104.1			**34.91**	**0.50***
plateau		MSWD=0.93	n=11	steps C-N	2003	104.1		100.0	**34.93**	**0.13***
NB-59 Illite, wt. = 10.64 mg, J=0.0037063, NM-80, Lab#=8602-01										
B	500	6.986	0.0055	3.780	89.6	92.7	83.7	1.8	38.69	0.17
C	550	17.14	0.0062	2.269	87.5	81.7	96.0	3.6	106.77	0.20
D	600	14.43	0.0074	1.240	34.7	68.9	97.3	4.3	91.51	0.28
E	625	15.41	0.0049	0.7376	308	103.8	98.5	10.5	98.71	0.19
F	650	16.01	0.0063	0.6135	409	80.7	98.7	18.7	102.74	0.18
G	675	16.36	0.0061	0.5560	558	84.3	98.9	30.0	105.05	0.18
H	700	16.71	0.0047	0.5889	681	108.8	98.8	43.7	107.20	0.27
I	740	17.21	0.0042	0.6749	993	120.1	98.7	63.7	110.20	0.21
J	780	19.88	0.0040	0.8429	882	127.8	98.6	81.4	126.56	0.29
K	800	28.88	0.0042	1.836	361	121.6	98.0	88.7	180.03	0.33
L	850	47.04	0.0043	2.302	242	118.6	98.5	93.6	285.94	0.58
M	900	72.48	0.0065	3.489	101	78.1	98.5	95.6	423.72	0.79
N	1000	64.71	0.0486	4.012	80.6	10.5	98.1	97.3	381.35	0.72
O	1650	5.729	0.0191	4.769	136	26.7	75.1	100.0	28.53	0.16
total gas age			n=14		4965	104.9			**131.52**	**0.54***

ID	Temp (°C)	$^{40}Ar/^{39}Ar$	$^{37}Ar/^{39}Ar$	$^{36}Ar/^{39}Ar$ (x 10^{-3})	$^{39}Ar_K$ (x 10^{-16} mol)	K/Ca	$^{40}Ar^*$ (%)	^{39}Ar (%)	Age (Ma)	±1σ (Ma)
93271 K-feldspar, wt. = 6.97 mg, J=0.0039260, NM-95, Lab#=9577-01										
A	700	8.384	0.0222	11.18	104	23.0	60.3	1.3	35.48	0.47
B	800	5.263	0.0125	0.4233	317	40.9	97.2	5.4	35.87	0.13
C	900	5.170	0.0097	0.2097	651	52.4	98.4	13.7	35.658	0.090
D	1000	5.149	0.0085	0.1580	1217	59.7	98.6	29.3	35.623	0.074
E	1100	5.138	0.0081	0.1011	1590	63.0	99.0	49.6	35.658	0.073
F	1200	5.155	0.0078	0.1150	1303	65.4	98.9	66.3	35.752	0.069
G	1250	5.146	0.0069	0.0412	1876	73.9	99.3	90.3	35.836	0.073
H	1300	5.137	0.0082	0.0648	758	61.9	99.2	100.0	35.729	0.078
total gas age			n=8		7815	63.1			**35.72**	**0.16***
plateau			n=8	steps A-H	7815	63.1		100.0	**35.72**	**0.06***
93271 Biotite, wt. = 8.35 mg, J=0.003911, NM-95, Lab#=9576-01										
A	*650*	*32.68*	*0.0674*	*103.6*	*126*	*7.6*	*6.3*	*1.6*	*14.5*	*1.1*
B	*750*	*7.611*	*0.0254*	*9.468*	*483*	*20.1*	*62.9*	*7.8*	*33.49*	*0.17*
C	830	5.493	0.0070	1.182	972	72.4	93.2	20.1	35.767	0.079
D	900	5.352	0.0060	0.6091	1122	85.2	96.2	34.4	35.966	0.075
E	970	5.403	0.0078	0.8376	935	65.4	95.0	46.3	35.848	0.080
F	1050	5.408	0.0124	0.7288	1149	41.0	95.6	61.0	36.111	0.071
G	1120	5.305	0.0214	0.5701	2200	23.9	96.4	89.0	35.724	0.073
H	1180	5.305	0.3993	0.7169	571	1.3	96.2	96.3	35.656	0.093
I	1240	5.406	0.6488	0.8043	257	0.79	96.2	99.6	36.32	0.15
J	1350	6.463	0.1303	3.989	35.2	3.9	81.6	100.0	36.81	0.92
total gas age			n=10		7849	43.1			**35.38**	**0.22***
plateau		MSWD=4.93**	n=8	steps C-J	7240	45.3		92.2	**35.88**	**0.14***
NB-102 Sericite, wt. 5.71 mg, J=0.0039223, NM-95, Lab#=9574-01										
A	600	25.59	0.0288	33.45	62.6	17.7	61.3	11.9	107.71	0.84
B	630	16.64	0.0190	2.594	68.8	26.9	95.3	25.0	108.79	0.53
C	660	15.96	0.0131	0.8573	54.3	39.0	98.3	35.4	107.68	0.63
D	690	15.47	0.0095	0.8151	35.0	53.5	98.3	42.0	104.50	0.94
E	720	15.05	0.0108	0.8740	63.5	47.4	98.1	54.1	101.56	0.55
F	750	14.64	0.0170	1.100	56.9	30.1	97.6	65.0	98.38	0.62
G	780	14.15	0.0256	0.8151	51.3	20.0	98.1	74.7	95.70	0.68
H	810	13.77	0.0349	0.8174	33.5	14.6	98.1	81.1	93.1	1.0
I	840	13.28	0.0415	0.9153	13.7	12.3	97.8	83.7	89.7	2.5
J	870	12.92	0.0547	0.0123	9.17	9.3	99.8	85.5	89.0	3.7
K	900	11.90	0.0578	0.4717	5.23	8.8	98.7	86.5	81.2	6.5
L	1000	9.373	0.0765	3.602	9.60	6.7	88.5	88.3	57.7	3.6
M	1100	6.075	0.0932	5.187	12.8	5.5	74.5	90.7	31.7	2.8
N	1200	4.227	0.0856	6.170	10.7	6.0	56.5	92.8	16.8	3.4
O	1300	4.426	0.0954	10.26	12.5	5.4	31.1	95.2	9.7	3.0
P	1650	11.76	0.1630	25.52	25.4	3.1	35.8	100.0	29.5	1.6
total gas age			n=16		525	26.3			92.0	1.1

ID	Temp (°C)	$^{40}Ar/^{39}Ar$	$^{37}Ar/^{39}Ar$	$^{36}Ar/^{39}Ar$ (x 10^{-3})	$^{39}Ar_K$ (x 10^{-16} mol)	K/Ca	$^{40}Ar^*$ (%)	^{39}Ar (%)	Age (Ma)	±1σ (Ma)
JM-coarse Biotite, wt. 2.77 mg, J=0.0078027, NM-100, Lab#=9912-01										
B	*680*	*13.54*	*0.1147*	*10.63*	*117*	*4.4*	*76.7*	*2.2*	*140.5*	*1.3*
C	750	11.86	0.0146	1.862	441	35.0	95.1	10.6	152.17	0.48
D	820	11.43	0.0035	0.3904	1168	147.6	98.8	32.7	152.30	0.47
E	900	11.40	0.0050	0.2238	946	103.0	99.2	50.6	152.59	0.39
F	950	11.43	0.0176	0.3452	363	28.9	98.9	57.5	152.44	0.43
G	1025	11.34	0.0298	0.3961	576	17.1	98.7	68.4	151.19	0.38
H	1200	11.43	0.0581	0.3363	1475	8.8	98.9	96.4	152.56	0.39
I	1300	12.89	0.7204	5.296	192	0.71	88.1	100.0	153.30	0.73
total gas age			n=8		5278	60.5			**152.08**	**0.95***
plateau		MSWD=1.91	n=7	steps C-I	5161	61.8		97.8	**152.24**	**0.33***
JM-fine Biotite, wt. = 3.41 mg, J=0.0076919, NM-100, Lab#=9914-01										
A	*600*	*9.180*	*0.0178*	*21.72*	*182*	*28.7*	*29.8*	*2.5*	*37.57*	*0.94*
B	*680*	*4.965*	*0.0074*	*6.569*	*221*	*69.3*	*60.4*	*5.6*	*41.12*	*0.61*
C	*750*	*3.351*	*0.0018*	*1.463*	*563*	*281.7*	*86.3*	*13.3*	*39.69*	*0.24*
D	*820*	*2.872*	*0.0011*	*0.3869*	*777*	*463.4*	*95.1*	*24.1*	*37.50*	*0.17*
E	900	2.724	0.0010	0.2206	979	528.8	96.6	37.6	36.15	0.16
F	950	2.766	0.0010	0.2928	632	530.9	95.9	46.3	36.44	0.20
G	1025	2.749	0.0011	0.2833	1319	474.7	96.0	64.5	36.24	0.12
H	1200	2.753	0.0032	0.2893	2226	161.2	95.9	95.3	36.272	0.094
I	1300	3.207	0.0124	1.668	343	41.1	83.8	100.0	36.91	0.36
total gas age			n=9		7242	330.2			**36.87**	**0.38***
plateau		MSWD=1.12	n=5	steps E-I	5500	336.8		75.9	**36.28**	**0.12***

ID	Temp (°C)	$^{40}Ar/^{39}Ar$	$^{37}Ar/^{39}Ar$	$^{36}Ar/^{39}Ar$ (x 10^{-3})	$^{39}Ar_K$ (x 10^{-16} mol)	K/Ca	$^{40}Ar^*$ (%)	^{39}Ar (%)	Age (Ma)	±1σ (Ma)
JM-coarse K-feldspar, wt. = 14.24 mg, J=0.0077880, NM-100, Lab#=9913-01										
A	450	312.0	0.0345	28.99	51.8	14.8	97.2	0.2	2188.1	3.8
B	450	7.912	0.0093	2.521	13.6	55.1	90.2	0.3	97.6	2.2
C	500	18.30	0.0155	1.543	61.8	33.0	97.4	0.6	234.49	0.74
D	500	5.459	0.0149	1.099	41.2	34.2	93.6	0.7	70.38	0.82
E	550	34.39	0.0161	1.996	190	31.8	98.2	1.6	421.30	0.85
F	550	4.466	0.0350	1.236	85.8	14.6	91.3	1.9	56.37	0.28
G	600	16.01	0.0416	1.356	238	12.3	97.3	3.0	206.66	0.42
H	600	4.046	0.0615	1.058	121	8.3	91.7	3.5	51.41	0.26
I	650	9.282	0.0631	0.8432	246	8.1	97.1	4.5	122.36	0.27
J	650	4.076	0.0739	0.9930	151	6.9	92.3	5.2	52.09	0.22
K	700	6.622	0.0724	0.6828	257	7.0	96.6	6.3	87.73	0.21
L	700	4.281	0.0707	0.8728	172	7.2	93.5	7.0	55.36	0.19
M	750	6.240	0.0671	0.9878	110	7.6	95.0	7.5	81.40	0.29
N	800	6.905	0.0705	0.5824	299	7.2	97.2	8.8	91.91	0.22
O	850	5.730	0.0615	0.3675	443	8.3	97.7	10.7	77.00	0.18
P	900	5.242	0.0677	0.3073	561	7.5	97.8	13.2	70.67	0.16
Q	950	6.134	0.0769	2.920	612	6.6	85.6	15.8	72.30	0.23
R	1000	6.161	0.0702	0.7217	640	7.3	96.2	18.6	81.40	0.19
S	1050	7.148	0.0494	0.3319	721	10.3	98.3	21.7	96.11	0.23
T	1100	8.676	0.0282	0.3747	908	18.1	98.4	25.6	116.17	0.27
U	1100	8.951	0.0172	0.4027	1483	29.7	98.4	32.0	119.66	0.26
V	1100	9.257	0.0144	0.4799	1721	35.4	98.2	39.5	123.39	0.26
W	1100	9.638	0.0147	0.7734	1886	34.8	97.4	47.7	127.24	0.27
X	1100	10.40	0.0158	0.9366	1833	32.3	97.1	55.6	136.61	0.37
Y	1100	11.44	0.0175	1.469	1816	29.1	96.0	63.5	148.01	0.29
Z	1230	11.90	0.0247	0.4127	649	20.7	98.8	66.3	158.00	0.32
ZA	1280	11.49	0.0191	0.2172	1969	26.7	99.2	74.8	153.50	0.51
ZB	1330	11.42	0.0116	0.1393	4440	44.0	99.4	94.0	152.86	0.37
ZC	1430	10.58	0.1661	0.4387	871	3.1	98.6	97.8	140.98	0.31
ZD	1530	10.43	0.1460	0.7142	449	3.5	97.8	99.7	137.93	0.33
ZE	1650	14.11	0.1750	9.826	63.6	2.9	79.3	100.0	150.84	0.72
total gas age			n=31		23101	26.6			**136.37**	**0.65***

ID	Temp (°C)	$^{40}Ar/^{39}Ar$	$^{37}Ar/^{39}Ar$	$^{36}Ar/^{39}Ar$ (x 10^{-3})	$^{39}Ar_K$ (x 10^{-16} mol)	K/Ca	$^{40}Ar^*$ (%)	^{39}Ar (%)	Age (Ma)	±1σ (Ma)
JM-fine K-feldspar, wt. = 9.73 mg, J=0.0076364, NM-100, Lab#=9915-01										
A	*550*	*10.91*	*0.0584*	*24.38*	*32.5*	*8.7*	*33.8*	*0.1*	*50.1*	*1.7*
B	*550*	*4.009*	*0.0446*	*3.615*	*13.3*	*11.4*	*72.8*	*0.2*	*39.7*	*1.9*
C	*600*	*3.187*	*0.0493*	*0.6886*	*17.5*	*10.3*	*92.9*	*0.3*	*40.3*	*1.4*
D	*600*	*3.195*	*0.0489*	*1.581*	*30.1*	*10.4*	*84.6*	*0.4*	*36.88*	*0.89*
E	*650*	*3.352*	*0.0496*	*3.578*	*14.7*	*10.3*	*67.8*	*0.5*	*31.0*	*1.7*
F	750	2.672	0.0170	0.3439	245.8	30.0	95.2	1.6	34.72	0.13
G	850	2.611	0.0070	0.1484	722.0	72.7	97.3	4.8	34.654	0.087
H	950	2.597	0.0061	0.0558	1493	84.2	98.3	11.6	34.839	0.074
I	1025	2.584	0.0059	0.0497	1800	86.6	98.4	19.7	34.685	0.088
J	1100	2.586	0.0057	0.0454	2434	90.3	98.4	30.6	34.726	0.082
K	1150	2.586	0.0056	0.0981	1569	91.1	97.8	37.7	34.519	0.074
L	1200	2.578	0.0056	0.0587	1952	91.2	98.3	46.4	34.571	0.071
M	*1250*	*2.584*	*0.0055*	*0.0381*	*3010*	*93.3*	*98.5*	*60.0*	*34.738*	*0.078*
N	*1350*	*2.600*	*0.0054*	*0.0218*	*6412*	*94.8*	*98.7*	*88.8*	*35.011*	*0.076*
O	*1600*	*2.676*	*0.0058*	*0.1642*	*2485*	*87.7*	*97.2*	*100.0*	*35.471*	*0.081*
total gas age			n=15		22232	89.5			**34.90**	**0.17***
plateau		MSWD=1.12	n=7	steps F-L	10216	86.3		46.7	**34.66**	**0.12***

Notes:
Isotopic ratios corrected for blank, radioactive decay, and mass discrimination, not corrected for interferring reactions.
Individual analyses show analytical error only; total gas age error includes error in J and irradiation parameters.
n= number of heating steps
K/Ca = molar ratio calculated from reactor produced $^{39}Ar_K$ and $^{37}Ar_{Ca}$.

* 2σ error

Sample	Mineral	Lab #	Plateau age (Ma)	Plateau Error (Ma)	Plateau MSWD	Steps (Plateau)	Isochron age (Ma)	Isochron Error (Ma)	$^{40}Ar/^{36}Ar_i$	$^{40}Ar/^{36}Ar_i$ Error	Steps (Isochron)	Isochron MSWD
Cortez	Biotite	7709	35.8	0.24	1.31	C-I	35.17	0.76	325	34	C-I	1.01
Cortez	K-feldspar	7705	34.93	0.13	0.93	C-N	34.92	0.15	296.2	8.8	C-N	1.16
93271	Biotite	9576	35.88	0.14	4.93*	C-I	35.83	0.59	310	35	C-I	8.78*
93271	K-feldspar	9577	35.72	0.06	1.04	A-H	35.72	0.08	293	12	A-H	1.38
JM-fine	Biotite	9914	36.28	0.12	1.12	E-I	36.12	0.22	332	42	E-I	0.32
JM-fine	K-feldspar	9915	34.66	0.06	1.98	F-L	34.67	0.11	290	58	F-L	2.88
JM-fine	K-feldspar	9915	-	-	-	M-O	34.78	0.47	603	100	M-O	11.1*
JM-coarse	Biotite	9912	152.2	0.33	1.91	C-I	152.1	0.46	310	22	C-I	2.19
JM-coarse	K-feldspar	9913	-	-	-	-	-	-	-	-	-	-

All errors 2σ

* MSWD ouside 95% confidence level, error multiplied by square root MSWD

APPENDIX G

ISOCHORES CALCULATIONS THAT TAKE GAS CONTENT INTO ACCOUNT

H2O-CO2-NaCl

Stack	Sample	Inclusion	Length	Width
NB107	NB107	1		

T	P (Bowers & Helgeson)
192.9	609
200	642
220	1190
240	1726
260	2250
280	2763
300	3268
320	3765
340	4255
360	4738
380	5215
400	5687

Tm clath	7.3
Th CO2 L-V	23
Th to	vapor
CO2 VolFrac	0.05
T of Estim	23
Th Total	192.9
L-V	L

Th	P @ Th
192.9	609

CO2 Den	0.22
CO2 MV	199.67
Aqueous Den	1.031
Molal NaCl	0.93
Wt% NaCl	5.154
X(NaCl)	0.016
Bulk XH2O	0.979
Bulk XCO2	0.005
Bulk XNaCl	0.016
Bulk Den	0.991
Bulk MV	18.98

Stack	Sample	Inclusion	Length	Width
NB107	NB107	2		

T	P (Bowers & Helgeson)
233	1544
240	1730
260	2251
280	2763
300	3266
320	3761
340	4250
360	4732
380	5209
400	5680

Tm clath	7.1
Th CO2 L-V	23
Th to	vapor
CO2 VolFrac	0.05
T of Estim	23
Th Total	233.1
L-V	L

Th	P @ Th
233.1	1544

CO2 Den	0.22
CO2 MV	199.67
Aqueous Den	1.034
Molal NaCl	0.997
Wt% NaCl	5.507
X(NaCl)	0.018
Bulk XH2O	0.978
Bulk XCO2	0.005
Bulk XNaCl	0.018
Bulk Den	0.993
Bulk MV	18.977

Stack	Sample	Inclusion	Length	Width
NB107	NB107	3		

T	P (Bowers & Helgeson)
225.2	1323
240	1720
260	2242
280	2754
300	3257
320	3752
340	4241
360	4723
380	5199
400	5671

Tm clath	7.2
Th CO2 L-V	23
Th to	vapor
CO2 VolFrac	0.05
T of Estim	23
Th Total	225.2
L-V	L

Th	P @ Th
225.2	1323

CO2 Den	0.22
CO2 MV	199.67
Aqueous Den	1.034
Molal NaCl	0.997
Wt% NaCl	5.507
X(NaCl)	0.018
Bulk XH2O	0.978
Bulk XCO2	0.005
Bulk XNaCl	0.018
Bulk Den	0.993
Bulk MV	18.977

Stack	Sample	Inclusion	Length	Width
NB107	NB107	4		

T	P (Bowers & Helgeson)
224	1293
240	1726
260	2250
280	2763
300	3268
320	3765
340	4255
360	4738
380	5215
400	5687

Tm clath	7.3
Th CO2 L-V	23
Th to	vapor
CO2 VolFrac	0.05
T of Estim	23
Th Total	224
L-V	L

Th	P @ Th
224	1293

CO2 Den	0.22
CO2 MV	199.67
Aqueous Den	1.031
Molal NaCl	0.93
Wt% NaCl	5.154
X(NaCl)	0.016
Bulk XH2O	0.979
Bulk XCO2	0.005
Bulk XNaCl	0.016
Bulk Den	0.991
Bulk MV	18.98

NB107	NB107	10			
T	P (Bowers & Helgeson)				
		Tm clath	7.9	CO2 Den	0.22
220.1	649	Th CO2 L-V	23	CO2 MV	199.67
240	1154	Th to	vapor	Aqueous Den	1.023
260	1646	CO2 VolFrac	0.08	Molal NaCl	0.727
280	2126	T of Estim	23	Wt% NaCl	4.074
300	2597	Th Total	220.1	X(NaCl)	0.013
320	3058	L-V	L	Bulk XH2O	0.979
340	3512			Bulk XCO2	0.008
360	3958			Bulk XNaCl	0.013
380	4399	Th	P @ Th	Bulk Den	0.958
400	4833	220.1	649	Bulk MV	19.55

NB107	NB107	11			
T	P (Bowers & Helgeson)				
214.7	677	Tm clath	7.8	CO2 Den	0.22
220	819	Th CO2 L-V	23	CO2 MV	199.67
240	1337	Th to	vapor	Aqueous Den	1.024
260	1841	CO2 VolFrac	0.07	Molal NaCl	0.761
280	2334	T of Estim	23	Wt% NaCl	4.256
300	2817	Th Total	214.7	X(NaCl)	0.014
320	3291	L-V	L	Bulk XH2O	0.98
340	3757			Bulk XCO2	0.007
360	4217			Bulk XNaCl	0.013
380	4670	Th	P @ Th	Bulk Den	0.968
400	5117	214.7	677	Bulk MV	19.358

NB107	NB107	12			
T	P (Bowers & Helgeson)				
210.5	721	Tm clath	6.3	CO2 Den	0.22
220	962	Th CO2 L-V	23	CO2 MV	199.67
240	1456	Th to	vapor	Aqueous Den	1.045
260	1943	CO2 VolFrac	0.06	Molal NaCl	1.264
280	2424	T of Estim	23	Wt% NaCl	6.878
300	2899	Th Total	210.5	X(NaCl)	0.022
320	3368	L-V	L	Bulk XH2O	0.972
340	3831			Bulk XCO2	0.006
360	4290			Bulk XNaCl	0.022
380	4744	Th	P @ Th	Bulk Den	0.995
400	5193	210.5	721	Bulk MV	19.149

NB107	NB107	13			
T	P (Bowers & Helgeson)				
203.7	561	Tm clath	7.9	CO2 Den	0.22
220	1009	Th CO2 L-V	23	CO2 MV	199.67
240	1544	Th to	vapor	Aqueous Den	1.023
260	2066	CO2 VolFrac	0.06	Molal NaCl	0.727
280	2575	T of Estim	23	Wt% NaCl	4.074
300	3074	Th Total	203.7	X(NaCl)	0.013
320	3564	L-V	L	Bulk XH2O	0.981
340	4046			Bulk XCO2	0.006
360	4521			Bulk XNaCl	0.013
380	4989	Th	P @ Th	Bulk Den	0.974
400	5451	203.7	561	Bulk MV	19.174

NB107 NB107
T P (Bowers & Helgeson)

300	1746
310	1892
320	2038
340	2326
360	2612
380	2894
400	3173
420	3448
440	3719

5

Tm clath	7.2
Th CO2 L-V	24.1
Th to	liquid
CO2 VolFrac	0.4
T of Estim	24.1
Th Total	310
L-V	L

Th	P @ Th
310	1892

CO2 Den	0.725
CO2 MV	60.733
Aqueous Den	1.032
Molal NaCl	0.964
Wt% NaCl	5.331
X(NaCl)	0.017
Bulk XH2O	0.82
Bulk XCO2	0.166
Bulk XNaCl	0.014
Bulk Den	0.909
Bulk MV	25.191

NB107 NB107
T P (Bowers & Helgeson)

300	1766
310	1911.5
320	2057
340	2346
360	2632
380	2915
400	3195
420	3471
440	3743

6

Tm clath	6.8
Th CO2 L-V	23.8
Th to	liquid
CO2 VolFrac	0.4
T of Estim	23.8
Th Total	310
L-V	L

Th	P @ Th
310	1911.5

CO2 Den	0.729
CO2 MV	60.387
Aqueous Den	1.038
Molal NaCl	1.098
Wt% NaCl	6.028
X(NaCl)	0.019
Bulk XH2O	0.817
Bulk XCO2	0.167
Bulk XNaCl	0.016
Bulk Den	0.914
Bulk MV	25.159

NB107 NB107
T P (Bowers & Helgeson)

221.6	1241
240	1730
260	2251
280	2763
300	3266
320	3761
340	4250
360	4732
380	5209
400	5680

7

Tm clath	7.1
Th CO2 L-V	23
Th to	vapor
CO2 VolFrac	0.05
T of Estim	23
Th Total	221.6
L-V	L

Th	P @ Th
221.6	1241

CO2 Den	0.22
CO2 MV	199.67
Aqueous Den	1.034
Molal NaCl	0.997
Wt% NaCl	5.507
X(NaCl)	0.018
Bulk XH2O	0.978
Bulk XCO2	0.005
Bulk XNaCl	0.018
Bulk Den	0.993
Bulk MV	18.977

NB107 NB107
T P (Bowers & Helgeson)

227.8	1047
240	1361
260	1859
280	2346
300	2825
320	3296
340	3759
360	4217
380	4668
400	5114

9

Tm clath	7.4
Th CO2 L-V	26.8
Th to	vapor
CO2 VolFrac	0.07
T of Estim	26.8
Th Total	227.8
L-V	L

Th	P @ Th
227.8	1047

CO2 Den	0.268
CO2 MV	164.472
Aqueous Den	1.029
Molal NaCl	0.896
Wt% NaCl	4.976
X(NaCl)	0.016
Bulk XH2O	0.976
Bulk XCO2	0.008
Bulk XNaCl	0.016
Bulk Den	0.975
Bulk MV	19.343

NB107 NB107 14
T P (Bowers & Helgeson)

		Tm clath	7.8	CO2 Den	0.22
227.9	1226	Th CO2 L-V	23	CO2 MV	199.67
240	1539	Th to	vapor	Aqueous Den	1.024
260	2058	CO2 VolFrac	0.06	Molal NaCl	0.761
280	2566	T of Estim	23	Wt% NaCl	4.256
300	3063	Th Total	227.9	X(NaCl)	0.014
320	3552	L-V	L	Bulk XH2O	0.981
340	4032			Bulk XCO2	0.006
360	4506			Bulk XNaCl	0.013
380	4973	Th	P @ Th	Bulk Den	0.976
400	5434	227.9	1226	Bulk MV	19.172

NB107 NB107 15
T P (Bowers & Helgeson)

		Tm clath	7.3	CO2 Den	0.713
		Th CO2 L-V	24.9	CO2 MV	61.72
		Th to	liquid	Aqueous Den	1.031
300	1571	CO2 VolFrac	0.45	Molal NaCl	0.93
308.7	1676	T of Estim	24.9	Wt% NaCl	5.154
320	1836	Th Total	308.7	X(NaCl)	0.016
340	2098	L-V	L	Bulk XH2O	0.793
360	2357			Bulk XCO2	0.194
380	2614			Bulk XNaCl	0.013
400	2866	Th	P @ Th	Bulk Den	0.888
420	3116	308.7	1676	Bulk MV	26.573
440	3361				

NB107 NB107 16
T P (Bowers & Helgeson)

		Tm clath	7.3	CO2 Den	0.708
		Th CO2 L-V	25.2	CO2 MV	62.118
		Th to	liquid	Aqueous Den	1.03
300	1548	CO2 VolFrac	0.45	Molal NaCl	0.93
312.8	1718	T of Estim	25.2	Wt% NaCl	5.154
320	1812	Th Total	312.8	X(NaCl)	0.016
340	2072	L-V	L	Bulk XH2O	0.794
360	2330			Bulk XCO2	0.193
380	2585			Bulk XNaCl	0.013
400	2837	Th	P @ Th	Bulk Den	0.886
420	3085	312.8	1718	Bulk MV	26.608
440	3330				

NB107 NB107 17
T P (Bowers & Helgeson)

		Tm clath	7.3	CO2 Den	0.729
		Th CO2 L-V	23.8	CO2 MV	60.387
		Th to	liquid	Aqueous Den	1.031
300	1563	CO2 VolFrac	0.5	Molal NaCl	0.93
310.3	1707	T of Estim	23.8	Wt% NaCl	5.154
320	1809	Th Total	310.3	X(NaCl)	0.016
340	2053	L-V	L	Bulk XH2O	0.757
360	2295			Bulk XCO2	0.231
380	2534			Bulk XNaCl	0.013
400	2769	Th	P @ Th	Bulk Den	0.88
420	3002	310.3	1707	Bulk MV	27.877
440	3230				

H2O-NaCl-[KCl]

Stack	Sample	Inclusion				
NB-33	NB-33	1				
T	P (Bodnar & Vityk)	P(gases)	P(Total)			
188.4	8				Tm ice	-5.4
200	206	911	1117		Th L-V	188.4
220	549	811	1360		Th to	L
240	891	714	1605		Molal NaCl	1.56
260	1233	625	1858		Wt% NaCl	8.38
280	1575	546	2121		X(NaCl)	0.03
300	1917	471	2388		Crit.Temp.	451
320	2259	405	2664		Crit.Press.	426
340	2601	348	2949		Bulk Den	0.942
360	2943	297	3240		Bulk MV	20.4
380	3285	253	3538			
400	3627	215	3842			

NB-33	NB-33	2				
T	P (Bodnar & Vityk)	P(gases)	P(Total)			
179.4	7				Tm ice	-5.2
180	18				Th L-V	179.4
200	369	911	1280		Th to	L
220	720	811	1531		Molal NaCl	1.51
240	1071	714	1785		Wt% NaCl	8.1
260	1423	625	2048		X(NaCl)	0.03
280	1774	546	2320		Crit.Temp.	449
300	2125	471	2596		Crit.Press.	419
320	2476	405	2881		Bulk Den	0.948
340	2828	348	3176		Bulk MV	20.27
360	3179	297	3476			
380	3530	253	3783			
400	3882	215	4097			

NB-33	NB-33	-4.9				
T	P (Bodnar & Vityk)	P(gases)	P(Total)			
202.5	9	911	920		Tm ice	-4.9
220	291	811	1102		Th L-V	202.5
240	614	714	1328		Th to	L
260	937	625	1562		Molal NaCl	1.42
280	1259	546	1805		Wt% NaCl	7.68
300	1582	471	2053		X(NaCl)	0.02
320	1905	405	2310		Crit.Temp.	445
340	2227	348	2575		Crit.Press.	408
360	2550	297	2847		Bulk Den	0.925
380	2873	253	3126		Bulk MV	20.36
400	3196	215	3411			

NB-33	NB-33	8				
T	P (Bodnar & Vityk)	P(gases)	P(Total)			
204.5	10	911	921		Tm ice	-5.1
220	259	811	1070		Th L-V	204.5
240	581	714	1295		Th to	L
260	902	625	1527		Molal NaCl	1.48
280	1224	546	1770		Wt% NaCl	7.96
300	1546	471	2017		X(NaCl)	0.03
320	1867	405	2272		Crit.Temp.	448
340	2189	348	2537		Crit.Press.	415
360	2510	297	2807		Bulk Den	0.925
380	2832	253	3085		Bulk MV	20.79

NB-33	NB33 CALCITE		9		
T	P (Bodnar & Vityk)	P(gases)	P(Total)		
222.8	14			Tm ice	-1.8
240	263	51	314	Th L-V	222.8
260	552	44	596	Th to	L
280	841	37	878	Molal NaCl	0.52
300	1130	31	1161	Wt% NaCl	2.96
320	1419	26	1445	X(NaCl)	0.01
340	1709	22	1731	Crit.Temp.	401
360	1998	18	2016	Crit.Press.	288
380	2287	15	2302	Bulk Den	0.862
400	2576			Bulk MV	21.37

NB-33	NB33 CALCITE		10		
T	P (Bodnar & Vityk)	P(gases)	P(Total)		
218.7	13			Tm ice	-2
220	32	59	91	Th L-V	218.7
240	326	51	377	Th to	L
260	619	44	663	Molal NaCl	0.58
280	913	37	950	Wt% NaCl	3.28
300	1207	31	1238	X(NaCl)	0.01
320	1500	26	1526	Crit.Temp.	404
340	1794	22	1816	Crit.Press.	296
360	2087	18	2105	Bulk Den	0.871
380	2381	15	2396	Bulk MV	21.16

NB-33	NB33 CALCITE		11		
T	P (Bodnar & Vityk)	P(gases)	P(Total)		
235.3	18			Tm ice	-2
240	83	51	134	Th L-V	235.3
260	359	44	403	Th to	L
280	636	37	673	Molal NaCl	0.58
300	912	31	943	Wt% NaCl	3.28
320	1189	26	1215	X(NaCl)	0.01
340	1465	22	1487	Crit.Temp.	404
360	1742	18	1760	Crit.Press.	296
380	2018	15	2033	Bulk Den	0.848
400	2295			Bulk MV	21.72

H2O-NaCl-[KCl]					
Stack	Sample	Inclusion			
NB47	NB-47		1		
T	P (Bodnar & Vityk)	P(gases)	P(Total)		
195.6	9			Tm ice	-4.5
200	81	214	295	Th L-V	195.6
220	409	195	604	Th to	L
240	737	176	913	Molal NaCl	1.31
260	1065	158	1223	Wt% NaCl	7.11
280	1393	141	1534	X(NaCl)	0.02
300	1722	124	1846	Crit.Temp.	440
320	2050	109	2159	Crit.Press.	393
340	2378	95	2473	Bulk Den	0.927
360	2706	83	2789	Bulk MV	20.3
380	3034	71	3105		
400	3362				

NB47 NB-47

T	P (Bodnar & Vityk)	P(gases)	P(Total)
168.6	6		
180	204		
200	551	214	765
220	898	195	1093
240	1246	176	1422
260	1593	158	1751
280	1940	141	2081
300	2287	124	2411
320	2634	109	2743
340	2982	95	3077
360	3329	83	3412
380	3676	71	3747
400	4023		

Tm ice	-3
Th L-V	168.6
Th to	L
Molal NaCl	0.87
Wt% NaCl	4.86
X(NaCl)	0.02
Crit.Temp.	419
Crit.Press.	336
Bulk Den	0.936
Bulk MV	20.11

NB47 NB-47 3

T	P (Bodnar & Vityk)	P(gases)	P(Total)
188.9	8		
200	192	214	406
220	525	195	720
240	857	176	1033
260	1190	158	1348
280	1522	141	1663
300	1854	124	1978
320	2187	109	2296
340	2519	95	2614
360	2851	83	2934
380	3184	71	3255
400	3516		

Tm ice	-4
Th L-V	188.9
Th to	L
Molal NaCl	1.16
Wt% NaCl	6.37
X(NaCl)	0.02
Crit.Temp.	433
Crit.Press.	375
Bulk Den	0.928
Bulk MV	20.28

NB47 NB-47 4

T	P (Bodnar & Vityk)	P(gases)	P(Total)
194	8		
200	107	214	321
220	436	195	631
240	765	176	941
260	1094	158	1252
280	1424	141	1565
300	1753	124	1877
320	2082	109	2191
340	2411	95	2506
360	2740	83	2823
380	3070	71	3141
400	3399		

Tm ice	-4.4
Th L-V	194
Th to	L
Molal NaCl	1.28
Wt% NaCl	6.96
X(NaCl)	0.02
Crit.Temp.	439
Crit.Press.	390
Bulk Den	0.928
Bulk MV	20.29

NB47 NB-47 5

T	P (Bodnar & Vityk)	P(gases)	P(Total)
195.3	9		
200	86	214	300
220	415	195	610
240	744	176	920
260	1073	158	1231
280	1402	141	1543
300	1731	124	1855
320	2060	109	2169
340	2389	95	2484
360	2718	83	2801
380	3047	71	3118
400	3376		

Tm ice	-4.6
Th L-V	195.3
Th to	L
Molal NaCl	1.34
Wt% NaCl	7.25
X(NaCl)	0.02
Crit.Temp.	441
Crit.Press.	397
Bulk Den	0.929
Bulk MV	20.27

NB47	NB-47		6	
T	P (Bodnar & Vityk)	P(gases)		P(Total)
178.8	7			
180	28			
200	379	214		593
220	731	195		926
240	1082	176		1258
260	1433	158		1591
280	1784	141		1925
300	2136	124		2260
320	2487	109		2596
340	2838	95		2933
360	3189	83		3272
380	3541	71		3612
400	3892			

Tm ice	-5.1
Th L-V	178.8
Th to	L
Molal NaCl	1.48
Wt% NaCl	7.96
X(NaCl)	0.03
Crit.Temp.	448
Crit.Press.	415
Bulk Den	0.948
Bulk MV	20.28

NB47	NB-47		7	
T	P (Bodnar & Vityk)	P(gases)		P(Total)
177.2	7			
180	56			
200	410	214		624
220	763	195		958
240	1116	176		1292
260	1469	158		1627
280	1822	141		1963
300	2175	124		2299
320	2528	109		2637
340	2881	95		2976
360	3234	83		3317
380	3588	71		3659
400	3941			

Tm ice	-5.1
Th L-V	177.2
Th to	L
Molal NaCl	1.48
Wt% NaCl	7.96
X(NaCl)	0.03
Crit.Temp.	448
Crit.Press.	415
Bulk Den	0.949
Bulk MV	20.26

NB47	NB-47		8	
T	P (Bodnar & Vityk)	P(gases)		P(Total)
179.6	7			
180	14			
200	344	214		558
220	675	195		870
240	1006	176		1182
260	1337	158		1495
280	1668	141		1809
300	1999	124		2123
320	2330	109		2439
340	2660	95		2755
360	2991	83		3074
380	3322	71		3393
400	3653			

Tm ice	
Th L-V	179.6
Th to	L
Molal NaCl	0
Wt% NaCl	0
X(NaCl)	0
Crit.Temp.	374
Crit.Press.	218
Bulk Den	0.891
Bulk MV	20.22

NB47	NB-47		9	
T	P (Bodnar & Vityk)	P(gases)		P(Total)
186.2	8			
200	245	214		459
220	588	195		783
240	931	176		1107
260	1275	158		1433
280	1618	141		1759
300	1961	124		2085
320	2305	109		2414
340	2648	95		2743
360	2991	83		3074
380	3335	71		3406
400	3678			

Tm ice	-5.2
Th L-V	186.2
Th to	L
Molal NaCl	1.51
Wt% NaCl	8.1
X(NaCl)	0.03
Crit.Temp.	449
Crit.Press.	419
Bulk Den	0.943
Bulk MV	20.4

NB47	NB-47		14	
T	P (Bodnar & Vityk)	P(gases)	P(Total)	
194.1	8			Tm ice -4.9
200	106	214	320	Th L-V 194.1
220	438	195	633	Th to L
240	770	176	946	Molal NaCl 1.42
260	1103	158	1261	Wt% NaCl 7.68
280	1435	141	1576	X(NaCl) 0.02
300	1767	124	1891	Crit.Temp. 445
320	2099	109	2208	Crit.Press. 408
340	2432	95	2527	Bulk Den 0.933
360	2764	83	2847	Bulk MV 20.18
380	3096	71	3167	
400	3428			

NB47	NB-47		15	
T	P (Bodnar & Vityk)	P(gases)	P(Total)	
172.8	6			Tm ice -6.4
180	139			Th L-V 172.8
200	507	214	721	Th to L
220	875	195	1070	Molal NaCl 1.84
240	1244	176	1420	Wt% NaCl 9.71
260	1612	158	1770	X(NaCl) 0.03
280	1980	141	2121	Crit.Temp. 463
300	2348	124	2472	Crit.Press. 459
320	2717	109	2826	Bulk Den 0.964
340	3085	95	3180	Bulk MV 19.94
360	3453	83	3536	
380	3822	71	3893	
400	4190			

NB47	NB-47		16	
T	P (Bodnar & Vityk)	P(gases)	P(Total)	
181.7	7			Tm ice -6.3
200	333	214	547	Th L-V 181.7
220	690	195	885	Th to L
240	1046	176	1222	Molal NaCl 1.81
260	1402	158	1560	Wt% NaCl 9.58
280	1759	141	1900	X(NaCl) 0.03
300	2115	124	2239	Crit.Temp. 462
320	2472	109	2581	Crit.Press. 456
340	2828	95	2923	Bulk Den 0.956
360	3185	83	3268	Bulk MV 20.11
380	3541	71	3612	
400	3897			

NB47	NB-47		17	
T	P (Bodnar & Vityk)	P(gases)	P(Total)	
175.6	7			Tm ice -6.4
180	87			Th L-V 175.6
200	452	214	666	Th to L
220	817	195	1012	Molal NaCl 1.84
240	1182	176	1358	Wt% NaCl 9.71
260	1546	158	1704	X(NaCl) 0.03
280	1911	141	2052	Crit.Temp. 463
300	2276	124	2400	Crit.Press. 459
320	2641	109	2750	Bulk Den 0.962
340	3005	95	3100	Bulk MV 19.99
360	3370	83	3453	
380	3735	71	3806	
400	4100			

NB47	NB-47		18	
T	P (Bodnar & Vityk)	P(gases)		P(Total)
178.2	7			
180	39			
200	400	214		614
220	761	195		956
240	1122	176		1298
260	1483	158		1641
280	1843	141		1984
300	2204	124		2328
320	2565	109		2674
340	2926	95		3021
360	3287	83		3370
380	3647	71		3718
400	4008			

Tm ice	-6.3
Th L-V	178.2
Th to	L
Molal NaCl	1.81
Wt% NaCl	9.58
X(NaCl)	0.03
Crit.Temp.	462
Crit.Press.	456
Bulk Den	0.959
Bulk MV	20.05

NB47	NB-47		19	
T	P (Bodnar & Vityk)	P(gases)		P(Total)
180.6	7			
200	354	214		568
220	712	195		907
240	1070	176		1246
260	1427	158		1585
280	1785	141		1926
300	2143	124		2267
320	2501	109		2610
340	2859	95		2954
360	3216	83		3299
380	3574	71		3645
400	3932			

Tm ice	-6.3
Th L-V	180.6
Th to	L
Molal NaCl	1.81
Wt% NaCl	9.58
X(NaCl)	0.03
Crit.Temp.	462
Crit.Press.	456
Bulk Den	0.957
Bulk MV	20.09

NB47	NB-47		20	
T	P (Bodnar & Vityk)	P(gases)		P(Total)
202.1	9			
220	299	195		494
240	624	176		800
260	948	158		1106
280	1272	141		1413
300	1596	124		1720
320	1921	109		2030
340	2245	95		2340
360	2569	83		2652
380	2894	71		2965
400	3218			

Tm ice	-5.1
Th L-V	202.1
Th to	L
Molal NaCl	1.48
Wt% NaCl	7.96
X(NaCl)	0.03
Crit.Temp.	448
Crit.Press.	415
Bulk Den	0.927
Bulk MV	20.74

NB47	NB-47		22	
T	P (Bodnar & Vityk)	P(gases)		P(Total)
204.8	10			
220	254	195		449
240	574	176		750
260	895	158		1053
280	1216	141		1357
300	1536	124		1660
320	1857	109		1966
340	2178	95		2273
360	2498	83		2581
380	2819	71		2890
400	3140			

Tm ice	-5
Th L-V	204.8
Th to	L
Molal NaCl	1.45
Wt% NaCl	7.82
X(NaCl)	0.03
Crit.Temp.	446
Crit.Press.	411
Bulk Den	0.924
Bulk MV	20.82

NB47	NB-47		23		
T	P (Bodnar & Vityk)	P(gases)	P(Total)		
179.2	7			Tm ice	-5
180	21			Th L-V	179.2
200	371	214	585	Th to	L
220	721	195	916	Molal NaCl	1.45
240	1071	176	1247	Wt% NaCl	7.82
260	1421	158	1579	X(NaCl)	0.03
280	1771	141	1912	Crit.Temp.	446
300	2121	124	2245	Crit.Press.	411
320	2471	109	2580	Bulk Den	0.947
340	2821	95	2916	Bulk MV	20.31
360	3171	83	3254		
380	3521	71	3592		
400	3871				

NB47	NB-47		24		
T	P (Bodnar & Vityk)	P(gases)	P(Total)		
177.2	7			Tm ice	-5.2
180	57			Th L-V	177.2
200	410	214	624	Th to	L
220	764	195	959	Molal NaCl	1.51
240	1118	176	1294	Wt% NaCl	8.1
260	1472	158	1630	X(NaCl)	0.03
280	1826	141	1967	Crit.Temp.	449
300	2180	124	2304	Crit.Press.	419
320	2534	109	2643	Bulk Den	0.95
340	2887	95	2982	Bulk MV	20.23
360	3241	83	3324		
380	3595	71	3666		
400	3949				

H2O-NaCl-[KCl]					
Stack	Sample	Inclusion			
104w	NB-104	6			
T	P (Bodnar & Vityk)				
196.5	9			Tm ice	-5.3
200	67	1124	1191	Th L-V	196.5
220	399	1000	1399	Th to	L
240	731	883	1614	Molal NaCl	1.54
260	1063	776	1839	Wt% NaCl	8.24
280	1395	679	2074	X(NaCl)	0.03
300	1727	592	2319	Crit.Temp.	450
320	2059	513	2572	Crit.Press.	422
340	2391	443	2834	Bulk Den	0.935
360	2723	381	3104	Bulk MV	20.57
380	3055	326	3381		
400	3387				

104w	NB-104	7			
T	P (Bodnar & Vityk)				
204.6	10			Tm ice	-5.2
220	258	1000	1258	Th L-V	204.6
240	580	883	1463	Th to	L
260	902	776	1678	Molal NaCl	1.51
280	1224	679	1903	Wt% NaCl	8.1
300	1546	592	2138	X(NaCl)	0.03
320	1868	513	2381	Crit.Temp.	449
340	2190	443	2633	Crit.Press.	419
360	2512	381	2893	Bulk Den	0.926
380	2834	326	3160	Bulk MV	20.76

104w	NB-104		8		
T	P (Bodnar & Vityk)				
198.1	9			Tm ice	-5.2
200	40	1124	1164	Th L-V	198.1
220	370	1000	1370	Th to	L
240	699	883	1582	Molal NaCl	1.51
260	1029	776	1805	Wt% NaCl	8.1
280	1358	679	2037	X(NaCl)	0.03
300	1688	592	2280	Crit.Temp.	449
320	2017	513	2530	Crit.Press.	419
340	2347	443	2790	Bulk Den	0.932
360	2676	381	3057	Bulk MV	20.63
380	3006	326	3332		

NB99	NB99		1		
T	P (Bodnar & Vityk)				
242.3	21			Tm ice	-3.8
260	264			Th L-V	242.3
280	538			Th to	L
300	812			Molal NaCl	1.11
320	1086			Wt% NaCl	6.08
340	1360			X(NaCl)	0.02
360	1634			Crit.Temp.	430
380	1908			Crit.Press.	367
400	2182			Bulk Den	0.867
420	2456			Bulk MV	21.72

NB99	NB99		2		
T	P (Bodnar & Vityk)				
237.2	19			Tm ice	-5.6
240	59			Th L-V	237.2
260	346			Th to	L
280	634			Molal NaCl	1.62
300	921			Wt% NaCl	8.65
320	1208			X(NaCl)	0.03
340	1495			Crit.Temp.	454
360	1783			Crit.Press.	432
380	2070			Bulk Den	0.897
400	2357			Bulk MV	21.45

NB99	NB99		3		
T	P (Bodnar & Vityk)				
217.1	12			Tm ice	-4.4
220	56			Th L-V	217.1
240	360			Th to	L
260	664			Molal NaCl	1.28
280	967			Wt% NaCl	6.96
300	1271			X(NaCl)	0.02
320	1575			Crit.Temp.	439
340	1879			Crit.Press.	390
360	2182			Bulk Den	0.904
380	2486			Bulk MV	20.82

NB99	NB99		4		
T	P (Bodnar & Vityk)				
224.1	14			Tm ice	-4.2
240	249			Th L-V	224.1
260	544			Th to	L
280	839			Molal NaCl	1.22
300	1134			Wt% NaCl	6.67
320	1430			X(NaCl)	0.02
340	1725			Crit.Temp.	436
360	2020			Crit.Press.	382
380	2315			Bulk Den	0.894
400	2610			Bulk MV	21.06

NB99 NB99 5

T	P (Bodnar & Vityk)
199.3	9
200	21
220	353
240	685
260	1018
280	1350
300	1683
320	2015
340	2347
360	2680
380	3012
400	3345
420	3677

Tm ice	-5.9
Th L-V	199.3
Th to	L
Molal NaCl	1.7
Wt% NaCl	9.05
X(NaCl)	0.03
Crit.Temp.	458
Crit.Press.	442
Bulk Den	0.938
Bulk MV	20.51

NB99 NB99 6

T	P (Bodnar & Vityk)
198	9
200	42
220	372
240	701
260	1031
280	1360
300	1690
320	2020
340	2349
360	2679
380	3009
400	3338
420	3668

Tm ice	-5.2
Th L-V	198
Th to	L
Molal NaCl	1.51
Wt% NaCl	8.1
X(NaCl)	0.03
Crit.Temp.	449
Crit.Press.	419
Bulk Den	0.932
Bulk MV	20.63

NB99 NB99 7

T	P (Bodnar & Vityk)
206.3	10
220	227
240	545
260	862
280	1179
300	1496
320	1814
340	2131
360	2448
380	2765
400	3083
420	3400

Tm ice	-4.7
Th L-V	206.3
Th to	L
Molal NaCl	1.37
Wt% NaCl	7.39
X(NaCl)	0.02
Crit.Temp.	442
Crit.Press.	401
Bulk Den	0.919
Bulk MV	20.48

NB99 NB99 8

T	P (Bodnar & Vityk)
222.8	14
240	267
260	560
280	854
300	1148
320	1441
340	1735
360	2029
380	2322
400	2616

Tm ice	-3.5
Th L-V	222.8
Th to	L
Molal NaCl	1.02
Wt% NaCl	5.62
X(NaCl)	0.02
Crit.Temp.	426
Crit.Press.	355
Bulk Den	0.887
Bulk MV	21.23

NB99	NB99	9		
T	P (Bodnar & Vityk)			
203.5	10		Tm ice	-3.3
220	268		Th L-V	203.5
240	581		Th to	L
260	895		Molal NaCl	0.96
280	1208		Wt% NaCl	5.32
300	1521		X(NaCl)	0.02
320	1834		Crit.Temp.	423
340	2147		Crit.Press.	348
360	2460		Bulk Den	0.906
380	2774		Bulk MV	20.79

NB99	NB99	10		
T	P (Bodnar & Vityk)			
205.2	10		Tm ice	-4.3
220	244		Th L-V	205.2
240	560		Th to	L
260	877		Molal NaCl	1.25
280	1193		Wt% NaCl	6.81
300	1509		X(NaCl)	0.02
320	1825		Crit.Temp.	437
340	2142		Crit.Press.	386
360	2458		Bulk Den	0.916
380	2774		Bulk MV	20.56

NB99	NB99	11		
T	P (Bodnar & Vityk)			
216.9	12		Tm ice	-3.7
220	59		Th L-V	216.9
240	359		Th to	L
260	660		Molal NaCl	1.08
280	961		Wt% NaCl	5.93
300	1262		X(NaCl)	0.02
320	1562		Crit.Temp.	429
340	1863		Crit.Press.	363
360	2164		Bulk Den	0.896
380	2465		Bulk MV	21.01

NB99	NB99	12		
T	P (Bodnar & Vityk)			
226	15		Tm ice	-4.9
240	222		Th L-V	226
260	519		Th to	L
280	815		Molal NaCl	1.42
300	1112		Wt% NaCl	7.68
320	1408		X(NaCl)	0.02
340	1704		Crit.Temp.	445
360	2001		Crit.Press.	408
380	2297		Bulk Den	0.901
400	2594		Bulk MV	20.9

APPENDIX H

Formulae for the salinity and temperature correction of Henry's Law Constants as supplied by Drummond (1981). These formulae are valid for 0 - 6 molal solutions in the temperature range of 25 - 400°C, pressures up to 500 bar and 3 mole percent of gas.

All determinations of fugacity is in the following form:

$$\text{fugacity} = K_H * X$$

where K_H is the value for Henry's Law constants and X is the molar concentration of the gas.

H_2

$$ln K_H = A + BT + C/T + DT^2 + Em$$

T = Temperature in Kelvin
m = NaCl molality
A = 5.91
B = 0.01632
C = -340.0
D = -2.769×10^{-5}
E = 0.2021

CO_2

$$ln K_H = A + BT + CX + D/T + E/X + FXT + GX/T + HT/X$$

T = Temperature in Kelvin
X = NaCl molality + 1.0
A = 20.244
B = -0.016323
C = -1.0312
D = -3629.7
E = 0.4445
F = 0.0012806
G = 255.9
H = -0.001606

CH_4

$$\ln K_H = A + BP + CT + DX + E/T + F/X + G/P + HP/X + IP/T + JTX$$

P = CH_4 pressure in atm.
T = Temperature in Kelvin
X = NaCl molality + 1.0
A = 26.187
B = 0.0013647
C = -0.026991
D = 0.1169
E = -3380.7
F = -0.2409
G = -0.2779
H = 0.0001919
I = -0.1428
J = 0.0002778

H_2S

$$\ln K_H = A + BT + CX + D/T + E/X + FXT + GX/T + HT/X$$

T = Temperature in Kelvin
X = NaCl molality + 1.0
A = 11.416
B = -0.007013
C = 0.2905
D = -2067.7
E = 0.5705
F = -0.0001574
G = -46.2
H = -0.001777

The following calculations for Henry's Law constants, applied to simple apolar gases, is taken from Prini and Crovetto (1989) and are valid from ambient temperatures to the Tmax show.

Formulae take the form of:

$$ln\ K_H = A_1 + A_2*10^3/T + A_3*10^6/T^2 + A_4*10^9/T^3 + A_5*10^{12}/T^4$$

System	A_1	A_2	A_3	A_4	A_5	σ	Tmax(K)
He-H_2O	-7.1725	5.9734	-0.9038			5.9	588.7
Ne-H_2O	-5.9825	5.5176	-0.8886			3.2	543.4
Ar-H_2O	-7.8972	7.0178	-1.2649			2.7	568.4
Kr-H_2O	-7.5642	6.8773	-1.3047			2.9	525.6
Xe-H_2O	-9.3604	7.9654	-1.5167			12.9	574.8
O_2-H_2O	-15.9766	15.7951	-4.3331	0.3502		5.0	616.0
CH_4-H_2O	-18.5223	17.7956	-4.8318	0.3856		3.3	633.0
H_2-H_2O	-46.0050	64.8729	32.9118	7.6094	-0.6673	10.8	636.0
N_2-H_2O	-55.5386	77.9340	-13.9781	9.2813	-0.8226	8.9	636.0

Above 573 K and up to the crtitical temperature, T_{cl}, the following formulae are better suited:

$$ln\ K_H = (B_0/T)*(T_{cl}-T).\ \ln((T_{cl}-T)/T_{cl}) + \sum_{i=0}^{n} (B_{i+1})/T^i\ (1000)^i$$

where B_0 has a value between 0 and -4, usually -1.

System	B_1	B_2	B_3	B_4	B_5	σ
He-H_2O	-6.4859	5.2327	-0.8086			6.5
Ne-H_2O	-5.3238	4.7936	-0.7959			2.1
Ar-H_2O	-7.1874	6.2632	-1.1676			1.5
Kr-H_2O	-7.0173	6.2204	-1.2220			4.0
Xe-H_2O	-8.7307	7.2588	-1.4265			11.8
O_2-H_2O	-13.3190	12.8557	-3.4516	0.2592		4.7
CH_4-H_2O	-15.5767	14.5624	-3.8519	0.2838		2.5
C_2H_6-H_2O	-20.6180	19.3949	-5.2453	0.3956		2.7
H_2-H_2O	-38.4512	53.4846	-27.4317	6.3522	-0.5590	10.6
N_2-H_2O	-47.7453	66.7623	-34.2820	7.9705	-0.7094	8.4